Development of a wearable tool for detecting ovulation in cattle : from the definition of microneedles to collect interstitial fluids, to the development of an aptasensor

Juliette Simon

THÈSE

Pour obtenir le grade de

DOCTEUR DE L'UNIVERSITÉ GRENOBLE ALPES

Spécialité : Matériaux, Mécanique, Génie civil, Electrochimie

Arrêté ministériel : 25 mai 2016

Présentée par

Juliette SIMON

Thèse dirigée par **Pascal MAILLEY**, Directeur de Recherche CEA-Leti; co-dirigée par **Fabienne BLANC**,Professeure VetAgro Sup et co-encadrée par **Thomas ALAVA**, Ingénieur de Recherche CEA-Leti

préparée au sein du **Laboratoire Chimie Capteur et Biomatériaux (CEA-Leti)** et de l'**UMR Herbivores (INRAe - VetAgro Sup)** dans **l'École Doctorale I-MEP2 (Université Grenoble Alpes)**

Développement d'un outil embarqué de détection des ovulations chez les bovins : de la définition d'un système de microaiguilles pour prélever les fluides interstitiels, au développement d'un aptasensor

Development of a wearable tool for detecting ovulation in cattle: from the definition of microneedles to collect interstitial fluids, to the development of an aptasensor

Thèse soutenue publiquement le **7 décembre 2021**,devant le jury composé de :

Monsieur Yoann ROUPIOZ DIRECTEUR DE RECHERCHE, CNRS	Président du jury
Madame Róisín OWENS PROFESSEURE, University of Cambridge	Rapporteuse
Madame Sylvie CHASTANT-MAILLARD PROFESSEURE, Ecole Nationale Vétérinaire de Toulouse	Examinatrice
Monsieur Jérome LAUNAY MAITRE DE CONFERENCE, Université de Toulouse 3 Paul Sabatier	Rapporteur
Madame Anne FERLAY DIRECTRICE DE RECHERCHE, INRAe	Invitée
Monsieur Vincent BOUCHIAT Grapheal	Invité
Monsieur Thomas ALAVA INGENIEUR DE RECHERCHE, CEA-Leti	Encadrant de thèse
Madame Fabienne BLANC PROFESSEURE, VetagroSup	Co-directrice de thèse
Monsieur Pascal MAILLEY DIRECTEUR DE RECHERCHE, CEA-Leti	Directeur de thèse

Remerciements

Il y a maintenant un peu plus de trois ans, je me lançais dans « La Thèse ». Quand on commence cet étrange voyage, c'est un peu comme se retrouver seul, à bord d'un petit vaisseau d'exploration lancé au milieu de l'espace. Notre mission peut paraître dix fois plus grande que nous, on se demande bien par où commencer et comment diable est-il possible de faire tout ce que l'on a prévu en seulement trois petites années. Dans mon cas je me suis aperçue bien vite que je n'étais pas seule à bord du vaisseau et qu'un solide équipage était là pour me guider et surmonter bon nombre d'obstacles, scientifiques bien sur … mais pas seulement !

Je tiens tout d'abord à remercier mes deux directeurs de thèse, Pascal Mailley et Fabienne Blanc, pour m'avoir fait confiance avec ce nouveau projet ambitieux qu'est SmartRepro. Ce fut un réel plaisir que de travailler avec vous. Tout au long de ma thèse nos échanges, vos conseils et vos encouragements m'ont amenée à m'aventurer dans des domaines scientifiques qui m'étaient inconnus jusqu'alors et à me lancer dans de nouveau défis. Cette thèse, je l'ai réalisée en allant chercher les technologies, les expertises aux quatre coins du CEA et même au-delà. Alors quand Pascal m'a proposée de me lancer dans les biocapteurs avec un certain Thomas Alava au DCOS, je n'ai pas hésité… et l'aventure SGFET a commencée. Nos discussions techniques (mais pas seulement !), le partage d'expérience… pour tous ces échanges à l'accent toulousain qui m'ont énormément aidée pendant ma thèse, je tiens à te remercier. Pour me montrer la voie dans l'univers des biocapteurs, j'ai aussi pu compter sur un très bon guide. Adrien, je te dois les solides bases d'une partie importante de ma thèse, ce fut un plaisir de travailler avec toi.

Mon travail sur les biocapteurs SGFETs a commencé sur la deuxième partie de ma thèse et réaliser des tests de fonctionnalisation et de détection biologique n'auraient pas été possible sans l'aide de plusieurs personnes que je tiens à remercier ici. Tout d'abord Maud Savonnet et Marie Gaillard qui m'ont guidée sur la voie des aptamères, un grand merci à toutes les deux. La Covid s'étant par le suite invitée dans nos quotidiens, la réalisation des tests de détection d'hormones n'aurait pas été possible sans l'aide de la startup Grapheal. Merci à toute l'équipe pour votre accueil, votre disponibilité et vos conseils. Travailler avec vous restera un très bon souvenir, je ne vous souhaite que du succès pour la suite !

Sur le plan technique, la création du premier prototype de patch fonctionnel, entre le dépôt du manuscrit et la soutenance a permis de réunir les différentes briques technologiques développées pendant la thèse sur une seule plateforme. Un grand merci à Mahfod Benessalah pour son investissement dans mon projet. Collaborer avec toi a été un grand plaisir !

Ma thèse est le fruit d'une collaboration entre le CEA Grenoble et l'INRAe Clermont-Ferrand. Si j'ai passé la majorité de ma thèse sur le site du CEA Grenoble, j'ai réalisé plusieurs séjours sur le centre de l'INRAe Clermont-Ferrand à l'occasion de présentations scientifiques ou pour participer à l'expérimentation animale décrite dans mon manuscrit. Merci aux équipes du centre pour leur accueil chaleureux à chacune de mes visites. Je souhaite particulièrement remercier Anne Ferlay responsable de mon équipe d'accueil à l'INRAe, ma directrice de thèse Fabienne Blanc bien sûr, Isabelle Constant pour son immense travail réalisé sur le dosage des

hormones, Pascale Berraud pour m'assister dans toutes mes démarches administratives ainsi que les animaliers d'Herbipôle pour leur implication dans mon projet de thèse.

Mes remerciements vont ensuite à l'ensemble des membres et invités du jury : Mme Róisín Owens, Mr Jérôme Launay, Mr Yoann Roupioz, Mme Sylvie Chastant-Maillard, Mme Anne Ferlay et Mr Vincent Bouchiat pour avoir accepté d'examiner et d'évaluer mon travail de thèse. Un grand merci aussi à Mme Alice Nicolas et Mme Marie Saint-Dizier qui ont suivies mon travail dès le début lors des Comités de Suivi Individuel (CSI).

Enfin, si le soutien scientifique et technique est primordial pour mener une thèse, il ne faut pas sous-estimer le soutien moral nécessaire pour parvenir jusqu'à la ligne d'arrivée ! Sur ce point là encore, j'ai été bien entourée.

Par mes encadrants bien sûr et par ma directrice de laboratoire au CEA, Séverine Vignoud que je tiens à remercier pour sa présence et son soutien tout au long de ma thèse et particulièrement lors des moments plus difficiles comme le premier confinement de mars 2020.

De ces quelques années au CEA, j'emporte une myriade de bons souvenirs… il faut dire que j'ai eu de super collègues dans ce labo du L2CB! Caro, voisine de bureau au top, nos discussions sur tout, les histoires du matin, ta bonne humeur et ton humour me manquent déjà. Bilal, you're the life of the party! Maxime, co-bureau de la « ThésardsCave » , merci pour tous les discussions à l'heure du déjeuner. Antoine: le seul thésard à avoir pu rester zen pendant l'intégralité de sa thèse, respect. Mathilde: partenaire natation et féministe dans l'âme. Prisca, fashion girl. Anouchka: spécialiste couture du labo, merci pour ta gentillesse et pour m'avoir encouragée dans mes débuts de couture. Paul et Amélia: merci aussi à vous deux pour votre gentillesse et pour les propositions de pauses café (c'était plus facile sur la fin ;)). Thibaut : toujours là pour soutenir ou pour une bonne discussion matinale sur l'actualité ;) . Charles, Sacha (2 points !), Mersha, Natalie merci aussi à vous tous pour votre bonne humeur quotidienne et les bons moments passés ensemble aux pauses cafés et à H3.

A la lisière du CEA il y a un lieu un peu magique où l'on oubli tous les tracas de la thèse pour quelques dizaines de minutes : la médiathèque de l'ALAS. Pendant plus de 3 ans, Ludivine et Sylvie m'ont fait découvrir une multitude d'univers à raison de quelques kilos de livres à chaque passage et surement quelques centaines d'emprunts. Un immense merci à toutes les deux pour votre bonne humeur, votre gentillesse, les discussions sur nos lectures et vos trouvailles en comics, BDs et autres, toujours géniales. Ces excursions hebdomadaires à la médiathèque vont me manquer !

Cette thèse, c'est aussi la dernière étape de mon cursus universitaire. Le trajet fut long et pas toujours de tout repos mais j'ai toujours été soutenue sans réserve par ma famille. Tout d'abord par mes parents à qui je dois énormément. Vous m'avez toujours encouragée et soutenue dans mes choix, vous m'avez appris le goût de l'effort et vous étiez là lors de mes moments de doutes comme lors de mes victoires. Charles, tous les deux nous avons toujours formé une sacrée équipe, pouvant toujours compter l'un sur l'autre. Ces dernières années, te voir évoluer, chercher et trouver ta voie a été une sacrée leçon de volonté, de courage et de détermination qui m'a aidée à ne rien lâcher jusqu'au bout. Merci aussi à mes quatre grands-parents, ma marraine et toute ma famille pour leur soutien inconditionnel, même si mes

histoires de microaiguilles, d'oreilles de vache et de capteurs pouvaient parfois paraitre un peu obscures !

Enfin, the last but not the least : Romain merci d'avoir été mon roc pendant cette aventure. Tu as été aux premières loges pour voir les effets des aléas de la thèse sur moi et je te remercie pour ta patience, pour m'aider à me déconnecter quand j'en avais besoin, pour tous ces petits plats qui m'attendaient quand je revenais tard le soir et bien sûr pour la découverte pas à pas du monde du cyclisme ! J'ai hâte de voir ce que la suite de l'aventure nous réserve.

Contents

Acronyms

Notation	Description
2PP	Two Photon Polymerization
AI	Artificial Insemination
BAW	Bulk Acoustic Wave
BioFET	Biosensor Field-Effect Transistor
BS	Blood Sampling
CAD	Computer-Aided Design
CEA	Commissariat à l'Énergie Atomique et aux Énergies Alternatives / The French Alternative Energies and Atomic Energy Commission
Cu	Copper
CVD	Chemical Vapour Deposition
DeepDeDeep	Derma
DMSO	Dimethyl sulfoxide
DNA	Deoxyribonucleic Acid
DI water	Deionized water
E2	17β-oestradiol
EIS	Electrochemical Impedance Spectroscopy
ELISA	Enzyme-Linked Immunosorbent Assay
FSH	Follicle-Stimulating Hormone
FTD	Fun To Do company

IFSET	Ion Sensitive Field Effect Transistor
$I_{leakage}$	leakage current
LH	Luteinizing Hormone
LETI	Laboratoire d'Électronique et de Technologie de l'Information / Electronics and Information Technology Laboratory
LITEN	Laboratoire d'Innovation pour les Technologies des Énergies Nouvelles et les Nanomatériaux / Innovation laboratory for new energy technologies and nanomaterials
LOD	Limit Of Detection
MN	Microneedle
P4	Progesterone
PBASE	1-PyreneButyric Acid N-hydroxySuccinimide Ester
PBS	Phosphate Buffer Saline
PCB	Printed Circuit Board
PEEK	Polyetheretherketone
PMMA	Polymethyl Methacrylate
PCR	Polymerase Chain Reaction
PTA	Plateforme de Technologie Amont (clean room)
QCM	Quartz Crystal Microbalance
RIA	RadioImmunoAssay
RNA	Ribonucleic Acid
SAW	Surface Acoustic Wave
SC	Stratum Corneum
SELEX	Systematic Evolution of Ligands by Exponential enrichment

SEM	Scanning Electron Microscope
SGFET	Solution-Gated Field Effect Transistor
Si	Silicon
SLA	Stereolithography
SOI	Silicon on insulator
SPR	Surface Plasmon Resonance
SupDe	Superficial Derma
V_{Gate}	Gate Source potential

Introduction

Over the past 50 years, the French cattle farming sector has undergone profound changes. To respond to changes in meat and milk consumption while coping with the decrease in the number of cattle farms, the size of dairy and suckling farms has almost tripled between 1983 and 2019 (Agreste, 2020). One of the keys to the economic success of a farm lies in the management of the herd's reproduction. Good reproductive management allows for optimal milk production in the case of dairy cows and an optimal number of calving per year in the case of suckling cows.

Artificial insemination (AI), one of the reproductive management tools, has been practised for about 50 years in France and is a widespread practice in French breeding. More than 75% of dairy calves are procreated by this method and about 13% of the calves from suckling farms (Allice, 2021). Successful insemination requires knowing the best moment to inseminate. Historically, the breeder would observe the herd several hours a day to spot heat associated behaviour expressed by the cows. To overcome the increase of the cows per herd, the lack of manpower on farms and the decrease in heat expression (Cutullic E., 2010), several tools to help detect cows in heat have been developed and are currently on the market. Most of these tools detect behaviours associated with the state of heat of the cow. The sensitivity, specificity, practicality and price of these tools cover a very broad spectrum (Allain C. et al., 2012). As the behaviours detected are not necessarily specific to the heat period, false positives can lead to unnecessary inseminations and therefore a financial loss for the farmer. Moreover, some cows show little or none of the expected behaviour during heat, and the farmer may miss an opportunity to inseminate, or may inseminate at the wrong time which also represents a loss of profit.

A new tool, the HerdNavigator® by Delaval, dedicated to ovulation detection provides promising results. Instead of relying on external signs of heat, this tool monitors the level of one of the reproductive hormones, progesterone, to predict ovulation and warn the farmer. This tool, which is more efficient than previous methods, doses the hormone in the milk of cows during milking. Although effective, it can only be used on dairy cows and is adapted for herds over 100 cows, requiring a significant investment by the farmer.

The CEA / VetAgro Sup / INRAe "SmartRepro" project, in which this thesis is included, aims to provide a new ovulation detection solution with the following specifications:

1. Monitoring of the evolution of hormones involved in the oestrus cycle of cows.
2. Applicable for both dairy and suckling cows.
3. Easy to use for the farmer.
4. Reasonable cost to be used by medium-sized farms (about 45 cows for dairy farms and 36 for suckling farms, (Alice, 2021)).

To meet these objectives, the tool displayed in Figure 0. 1 was imagined.

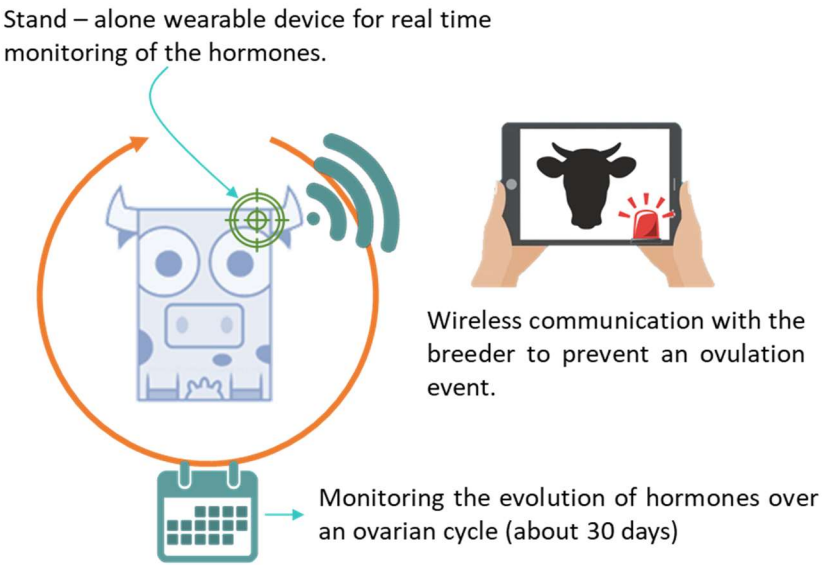

Figure 0. 1 Schematic view of the SmartRepro tool for ovulation detection.

This tool, in the form of a patch, will consist of an on-board biosensor capable of analysing one or more hormones involved in the oestrus cycle of the cow in real time. These hormones, being present for example in the blood (Dieleman et al., 1986; Martin et al., 2013), will have to be collected and transferred to the biosensors embedded in the patch. The patch is intended to be worn for at least 30 days, to be sure to include an entire oestrus cycle and eventually detect some abnormalities (prolonged luteal phases or interruption of cyclicity) (Disenhaus C et al., 2008), without requiring any maintenance by the farmer. The design makes the tool easy to use for suckling cows, spending part of the year on pasture, but also dairy cows in pasture-based systems. When the biosensor detects an ovulation, the patch will transmit the information to the farmer.

As the SmartRepro project started with this thesis, I chose to focus on three axes during the three years of research:

1. Determine the location of the patch. This location must allow for hormone collection, be easily accessible to the farmer and be protected from the cow's daily activities to remain in place for the required 30 days.
2. Develop a way to reach the hormones and transfer them to the biosensor.
3. Develop a biosensor for real time monitoring of the hormones. The selected technology should combine sufficient sensitivity and specificity, be suitable for stand-alone wearable device integration and have low production cost for possible industrialisation further down the line.

The following manuscript presents the reasoning in the choice of technologies selected to meet the specifications and the solutions developed during this thesis.
The first chapter will first provide a brief presentation of this thesis context in regard to the reproduction management in French herds as the different solutions already on the market to help heat detection. In a second part, an overview of the different technologies available

to fulfil the thesis objectives will be introduced and discussed with the prism of the SmartRepro application and constraints.

Defining the location of the patch was the first step of the development process as it would impact the type of fluids analysed and how to reach them. The strategy to determine the location of the patch and the tissues analysis to refine the emplacement choice will be presented in Chapter 2. These data led in the second time of this chapter to the design and the creation of hollow microneedles (MNs) to sample and transfer the fluids containing the hormones to further parts of the patch.

To monitor the evolution of the hormones in real time, a biosensor was developed and characterized electrochemically. Before conducting hormones detection tests, detection of molecules whose interactions are well known in the literature were performed. The objective of these experiments was to understand the inner mechanisms of the biosensor and its unique detection structure when operating in a liquid environment. The fabrication process and electrochemical tests results will be presented in Chapter 3.

Finally probes to detect the targeted hormones with high sensitivity and selectivity were selected and tested. The first hormones detection tests and results will be presented in the last chapter.

- Chapter 1 –

State of the art

Introduction

This thesis presents a multidisciplinary work that has linked animal sciences with biosensors with the objective to develop a new device dedicated to help farmers to find the best time to inseminate their cows. This first chapter depicts the context of this work and provides a synthetic review of the main biological and technological knowledge that have been used to refine our scientific position and research strategy.

Over the last decades artificial insemination (AI) has considerably increased in dairy herds as a way to increase genetic gain and to control the spread of sexually transmitted diseases. At the time of writing, about 79% of the dairy cows are inseminated in France whereas AI only concerns 13% of beef cows (Allice, 2021). New perspectives of AI development can be pointed out in beef with the opportunities from genomic selection (Pimentel & König, 2012) and with the recent development of insemination by the breeder.

Successful AI relies on the farmer's ability to detect when a cow is about to ovulate and to determine the best time for insemination (Roelofs, 2005). Traditionally, the detection of the ovulation time in cyclic cows relies on visual observation of oestrus (or heat) that is a period occurring around 20 to 30 hours before ovulation where cows express sexual behaviours (Roelofs et al., 2005). Oestrus detection is necessary to determine when to inseminate cows. It plays a key role in the profitability of artificially bred dairy and beef herds as if cows are inseminated too early or too late, the chance of fertilization can be affected and, if fertilization occurs, the early embryonic development can be altered (Roelofs, 2005) leading to reproductive failure. Such reproductive failures have great consequences both on farm profitability, as lack of calving means less income (milk and calves), and on cow longevity, as failure to conceive often means culling (Bascom & Young, 1998; Hadley et al., 2006).

Standing to be mounted is the gold standard indicator that a cow is in oestrus (Van Eerdenburg et al., 1996) but it is frequently not observed due to either poor intensity of oestrus expression (cow effect) or insufficient observation (human effect) or both (Moore et al., 2021). Several studies have reported that the mean duration of standing oestrus is less than 10 hours in both dairy and beef cows and that some oestrus may occur without any standing behaviour (Bedere, 2017; Blanc et al., 2010) (Figure 1. 1). Oestrus detection has thus become a major limiting factor of reproductive performance and profitability in modern dairy herds.

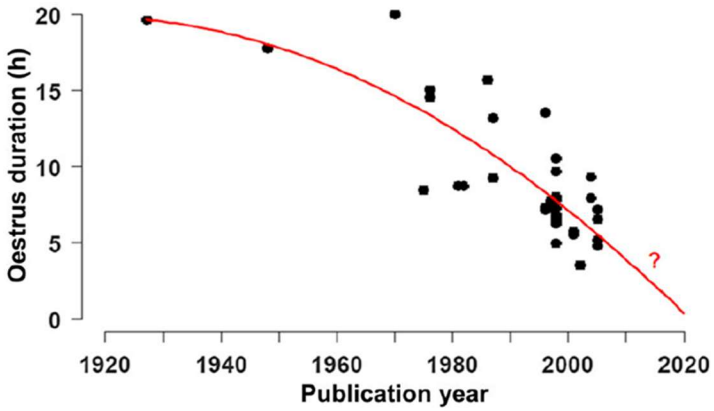

Figure 1. 1 From (Bedere, 2017). Duration of the oestrus (heat) in dairy cattle through time (quantitative review of 39 records from 25 studies between 1927 and 2005: reprinted from (Cutullic E., 2010))

To improve oestrus detection rate and help farmers to determine the right time for insemination, automated oestrus detection systems have been developed (Saint-Dizier & Chastant-Maillard, 2012; Moore et al, 2021). Most of them consist in monitoring mounting behaviours, activity or locomotion but few rely on the monitoring of physiological traits that can be associated with ovulation. The SmartRepro project in which this thesis is included proposes an alternative solution that could be used both in suckling and dairy cows bred in pasture-based systems with the objective to be easy to use, more reliable and less expensive than the currently available solutions.

The first part of this "state of the art" chapter proposes a critical analysis of available oestrous detection devices in order to highlight their strengths and limitations. The second part is dedicated to biosensors with the aim to analyse what solutions would be interesting to deploy for the detection of ovulation time. With the important evolution of micro and nano technologies over the last decades, biosensors have taken an important place in our daily lives, whether in the medical, agricultural, environmental or, more recently, welfare fields. Through the prism of the SmartRepro project, the range of technological solutions developed for these applications will be presented.

1.1 Ovulation detection in cows, a critical point in the management of reproduction

1.1.1 Controlling reproduction in dairy and suckling herds: a key issue for breeding

1.1.1.1 Herd profitability relies heavily on reproductive success

Depressed reproductive performance of a cow herd affects its profitability through additional expenditures and reduced incomes (Seegers, 2006). Additional expenditures are extra straws and extra charges for repeat services by AI technicians, more frequent veterinary

examinations and interventions, extra hormonal and other treatments units, additional expenses in other corrective or preventive measures (nutritional supplementation, heat detection aid devices) and extra labour time for the farmer to manage the problem of cows. Reduced incomes result from lengthened calving intervals that induce calf crop reduction and reduction in milk yield per year-present cow (Seegers, 2006).

Besides these direct additional expenditures and reduced incomes, indirect costs are also induced from culling due to reproductive problems. In most of dairy and beef herds, reproductive failure is one of the main causes of involuntarily culling (Ahlman et al., 2011) and leads to reduced cow longevity. Involuntary culling has detrimental economic consequences as it means an anticipated exit of the cow in comparison to the optimal culling age (Brzáková et al., 2019; Hadley et al., 2006; Seegers, 2006). Consequently, the annual production costs associated with raising replacement heifer increase: more replacement stock has to be brought in and rearing or purchase costs of heifers are amortised on a lower milk yield (Beaudeau et al., 1995) (Figure 1. 2) or a lower number of calves from first calving to exit. Another economic impact is that culling for reproductive problems lets less possibilities for voluntarily culling of cows having low genetic merit for production traits (Seegers, 2006). In dairy herds, total loss due to reproductive failure was estimated to 10 % of the farmer income (Dijkhuizen et al., 1985). In beef herds, Boyer et al. (2020) reported that a suckling cow stops to be profitable to the breeder after two reproductive failures.

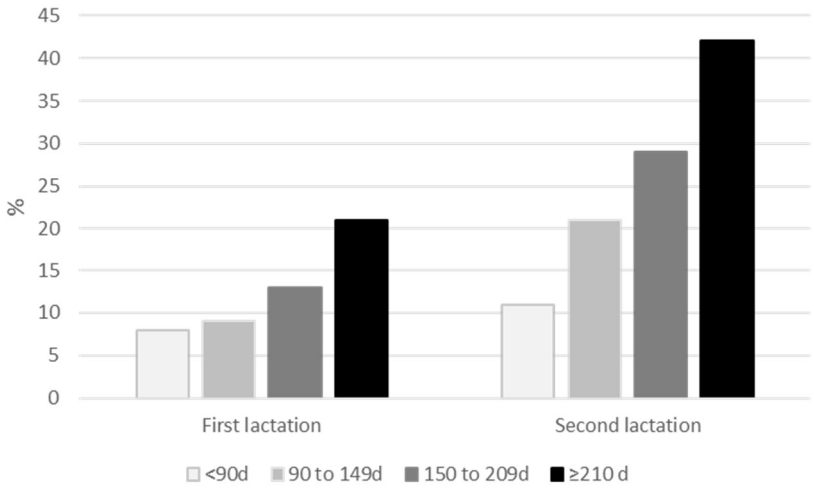

Figure 1. 2 Estimated probability (%) for a cow to be culled in first and second lactation according to the postpartum days open observed in the same lactation (from Beaudeau et al., 1995)

Such results clearly highlight why reproductive success is a major issue for dairy and beef herds' profitability.

1.1.2.2 Artificial insemination (AI): a dominant practice in dairy herds, more rare in suckling herds

AI is a widely used technique in dairy herds as 80% of the dairy cows are inseminated in Europe (Alice, 2021). The significant deployment of this technique can be justified on two main grounds:

- **Sanitary.** As all seeds are checked by the seed collection centres, the risk of transmission of venereal diseases is considerably reduced.
- **Genetic.** Each breeder cannot rear as many bulls as desired to improve productive and functional traits within his herd. An access to a catalogue of bulls' seeds with identified characteristics can allow rapid improvement of the targeted characteristics. AI can also be used as a lever to increase genetic diversity within a herd (Rodgers et al., 2012).

Despite the interests of AI, this technique is still little used in beef production. In France, only 15 to 17% of suckling herds use AI (Chanvallon et al., 2015; Boÿreau, 2019). Several reasons can partly explain this large gap between dairy and beef herds. First, a large part of the beef herds are located in areas were often fewer veterinaries are available to practice AI. Secondly, the breeding period often occurs in spring when cows are at pasture and practising AI means to spend time to observe cows in paddocks that sometimes are quite far from the farm, to isolate cows in oestrous and block them in a stalling device to practice AI. All these steps have to be repeated in case of conception failure.

In her veterinarian thesis, Boÿreau (2019) conducted a survey of breeders and veterinaries to identify the obstacles for AI in suckling herds. The study took place in the Creuse department (France), which has the largest number of suckling herds in France (22% of the French beef herds). From the breeders' point of view, the main obstacles to AI are:

- the fact that beef cows spend a majority of their time outdoors,
- the low profitability of AI compared to natural mating,
- the amount of time required to observe the cows and to detect oestrus as 93% of the breeders interviewed do not use tools for heat detection.

Veterinarians identified two main obstacles:

- The lack of veterinarians in rural areas. On average in the Creuse department, a veterinarian structure (two to four practitioners) has on average 133 beef herds to follow. With pastures often far apart and sometimes difficult to access, it is not possible to offer this service to all herds.
- Very few vets offer this service (only 10% according to the survey) and as the demand from farmers is quite low there is a lack of technical training on AI and heat detection tools.

With the increase of herd size, suckling farmers gave priority to work simplification at the detriment of the development of practices that take time like AI. However such a choice may evolve in the future as insemination by the farmer is now possible, provided that easy to use and reliable tools are available for oestrus detection at pasture and that devices are accessible to block the cows at pasture in order to inseminate them.

1.1.2 Inseminating at the right time requires to assess the reproductive status of females

1.1.2.1 Summarized presentation of the oestrus cycle of the cow and the dynamics of reproductive hormones during the cycle

The ovary of the cow ensures two main functions: the production of the female germ cells (oocytes) and the synthesis of steroid hormones: progesterone (P4) and oestrogens. Each oocyte develops within a structure named a follicle that will also develop itself during the oestrus cycle. Folliculogenesis can be divided into three phases according to follicular dynamics (Bedere, 2017) (Figure 1. 3):

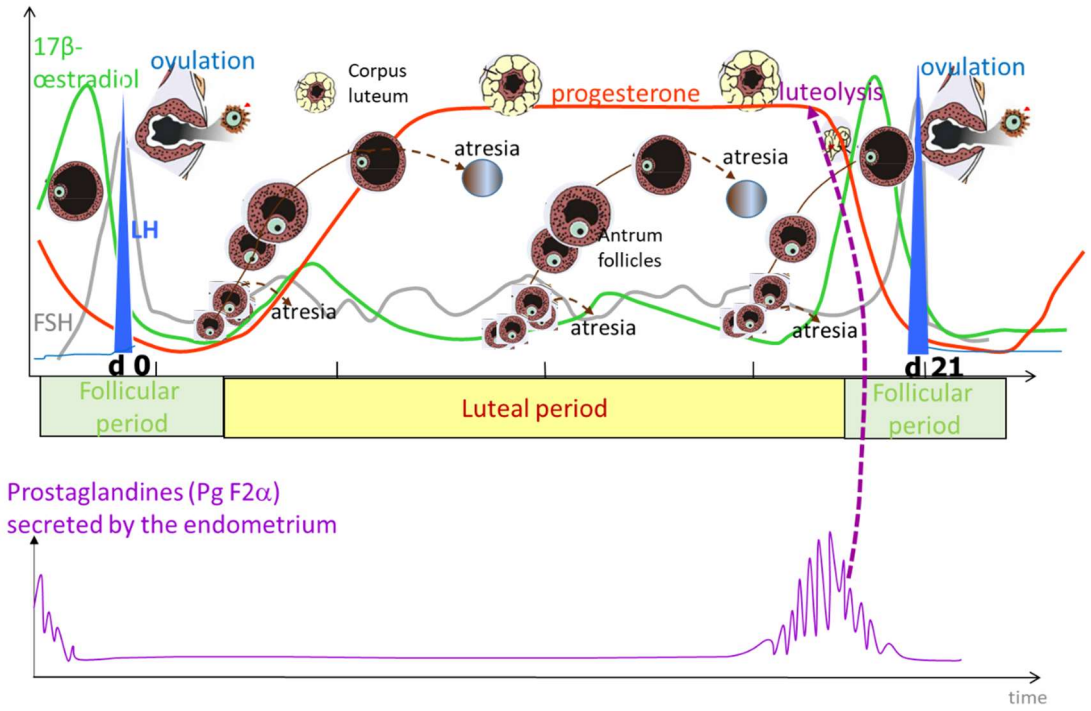

Figure 1. 3 Schematic representation of hormones and follicles dynamics during the oestrus cycle of a cow with the follicle-stimulating hormone (FSH; grey), the luteinizing hormone (LH; blue), the 17β-oestradiol (E2; green), the progesterone (P4; red and luteolysing prostaglandins (PGF2α; purple)

1. **The basic follicular growth**

During this phase a cohort of primordial follicles is recruited. Each of them contains an oocyte. Primordial follicles develop into primary and then into secondary follicles. During this phase follicles are not sensitive to gonadotrophins (follicle stimuling hormone, FSH and luteinizing hormone, LH) secreted by the pituitary.

2. **The follicular period**

In this phase a vascularised layer of endocrine cells (*theca interna*) appears around the secondary follicles. These theca cells make the follicle sensitive to the increase in plasmatic FSH concentration. During the follicular period only 2 or 3 follicles are selected from the cohort in response to the increase in FSH. Their granulosa develops, their *theca interna* starts

producing 17β-oestradiol (E2) and cavities filled with follicular fluid appear. The E2 production of the selected follicles applies a feedback on the pituitary gland, stimulating the production of LH. At the same time, FSH stimulates the secretion of inhibin by the granulosa which, together with E2, applies a feed-back on the hypothalamus which is inhibiting the secretion of FSH itself. While being exposed to FSH produced by the pituitary, one of the selected follicles acquires LH receptors and becomes dominant. The dominant follicle finishes its development under LH and growth factors control and the others selected follicles are resorbed (Figure 1. 3). The increased magnitude and frequency of LH pulses until the LH peak induce important changes in the follicle (growth and meiosis of the oocyte proceeds again) and the LH surge induces ovulation. The oocyte that was contained into the follicle is released near to the fallopian tube.
During an oestrus cycle, with the FSH dynamics, follicular waves leading to the emergence of a dominant follicle occur every 7 to 10 days.

3. The luteal period

Once an oocyte is successfully ovulated, the rest of the follicle forms a new structure, the *corpus luteum* that no longer produces E2 but progesterone (P4). P4 has antagonist effects of E2 and applies a feed-back on the hypothalamic-pituitary axis which causes LH and FSH drops. In consequence, no ovulation can occur as long as the *corpus luteum* is present and P4 level is high. If there is no conception after ovulation, the corpus luteum will be lysed (i.e. luteolysis induced by prostaglandins secreted by the endometrium), P4 levels will drop and a new cycle will start (Figure 1. 3).

If the oestrus cycle of cows lasts for approximately 21 days, a large variability exists. In reality, oestrus cycles of dairy cows were described to range from 19 to 26 days (Disenhaus et al., 2008). Such a variability has an impact on the management of reproduction and increases the probability that the farmer misses oestruses.

1.1.2.2 Oestrus: behavioural changes that announce the occurrence of an ovulation

At the end of the follicular phase (before ovulation), the dominant follicle synthesizes and secretes increasing quantities of E2. The concentration of E2 circulating in the systemic blood reaches a threshold which causes two closely linked events due to positive feedback on the brain:

1. a behavioural response named oestrus,
2. the surge of release of pituitary gonadotrophic hormones, especially LH, resulting in a peak of gonadotrophins that prompts the process of ovulation at a related time, commonly some 20-30 h later (Roelofs et al., 2010).

Oestrus is characterized by the acceptance by the female of the male for mating. In artificial inseminated bred herds there is no bull and a cow is considered to be in true oestrus when she is standing immobile when being mounted by another cow. However, standing to be mounted is not the only sexual behaviour that is observed during oestrus. During oestrus there is also an increase in the occurrence of other sexual behaviours: mounting, being mounting, flehmens, chin resting or sniffing/licking the vulva of other cows (Chanvallon et al., 2015; Van Vliet & Van Eerdenburg, 1996) (Figure 1. 4).

Figure 1. 4 Pictures extracted from (Chanvallon A. et al., 2015). Behaviours associated with the oestrus event for beef herds: A) Ano-genital sniffing B) chin resting and C) mounting and standing to be mounted.

Standing to be mounted is not a highly expressed behaviour. In beef cows, it is observed in 90 to 100 % of the oestruses but it represents 2 to 4 % of the total behaviours that are expressed during oestrus (Blanc et al., 2010; Chanvallon et al., 2015) (Table 1. 1). In dairy cows (Roelofs et al., 2005) observed standing to be mounted in only 58 % of the oestruses and when it was expressed it represented less than 3 % of the total sexual behaviours (Figure 1. 5).

	Oestrus period	Luteal period	P (Wilcoxon test)
Total number of sexual and social behaviours	812 ± 537	80 ± 44	<0.05
Proportion of social behaviours (%)	59 ± 11	92 ± 9	<0.05
Proportion of sexual behaviours (%)	41 ± 11	8 ± 9	
Proportion of flehmen + sniffing or licking of the vagina of another cow + resting with the chin on another cow (%)	30 ± 10	8 ± 9	<0.05
Proportion of mounting + being mounting + mounting the headside (%)	9 ± 5	0 ± 0	<0.05
Proportion of standing to be mounted (%)	2 ± 2	0 ± 0	<0.05

Table 1. 1 From (Blanc et al., 2010). Proportion of sexual and social behaviours observed during the oestrus and the luteal period in Charolaise cows (n=69 oestruses)

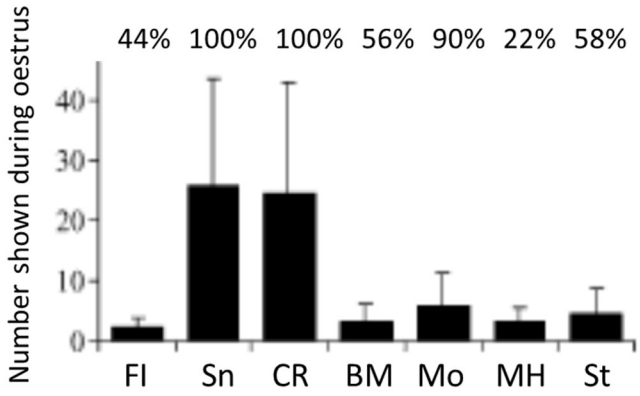

Figure 1. 5 From (Roelofs et al., 2005). Mean number of different signs shown during oestrus (mean ± sd)(Fl: flehmen, Sn: sniffing the vagina of another cow, CR: resting with the chin on another cow, BM: being mounted, Mo: mounting, MH: mounting the headside; St: standing heat). Above the bars, the percentage of oestrus periods in which the sign was displayed at least once is shown.

Besides the low expression of standing to be mounted, it was observed that the duration of oestrus measured by the interval between the first standing to be mounted to the last one has decreased over the past decades (Figure 1. 1). In dairy cows, the duration of oestrus has been halved, from 15 h to 4-8h, in forty years. In beef cows, (Blanc et al., 2010) reported durations ranged from 10 to 6 hours according to the breed.

Because standing to be mounted is rare and may not be expressed during some oestruses, it has been concluded that standing behaviour could not be the only evidence of oestrus in dairy and beef cows (Bedere, 2017) and that other signs have to be considered. Van Eerdenburg et al., (1996) proposed to rank the different oestrus behaviours and to give them a score according to their specificity. A cow is then considered in oestrus when the cumulative score reaches a threshold. Chanvallon et al. (2015) reported that when oestrus is defined as the period when secondary sexual behaviours (*flehmen + sniffing or licking the vagina of another cow + resting with the chin on another cow)* significantly increase, the duration of oestrus is 2 to 5 hours higher than the duration defined on standing to be mounted behaviours (Table 1. 2).

Breed	***Based on Standing to be mounted (h)***	***Based on the expression of secondary sexual behaviours (h)***
*Charolaise_1**	7.6 ± 4.6	12.4 ± 3.9
*Charolaise_2 **	9.9 ± 3.7	12.1 ± 4.1
Limousine	8.2 ± 6.3	11.1 ± 4.0
Blonde d'Aquitaine	6.2 ± 3.4	11.0 ± 2.4

*Table 1. 2 From (Chanvallon et al., 2015), translated from French. Duration of oestrus for beef herds (hours, mean ± standard deviation). The duration of the oestrus was defined by the time laps in between the first and the last standing to be mounted, or by the time laps between the increase and the significant decrease of the secondary sexual behaviours (flehmen + sniffing or licking the vagina of another cow + resting with the chin on another cow). * The two tests on the Charolaise breed were realized on two different herds and the results were analysed separately.*

With the view of detecting ovulations from oestrus detection several issues have to be pointed out. First, several studies have reported that some ovulations (8 to 15%) are not accompanied by behavioural changes. They are called “silent ovulations” (Chanvallon et al., 2015; Kerbrat & Disenhaus, 2004; Palmer et al., 2010; Ranasinghe et al., 2010). Second, behavioural traits are difficult to measure and to interpret. When a cow is mounting another one, it is not always obvious to know which of the two is in true oestrus. Likewise, when only secondary sexual behaviours (licking, sniffing, chin resting) are observed detection errors can occur leading to false detected ovulations (detections that occur during the luteal phase). Last, oestrus expression is characterised by a high variability, both in duration and in expression (type of behaviours expressed and frequency). Several endogenous and exogenous factors are known to have an effect on oestrus expression and to enhance this variability in oestrus expression (Blanc et al., 2010; Cutullic et al., 2009; Roelofs et al., 2005):

- Animal factors. Differences between breeds in oestrus expression have been reported both in dairy and beef cows (Blanc et al., 2010; Cutullic et al., 2009). In Holstein cows Roelofs et al. (2005) observed that oestrus was more intense in primiparous cows than in multiparous cows. Productive traits can also affect oestrus expression. Several works have demonstrated that high milk production is associated with poor oestrus behaviour Cutullic et al (2009), Lopez et al (2004) and other studies have pointed out that oestrus expression can be modulated by the nutritional status of cows (Cutullic et al., 2009; Blanc et al, 2010). At last, health issues like lameness have been associated with a reduction of oestrus intensity in dairy cows. This reduced oestrus expression may be caused by physical limitations of the lameness itself inducing a reduced frequency of mounting behaviours (J. Roelofs et al., 2010).
- Environmental factors : The expression of oestrus is influenced mainly by the number of cows in oestrus at the same time ((Blanc et al., 2010; Roelofs et al., 2010). When the herd is larger, the number of interactions between animals is greater and the possibility of forming sexually active groups is higher. Other environmental factors like housing conditions, presence of a bull (Roelofs et al., 2008), season (better expression in fall and winter) or time of the day have been shown to interfere with the intensity of oestrus. Barn housed cattle exhibit more mounts per hour during oestrus than cattle housed on pasture mainly because cows on pasture spend more time grazing than animals confined in barns (Roelofs et al., 2010). The substrate of the floor on which cattle are housed also affects oestrus behaviour. Mounting activity is less frequent on slippery surfaces or areas at grazing with steep slopes (Chanvallon et al., 2015). Vailes & Britt, (1990) showed that duration of oestrus and number of mounts were longer and greater on dirt than on concrete floors. As for the effect of timing in the day Kerbrat & Disenhaus (2004) reported that sexual behaviours were mostly expressed during the night (from 1 to 7 o’clock in the morning).

Causes of variability in oestrus expression are thus quite numerous and clearly make oestrus detection a critical step in the management of reproduction.

1.1.2.3 Other changes associated with oestrus period

As already mentioned behavioural changes observed during the oestrus period are due to hormonal changes preceding ovulation. They are thus associated with physiological changes and changes in activity patterns.

1. **Activity pattern.**

It has been observed that the physical activity of cows increases during the oestrus (Silper et al., 2015). Allrich, (1993) and co-workers equipped dairy cows with pedometers and measured that their activity pattern increased by a factor of four when they were in oestrus. Kiddy, (1977) and co-workers observed the same tendency for dairy cows in comfort stalls with an activity 2.75 times higher for cows in heat. Blanc et al (2010) reported in Charolaise, Limousine and Blonde d'Aquitaine that time spent standing was significantly higher during oestrus than during the luteal phase.

2. **Physiological traits.**

Changes in progesterone and/or oestradiol levels that occur at the end of the follicular period have a strong correlation with oestrus. Other physiological changes have been reported to change when cows were in oestrus and were analysed as potential markers of oestrus: reduction in body temperature, decline in milk yield or a decrease in vaginal mucus resistance (Firk et al., 2002; Saint-Dizier & Chastant-Maillard, 2012).

Overall, when they have to confirm that a cow is in heat and has to be inseminated, farmers pay attention to several oestrus signs and give them different levels of reliability. (Ponsart et al., 2010) reported that standing heat is the sign farmers consider to be the most reliable to validate an oestrus. They also give a high reliability to vaginal mucus discharges and to the expected occurrence of oestrus planned from the reproductive planning. Chin resting, bawling and nervousness appeared to be more taken into account by dairy farmers than by beef farmers (Table 1. 2).

Signs	***Mean score/10 Beef farmers (n=255)***	***Mean score/10 Dairy farmers (n=64)***
Standing to be mounted	9.3 ± 1.2	9.0 ± 1.4
Mounting	7.1 ± 2.4	6.7 ± 2.4
Chin resting	3.7 ± 2.5	4.6 ± 2.9
Bawling	4.2 ± 2.9	7.0 ± 2.3
Sniffing the vagina of another cow	5.9 ± 2.4	4.8 ± 2.4
Nervousness	5.2 ± 2.7	6.1 ± 2.3
Standing	3.5 ± 2.9	3.6 ± 2.6
Vaginal mucus	8.2 ± 2.0	7.7 ± 2.4
Expected time of oestrus from the reproductive planning	6.3 ± 3.3	6.5 ± 3.4

Table 1. 2 From (Ponsart et al., 2010)*, translated from French. Average (± sd) scores given by the breeders to judge the reliability of the heat signs in beef and dairy herds. (1= low reliability; 10= high reliability).*

Interestingly, another study conducted by Cutullic et al (2006), showed in dairy cows (Holstein and Normande) that conception rates differ according to the signs that are considered to confirm oestrus. The highest rate of successful AI (50%) is observed when the decision to inseminate a cow is made on the criterion of standing to be mounted (Figure 1. 6). This rate

drops to 36 % when insemination is made from mountings signs and decreases to only 28 % when insemination is made from slight signs (sniffing, licking, flehmen, chin resting).

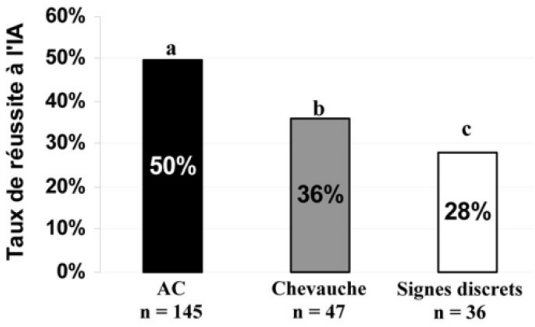

Figure 1. 6 From (Cutullic et al., 2009). Success rate of artificial insemination according to the detection "sign" mode, Normande and Prim' Holstein breeds combined (n=228). A) Overlap acceptance, B) Mounting, C) Secondary signs.

1.1.2.4. A reliable oestrus detection is necessary to define when to inseminate the cow

Behavioural changes that can be observed during oestrus are of great interest to predict the occurrence of an ovulation as they account for the underlying physiological status of the cow. When oestrus is expressed, it means that the oestrus cycle is at the end of the follicular period and that ovulation will occur. Several studies have measured the interval between the onset of the oestrus and the ovulation (Figure 1. 7). It appears that this interval is highly variable. On average, it ranges between 25 to 30 hours (except in Saumande & Humblot, 2005).

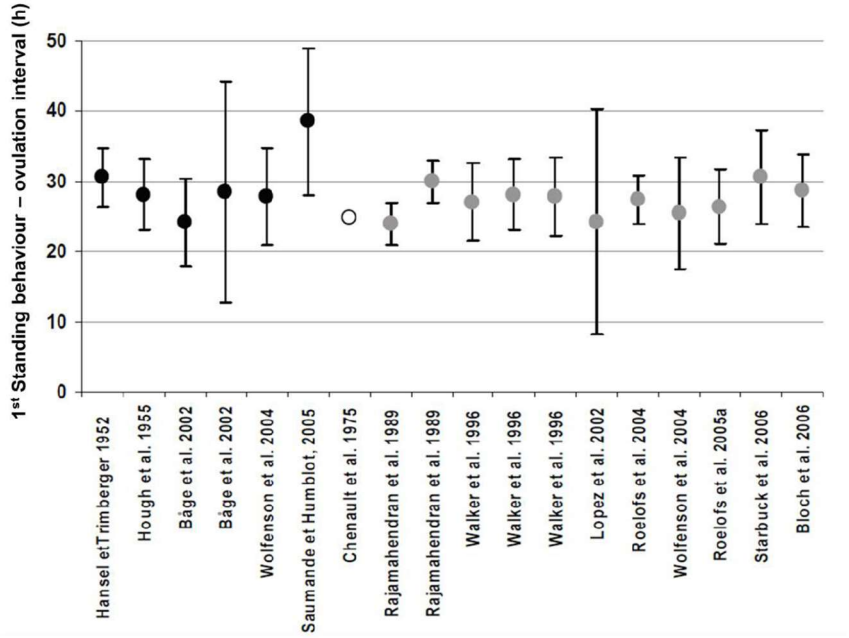

Figure 1. 7 (From Bedere, 2017, reprinted from Cutullic E., 2010). 1st standing to be mounted –ovulation interval (means and standard deviations) of 18 populations of heifers (black circles), cows (grey circles) or both (white circles) reported in 18 studies.

To go further, several authors studied the influence of the timing of artificial insemination relative to the timing of oestrus. Insemination time has been shown to influence fertilization rate and embryo quality. Dalton et al., (2001) tested three intervals between the onset of oestrus and insemination (0h, 12h and 24h). They observed that early insemination results in lower fertilization rates (AI 0h : 67%, AI 12h : 79%, AI 24h : 98%) but good embryo quality, whereas late insemination (24h after the onset of oestrus) reduced embryo quality but the fertilization rate was good. These results indicate that AI 12h after the onset of oestrus (1st standing heat) provides a good compromise between potential fertilization failure (AI 0h) and embryo failure (AI 24h). These results support the practical a.m-p.m rule used by farmers: cows first seen in standing to be mounted in the morning (a.m) would be inseminated in the afternoon (p.m) and those observed in standing heat in the evening would be inseminated the next morning. They also highlight the importance of performing oestrus detection of high quality (determining oestrus onset with precision) to determine the best time to inseminate. Such a challenge clearly explains why several devices have been developed to help the farmer detecting oestruses (see 1.1.3). Their interest is all the more important that standing heats are low expressed and that variability in oestrus expression is high.

Another strategy to predict time of ovulation and time to inseminate the cow is to rely on the hormonal changes that occur within the hours preceding ovulation.
LH has been considered as a relevant candidate to predict ovulation time as ovulation is triggered by the LH surge. Several studies have thus measured the interval between the LH peak and ovulation and have reported that LH peak occurs approximately 25h before ovulation (Roelofs, 2005). However, to be able to detect LH surge, blood samples have to be taken at short intervals (every 4 hours, Saumande & Humblot, 2005), which is not realistic in practice.

Surprisingly few works have studied the correlation between levels of oestradiol and timing of ovulation. Lopez et al. (2002) reported in primiparous Holstein cows that mean duration from the highest level of oestradiol measured in milk until onset of standing behaviour was 21 ± 3.7 h and until ovulation was 46.7 ± 5.3 h. The mean duration from onset of standing behaviour until ovulation was 26.4 ± 4.2 h. Saumande & Humblot (2005) found that the mean interval between the highest concentration of oestradiol and ovulation ranged from 22 to 34 h in Holstein heifers. (Roelofs, 2005) underlined that monitoring of oestrogen levels is unsuitable for the prediction of time of ovulation on the farm, because of the large variation between animals to time of ovulation and because currently measurements of oestrogens levels cannot be easily automated.

The last hormone candidate to predict time of ovulation is progesterone. Progesterone concentrations can be measured in milk and in blood. The possibility of using progesterone concentrations to detect the ovulation has been investigated by several studies (Friggens & Chagunda, 2005). (Roelofs, 2005) measured the progesterone concentrations in milk and plasma of Holstein cows throughout the oestrus cycle. In milk, progesterone concentration dropped from levels higher than 15 ng/ml at 97.7± 17.8 h before ovulation to levels around 2 ng/ml at 70.7±16.8 h before ovulation. Here again, (Roelofs, 2005) outlined the large variation in timing of decrease of progesterone concentrations relative to ovulation between animals (at best the range is about 2 days) and concluded that monitoring progesterone alone was not sufficient to predict ovulation. Such a variability in progesterone profiles has been explored by (Blavy et al., 2016) from a large data set (26 dairy herds) and progesterone profile features (slope, cycle length, cycle height) were included in a model to estimate the probability of insemination success in Holstein cows (Blavy et al., 2018).

From these data collected in the literature, it is easy to understand that prediction of the timing of the ovulation is not an easy task because of the high variability in changes of both physiological and behavioural traits that occur during oestrus. However as it was shown that insemination time influences fertilization rates, increasing the accuracy of ovulation detection is still of high interest. As single parameter approaches have revealed their limits, a significant improvement in ovulation detection may come from approaches that will combine several predictors.

Controlling the reproduction is a key issue for the profitability of the herd. However, in the previous paragraphs, we have seen that oestrus detection faces the same difficulties in suckling and dairy cows with an extreme variability in oestrus expression in between type of herds, breeds and even individuals. However, being able to predict impending ovulation and its timing is an essential parameter for the success of the AI. Many articles report the predominance of discrete signs with little specificity to oestrus, short oestrus durations and high variability in their expression. There is therefore a great risk of missing an oestrus or misinterpreting the signs. This observation demonstrates the interest in developing tools for the detection

of ovulation and not oestrus (Walsh et al., 2011a). Both dairy and suckling farms could benefit from this type of detection aid.

1.1.3 From oestrus to ovulation detection

Traditionally, oestrus detection was performed by visual observation for signs of mounting behaviour. If this detection method is still practiced in some farms, visual detection of the oestrus is less used nowadays due to several reasons:

- The increase of the herd size. 30% of American herds have more than 500 cows, (Lucy, 2001).
- The reduction of the available labour force per cow.
- The decrease in oestrous duration and intensity due to an over selection of the cows criteria, mostly for dairy cows, during the last decades (Cutullic et al., 2009).

These changes reduce the opportunities for visual observation, and lead to an oestrus detection often below 50 % (Van Eerdenburg, 2002; Roelofs, 2005).

1.1.3.1 Methods of oestrus detection based on behavioural and activity parameters

Over the past decades, breeders have shown a real interest in sensors for oestrus detection. According to Rutten (2014, 2018), the investment is considered a "price worth paying" to improve the economic health of the herd. The different oestrus detection methods and tools available in the market are presented in this section and summarized on Figure 1. 8. If no reference is provided, information comes from Allain and coworkers (2012).

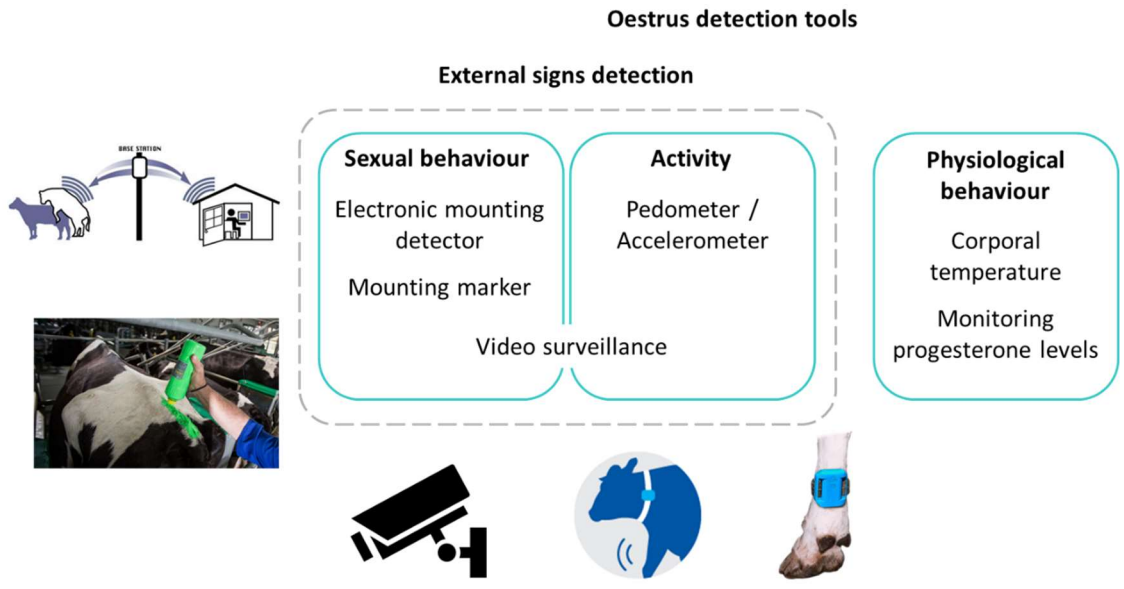

Figure 1. 8 Schematic summary of the main oestrus detection methods currently available on the market.

1. Visual oestrus detection

This is the traditional way to detect the oestrus. All the external signs of the oestrus are observed by the breeder, daily. Firk et al., (2002) reports that five observations of twenty to thirty minutes are necessary to detect the majority of the oestrus events. This method is extremely time consuming and cannot be applied for large herds.

2. Mounting acceptance detection

Standing to be mounted is the most specific sign of oestrus but as shown previously it is rarely expressed. Firk et al. (2002) report that if we only consider standing to be mounted only 20 % of the oestruses can be detected visually with two to three observation sessions of 30 minutes per day. Three types of tools have been developed to record being mountings.

- Electronic. A patch containing the sensor is glued on the cow rump as presented in Figure 1. 9.A. The pressure of the mounting cow will trigger the sensor and after two seconds of detected pressure an alert will be transmitted to the breeder by a software. The tool reliability is variable with a heat detection rate of 69 to 92 %. The reliability of alerts is around 96 to 100 % (so a maximum of 4% of false positive alarm) which makes it potentially an interesting product. Additional study carried out by At-Taras & Spahr, (2001) validates this detection rate with 86.8 and 71.1% of detected oestrus in two different trials using electronic sensors. The investment is about 6.5k€ for fifty cows. The limit of this device could be its sensitivity when the herd is in barns where cows do not necessarily have the possibility to escape a mounting because of lack of space. The two seconds required to validate standing to be mounted could also be the source of loss of sensitivity in relation with the advertised value (Saint-Dizier & Chastant-Maillard, 2012a). Furthermore, Firk et al. (2002) reported that chin rubbing of other cows on the rump often result in error messages.
- Mechanical. A patch containing an encapsulated coloured liquid is glued on the cow rump as presented on Figure 1. 9.B. The pressure of a mounting cow will pierce the capsule and the liquid will spread to the rest of the patch, an indicator that will be perceived by the breeder. The heat detection rate is reported to be around 71 to 86% according to At-Taras & Spahr, (2001). This device can be found around 2€ a piece on catalogues. It can be used only one time and needs to be changed when the capsule is burst. It is thus more time consuming than the electronic version. The breeder has to verify each cow several times per day and substitute burst detectors with new ones. If this can be manageable for small to medium herd size, this cannot be used for large herd or beef herds during the grazing period.
- Marker. Some paint is applied on the cow rump. By friction, the mounting cow will remove part of the paint. On Figure 1. 9.C the left cow has an intact paint strip whereas the right one had its paint strip removed. A regular observation from the breeder leads to detect in heat cows. The cost is low: under 20€ to mark thirty to forty cows but its low cost is offset by its controversial effectiveness. Boyd (1984) detected mainly false-detected oestrus as the cows rubbed the paint off their rump herself. Additionally, it seems that the paint was not always removed when the cow was mounted. On these points, it is possible that the quality and characteristics of the paint have evolved since 1984. A more recent study by Xu et al., (1998) reports that the combination of paint and visual observations led to a detection rate of 98.4 % with only 2.4 % of false positive detections. However, this type of tool still needs a lot of implication from the breeder when one of the objective of using an oestrus detection tool is to reduce the workload of the breeder in addition to herd costs. As

often with the detection tools, this option cannot be used for the suckling cows when they are at pasture.

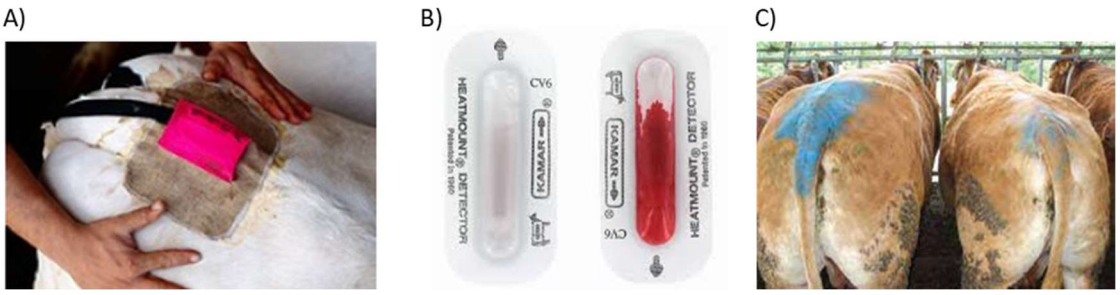

Figure 1. 9 The three types of overlap detection. A) Electronic detector, B) Mechanical detector before/after the mounting and C) Paint stripe before/after mounting.

3. Video surveillance

When the cows are in a barn, the building can be filled with cameras. According to (Firk et al., 2002; Roelofs et al., 2010), viewing the recordings three times thirty minutes per day is enough to have an oestrus detection rate in the 74 to 90 % range. The investment is quite significant with a budget of 3.5 to 5 k€ for two to three cameras. This kind of tool can be very effective as all the signs (mounting acceptance and secondary signs) are visible and even other data such as injuries can be recorded and detected by the breeder. Nevertheless, this solution still asks for a considerable amount of time from the breeder to watch all the footages as no effective software to automatize the detection is on the market yet (Alawneh et al., 2006). This type of tool is also mostly used for dairy herds and maybe for suckling herds when in barns during the winter.

4. Pedometer / accelerometer

Mostly used in dairy herds, the activity monitoring can be done using three types of tools:

- A pedometer fixed to a cow leg recording the number of steps per time unit.
- An accelerometer fixed around the neck and recording movement in the three axial directions.
- An accelerometer fixed to the leg to record the steps but also the lying / standing behaviours switches (Saint-Dizier & Chastant-Maillard, 2012a).

The data recorded by the device are transmitted to a software by radiotelemetry. The activity of each animal is analysed and compares it to previous reference period. The reliability of this type of detection tool is highly variable with a heat detection rate of 63 to 90 % for the pedometers and of 59 to 83 % for the accelerometers. The false positive alerts are respectively in the 6 to 29 % range for the pedometer and in the 6 to 20 % range for the accelerometer.
The initial investment can be considered as moderate as it stays within the 4.5 to 8 k€ to equip fifty cows.
The limits of this type of equipment are:

- Difficulty to interpret the data when going from barns to pasture
- Necessity to manipulate the cows individually to install and remove the sensor.
- Do not give the optimal insemination window (see section 1.1.2.1)
- The device cannot operate as wanted if the cow has a lameness or other issue that limits its movement.

In suckling herds, an additional issue is that, at pasture, cows may cover different distances from one day to another according to the availability of forages resources, weather, temperature etc. In these conditions' detection by comparison with the previous data (hours or day) can be biased.

1.1.3.3 Methods of ovulation detection based on physiological parameters

In addition to sensors developed to detect external signs of heat, sensors to monitor physiological parameters have entered the market more recently. This new option may help to detect oestrus in all cows, including those that do not express specific behaviour during this period of their oestrus cycle.

1. Corporal temperature

Fisher et al (2008) tried a new approach of ovulation detection based on the monitoring of body temperature. They succeed to correlate variations in body temperature with the time of the LH peak: a decrease in temperature two days before the LH peak was measured followed by an increase of 0.48°C within the 4 h period of the LH surge. A recent product named Anemon was recently launched and combines a vaginal thermometer with a transmitter / accelerometer collar (Kohler et al., 2010). An alarm is sent to the breeder's phone when an increase of activity is associated to a decrease followed by an increase in temperature. The system was finalized in 2010 but only data providing from the product developer were found. Claims for the Anemon system developer (Brielmann, 2014) are a heat detection of 87,5 % but no other study was found to challenge these results.

2. Progesterone levels

Claus et al., (1983) measured progesterone in milk fat. Results showed that 32 % of the oestruses detected from P4 data were not recognised by the farmer. From this observation, several products have been developed and put on the market. Actually, two devices are marketed:

- eProCheck ® by Minitüb (Figure 1. 10.A). This tool allows the concentration of P4 to be measured in the milk or plasma of the cow. The sample is hand-collected and prepared by the user and then analysed by a portable analyser. Interpretation of the results is left to the user, who must be trained personnel (veterinarians or inseminators). Cost of the equipment and performances were not found.
- Herd Navigator ® by a Foss and Delaval collaboration (Figure 1. 10.B). This device is associated with a milking robot and is therefore exclusively reserved for dairy cows. During milking, the device takes a milk sample and analyses its P4 concentration. The Herd navigator monitors each cow individually and can warn the farmer when ovulation is imminent (drop in P4 concentrations). With this device, the farmer can manage the cycle of his cows on his own with the possibility of adapting the periods and frequency of dosage while proposing the analysis of other biomarkers. The heat detection rate is particularly high, within a 93 to 99 % range. The investment however is around 40 to 50 k€ (+55€ /cow/year) and makes the system unaffordable for many French farms where the number of cows remains below 100.

Figure 1. 10 A) eProCheck ® by Minitüb system and B) Herd Navigator ® by a Foss and Delaval system operating principle

Overall, the tools to help predict oestrus and ovulation are now playing an important role in bovine reproductive control. Tools based on detection of external signs give a wide range of results with very few options that are suitable for both suckling and dairy herds, and that require minimal maintenance time from the breeder. Techniques based on monitoring physiological parameters are very promising as they allow a more successful and accurate assessment of the ovulation event, even in cows that do not express any external specific signs of heat. Monitoring the hormones involved in the oestrus cycle seems to be an interesting path to explore with two products already on the market. Based on the literature, the sensor developed for the SmartRepro project should use this detection strategy. Real time monitoring of hormones implies the need for two main components in our system: a way to access a cow fluid (milk, blood or interstitial fluid) where the hormones are located and a biosensor to dose in real time these hormones through the oestrus cycle to detect the approach of the ovulation event.

1.2 Detection of physiological parameters in living organisms

The ovulation detection patch proposed in SmartRepro implies to transfer a biological fluid into contact with a biodetection system for real time analysis. More concretely, two technological building blocks have to be developed:

- A biosensor to measure the hormones contained in the interstitial fluid.
- A system to transfer the interstitial fluid from the cow's dermis to the sensor.

In recent years, sensors have become the object of a real interest for farmers, but it can represent a significant investment that is sometimes difficult to justify. If ovulation detection sensors are very popular as they have a direct economic impact on the farmer rent (Rutten et al., 2014, 2018), welfare sensors are not yet sufficiently attractive because of an uncertain return on investment.

The sensors used by the breeder presented in Figure 1. 11, can be organized in three categories:

- The at cow sensors. Represented in red zone of Figure 1. 11, they include accelerometers, temperature and heart rate monitoring or pH analysis. They can be worn, swallowed or inserted into the cow digestive system.
- The near cow sensor. Represented in the blue zone of Figure 1. 11, they include video and sound analysis, climate analysis, feed analysis or GPS.
- The from cow sensor. In green on Figure 1. 11, they monitor products coming from the cow (milk, hair, saliva, sweat, nasal secretion, breath, faeces, etc.).

Figure 1. 11 Extracted from (Knight, 2020a). Overview of sensor technologies associated with dairy animals (can be extended to suckling breeds). The red zone and individual red dots show 'At Cow' sensors, the blue zone shows 'Near Cow' sensors and the green zone shows 'From Cow' sensors.

If it is recognised that biosensors are valuable to the livestock industry in several domains (infection and disease detection, reproduction, nutrition…) (Chastant-Maillard & Saint-Dizier, 2016), only few of them have access the market despite a regular research on it. The only ovulation detection sensor that is available on the market is the HerdNavigator ®, introduced in 2008, which is a "from cow sensor" and doses the progesterone in the milk from sampling during the milking sessions. So, it is not a wearable device. There is no mention of a ready for the market wearable biosensing device in the literature for the ovulation detection. This situation is partly due to the difficulty to measure hormones (small molecules and small concentrations), to have cheap and reliable production methods for the biosensors, to issues

to integrate the sensor in a bigger system as well as stabilization and storage issues(Velasco-Garcia & Mottram, 2001).

Despite these difficulties the market seems to be favourable for ovulation detection sensors with possible application both in suckling and dairy cows but also in small dairy ruminants where AI is also commonly used. The patch developed by SmartRepro should be interesting for breeders and competitive with the products already available. It is essential that the sensor developed in the project exhibits performances at least equal to the solutions already on the market (oestrus detection devices), is affordable and easy to use. The first two points are directly related to the type of developed biosensor.

1.2.1 Biosensors

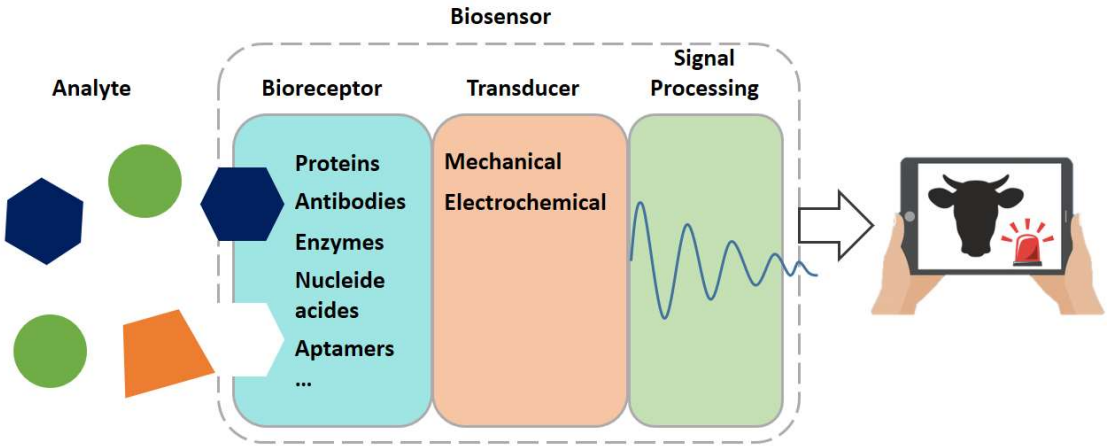

Figure 1. 12 Schematic of a biosensor technological parts

A biosensor is a device using specific biochemical reactions mediated by isolated enzymes, immunosystems, tissues, organelles or whole cells to detect chemical compounds usually by electrical, thermal or optical signals (Gold, 2019). It is basically composed of the four components presented in Figure 1. 12.

1. **The analyte.** The biosensor is brought into contact with a fluid (liquid or gas) that contains the element to be detected.
2. **The bioreceptor layer.** This layer, in contact with the analyte will bind specifically to the targeted molecule. Different kinds of bioreceptors were developed and used through the years as presented in Figure 1. 12.
3. **The transducer element.** This layer converts the biorecognition event into a measurable signal (optical or electrical mostly).
4. **The signal processing module** to amplify, analyse and prepare the signal for display.

The conception of biosensors was first described by Clark an Lyons in 1962 with the “enzyme electrode” (Clark & Lyons, 1962). This first biosensor was dedicated to the glucose detection in blood. The glucose presents in the blood paired with an enzyme and O_2. This reaction oxidizes the glucose into gluconic acid and hydrogen peroxide. The oxygen electrode developed few years prior to this experiment by Clark then monitor the O_2 concentration

present in the analyte. The concentration of glucose present in the blood sample is deduced from the decrease of O_2 concentration.

Since this first application, the development of biosensors for a still increasing number of applications can be witnessed all around the world. Point of care monitoring of treatment and disease progression, environmental monitoring, food control and biomedical research are a few of these application fields (Mehrotra, 2016).

If the applications and used technologies can differ, the performance of each biosensor can be evaluated on these following points (Morales-Narváez et al., 2016):

1. The selectivity. The bioreceptor can bind to the target with more or less specificity. A high selectivity means that in theory the bioreceptor will only bind to the target while totally ignoring the rest of the molecules in the analyte. In practice, the association of the bioreceptor with the transducer layer can impact the selectivity of the probe.
2. The sensitivity. The sensitivity is the amplitude of the transduced signal upon the variation of the analyte concentration. This characteristic can be linked to the limit of detection (LOD), the minimal concentration of the target that can be detected.
3. The reproducibility of the results.
4. The reusability of the biosensor. If the sensor is to be used several times, it must be able to deliver the same response quality from one use to the next.
5. The reversibility of the biosensor. The ability of the bioreceptor to release the target naturally or under external stimuli. This characteristic particularly important for real time monitoring biosensors.

Other criteria can be used as the fast response time, the biocompatibility, the portability or the price according to the application.

The use of biosensors in numerous fields of application has many advantages compared to traditional analytical techniques. Miniaturization of the size of the sensor to micro or nano scale has improve the signal to noise ratio (Bhalla et al., 2016) and allow to use smaller sample volumes implying a reduction of the assay costs. Increasing the surface to volume ratio of the sensing layer has led to the creation of probes of size similar to the targets. Such a step forward leads to the reduction of the non-specific binding and increase binding performance towards the target molecule (Fowler et al., 2008).

As indicated at the beginning of the section, several types of probes can be functionalized on the transducer surface to detect the reaction or recognition of interest. For the SmartRepro project, the types of probe we are interested in are those capable of molecular recognition.
Two types of probes can be used for molecular detection. First antibodies, which are the most popular probes for molecular detection. These proteins also known as immunoglobulins, are a large family of glycoproteins capable of recognizing antigens with high specificity with their binding domains located on the parathope of their “Y” shape. Another type of probe, aptamers or small oligonucleotides single strands, can also be used for molecular detection. This second type of probe will be discussed later in this chapter.

1.2.1.1 Immunosensors

Biosensors using antigens as a probe are called immunosensors. The detection event is due to interactions between antibodies and antigens on the transducer surface.

Before going any further, there is a delicate distinction between immunosensors and immunoassays. For the immunosensor, the formation of the antibody/antigen complex happens on the same platform as the recognition process. For the immunoassay, the diagnosis following the formation of the immunocomplex takes place elsewhere.
The difference between the immunosensor and immunoassay is presented on Figure 1. 13.

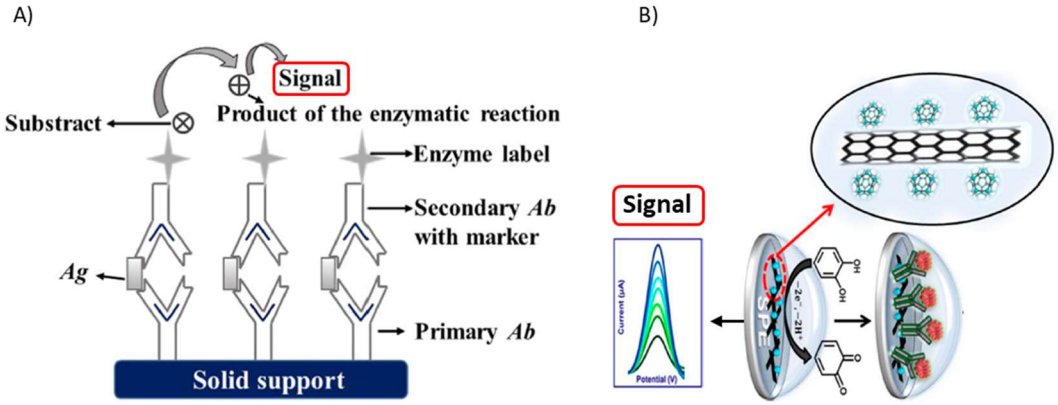

Figure 1. 13 A) From (Felix & Angnes, 2018). Schematic representation of an immunoassay detection steps for sandwich-type ELISA (enzyme-linked immunosorbent assay). Ag = antigen and Ab = antibody. The detection signal happens away from the detection platform. B) Adapted from (Mollarasouli et al., 2019). Schematic representation of Fullerene (Carbon allotrope)-Functionalized Carbon Nanotubes/Ionic Liquid based for tumour detection. The signal is emitted from the same platform where the recognition event happens.

The antigen-antibody bind is often characterized with high selectivity and high affinity. For the immunosensor to detect the recognition event, a transducer layer is needed. The next section presents an overview of the possibilities for the transducing layer.

1.2.1.2 Immunosensor detection strategies

Immunosensors detection strategies are using label free techniques in contrast with the labelling techniques. The use of the labelling techniques is mainly reserved for the immunoassays in which a marker binds to the target and leads to a discrete measure at the end of the reaction. Mainly, this technique is used to increase the sensitivity of the detection through enzymatic amplification and photon counting. The most common method is the use of fluorescent probes (example). This technique, although inexpensive, is generally limited by its sensitivity to environmental conditions (pH and temperature which impact probe quenching). Furthermore, the labelling techniques require a significant investment of time on the part of the user (preparation, analysis of the assay) and cannot be adapted for integration into a wearable device or for a stand-alone real-time monitoring application.

The bovine ovulation detection tool developed by SmartRepro cannot use such techniques for these reasons. Therefore, in the rest of this chapter, we will orientate our bibliographic work on the so-called "label free" techniques.

Label free immunosensors can be classified based on their transduction mode:

1. **Optical and photonic**

On the same model than the ELISA test presented in Figure 1. 13, the binding of the target to the probe can realise or activate photoreactive products. Coloration of the reaction environment or fluorescence observation under microscope can indicate if the target molecule was detected. With this type of assay, the intensity of the signal can be proportional to the concentration of the target to a certain extent. Nonetheless, this could not be used in this thesis as it cannot deliver real time monitoring.

A photonic detection option is surface plasmon reasonnance (SPR). The sensitivity of the SPR can reach the nanomolar range and the detection method is simple, and the assay is inexpensive. The operating principle of the SPR is presented on Figure 1. 14.

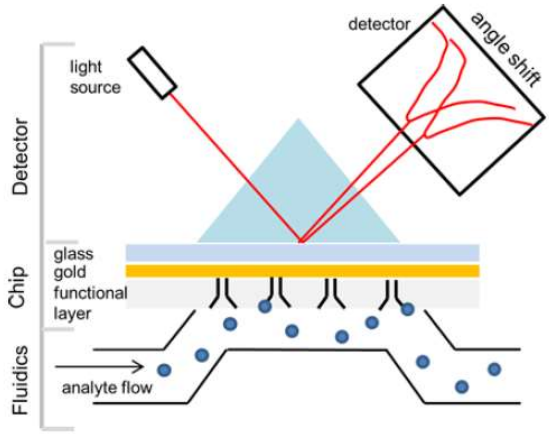

Figure 1. 14 Operating principle of a SPR biosensor (Damborský et al., 2016).

In this system, a thin metal layer (often gold) is applied on a prism. The probe is immobilized on this metallic layer. When the target molecule bind to the probe, it creates a local increase of the refractive index at the metal surface. The variation of the refractive index induces a shift of the resonance angle, proportional to the density of analyte detected. The sensor can then be operated by monitoring the resonant incident angle shift (Homola, 2003). This technique allows real time measurement. However, it remains an expensive laboratory system that cannot be integrated into a wearable device.

Other optical detection, label free biosensors exist (optical ring resonators (Iqbal et al., 2010), wave guides (D. Sun et al., 2014), wave-guide (Yih et al., 2006) or photonic crystals (Shafiee et al., 2014)) but they all face the same problem when it comes to miniaturisation, complexity and cost of the set up. If very good results can be obtained with these techniques, they are not adapted to the project of the thesis.

2. **Micrograviметry**

Another renowned tool for use in biosensors is the quartz crystal microbalance (QCM). This biodetection system, whose operating principle is presented in Figure 1. 15, is based on the use of the piezoelectric effect. The probe is anchored to a gold layer, on a QCM. An alternative electric field is applied to the QCM inducing constraints in the quartz lattice (expansion and

contraction). The resulting resonance frequency of the QCM is related to its thickness or mass and it will change according to the probe / target binding event. The QCM is sensitive in the nanogram range. This technique was used for different applications like the detection of disease biomolecules (Pesquero et al., 2017; Zhou et al., 2002). Nonetheless, like the SPR, it is a laboratory instrument, costly and cannot be integrated into a wearable device.

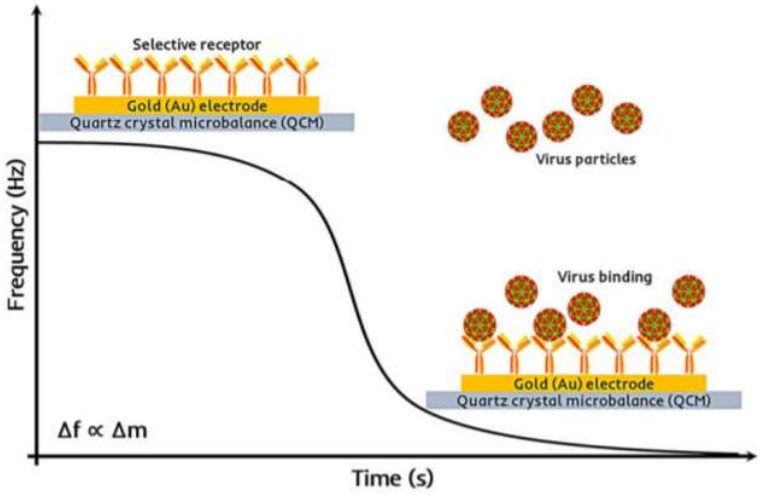

Figure 1. 15 Operating principle of a QCM biosensor (Afzal et al., 2017).

If the QCM cannot be miniaturised for further integration in a wearable device, other types of biosensors based on the same measurement method are available like SAW (surface acoustic wave) or BOW (bulk acoustic wave). Surface acoustic wave sensors rely on the fact that mechanical vibrations propagate under piezoelectric solid surfaces when surface or bulk acoustic waves Changes in the velocity of the SAW can be correlated to changes in surface temperature, viscosity and mass loading. If this type of biosensors is highly sensitive in aqueous environment, the biosensor loss in performances in complex medium like blood.

3. Electrochemical

The previous detection methods use variations in the reflective index or mass induced by biological recognition and then convert this signal into an electrical signal. A first advantage of electrochemical detection techniques is that biological detection directly induces an electrical signal. In addition, sensors using this type of detection technique are generally inexpensive, space-saving and easily integrated into portable devices.

The biosensor introduced by Clark and Lyons uses the most widespread electrochemical detection technique: amperometry. The concept is based on the measurement of the current induced by electrochemical oxidation or reduction of electroactive species at the surface of the Clark electrode. This electrode, also called the “working” electrode, has a constant potential with respect to a reference electrode. This technique being the most common electrochemical detection technique, is included in this section. However, amperometric technique uses secondary enzymes or aptamer labels since antibodies and most proteins do not present redox catalytic sites electrochemically active in the potential range of measurement (Vestergaard et al., 2007).

Electrochemical Impedance spectroscopy (EIS) is also a widespread electrochemical technique. This technique is well suited for a label-free biosensing application with a low LOD in the range of 0.01–100 ng.mL^{-1} (Luo & Davis, 2013). The LOD of impedimetric biosensors is recognized to be lower than for the amperometric sensors by three orders of magnitude according to (Bahadır & Sezgintürk, 2016). The concept of this technique relies on the use of a small amplitude alternating current (AC) to study the impedance characteristics of the cell. Both the amplitude modulation and the phase shift between the AC voltage and the current output. With this technique, the surface property of the biosensing part that are exclusively due to the analyte binding at the biosensor surface. However, even with higher sensitivity than most amperometric biosensors, the fact is that this technique can hardly be miniaturized, and this greatly limits its potential applications in ovulation sensor development.

Finally, a third type of electrochemical detection method was developed.
First reported in the literature by Bergveld (1970), the advent and widespread use of BioFETs (Biosensor Field Effect Transistors) owes much to the rise of microelectronic techniques. The first version of the BioFET sensor, called an ISFET (Ion Sensitive Field Effect Transistor) combines the principles of a MOSFET Metal Oxyde Field Effect Transistor), widely used in electronics and an external electrode (see Figure 1. 16.B).

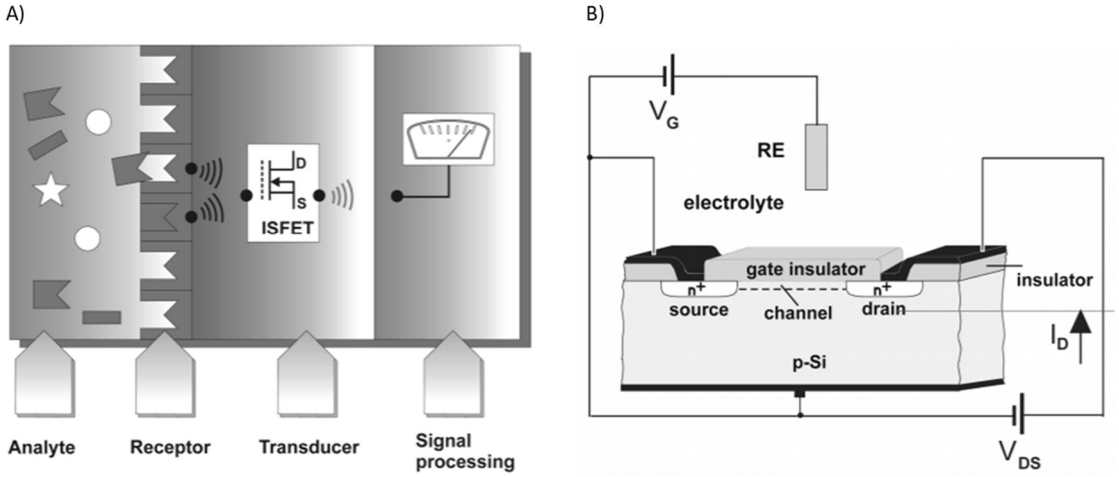

Figure 1. 16 From (Schöning & Poghossian, 2006). A) Schematic of a Biosensor based on the ISFET technology. B) Schematic functioning of the ISFET.

The transistor is made of a p-doped silicon (Si) substrate with two n-doped regions: the source and the drain electrodes. The two electrodes are connected by a channel made of a dielectric material (typically silicon dioxide, SiO_2). When used for biological detection, the transistor and the reference electrode (RE on Figure 1. 16.B) are immersed into a solution. A positive potential is applied between the RE and the Si bulk which creates a depletion region in the channel, electrically linking the two electrodes (source and drain). When a difference of potential is applied between these two electrodes, electrons will flow from the one electrode to the other. The presence of charged molecules at the surface of the dielectric will alter the electric field, shifting the potential experienced by the transistor channel and leading to a modulation of the output current. The overall structure is highly sensitive and the ISFET has

been adapted to many applications since for the detection of enzyme, DNA or different ions (Fritz et al., 2002; Gumbrecht et al., 1990; Souteyrand et al., 1997).

The immunosensing combines the advantages of good sensitivity and high selectivity. Some of the detection methods as the BioFET can be miniaturized to be integrated into stand-alone real-time monitoring devices. Yet, if the production of antibodies is nowadays well mastered by the industry, their production remains complex and necessitate the use of living organisms from the animal to the plants. This type of probe is also oversized for the detection of smaller molecules like hormones which are about a third of the antibody size (10 – 15 nm) and lack of stability. Around the world, many studies report the development and use of new type of probes, not necessary belonging to the antigen / antibody category.

1.2.1.3 Aptamers, a new type of probe

Aptamers are oligonucleotides (RNA or DNA single strands) or peptides molecules capable to bind specifically to a wide range of analytes with a nanomolar affinity. Aptamers can be select using the SELEX method (systematic evolution of ligands by exponential enrichment), introduced by Ellington and Tuerk in the nineties (Ellington & Szostak, 1990; Tuerk & Gold, 1990a). The concept of this method is presented Figure 1. 17. The targeted molecule is put in contact with a DNA/RNA library and goes through several selection rounds until high degree of selectivity and affinity binding is obtained (Gold L., 1995). When an aptamer is selected, its sequence is amplified using the classic PCR (Polymerase Chain Reaction) method. Once the aptamer sequence known, it can be artificially produced for further batches. This process is cheaper and simpler than the production of antibodies and does not require the use of living organisms.

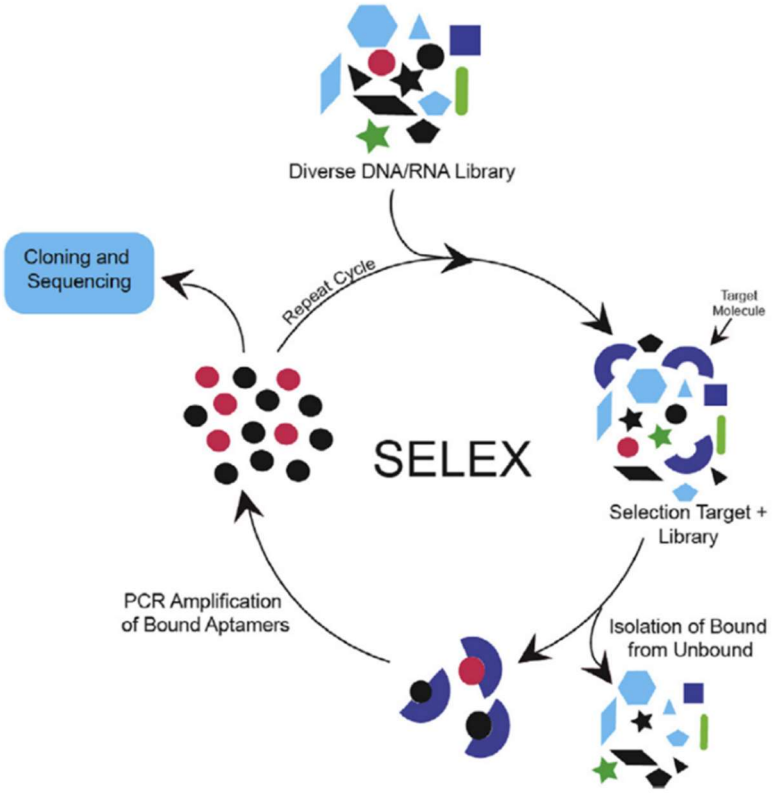

Figure 1. 17 From (Wu & Kwon, 2016). Schematic of the SELEX in vitro selection of aptamers.

The variety of the potential targets is vast, including peptides (Baines & Colas, 2006), toxins (Bazin et al., 2017), viruses, bacteria, proteins or hormones. An interesting property for this thesis real time monitoring project is the stability of the aptamers across a broad range of physiological environments (Cao-An Vu & Wen-Yih Chen, 2020). However, the second structure of aptamers can be reversibly denaturated with temperature unlike antibodies. This typical feature allows the regeneration of the biosensor aptamer probes after target binding (Pereira et al., 2018).

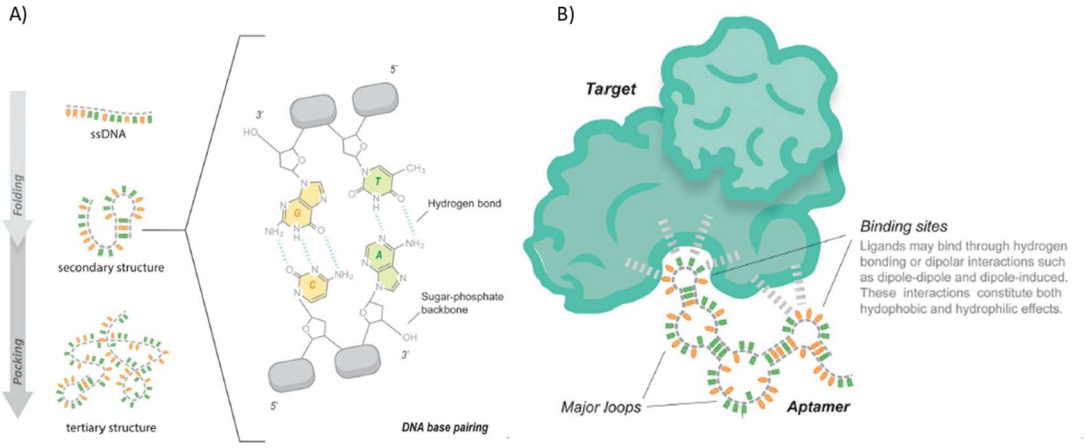

Figure 1. 18 Adapted from (Pereira et al., 2018). Aptamer structure, from its production to its interaction and bonding with the target. A) The ssDNA fold into secondary and tertiary structure. B) The bases not involved in the 3D configuration of the aptamer create loops that can interact with the target (binding sites) through hydrogen bond or dipolar interactions.

1.2.1.4 From immunosensors to aptasensors

Aptasensors are biosensors using aptamers as a recognition element. This type of sensor is more recent than the classical immunosensor and is still subject to numerous explorations and optimisations. Piro et al (2016) reports that aptasensors have a LOD about three orders of magnitude higher than immunosensors due to the highest affinities of antibodies. Cao-An Vu and co-workers (2020) acknowledge that at the beginning of the aptamers development, aptamer sequences and their binding targets was relatively weak, with most of the dissociation constant (K_D) value ranging from the hundreds of nanomolar to milimolar range. Lowering this K_D value was therefore the first challenge to optimize this new type of probe. Numerous teams around the world consumed much time and effort in this direction.

As a first step, this affinity of the aptamers with their target molecule can be significantly reduced by reworking the sequence of the aptamer. Hilder and Hodgkiss (2017) evaluated the affinity of several aptamers designed to bind to the hormone oestradiol, a target hormone in this project. Depending on the sequence: presence of loops (Figure 1. 18.B), their size and structure or the aptamer length, different affinity values were obtained. For example, the 76 bases long aptamer developed by Kim and co-workers (2007) and the 22 bases long version developed by Svobodová (2017) has respectively a dissociation constant (K_D) of 130 and 98 nM.

Another path to improve the LOD value was explored with the optimisation of the transducer part of the aptasensor. Detecting E2 is the subject of numerous articles for both immunosensing and aptasensing methods.

On the immunosensing side, reported LOD values ranged between 0.1nM (K_D estimated around 10^{-7}M) (Kuramitz et al., 2003) to 0.1pM using EIS technique (K_D estimated at 5pM) (X. Liu et al., 2012). If the first E2 detection using aptamers gave LOD value around 0.1 nM in 2010 (Olowu et al., 2010), progresses were quickly made and in 2014 and Ke et al (2014) obtained a LOD of 5 fM using EIS technique.

Among the various biosensors, one in particular has benefited from the advent of aptamers: the BioFETs. Since their first use, antibodies were the most widely applied recognition factor (Cao-An Vu & Wen-Yih Chen, 2020). However, one of the BioFET limitation is the Debye length.

When the BioFET is used in liquid conditions, ions from the solution will accumulate at the electrode surface to maintain the electroneutrality of the system.

The behaviour of the charges at the electrode/electrolyte interface has long been studied. From the double layer model proposed by Helmotz in 1986, through the introduction of the diffuse layer by Gouy and Chapman (1910 and 1913 respectively) to the combination of these two models by Stern (1924) (Bard & Faulkner, 2001), a stable model of charge interactions at the interface can now be proposed (Figure 1. 19).

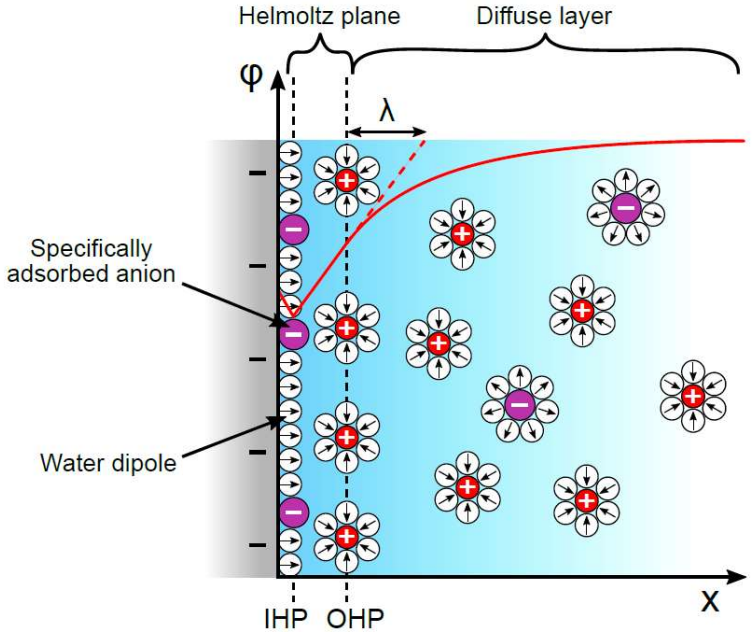

Figure 1. 19 From (Hugo, 2020). Schematic of the double-layer structure in the case of a negatively charged surface. The potential drops across the double-layer is depicted in red, and the Debye length indicated (λ). IHP=Inner Helmotz Plane; OHP = Outer Helmotz Plane.

In this model, the Debye length is the scale over which charged molecules screen out electric fields. In other words, it is the maximum distance at which a molecule can be detected by the sensor. The Debye length is typically of a few nanometers and the aptamers with a more compact structure than the antigens are more likely to detect the target under the Debye length where electrical signal is detectable (Cao-An Vu & Wen-Yih Chen, 2020).

While the antigen/antibody detection system is widely used for several applications, the size of these probes is less suitable for detecting small molecules (e.g. toxins, hormones). To meet this need, new types of probes have emerged over the last twenty years, which avoid the use of living organisms during their manufacture. These aptamers, which are highly selective have been developed for several years and are now used for

detection purpose in many fields. This recognition technique can be coupled in an interesting way to BioFETs. These biosensors have a high sensitivity and selectivity but are limited by a low Debye distance. Due to their compact nature, aptamers allow the detection of the target under this Debye limit unlike antigens.

1.2.1.5 Graphene – based SGFET. An emerging technology with great potential for the health field

As introduced previously, BioFETs sensors associated with aptamers for the detection of small molecules has a great potential for the biosensor's applications. Amid the various types of BioFETs, the Gr-SGFET (Graphene based, solution-gated field effect transistor) is a transistor device with a graphene channel.

Graphene and its derivatives have attractive properties for biosensing like their heterogeneous chemical and electronic structure, their renowned capabilities for direct binding to biomolecules, the possibility to be processed in aqueous conditions and the ability to be tuned as an insulator (Morales-Narváez et al., 2016). Graphene exists under different forms presented in Figure 1. 20.

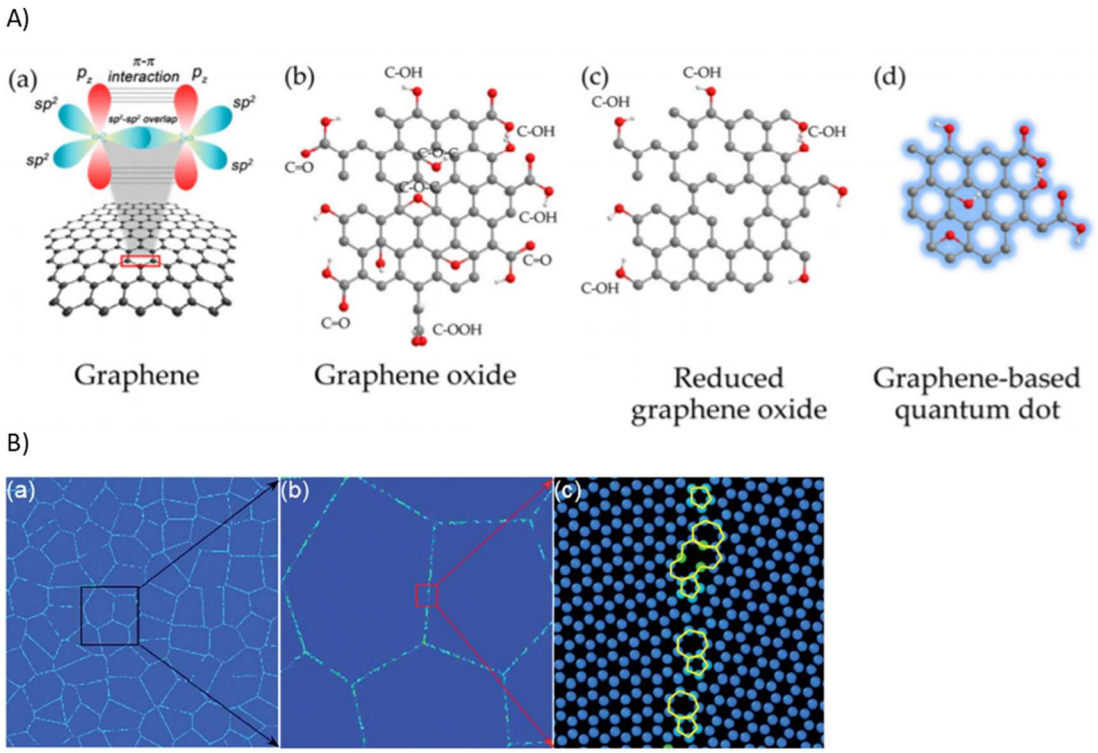

Figure 1. 20 A) From (Phitsini Suvarnaphaet et al., 2017). From left to right: pristine graphene single layer with honeycomb lattice; graphene oxide; reduced graphene oxide; graphene quantum dots. B) From (Yang et al., 2017) polycristaline graphene with close up on the grains boundaries and atoms organisation on these spots.

Pristine (singe crystalline grain), polycrystalline (single crystalline grains of distinct orientations), quantum dots (nanocrystals) or (reduced) graphene oxide (sp^2 carbon atoms

lattice, disrupted by sp^3 carbon bonds, oxygen-containing groups) can all be used in biosensing but must be chosen carefully according to the application. For example quantum dots have photoluminescent properties that can be tuned with their size and surface chemistry (Morales-Narváez et al., 2016). In the case of the Gr-SGFET, an atomic layer of polycrystalline graphene is used. The objective is to have a channel with less defects as possible (seal grains, rip in the graphene layer) to avoid the creation of chemically active region that will react with the species presents in the electrolyte and will noise the signal.

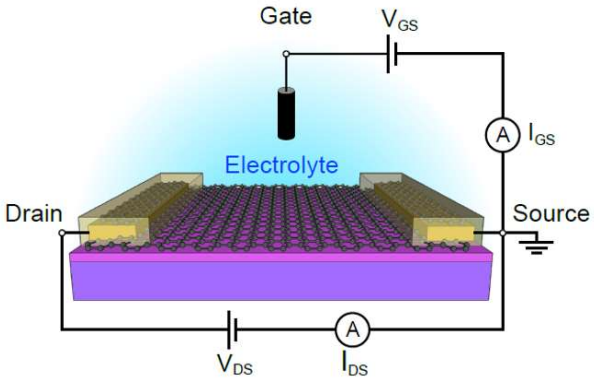

Figure 1. 21 From (Hugo, 2020). Graphene SGFET structure with the graphene layer on Si/SiO2 substrate and contacted by metallic electrodes passivated from the liquid environment. An out of plane electrode is inserted in the electrolyte to serve as a gate.

When in liquid environment, the graphene is directly exposed to the electrolyte containing charged species. Unlike the ISFET, introduced in section 1.2.1.1 Immunosensors, the Si bulk is not used to electrostatically gate the graphene channel through the dielectric layer. Instead an independent gate is introduced in the electrolyte (see on Figure 1. 21) and maintains a fixed potential in the solution. The advantage of the Gr-SGFET relies in the graphene layer. The high mobility (up to 5 x 10^{-4}cm.V^{-1}.s^{-1} at room temperature according to Petrone et al. (2012)) of the charge carriers directly available at the graphene channel surface is exploited to enhance the sensibility of the graphene (Hugo, 2020). This characteristic associated with those already presented of the BioFETs (miniaturisation, real time monitoring, small amount of biological sample needed) is a promising solution for highly sensitive detection in liquid environment and so for this thesis project.

Advanced biosensing technologies are present in various fields like environment, food, and medical or even for large public to enhance sportive performance or quality of life. Often presenting high selectivity and sensitivity, miniaturization at affordable price cannot be achieved for all of them.

Gr-SGFETs are interesting biosensors as they present all the criteria required: high sensitivity and ease of miniaturisation. To detect the targeted hormones, combination of Gr-SGFET technology and aptamers was finally chosen. This new type of probes allows the detection of small molecules like hormones and can be highly selective according to the degree of optimisation of the aptamer. Their fabrication process is also affordable and

do not involve the use of living hosts (animals, in vitro cells or plants) to be produced. Moreover, they have the ability to release their target naturally (according to their K_D value) or under a temperature stimuli that liberate the binding site and allow to have real time analysis.

1.2.2 Microneedles

While a promising lead has been selected to detect the hormones progesterone and oestradiol in the cow's fluids (interstitial fluid or blood), a way to access this fluid has yet to be selected. Prior to any test phase, a set of specifications was discussed to guide the research. The stand-alone tool to develop will be worn by the cow during approximately thirty days and regular sampling of fluids will be realized to follow the hormones levels in real time. On the basis of these facts, three challenges were identified:

How to reach the fluid? The fluids to sample are located underneath the cow's skin and the first challenge will be to bypass this outer protective layer.
How to transport the fluid from the sampling site to the biosensor? The sampling will happen up to several times a day during thirty days, without any maintenance from the breeder. A channel should allow the fluid to go from the source of collection to the biosensor. Classical hypodermic needles used humans fulfil perfectly this role.
Animal welfare. The cow will have to keep this device implanted in the skin for several weeks. Wearing the patch this long can be painful as the nerves located under the skin could be reached.

Solutions responding to this type of request already exist for the humans since a few decades. For people with diabetes, insulin delivery can be realized using a pen equipped with a needle penetrating under the skin (Figure 1. 22). Glucose monitoring has been recently available from diabetic patients but also to improve sport performance of high-level or amateur athletes.

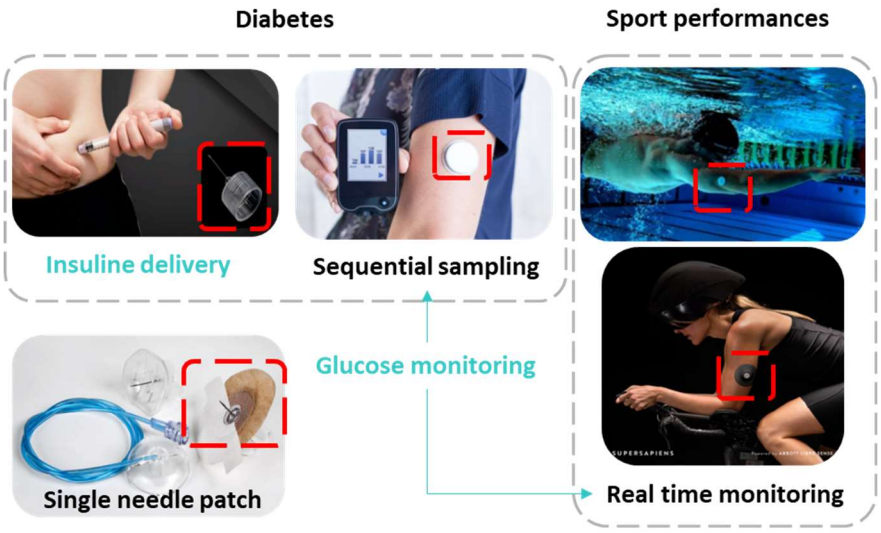

Figure 1. 22 Overview of the different uses and packaging of single needle patch. For medical care or welfare use, to sample fluids, these patches do not require professional assistance to install or remove them. The patch can also contain biosensors with data analysis available for the consumer on an associated application.

To access the glucose or to inject insulin, patch containing one short hypodermic needle or also called "microneedle" with length ranging between 4 and 8mm is inserted under the subcutaneous layer of the skin (see Figure 1. 22). This layer also called the hypodermis is made of fat and connective tissues containing blood vessels and nerves. A longer needle would increase the chances to touch muscles, to bleed which would also increase the pain level and leave bruises. If sampling solution for glucose monitoring are already widespread on the market, current studies for fluids delivery via a microneedle (mostly insulin) are currently under development and tests.

Microneedle (MN) use comes with a series of advantages: no pain during the wearing time, no need for professional help to place and remove the patch and less inflammations and infection issues (Larrañeta et al., 2016a; Prausnitz, 2004).
From a practical point of view, the needle patch can also integrate a biosensor for glucose monitoring. The glucose profile is then available for consultation on the user smartphone for example. This type of device is really interesting for our project as it seems to respond to the different challenge with maybe the need to adjust the needle length for the cow.

However, one of the major limitation of this type of product is its lifespan. After 3 to 4 days, the needle must be changed as cannot drain enough fluid any more as the needle channel gets clogged by tissues or due to the development of scar tissues around the needles.
A first way to prolong the lifespan of the needles or to have the capacity to drain enough fluids for a longer time is to have needles arrays instead of one. This type of patch with arrays of hollow needles does not exist yet. Generally speaking, the actual hollow needle patches are created by cutting a pre-existing hypodermic needle to the desired length. Manually creating arrays of this type of needles would be time consuming and not transferable for mass production.

While this first, rather rudimentary, type of microneedle is now well known to the general public, the many advantages associated with the MN concept have raised the interest of many research teams around the world and a large number of microneedles have been developed for a variety of applications. In the context of this thesis, we were interested in the leads and results of different teams around the world, in order to create an adapted fluid sampling solution for the project.

1.2.2.1 Emergence and use

MN arrays were introduced in the seventies by Gerstel and Place (1971) with a patent describing “drug delivery device for use in the percutaneous administration of a drug for local therapy or systemic therapy”. If the general idea was already there, the term “microneedles” was not used yet and it is only in the nineties in parallel to the rise of the microfabrication techniques that the MNs really started to be developed (Prausnitz, 2004).
Since then, numerous paths were explored and better knowledge about the length, the shape and the materials of the MNs was acquired. At the time this manuscript was written, more than 3 000 publications about microneedles are available (World of Science). MNs have been produced and used in a wide range of applications from medical applications like the delivery of drugs like insulin (see previous section), fluid sampling or even cosmetic treatments.

1.2.2.2 A variety of shapes and material

Several types of MNs exist as presented on Figure 1. 23. If their design can vary, fabrication methods and used materials also offer many possibilities for the creation of a MN according to the final application.

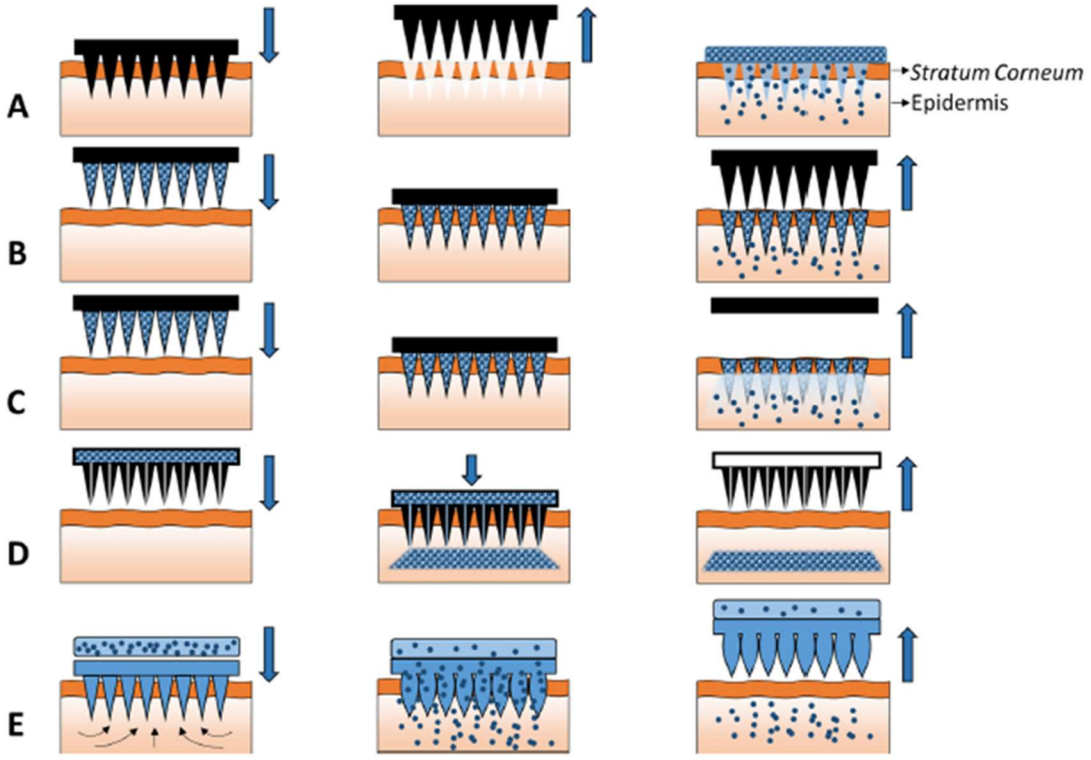

Figure 1. 23 From (Larrañeta et al., 2016). Schematic representation of the different types of microneedles present in the literature. A) Solid microneedles; B) Coated microneedles; C) Dissolvable microneedles; D) Hollow microneedles; E) Hydrogel microneedles.

1. **Solid MNs** (Figure 1. 23.A)

The primary goal of solid MNs is to create some holes or cracks in the sratum corneum (SC) barrier to help the delivery of a transdermal formulated drug (cream, gel or lotion). This type of MN can be fabricated with a large panel of materials. Generally speaking, few considerations have to be kept in mind for MNs fabrication: the material should have sufficient mechanical strength to penetrate the SC, the geometry must be thought to facilitate

the implantation and minimize the pain of the patient. Respecting these criteria, many examples of MNs can be found with different materials and shapes Figure 1. 24:

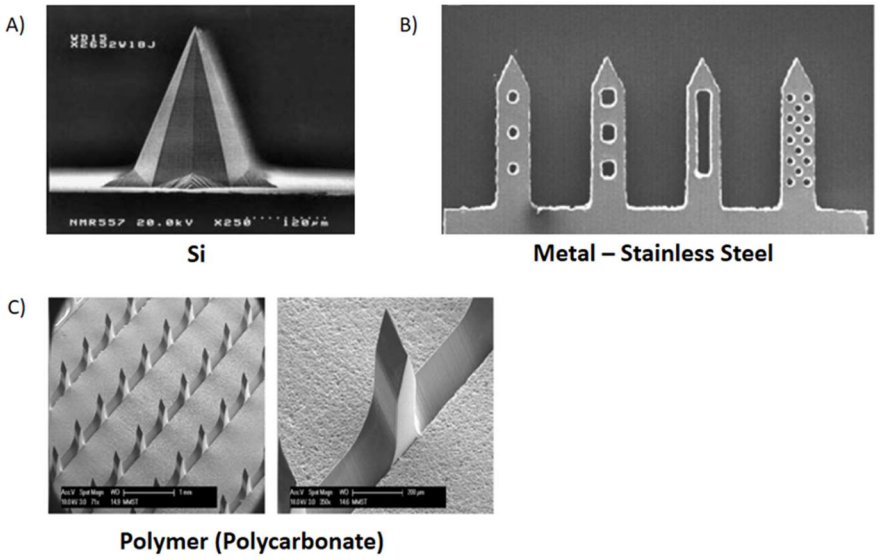

Figure 1. 24 Solid microneedles of different shapes and materials (Gill & Prausnitz, 2007a; Oh et al., 2008; Wilke et al., 2005).

Advances in microelectronics led to the creation of MNs within the micron range with nano features structures as seen in Figure 1. 24.A (Donnelly et al., 2009). Taking advantage of microelectronics production techniques, the fabrication of silicon MNs is easily industrialisable at relatively low cost. Their height is limited by the thickness of the Si wafer and is around a few hundreds of micrometres.
Metal MNs presented on Figure 1. 24.B are realized using laser cutting technique on a 75 µm stainless steel sheet. Electropolishing was used to soften the MNs edges. MNs were then bended to create “out of plane” MNs (Gill & Prausnitz, 2007a).
The solid polymer MNs (Figure 1. 24.C) are made of polycarbonate, a biocompatible polymer. A negative mould of the MNs was used to realize hot embossing on the polymer sheet. Their height can vary between 200 and 500µm (Oh et al., 2008).
We can already acknowledge that all the MNs have a tip radius thinner than the base of the MN body. This configuration allows to decrease the penetration force needed to implant the MNs patch under the skin (Wilke et al., 2005).

2. **Coated MNs** (Figure 1. 23.B)

If previously the MNs were only a tool to create cracks into the SC layer, solid MNs can also be used to deliver drugs by coating the MN body. Gill and Prausnitz (2007 b) estimated to 1mg the amount delivered by a small MNs array and tests were realized with hyaluronic acid, proteins, insulin (…). Figure 1. 25 displays examples of MNs coating tested by Gill and co-workers.

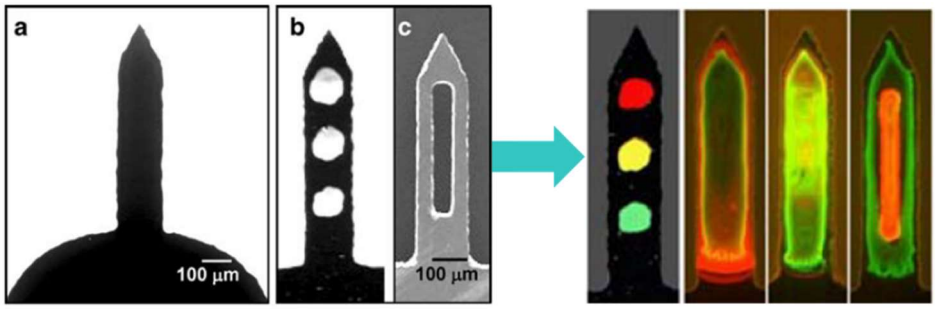

Figure 1. 25 From (Gill & Prausnitz, 2007b). Before and after coating of three different design of stainless steel, in-plane microneedles.

MNs designs with cavities in their body were tested. Drugs were loaded in it to reduce the amount of drugs wiped off by the skin during the MNs insertion. If this type of MN does not present the channel needed for the project, a coating of the body or of the channel could be interesting. An outside coating could load anti-inflammatory drugs to delay the clogging issue after several days of use.

3. **Dissolving MNs** (Figure 1. 23.C)

Dissolving MNs are of real interest for drug delivery. Their use is very simple as the MNs array is left to dissolve under the skin, releasing the drugs encapsulated in the polymer matrix within a few minutes. Many polymer formulations are used to create these MNs. Figure 1. 26 and Figure 1. 27 present MNs realized with six different shapes and formulations.

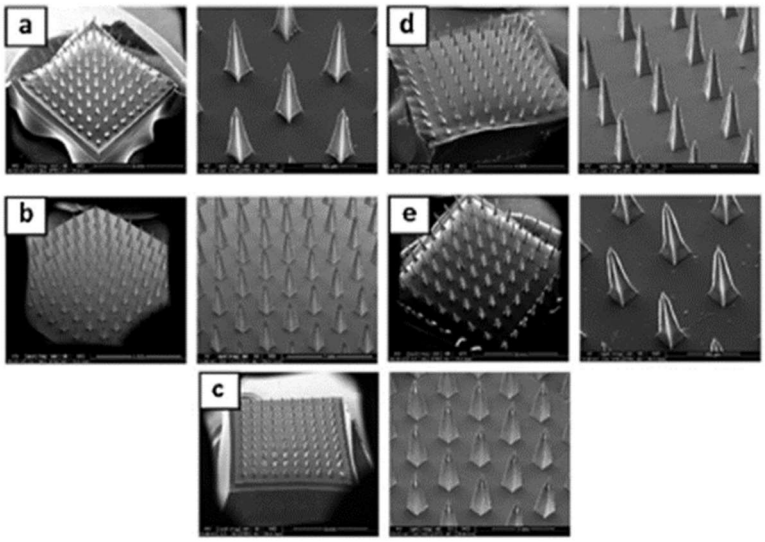

Figure 1. 26 From (Larrañeta et al., 2016a). SEM photographs of parts from 10 x 10 MN arrays made of: (a) alginat, (b–c) hydroxypropyl cellulose, (d) cross-linked PVA-gelatin, and (e) chitosan.

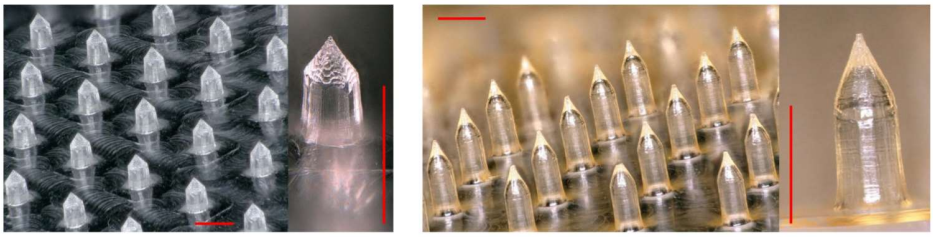

Figure 1. 27 From (Champeau M., 2020). Patch of hyaluronic acid-based microneedle fabricated by solvent casting molding method.

These MNs are often made by casting methods but Lee and co-workers (2011) introduced a controlled drawing technique to produce polymer MNs. With the matrix MNs made of maltose and a lithography-based process (illustrated on Figure 1. 28 (left)), Lee and his team were able to obtain MNs about 1,2mm high.

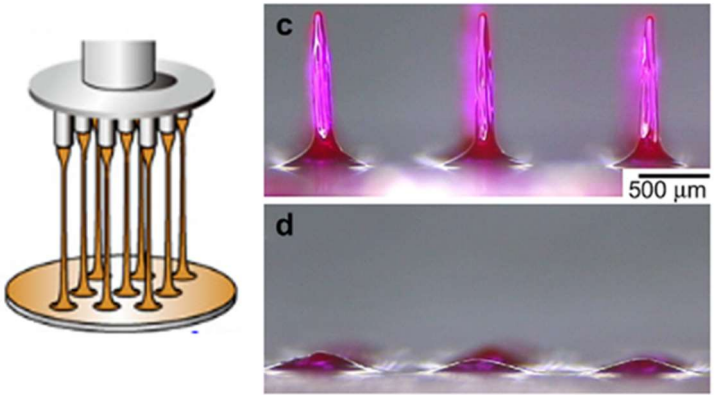

Figure 1. 28 Extracted from (Lee et al., 2011) Schematic of the lithography process for microneedles printing (left) and obtained microneedles before and after 20 minutes under the skin (right).

An interesting point in the use of water-soluble materials is that it eliminates the potential risk of leaving biohazardous sharp waste in the skin as opposed to the previously seen solid MNs.

4. **Hydrogel MNs** (Figure 1. 23.E)

The hydrogel forming MNs are relatively new in the MN landscape with the first version created by (Donnelly et al., 2012). Realized using micro-casting methods, these MNs can deliver drugs as well as sample fluids (blood or interstitial fluid) without dissolving. In the case of fluid sampling, once inserted under the skin the MN swell, taking up the fluid (Romanyuk et al., 2014) for further analysis of analytes or biomarkers in a laboratory setting.

This MN technology is the first to enable sampling of fluids. Nevertheless, this type of MNs only enables single shot measurement so it is not possible to use it for the thesis project.

5. **Hollow MNs** (Figure 1. 23.D)

Hollow MNs have a high potential for the thesis application as it could be the easiest way to sample the cow fluids and to bring them to the biosensor. The variety of shapes and biocompatible materials to fabricate them is displayed in the literature. Examples are shown on Figure 1. 29 and Figure 1. 30.

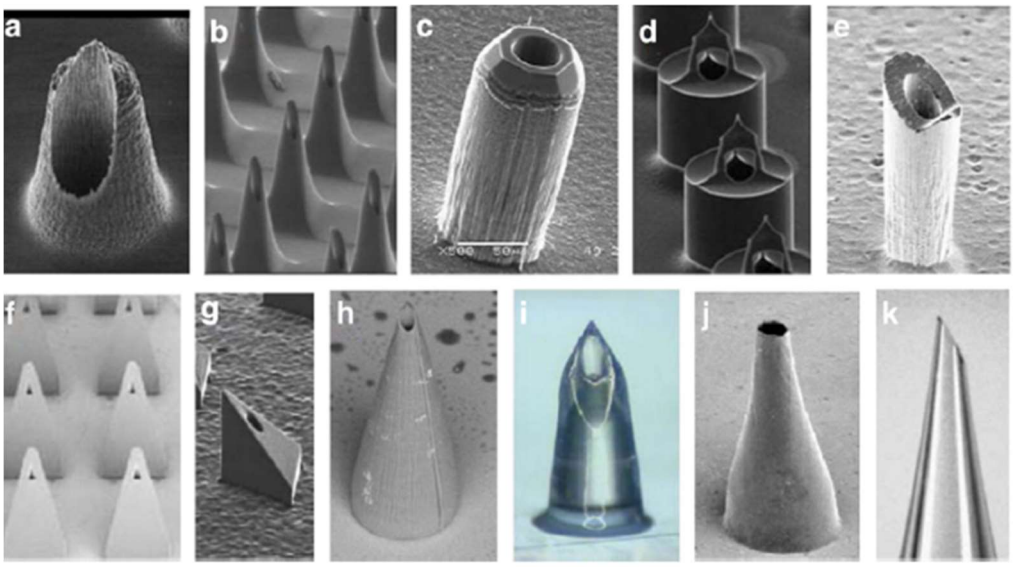

Figure 1. 29 From (Y.-C. Kim et al., 2012). All the presented hollow microneedles are made of silicon except for (i) and (k) which are made of glass.

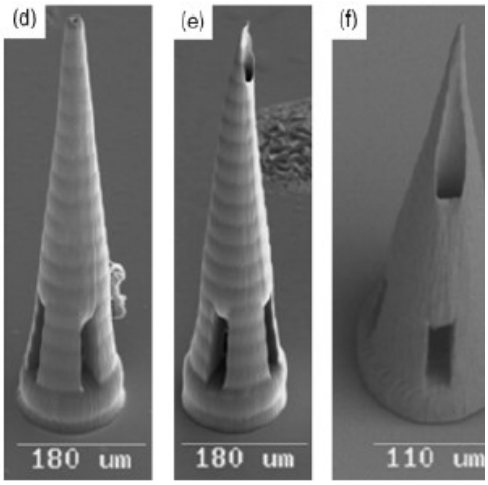

Figure 1. 30 From (Ovsianikov et al., 2007). Ceramic (Ormocer) made hollow microneedles using 2 photons polymerization technique.

Most hollow MNs are made of silicon (Figure 1. 29), due to its biocompatibility and the use of microelectronic technologies that allow great freedom of shape. For the shape of the tip different options have been tested like straight, tapered or pyramidal. However, there is a preponderance of tapered MNs, which allow for easier insertion of MNs and reduces the chances of the channel being clogged during insertion (Chua et al., 2013a).

Hollow MNs made of silica glass as shown on Figure 1. 29 can be found in the literature. However, this material is brittle and fabrication of glass MNs is not time efficient, since it is typically performed by hand (McAllister et al., 2003). Today, the are mainly used for laboratory use but have not been recognized viable yet for commercialisation of drug delivery (P. M. Wang et al., 2006).

Hollow MNs in Figure 1. 30 are made of a biocompatible hybrid material (Ormocer®) containing polymer and ceramic. Ovsianikov and co-workers (2007) used this material with an interesting fabrication technique called two photon polymerization (2PP). A femtosecond laser radiation induces a highly localised chemical reaction leading to polymerization of the photosensitive material with current resolution down to 100 nm. MNs of a few hundreds of micrometres height were produced so far. This additive technique is an interesting path to investigate for the SmartRepro application.

Hollow MNs have emerged as an effective means of reaching the fluids containing the hormones and delivering them to the sensor.
If silica made hollow MNs also have a great potential, they are limited by the wafer height. The cow skin being potentially thicker than the human one, this fabrication technique might be discarded by this parameter. The additive fabrication methods, 2PP or even precise 3D printing could be another solution to explore.

The other MNs fabrication techniques are not suited for the project as they don't have a channel. Nonetheless, some of their characteristics could be integrated in the SmartRepro MNs like the release of anti-inflammatory drugs in the form of a coating or dissolvable parts. The channel could also be coated to help keep the channel unclogged for a longer time.

Conclusion.

This first chapter presents the context of this thesis. With increasing herd size and decreasing manpower, heat detection in cows is becoming difficult. The control of reproduction is a key element of the economic success of a dairy or suckling farm and artificial insemination is a common practice in France. With a decrease in the time length and intensity of heat signs expressed by cows over the last few decades, the farmer needs tools to help detect heat.
In this chapter, the various commercialised heat detection tools have been critically presented. From the observations made, it became clear that none of these products combine the three following criteria:

- Accurate detection of ovulation (no false positives, no missed heats and estimation of ovulation to optimise the chances of successful AI).
- Low cost.
- Ease of use for the breeder.

The objective of the SmartRepro project is to develop a tool combining these three criteria. In the framework of this thesis, the objective over three years was to develop a first prototype of a patch. The first task was to identify the technological building blocks to be developed, as presented in Figure 1. 31.
To be efficient, the patch will be worn about 30 day by the cow (oestrus cycle) and the hormone levels will have to be dosed frequently.
From hormone monitoring to technical solutions to access them in the cow body (blood or interstitial fluids) and transport them to the biosensor, options present in the literature were explored in the second part of this chapter.
To analyse the fluids, biosensor Gr based SGFET is a promising technology with high sensitivity and easily miniaturized for integration into an integral into a stand-alone wearable patch. To detect the hormones, aptamers (small oligomers) are a rising option to detect small molecules with high affinity and sensitivity. Moreover, this type of probe can release the target (hormone) under stimulus (naturally or through an increase of the temperature). This would make possible to clean the sensor regularly and to allow real-time measurement over several days.
To access the fluids, hollow MNs were chosen. The MN technology has several advantages like easy manipulation, avoid pain and infections compared to traditional hypodermic needles. From the literature reviewed in this chapter, a hollow MN responding to the needs of this thesis will be developed in Chapter 2.

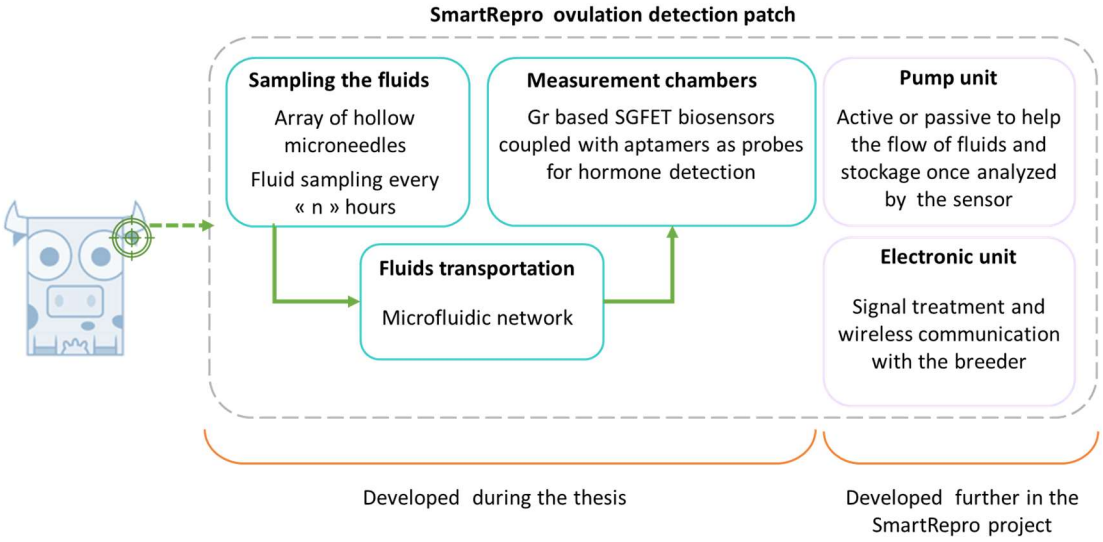

Figure 1. 31 Schematic view of the SmartRepro patch.

- Chapter 2 –

Microneedles

Introduction

The patch developed in the SmartRepro project is composed of four main elements:

- a hollow microneedle (MN) array to reach and sample the interstitial fluid containing the hormones
- a fluidic network to forward the fluid into the measuring chamber
- a sensor to dose in real time the level of hormones in the fluid
- a pump to help the fluid to travel from the MNs to the measuring chamber.

The MNs are the primary element of this patch as they sample the interstitial fluid, containing the two targeted hormones: oestradiol and progesterone. This fluid is located in the dermis layer of the skin, underneath the stratum corneum (SC), the outermost layer. The SC is mainly composed of dead tissues (corneocytes arranged in vertical, interlocking columns) and has a protective purpose for the body (Elias, 2012). The first challenge of the MN is then to go through this extremely cohesive layer. Once this barrier has been passed, their role is to sample the interstitial fluids in the dermis. Thus, to drain the fluids the MNs have to be hollow. The use of MNs for medical purpose is well covered in the literature with more than 3,200 published articles to this day (September 2021). With a variety of shapes and materials, MNs can be used for a large range of applications. In the nineties, MNs were first used to create holes into the SC (Henry et al., 1998) as the short term created holes facilitates the delivery of drugs in the skin derma. Over the last twenty years, new types of MNs have emerged with the capacity to directly deliver drugs or sample fluids in human dermis. To respond to application needs, a large panel of material and fabrication techniques were developed to create MNs. Coatings, dissolvable materials and porous hydrogel were frabricated either to infuse drugs or to sample fluids (Larrañeta et al., 2016b). Hollow MNs appeared in the early 2000's. Made of silicon, metal, polymers or ceramic, they are often used to deliver drugs into the dermis. One can notice that all of the MNs in the literature are designed to be implanted under the skin for a period ranging from a few minutes to a few days (less than a week). After a few days, scar tissues tend to develop around the MNs, cutting them from the biological environment.

A large panel of MNs already exists for medical applications. Information about where to implant them, their height, shape and required implantation force can easily be found in the literature. In contrast, information on the subject is limited for cattle use. Dowling and co-workers (1955) made a first attempt to measure the thickness of the cattle skin but the measurements were limited to "the left side behind the shoulder and on the mid-side over the second rib". This study was recently used to support Steinbach and co-workers work (2021) on the feasibility to sample interstitial fluids from these areas, using steel MNs. The MNs made of steel and coated with an absorbing hydrogel, are designed to sample, within minutes, interstitial fluids for further laboratory analyses. This study supports our interest in using MNs for health monitoring in cattle but the application and so the MNs design differs. Indeed, we intend to use hollow MNs to sample fluids during the entire oestrus cycle (about a month) with on board analysis.

This chapter presents the specifications to select the position of the patch on the cow to define the best implantation area for the MNs. Deeper tissue analysis (composition and thickness) of the selected area were performed to refine the location choice for the MNs in

terms of site and depth of implantation. During this thesis, different fabrication methods were explored to obtain a micrometer diameter range channel inside the MNs alongside a good global definition of the design of the microneedle. The research for the optimal process to produce the MNs is also presented in this chapter.

2.1 Defining the implantation area

2.1.1 On-board tool specifications

It is important to provide primary specifications to define the optimal implantation area for the MNs. Discussion within the SmartRepro group led to the following specifications:

1. **Accessibility**. The breeder has to be able to place and remove the patch by himself, without the help of a veterinarian, so the implantation site should be easy to access. The patch also has to stay in place during the oestrus cycle – roughly four weeks – to not miss the ovulation. The device must remain in place despite the daily activities of the cow such as walking, feeding, lying down, social interactions or rubbing against features headlocks or fences present in its environment.
2. **Design**. The first purpose of the MNs is to penetrate the SC and the design has to facilitate this step. A channel is also needed to sample the fluids. The shape and the material selected for the MNs have to be chosen carefully to fulfil these two requirements.
3. **Length**. The MNs have to be long enough to go through the SC and the tip of the MNs should be implanted in the underneath tissue to reach the interstitial fluid.

These technical specifications are mandatory for the wearable monitoring tool to fulfil its ovulation detection task. It should also be kept in mind that the overall system should be user friendly and affordable to be accessible to the largest public.

2.1.2 Determination of the implantation area for interstitial fluid extraction in cows and feasibility of adapted microneedles

The determination of the implantation area for the MNs on the cow is of paramount importance to ensure the proper functioning of the patch along the four cycles. Upstream of the thesis, areas were preselected on the cow with three specifications inspired by those from the Section 2.1.1:

- Accessibility to the area for the breeder to position and remove the patch.
- Accessibility to the fluid. The skin of the cow should be thin enough to increase the chances for the MNs to pass through the SC and reach the interstitial fluids.
- An area protected from the cow daily activities to avoid scratching and removal of the patch.

Ultrasound was used to investigate these areas and the ear of the cow seemed to be the most suitable for the implantation site. The composition of the tissues of this area is not well described in the literature. During this thesis, a more detail analysis of the ear tissues was realized for seven different breeds of dairy and suckling cows. As a result, the depth of the tissue to reach with the tip of the microneedle and the thickness of tissue to be crossed to reach it were determined. These two parameters are essential to set the microneedle height and from there, several attempts for producing MNs were made (see 2.2.3 Fabrication). The ears measurement campaign and its outcomes are presented in the following article, submitted in Biosystem Engineering journal (August 12th 2021).

Determination of an implantation area for interstitial fluid extraction in cows and feasibility of adapted microneedles

Article submitted on August 12th, 2021 in Biosystem Engineering.

Authors

Juliette Simon[1,2,3] juliette.simon@cea.fr, Pascal Mailley[1,2] pascal.mailley@cea.fr, Fabienne Blanc[3] fabienne.blanc@vetagro-sup.fr, Didier Pin[4] didier.pin@vetagro-sup.fr, Sophie Mailley[1,2] sophie.mailley@cea.fr , Thomas Alava[1,2] thomas.alava@cea.fr , Anne Ferlay[3] anne.ferlay@inrae.fr,

[1] Univ. Grenoble Alpes, F-38000 Grenoble, France
[2] CEA, LETI, Minatec Campus, F-38054 Grenoble, France
[3] Université Clermont Auvergne, VetAgro Sup, INRAE, UMR Herbivores, F-63122 Saint-Gènes-Champanelle, France
[4] Université Lyon, VetAgro Sup, UPSP ICE, F-69280, Marcy l'Etoile, France

Corresponding author: Juliette Simon

Abstract

We present a preliminary study of a wearable system to monitor biomarkers for dairy and suckling cattle. Finding the optimal location on the cow body (ears) and designing the adapted microneedles to reach the interstitial fluids underneath the cow skin are the two points addressed here.
For the selection of the location, 4 breeds of suckling cows (Aubrac, Charolaise, Limousine, Salers) and 3 breeds of dairy cows (Abondance, Montbéliarde, Holstein) were chosen. Measurements of the thickness of the ear tissues were conducted on three areas of the ear (top, apex and base of the pinna), on the external and internal sides. Results show that the apex of the pinna, external side is the best area for microneedle implantation with an implantation window of 1403±589 µm (DeepDe), considering all breeds. To reach this

implantation window located between the stratum corneum and the cartilage, the microneedle has to pass through 1323±404 µm of tissues (SupDe), considering all breeds.

From these results, a microneedle design was made on SolidWorks. With a conical shape 2.89 mm in height and a conical channel 300 µm in diameter (at the tip of the microneedle), the model was made using 3D printing. The resulting microneedles respect the SolidWorks design with fair accuracy. They were connected to a microfluidic channel for sampling or releasing fluids.

Keywords

Livestock; biosensor; cow; microneedles; 3D printing

Nomenclature

SupDe: Superficial Dermis, distance from epidermis to the beginning of the deep dermis
DeepDe: Deep Dermis, distance from the end of the SupDe to the cartilage
EpCart: distance from the epidermis to the cartilage

Introduction

Precision livestock farming appears to be a relevant way to compensate for increasing herd sizes, to support the farmer in optimising and reorganising his time and to make livestock work more attractive for young people (Hostiou et al., 2017). In ruminant farms, and more particularly in dairy cattle, many technologies, robots and sensors have been developed to monitor and improve dairy cow production, reproduction, health or welfare (Knight, 2020b). Among these devices, oestrus detection sensors are currently dominating the market (Knight, 2020b). They were developed to help the farmer define the optimal time to inseminate the cow and consequently to improve herd fertility and profitability. The need for automated systems for oestrus detection has increased over recent decades, while expression of oestrus behaviours became more discrete in high-producing dairy cows (Walsh et al., 2011b). Moreover, herds have become larger and the labour time available for individual visual observation of cows has declined. A wide variety of oestrus detection tools has been proposed (Mottram, 2016; Saint-Dizier & Chastant-Maillard, 2012b) and corresponds to the three broad categories of sensors described by (Knight, 2020b): “at cow” sensors, “near cow” techniques and “from cow” sensors.

“At cow” sensors (like body temperature sensors or activity meters) are carried by the cow or swallowed into the reticulorumen or inserted into the reproductive tract. They enable individual and real-time monitoring for each cow. For example, they can detect a specific behaviour associated with oestrus, like an increase in activity, overlap acceptance or an increase in body temperature.

“Near cow” techniques relate to remote systems that can watch, listen to or track cow activity, like a camera-software system that records cow activity and its expression in sexual behaviour. These techniques allow global monitoring of the herd within a defined area (camera coverage area or under relay signal range). Like “at cow” sensors, these techniques provide real-time analysis by making nonspecific measurements based on the cow’s behaviour.

Finally, “from cow” sensors collect and analyse data related to products from the cow, as with milk progesterone assay.
Currently, commercially available systems dedicated to oestrus detection represent essentially “at cow” sensors and “near cow” techniques. However, “at cow” sensors and “near cow” techniques are mainly oestrus detection devices since they do not detect ovulation per se but rather behaviours and activity changes that begin approximately 30 h before ovulation, (J. B. Roelofs, 2005). Only one automated but costly system uses the “from cow approach”: the Herd Navigator® by Delaval which is available to detect ovulation by measuring milk progesterone levels (Saint-Dizier & Chastant-Maillard, 2012b). Its detection performances are high (Mottram, 2016), but it performs discrete measurements. This system is also not fully versatile since it cannot be used to detect ovulation in non-milking females (heifers, dry or suckling cows). For these animals, plasma immunoassays represent the only alternative. However, this methodology is time-consuming and invasive since it requires manipulation of the animals several times a day for regular blood sampling. This involves keeping the non-milking cows indoors, which is not in accordance with animal welfare considerations.
In fact, physiological indicators, such as progesterone level, appear to be more accurate than behavioural indicators in detecting cow oestrus period (O’Connor, 2009). However, they are not widely used due to the constraints inherent to the detection methodology, including extended handling time, stress on the animals, invasive manipulations and complexity of the detection tool. Finally, the aforementioned considerations clearly highlight the need for a versatile monitoring tool, working in fields or indoors, which enables the real-time detection of physiological oestrus biomarkers in a less invasive manner while being less stressful for the animal.
A wearable monitoring system, which embeds a biological-fluid sampling tool, an ovulation biomarker sensor and a data processing and management system would answer this typical need. Here, we focus on the first component of the aforementioned monitoring system which relies on biological fluid sampling. This consists of an array of hollow microneedles that manages transcutaneous extraction of biological fluids of interest (i.e. capillary blood and/or interstitial fluid). The inner channels of the microneedles will be further connected to a microfluidic network equipped with a pump and sensors for real-time analysis of progesterone or oestrogens. To our knowledge, such a device has not been yet been described in the literature on precision livestock farming, so that proof of concept is still to be achieved.
This paper focuses more particularly on the selection of the optimum area for positioning of the microneedle array on the cow and the resultant design of the microneedles according to the following requirements: i/ The farmer will have to position and remove the embedded system on the cow without external assistance of a veterinarian. ii/ The implantation area has to be easily and safely accessible to the farmer. iii/ The system has to be implanted in an area not easily accessible by other cows in order to avoid scratching. iv/ The target fluids (capillary blood and/or interstitial fluid here) have to be accessible with microneedles. In the last part of the article, microneedles array connected to a simple microfluidic channel are presented as a first proof of concept to study the feasibility of the monitoring system.

Material and methods

1. Defining the target area for implantation

Cow ears have been considered as a relevant target area for implantation of the future device as they are quite easily accessible and can be manipulated by the farmer when cows are

blocked at the headlock barrier. Ears have also already been selected in previous studies to receive implantable biosensors to monitor body temperature (Chung et al., 2020) or hormonal subdermal implants to control the ovarian cyclicity of cows (Sá Filho et al., 2013). However, no publication providing quantitative data about the thickness of cow ear tissues – all breeds combined – was found in the literature. In order to be sure that it would be possible to cross the epidermis of ears and find a sufficient thickness of dermis to host microneedles, ultrasound measurements were performed on 3 Charolaise and 3 Holstein cows to measure the variability of dermis thickness at different parts of the ear: external face near to the apex of the pinna (Figure 2. 2.A), internal face near to the apex (Figure 2. 2.B) and internal face at the middle of the pinna (Figure 2. 2.C). Measurements were performed using an Aloka Prosound 2 unit equipped with a linear probe (ref. UST5820 at 5 MHz; Hitachi Medical Systems, Saint Priest, France). The distance from the surface to the white line (cartilage) was measured for each ultrasound image and defined as skin thickness (Figure 2. 1).

Figure 2. 1 Measurement of skin thickness defined as the distance from the surface to the white line on an ultrasound image.

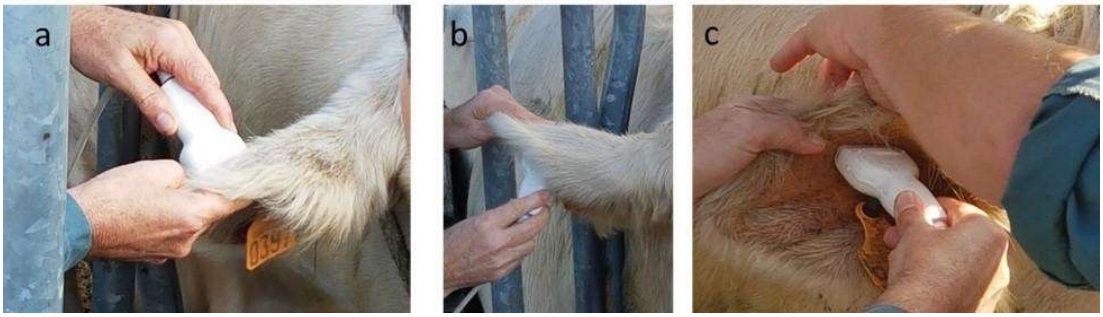

Figure 2. 2 Three areas were considered to measure skin thickness by ultrasound on live cows (n=6): a) external face near the apex, b) internal face near the apex, c) internal face middle of the pinna.

2. Ear samples

Ears from seven different breeds of dairy and suckling cows (Table 2. 1) were collected from private slaughterhouses located in Auvergne, France. Ears were cut from the animals at the end of the slaughter line. For a given cow, the ear without an ear tag was chosen and the pinna was removed from the head with a knife, put into a tight plastic bag including a paper giving information on the cow number, its breed and sex. It was then stored at 4°C until slide preparation and analysis. Seventy-one ears were collected from Holstein (n=11), Montbéliarde (n=12) Abondance (n=5) Charolaise (n=11), Limousine (n=12), Aubrac (n=10) and Salers (n=10) breeds in order to explore the variability among genotypes.

3. Slide preparation and analysis

Histological slides were prepared at the histopathology laboratory of VetAgro Sup. To select the optimal site to implant our system, cross-sections were made at three different sites on the pinna: top of the pinna, dorsal edge (top_pinna); apex of the pinna (apex_pinna); base of the pinna, ventral edge (base_pinna), (Figure 2. 3).

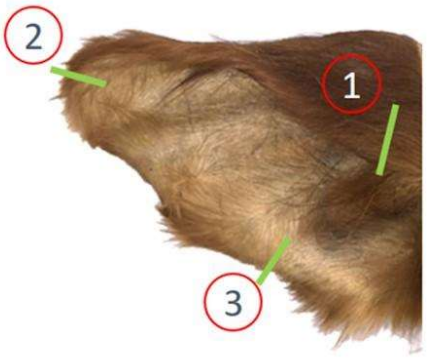

Figure 2. 3 The three sampling areas considered for histological analyses: (1) Top of the pinna, dorsal edge, (2) Apex of the pinna, (3) Base of the pinna, ventral edge. Green lines indicate the direction of the incision.

At each site, a 5 cm x 5 mm sample was collected and fixed in formalin solution, dehydrated and embedded in paraffin. The samples were cut into 5 micrometre sections using a microtome, deparaffinised and rehydrated. The sections were stained with hemalun–eosin and mounted between slides and coverslips, ready for observation. Slide analysis was done on a Zeiss Olympus Bx53 microscope (magnification *1.25) and with the associated CellSens (standard version) software at the Clinatec Institute (Grenoble, France). For each sample, two types of measurements were performed on both sides of the cartilage (internal side – INT and external side – EXT): distance from epidermis to cartilage (EpCart) and distance from epidermis to the line that delimits heterogeneous and clear dermis (SupDe) (Figure 2. 4). The total number of analysed glass slides is detailed in Table 2. 1.

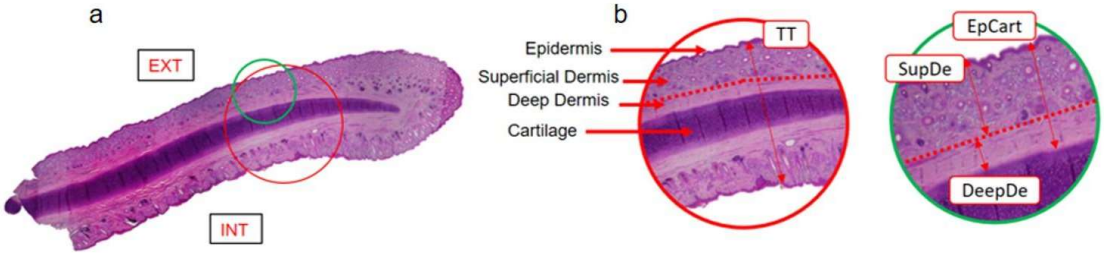

Figure 2. 4 A) Picture of a sample taken on top of the pinna. The internal (INT) and external (EXT) sides of the ear are indicated. B) Close-ups of the slide showing part of the dermis tissues. The superficial dermis (SupDe) is heterogeneous and contains follicles and glands, whereas the deeper layer of the dermis (DeepDe) is homogenous and contains no hair follicles. The cartilage is also clearly visible (darker layer). Three types of measurements were made on each sample: EpCart, the distance from epidermis to cartilage; SupDe, the distance from epidermis to the deep dermis; DeepDe, the thickness of the deep dermis.

EpCart and SupDe measurements were repeated up to 3 times on each side of the cartilage (INT and EXT) for each sample. The mean of these three measurements was used for statistical analyses.

Breeds	Ear sampling area					
	Top of pinna		Apex of pinna		Base of pinna	
Dairy cows	External side	Internal side	External side	Internal side	External side	Internal side
Abondance	4	4	3	5	4	4
Montbéliarde	11	11	9	10	11	10
Holstein	12	12	7	9	12	12
Suckling cows						
Aubrac	9	9	7	7	10	10
Charolaise	6	7	5	8	11	11
Limousine	10	10	8	10	12	12
Salers	5	3	3	3	9	10

Table 2. 1 Number of slides analysed per breed and ear sampling area.

4. Designing the microneedle unit and manufacture

The microneedles were designed using SolidWorks ® software. Once converted from SLDPRT to STLformat, the design was printed using a MiiCraft 125 series 3D printer and the YOE Mikrofluidic resin. The software used to print the units was MiiUtility (Vers3.2.7).
Printing parameters: Curing time: 4s, Gap adj(mm):0, Base layer: 2, Base curing: 25s, Buffer layer: 4.
Once printed, the microneedles were washed out three times for 3 minutes into isopropanol and for 10 minutes in isopropanol + ultrasound in order to get rid of non-polymerised resin remaining on and in the microneedles.
Visual characterization was done using the Keyence VHX 7000-970F numerical microscope and the associated software to take pictures and perform measurements.

Theory/calculation

Differences in skin thicknesses measured on ultrasound images at the apex (external and internal) and at the centre of the pinna were tested using Wilcoxon's test for paired values. For histological data, thickness of the deep dermis (DeepDe) was calculated for each sample from the difference between EpCart and SupDe. Effects of breed (Aubrac, Charolaise, Limousine, Salers, Abondance, Holstein, Montbéliarde) and ear sampling area (Top_pinna_Ext, Top_pinna_Int, Apex_pinna_Ext, Apex_pinna_Int, Base_pinna_Ext and Base_pinna_Int) on EpCart, SupDe and DeepDe were analysed using non-parametric tests as normality of the residuals was not observed when using mixed linear models. The Friedman test was used to test the effect of ear_sampling_area (repeated measurements from the same cow) and the Kruskal-Wallis test was used to analyse the breed effect. Wilcoxon tests were used to compare differences between groups. These analyses were performed with the statistical software R© (version 4.0.0, (R Development Core Team, 2008). Results were considered significant when P≤0.05.

Results

1. Validation of the target implantation area from anatomical characteristics of the ear

Ultrasound measurements revealed that skin thickness varies along the pinna with values being significantly higher in the middle (internal side, (5.45 [4.92-6.35] mm) than near the apex (3.10 [3.02-3.17] mm (P<0.03) and 3.40 [3.32-3.47] mm (P<0.03) for internal and external face of the apex, respectively).
Analysis of histological slides showed that ear skin is composed of four layers whose thickness varies between the three sampling areas. Beside the classical epidermis, dermis and cartilage division, we found that dermis is divided into two sub-layers. As shown in Figure 2. 4.B, the superficial part of the dermis adjacent to the epidermis contains hair follicles and glands, blood vessels and hair bulbs (SupDe, Figure 2. 4.B). The second sub-layer of the dermis, located deeper, just above the cartilage, appears to be free of follicles and glands and is called the deep dermis (DeepDe). Because it is free of hair follicles and glands, the deep dermis would be an interesting implantation window for the microneedles, as no "parasitic" fluids from glands would complicate hormone detection.

1.1 Dermis and ear thickness

Variables	Ear sampling area						p[1]
	Top of pinna		Apex of pinna		Base of pinna		
	External side	Internal side	External side	Internal side	External side	Internal side	
EpCart (µm)	1379 [1222-1720] d	1328 [1225-1815] d	2668 [2344-3158] a	1949 [1649-2588] b	990 [894-1110] c	971 [857-1104] c	<0.0001
SupDe (µm)	816 [687-904] e	763 [682-879] e	1251 [1069-1500] a	1093 [811-1317] b	582 [530-686] c	535 [468-625] d	<0.0001
DeepDe (µm)	610 [485-833] d	610 [461-740] d	1328 [1089-1700] a	912 [758-1280] b	397 [306-482] c	428 [341-483] c	<0.0001

Table 2. 2 Effect of ear sampling area on the distance from epidermis to cartilage (EpCart), distance from epidermis to deep dermis (SupDe) and deep dermis thickness (DeepDe).
Data represent median and interquartile interval (Q1-Q3)
[1] Ear sampling area effect was tested using the non-parametric Friedman test
Variables presenting the same letters on the same line are not significantly different. Differences between groups were tested with the Wilcoxon test

	Breed							
	Suckling Cows				Dairy cows			
	AU	CH	LI	SA	AB	HO	MO	p
EpCart (µm)	1358 [1084-1789] ac	1423 [1112-2001] a	1427 [1059-2034] a	1125 [930-1345] bc	1293 [1171-2140] ac	1081 [894-1525] bc	1255 [1065-2171] a	<0.01
SupDe (µm)	716 [585-757] a	780 [651-1055] ab	752 [564-1072] a	626 [539-765] ac	847 [749-1098] b	636 [529-806] c	825 [641-1191] b	<0.001
DeepDe (µm)	666 [455-890] ac	612 [448-1071] ac	646 [448-1068] c	518 [363-694] ab	518 [404-902] abc	455 [336-677] b	512 [391-747] ab	<0.01

Table 2. 3 Effect of breed on the distance from epidermis to cartilage (EpCart), distance from epidermis to deep dermis (SupDe) and deep dermis thickness (DeepDe)

Suckling cows: AU = Aubrac, CH = Charolaise, LI = Limousine, SA = Salers,

Dairy cows: AB = Abondance, HO = Holstein, MO = Montbéliarde

Data represent medians and interquartile intervals (Q1-Q3)

[1] Breed effect was tested using the non-parametric Kruskal-Wallis test

Variables presenting the same letters on the same line are not significantly different. Differences between groups were tested with the Wilcoxon test.

Ear area effect:

Independently of breed, the thicknesses of dermis tissues (EpCart, SupDe and DeepDe) were significantly higher at the apex than at the base or at top of the pinna ($p<0.001$, Table 2. 2). The lowest values of EpCart, SupDe and DeepDe were observed at the base of the pinna, with thicknesses being 1.4 times lower than at the top. No difference between internal and external sides was found in EpCart, SupDe and DeepDe when measured at the base and at the top of the pinna (Table 2. 2). However, at the apex of the pinna, tissue thicknesses were higher on the external side (Table 2. 2).

Breed effect:

Significant differences in EpCart, SupDe and DeepDe were observed between breeds (Table 2. 3). EpCart was thinnest in Holstein and Salers cows (1081[894-1525] µm and 1125 [930-1345] µm, respectively) and thickest in Charolaise, Limousine and Montbéliarde cows (1423 [1112-2001] µm, 1427 [1059-2034] µm and 1255[1065-2171] µm, respectively). SupDe, which is the layer to be crossed by microneedles to reach DeepDe, was significantly thicker in Montbéliarde and Abondance cows, with median values of 825 [641-1191] and 847 [749-1098] µm, respectively, and was significantly thinner in Holstein and Salers cows (636 [529-806] and 626 [539-765] µm, respectively).

DeepDe, which is the target layer for microneedles, was quite heterogeneous between breeds. The thinnest DeepDe was observed in Holstein cows (455 [336-677] µm) and the thickest in Aubrac cows (666 [455-890] µm). DeepDe was very similar in Charolaise and Limousine cows (Table 2. 3).

1.2 Definition of the optimal implantation area: a compromise between thickness and tissue composition

The implantation area of the device has to be chosen where DeepDe is as thick as possible in order to be sure to have enough thickness at the end despite of the variability observed between cows. At the base and top of the pinna, DeepDe thickness is under one millimetre, whatever the edge considered (internal or external) (Table 2. 4). In contrast, we observed in all breeds that DeepDe exceeds one millimetre on the external side of the apex (Table 2. 4). Therefore, from the implantation window point of view, the apex of the pinna, external edge seems to be the best location.

	Breed						
	Suckling Cows				Dairy cows		
Ear area	AU	CH	LI	SA	AB	HO	MO
Top_pinna_Ext	723.1 [333.6]	698.8 [204.6]	841.3 [393.2]	608.4 [164.9]	427.2 [226.7]	523.1 [206.9]	495.1 [115.9]
Top_pinna_Int	619.5 [215.7]	698.6 [275.1]	707.0 [201.9]	619.4 [168.8]	662.4 [479.6]	446.4 [168.8]	519.0 [193.5]
Apex_pinna_Ext	1308.0 [718.2]	1328.3 [363.2]	1693.1 [463.8]	1523.9 [477.3]	1073.3 [173.6]	1126.5 [645.1]	1250.8 [443.1]
Apex_pinna_Int	794.9 [212.7]	1268.9 [326.1]	963.0 [524.5]	885.5 [702.8]	764.3 [245.5]	911.2 [226.8]	933.9 [532.1]
Base_pinna_Ext	367.7 [200.4]	432.0 [196.8]	405.6 [78.2]	404.6 [81.8]	348.5 [112.6]	316.2 [178.1]	377.4 [142.0]
Base_pinna_Int	428.0 [188.1]	438.1 [72.5]	461.2 [216.1]	455.0 [192.8]	389.2 [114.1]	370.6 [188.3]	366.7 [93.4]

Table 2. 4 Medians and interquartile ranges (in brackets) of deep dermis thickness (DeepDe, µm) according to ear area sampling and breed. Medians and interquartile ranges (in brackets) of deep dermis thickness (DeepDe, µm) according to ear area sampling and breed (Suckling cows: AU = Aubrac, CH = Charolaise, LI = Limousine, SA = Salers - Dairy cows: AB= Abondance, HO=Holstein, MO= Montbéliarde)

The second parameter considered in order to choose the implantation area of microneedles is the thickness of the SupDe layer and its homogeneity (i.e., low variability) between cows as the microneedle is designed to be used on all the different breeds presented in this article. An important SupDe layer is interesting as it would help to maintain the microneedle in place during the system wear time. In all breeds, SupDe thickness is greater at the external side of the apex (Table 2. 5, thickness results). However, this location also has the highest variability results (highest interquartile range [IQR], Table 2. 2 and Table 2. 5). Based on IQR criteria, the top and base of the pinna would be more suitable locations for the microneedles, whereas based on the thickness criteria, the apex appears to be more relevant.

	Breed						
	Suckling Cows				Dairy cows		
Ear area	AU	CH	LI	SA	AB	HO	MO
Top_pinna_Ext	836.7 [208.4]	1016.7 [102.4]	826.0 [310.6]	765.4 [314.0]	836.7 [208.4]	689.0 [74.9]	839.7 [165.3]
Top_pinna_Int	746.7 [93.8]	877.8 [323.4]	799.7 [390.3]	748.9 [74.0]	746.7 [93.8]	674.1 [201.1]	754.1 [175.1]
Apex_pinna_Ext	1229.4 [247.1]	1462.9 [417.7]	1335.5 [418.6]	1336.8 [19.8]	1229.4 [247.1]	1048.8 [139.5]	1288.9 [460.4]
Apex_pinna_Int	845.6 [298.6]	1131.9 [402.6]	937.6 [517.5]	825.1 [522.4]	845.6 [298.6]	806.5 [386.0]	1335.3 [939.4]
Base_pinna_Ext	584.0 [100.7]	635.5 [179.5]	572.1 [118.2]	551.7 [132.9]	584.0 [100.7]	510.4 [138.9]	687.1 [193.1]
Base_pinna_Int	495.5 [225.7]	574.6 [268.6]	521.4 [119.3]	568.5 [158.6]	495.5 [225.7]	503.1 [61.9]	555.6 [191.3]

Table 2. 5 Medians and interquartile ranges (in brackets) of superficial dermis (SupDe, µm) according to ear area sampling and breed (Suckling cows: AU = Aubrac, CH = Charolaise, LI = Limousine, SA = Salers - Dairy cows: AB = Abondance, HO = Holstein, MO = Montbéliarde)

2. Microneedle results

Once the technical constraints were known, microneedles were designed in-house. The design, made on SolidWorks®, was thought to sample the DeepDe interstitial fluids of the external face of the apex of the pinna. To reach this sub-layer, the microneedle must pass through the SupDe layer of 1323±404 µm, considering all breeds. Several studies on microneedles for medical applications show that only about 50 to 60% of the microneedle body penetrates underneath the stratum corneum, the upper layer of the skin. According to these studies (Chua et al., 2013b; Hutton et al., 2018), we designed a 3 mm microneedle to reach the implantation point, in the DeepDe sublayer (1403±589 µm thick when considering all breeds).

A judicious choice of the external microneedle design would facilitate the system-positioning step and avoid occlusion of the microneedle channel when penetrating tissues. From the main shapes reported in the literature (triangular, straight or tapered, (Larrañeta et al., 2016b), the tapered shape was chosen as it presents the lowest penetration pressure and reduces the risk of channel occlusion (Chua et al., 2013b).

For the channel design, two factors were considered. First, the interstitial fluid, which is meant to be sampled by the microneedles, is viscous (significantly thicker than blood, (Zurovsky et al., 1995)). For this reason, the diameter of the channel must be large enough to allow the fluid to cross it. On the other hand, capillarity is an important phenomenon to consider in bringing the liquid into the channel. To use the capillarity phenomenon, at least to initiate fluid sampling, the channel of the microneedle has to be thin enough according to Jurin's law.

To produce the microneedles, we used a 3D printing method as it allowed quick, easy and low-cost prototyping and is of real interest for potential batch production, once the prototype is validated. The principal limitation of the 3D printing method is its accuracy and the microneedle prototype has a high aspect ratio with a 3 mm height and hence a 3 mm long channel.

The channel was the most challenging part to design, as it has to be large enough for viscous fluids to cross, thin enough to have a capillarity effect, and be within the 3D printer technical limitations. Several printing tests led to a two-segment channel design as presented in Figure

2. 5. The first part (Figure 2. 5, in red) is a 150 µm radius microchannel. The second part of the channel (in green) is a conical (from 150 µm to 900 µm radius) channel whose function is to avoid the occlusion of the channel during the printing step. Liquid resin is likely to stay trapped inside a 3 mm long 150 µm radius channel and residual polymerization could lead to the occlusion of the channel by the end of printing. The conical channel allowed the evacuation of all of the non-polymerized resin before reducing the channel radius near the tip of the microneedle.

The final prototype can be observed in Figure 2. 6. For a first prototype, an array of three microneedles was printed with a distance of 1200 µm between each microneedle. The spacing is 8 times the minimal distance needed not to increase the force required penetration of human skin (Olatunji et al., 2013).

The channel and the external aspect were checked using numerical microscopy (VHX 7000-970F numerical microscope and associated software). Comparison between the SolidWorks design and the printed product showed that the design was very well conserved, with a difference of 2 to 4% (see Appendice A.A). The microneedle array was tested for sampling and injecting water and foetal bovine serum (see Appendice A.B). As the final goal is to integrate the microneedles into an on-board device, they were also connected to a basic fluidic card for a first fluidic check. The connection to the fluidic card was done using some thin double-sided adhesive from 3M. A syringe located at the other end of the fluidic card allowed to manually inject or sample fluids (foetal bovine serum). No leakage was observed and in sampling mode, the liquid would filled the microneedles by capillarity, the syringe would then be used to fill the microfluidic channel.

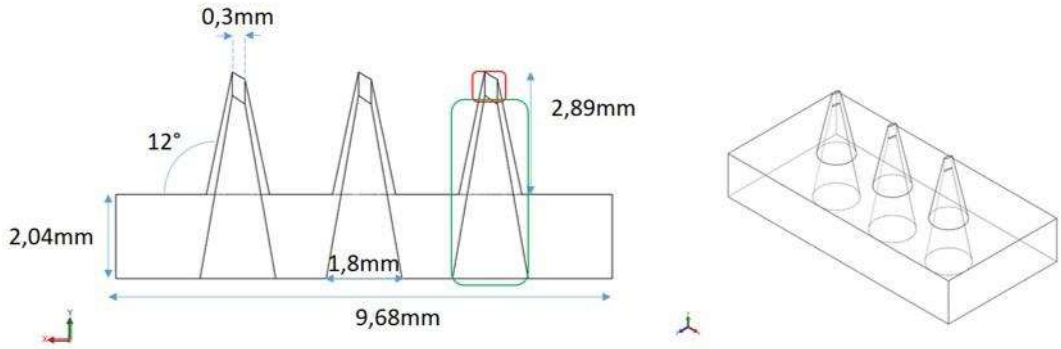

Figure 2. 5 SolidWorks design of the microneedle array. The channel is composed of two segments: conic (green) and straight (red).

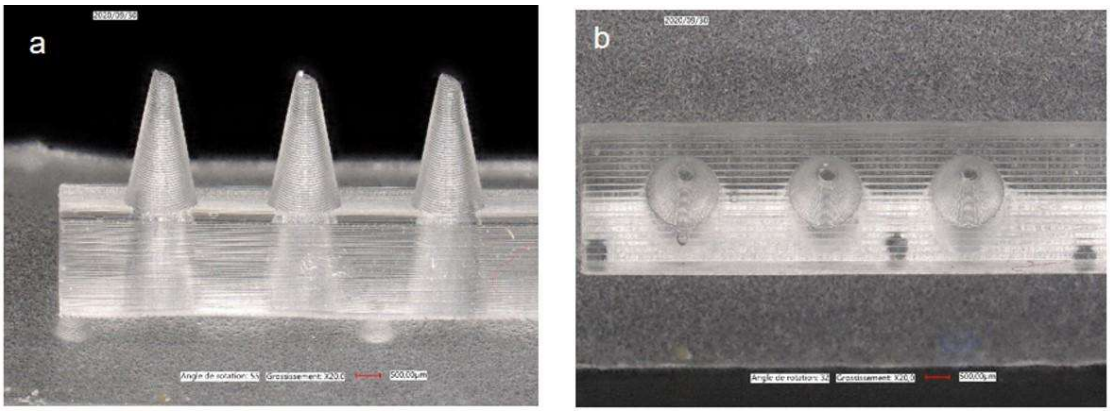

Figure 2. 6 Front view (a) and upper view (b) of the 3D-printed microneedle array. The upper view shows the channels. Pictures taken with the VHX 7000-970F numerical microscope.

Discussion / Conclusion

Physiological indicators are rarely used in livestock farming because they demand many manipulations of the animal by the breeder and can be stressful for the animal. This stress can affect the results of sample analysis in a laboratory. Easy access to targets such as hormones or proteins would facilitate the use of this kind of indicator. Here, we present our preliminary research on building an on-board tool to monitor physiological indicators. The ear of the cow was chosen as the optimal implantation area, following the specifications described in the introduction section. Further analyses of the ear tissues were indicated the optimal implantation site on the ear. Of the three potential microneedle implantation areas, the SupDe skin sub-layer, which contains hair bulbs, glands and blood vessels, is not suitable because of the random bio-materials the microneedle would encounter once implanted (blood, sweat glands, hair bulb, grease…). In this situation, whereas the microneedle would be used to inject or sample some fluids, the results would be random. The location chosen must be a compromise and the apex of the pinna, external face seems to be the best one. The DeepDe layer is the thickest in this area and the quite consistent thickness of the SupDe could allow the microneedles to be more firmly embedded in the ear. The standard deviation of the SupDe values should be taken into account during microneedle development to reduce its impact when positioning the microneedles in the ear.

The microneedle array prototype is the first step in the production of wearable sensors for in situ analysis or automated delivery of drugs for veterinary use. The material used to make the microneedles should be chosen carefully because it must be biocompatible and not break during positioning and removal, or even during wearing. Ceramics would meet biocompatibility and durability expectations, but we chose to use basic resistant polymer for reasons of availability and cost. We wanted to show that the printing of such a design is feasible, thus laying the foundations for more complex designs in the future, while being aware of the technical limitations of 3D printing. Our microneedles array are 2.89 mm long and have good external and internal definitions. The tip canal has a radius of 150 µm and widens to a radius of 1.8 mm at the base of the microneedle.

Acknowledgments
The authors thank the slaughterhouses of Villefranche d'Allier Brioude and Egletons; Didier Bany and Jean Michel Giraud of INRAe for the ear ultrasound measurements; Isabelle Constant and Chirstophe Mallet of INRAe for ear sampling; Sylvie Bouteille and Sylvie Rapiteau from the VetAgro Sup histopathology laboratory and Dr Pauline Panzuti from the European College of Veterinary Dermatology for the preparation of the ear samples; Christophe Gaude and David Ratel from the Clinatec Research Centre for access to the microscope and associated software ; Alice Nicolas from the CNRS – LTM laboratory for access to the 3D printer.

Formatting of funding sources
This work was supported by the Région Auvergne – Rhône-Alpes [SmartRepro project], the The French Alternative Energies and Atomic Energy Commission (CEA) and the National Research Institute for Agriculture Food and Environment (INRAe).

In this article the histological analysis of 71 ears from six breeds, both dairy and suckling was realized. The results highlight that the apex of the pinna, external side, is the best emplacement for the ovulation detection patch for all the breeds. This site has a large implantation window (DeepDe[1]: 1403 ±589 µm) and a rather uniform SupDe[2] sublayer for all breeds (SupDe: 1323±404µm). It respects the practical specifications as previously stated (see 2.1.1) and allows satisfactory implantation conditions for the MNs.

We show in the previous article that hollow MNs could be prototyped and produced using 3D-printing technology. The objective of this first prototyping phase was to prove that it is possible to obtain a 3 mm long channel inside the MN, without any debris inside (resin residue). This step didn't require biocompatible ink and a standard one was mainly used. Nevertheless, this type of ink exists like ceramic based ones (silica-filed photopolymer resin) which can be used for dental applications. Some tests were realized also wit this type of resin and the results are presented section 2.3.2 Compression test

2.2 Design and fabrication of the microneedles

2.2.1 Choosing the fabrication process

The campaign realized on the cows' ears in 2.1.2 gives a first idea of the future design of the MNs. With these characteristics in mind, several fabrication methods were preselected and investigated at the CEA Grenoble. It appeared quickly that the main challenge in creating

[1] Deep Derma
[2] Superficial Derma

hollow MNs was to be able to obtain the 3 mm long (see previous article) and few hundreds of micrometres diameter channel inside, without clogging issues. An in-house (CEA Grenoble, France) prototyping was favoured to have full control of the tests. We also kept in mind to choose a fabrication technique that could make biocompatible MNs from the prototyping step or later in the MNs development.

The CEA Grenoble offers a wide range of techniques and associated equipment in additive or subtractive manufacturing. During this thesis, I had the opportunity to explore and experiment with several fabrication methods using the CEA resources present in the LETI or the LITEN.

1. Hypodermic needles reshaping

A simple way to produce MNs is by using classical hypodermic needles. Usually made of stainless steel, the tip of the hypodermic needle is cut and fixed to a patch. Becton Dickinson patented such device in 2002 and a few companies use these single MN for insulin administration or glucose monitoring survey for example. In the case of the SmartRepro project, rather than a unique MN, an array of MNs is needed for three main reasons:

- If during the four weeks use a MN gets blocked, the rest of the MNs should compensate.
- Distributing the needles over the area would ensure that enough fluid is drained.
- If few MNs get damaged during the implantation step, the rest could compensate.

Arrays of MNs could be created using hypodermic needles but the process remains artisanal and should not be considered as a solution for a possible industrialisation. For this reason, using hypodermic needles was discarded.

2. Subtractive fabrication techniques

It has been reported that microelectronic fabrication process, using subtractive manufacturing, can be used to create hollow MNs arrays (Gardeniers et al., 2003; Roxhed, Griss, et al., 2008). Using lithography etching and metal deposition techniques (Figure 2. 7), patches of MNs can be produced with exotic designs and channel (50 to 70 µm of diameter). In other studies (Stensaas & Stensaas, 1978; Voskerician et al., 2003), silicon has been used in brain and subcutaneous implants, validating the silicon for medical implants use. Furthermore, microelectronics fabrication techniques can easily be transferred for industrial production, advantageously reducing the cost of production. However, the limitation of the technique for the application is the maximum height of the MNs. Silicon MNs are made from a 700 µm thick silicon wafer. In some case, two wafers can be assembled to reach around 1mm thick (SOI – silicon on insulator process). From the results presented in section 2.1.2, the MNs need to be around 3 mm high. Unfortunately, this height cannot be achieved using silicon substrate and microelectronics fabrication techniques.

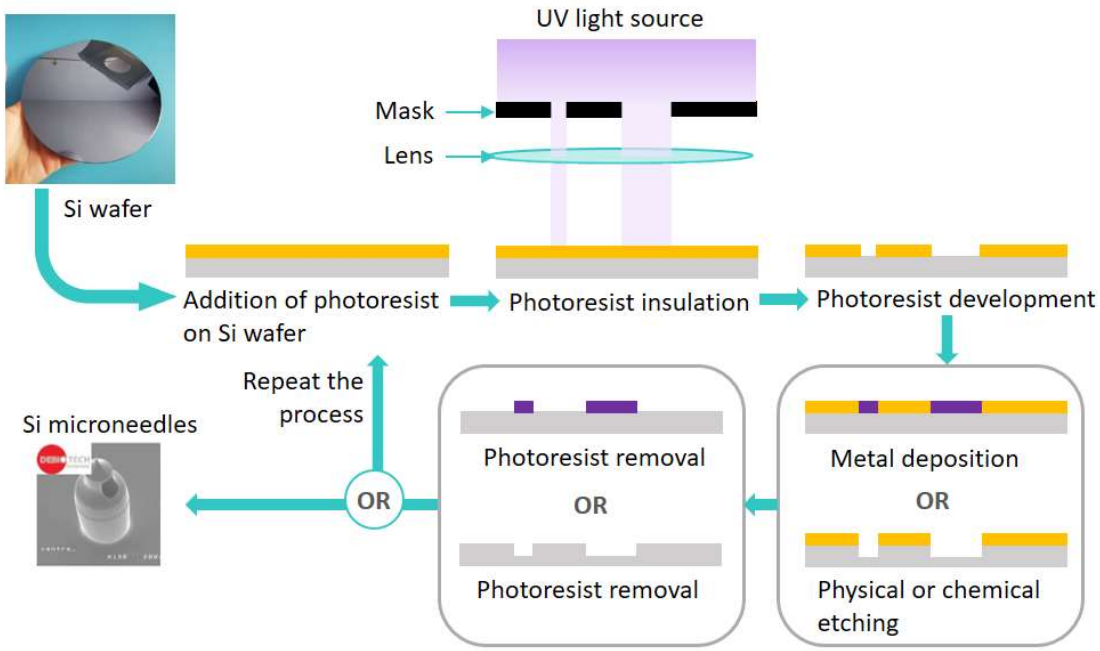

Figure 2. 7 The principal stages of microelectronics processing for Si hollow microneedles production.

3. Injection – moulding techniques

Injection-moulding techniques, available at LITEN, were considered as they can offer great accuracy in the details, reproducibility and allow a one-step fabrication (Figure 2. 8). The first exchanges with experts in this domain gave us the confirmation that the creation of the MNs patch as well as the inner channel using the injection moulding technique was challenging but possible. Biocompatible materials such as PMMA (polymethyl methacrylate), PEEK (Polyetheretherketone), metallic powders or ceramics can be used for injection moulding whose process is described on Figure 2. 8.

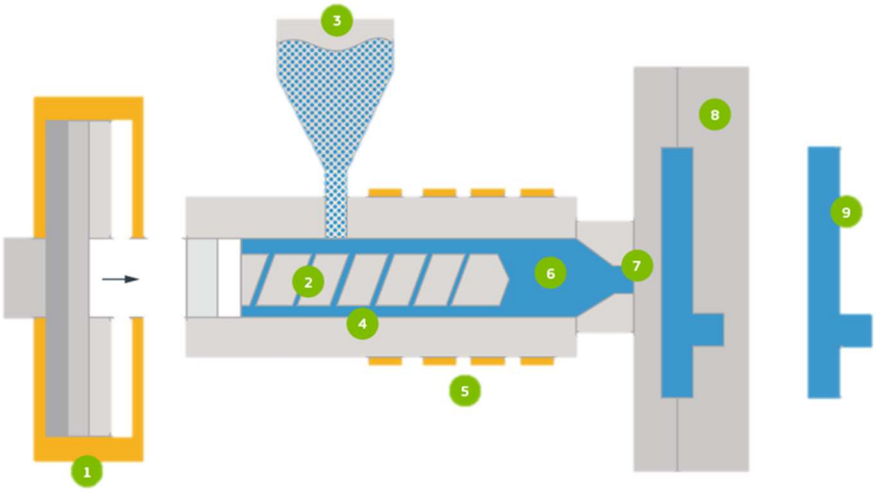

Figure 2. 8 Presentation of the plastic moulding injection process. 1. Piston 2. Srew 3.Hopper 4.Barrel 5.Heating elements 6.Material 7.Nozzle 8.Mould 9. Final product. Reproduction from Protalabs website.

For particular materials such as ceramic, the fabrication process can imply an annealing step, post injection. This sintering at high temperature leads to a controlled withdrawal of the moulded piece. This can be an advantage for MNs fabrication to obtain thinner features (height, channel diameter).

If most of the requirements are validated to produce the MNs patches, the prototyping of the MNs design cannot be done using this technique, as the creation of the aluminium moulds is expensive (several thousands of euros for one mould). The aim of the prototyping step is to test various designs for the channel or the general shape of MNs. For this reason, this technique was not selected for the early stages of MNs prototyping.

4. Additive fabrication techniques

In recent years, additive fabrication techniques have become more accessible and popular thanks to the arrival on the market of affordable and precise 3D-printers. It responds to a large range of applications with a wide variety of raw material including photoresists: basic polymers, biocompatible ones, polymer/ceramic mix and many others. With a maximum accuracy around tens of micrometres depending of the model and the type of resin, this solution offers great perspectives for rapid and relatively cheap prototyping.
The CEA has several models of 3D printers, from filament-based technologies to stereolithography (SLA) based technologies. Two kinds of SLA 3D printers were investigated during this thesis. Series of protocols were tested to obtain, at the best of the machine capabilities, the prototyped MNs (see 2.2.3).

The first step for the microneedle prototyping was to be sure that the technique could produce a continuous channel inside the MN with a good printing quality. The machine prints layers of what can be called “3D pixels”. This minimum detail induces a roughness on surfaces including the internal walls of the channel. To use this fabrication technique for microfluidic purpose, a characterization of the channel surface must be made to ensure it won’t be an

issue for fluid transport. Two equipment were in concurrency at the end of the series of trials: the “125 series” 3D printer by MiiCraft (propriety of the CNRS – LTM) and the “Form 3” 3D printer by Formlabs. These two equipments claimed a precision of 15 and 25 µm respectively. Figure 2. 9 presents the global printing process for an SLA type equipment.

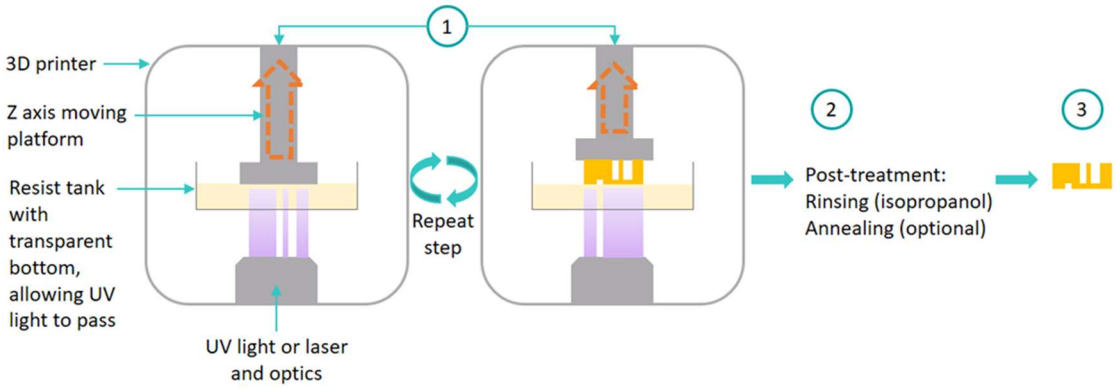

Figure 2. 9 Presentation of 3D-printing process using SLA technology. 1. Step by step printing of the design on the platform 2. Post treatment of the printed piece once removed from the platform 3. Final piece

Series of MNs were printed (see section 2.2.2.3) on the Miicraft 3D-printer and on the Form3 3D printer. The goal was to assess the limits of the printer. MN will be designed taking into considerations the limits of the 3D printer.

2.2.2 Designing the microneedle for SLA 3D printing

2.2.2.1 The shape

Chapter 1 displays a great variety of shapes for MNs. The need to create a channel inside the microneedle restricts the possibilities to three main 3D shapes: straight, tapered or pyramidal. The main requirement for the MNs is to penetrate biological tissues and especially the SC, without breaking or bending. The MNs should also verify a low insertion force and high fracture force (Larrañeta et al., 2016b). For the hollow MNs, another requirement is to avoid a blockage by residual biological tissues when introduced under the SC.

If the material choice is obviously important, the design plays a leading role to fulfil these requirements. Several studies (Chua et al., 2013b; Davis et al., 2003; Kochhar et al., 2013; Sabri et al., 2020), report that external MN designs can have an important impact on the force needed for MNs mechanical insertion under the skin. The conclusions were the following:

- A sharp tip (bevelled) helps the tissues penetrations.
- A small tip (50 µm diameter compare to 75 µm diameter for electroplated nickel MNs in Davis study) and a proportionally large base (up to 300 µm diameter) has also an impact on the penetration force required.
- Thick enough walls are needed to withstand the insertion pressure (10µm in Davis study).

- MNs must be at a minimum distance from one another with a minimum of 150 µm on a same array. If the density of the MNs is too important, they will form a “bed of nails” and prevent MN penetration.

The straight and conic designs seem to respond effectively to these considerations. The pyramid design was left aside at this point as it did not bring additional gain to the other designs and maybe more difficult to obtain depending on the fabrication method.

In between the straight and conic designs, Chua and co-workers (2013) point out two main differences. First, the theoretical minimum applied pressure to penetrate the skin is about $22x10^6$ Pa for the conic design while it is one order of magnitude higher for the straight design ($198x10^6$Pa). These values were calculated for MNs patches of the same material (silicon) having the same number of MNs and the same centre-to-centre spacing. This article also demonstrated that the channel of the straight design is more likely to be obstructed by biological material displacement than the conic one during the insertion under the skin. When inserted under the skin, the straight design induces “rings cracks” whereas the conic design creates “planar cracks” as illustrated in Figure 2. 10. Considering these informations, the conic shape was finally selected.

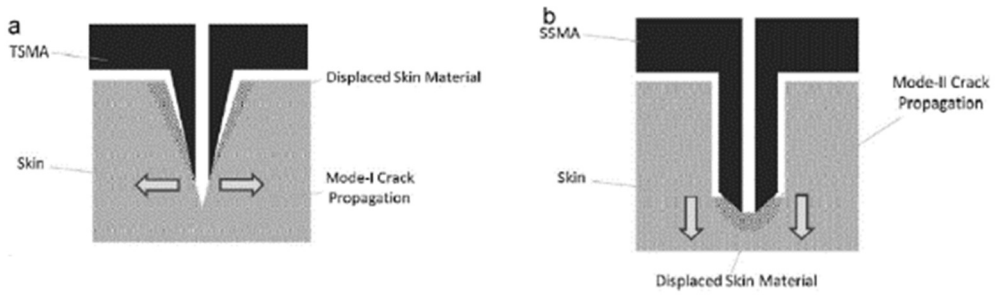

Figure 2. 10 Reproduction from Chua et al. 2013. TSMA (Tapered Silicon Microneedle Array) penetration via formation of planar mode-I crack with the arrows depicting the tensile forces propagating the crack. B) SSMA (Straight Silicon Microneedle Array) penetration via formation of mode-II ring crack with the arrows depicting the shear forces propagating the crack.

2.2.2.2 The size

In the 2.1.2 Determination of the implantation area for interstitial fluid extraction in cows and feasibility of adapted microneedles section, the emplacement for the patch was chosen. The external side of the apex of the pinna presents the best features to implant the MNs as it has a large implantation window (DeepDe: 1403 ±589 µm) and a uniform SupDe layer (1323±404µm) to go through for all tested breeds, compared to the two other sites.

These data are of primary importance to know the target depth where the tip of the microneedle should be inserted. If the tip of the microneedle is ideally expected to be located in the middle of the DeepDe sublayer, the target depth should roughly be in the [1,3 mm; 2,7 mm] range. The median would be around 2 mm. This case is presented in Figure 2. 11.A.

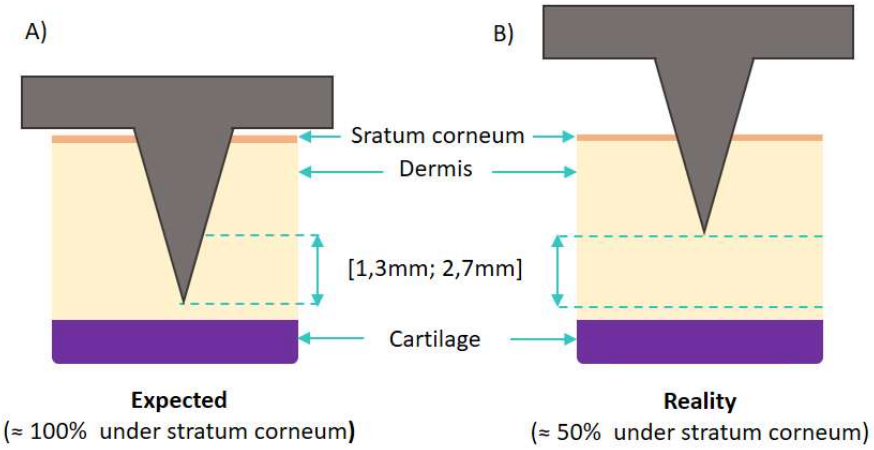

Figure 2. 11 Expected and real behaviour of microneedle inserted under the stratum corneum.

When inserted under the skin, the microneedle is unlikely to have the total height of its body under the SC as presented in Figure 2. 11.A. According to the literature, only 50 to 60% of the MNs will bypass the first skin layer ((Chua et al., 2013b), (Hutton et al., 2018)) as presented in Figure 2. 11. B. A height of approximately 3 mm was chosen for a microneedle design to have 1,5mm to 1,8 mm of the microneedle under the SC once inserted.

2.2.2.3 SolidWorks® designs

Once the principal features of the MNs had been optimised, the design was created on SolidWorks®. SolidWorks® is a 3D modelling computer-aided design software (CAD) published by Dassault Systems. This software was used to design all the MNs during this thesis. A wide variety of options were explored for the microneedle body, tip and channel. All of the fabrication processes considered for prototyping MNs in this thesis need a CAD file, so this step was not only an exploration of all the possibilities that crossed our mind but really a preliminary step for the fabrication process.

Some designs were realized to test the limits of the 3D printer for our application. Channels of different heights and diameter were printed as presented on Figure 2. 12, Figure 2. 13 and Figure 2. 14. For this evaluation step, definition of the body and tip of the MN and possibility to create a neat channel of various diameters were the points of interest (see section 2.3).

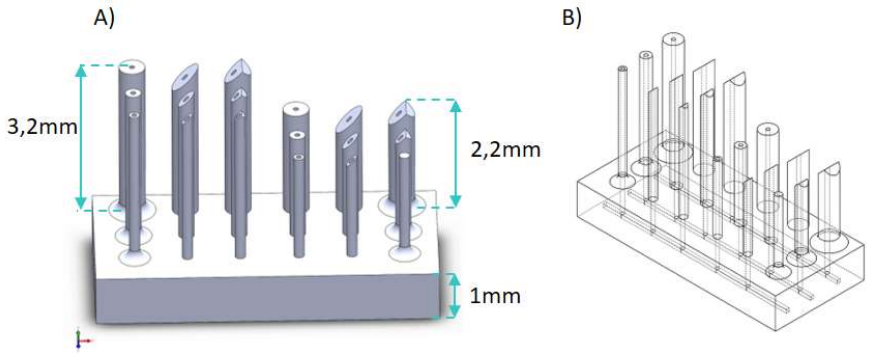

Figure 2. 12 Microneedles patch design for fabrication process testing. Different microneedle body diameters were designed: 500, 300 and 200µm (from the last to first row) with a 100µm diameter channel and three tip designs were tested: plane, 45° bevel, double 45° bevel.

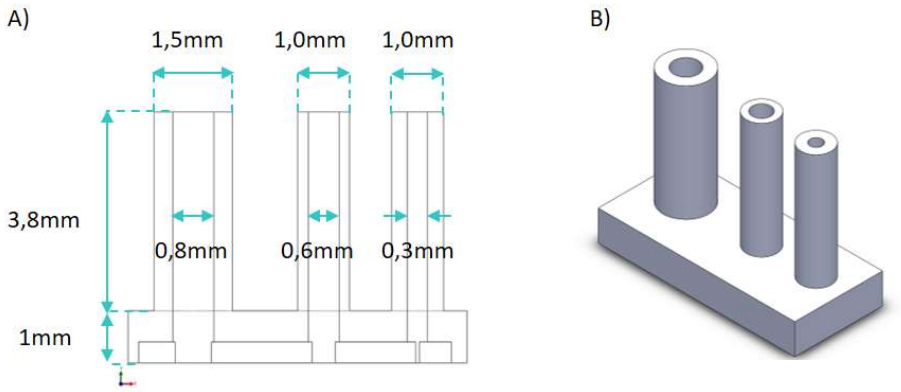

Figure 2. 13 Microneedles patch design for channel diameter test. A) Sectional view B) Design overview.

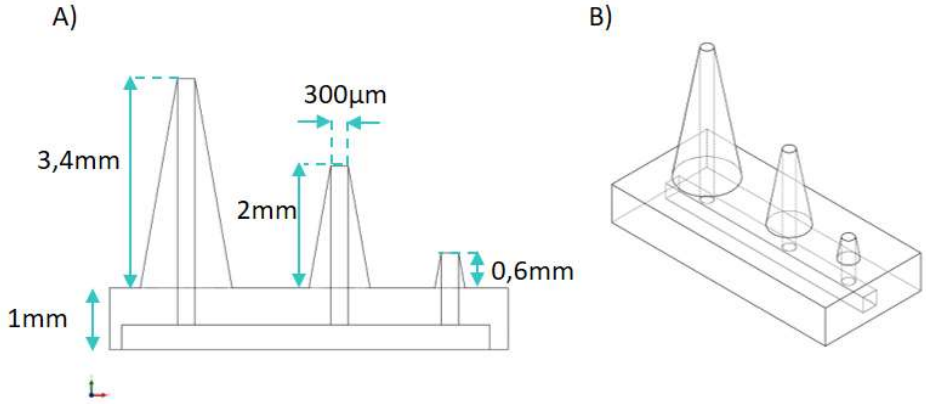

Figure 2. 14 Design of three microneedles with the same channel diameter but three heights A) Sectional view B) Design overview.

The fabrication of these designs with an always evolving protocol (printing parameters and post-printing treatment) led to the conclusion that it was not possible to obtain a nearly 3mm long microchannel with a straight channel as presented in Figure 2. 14. When the design is

printed, layer by layer (see Figure 2. 9), some non-polymerized resin is trapped in the growing channel as its diameter is not wide enough to facilitate the resin to flow. This resin, stocked in the channel will eventually polymerize during the following step of the printing, thus blocking the channel like presented in the picture underneath.

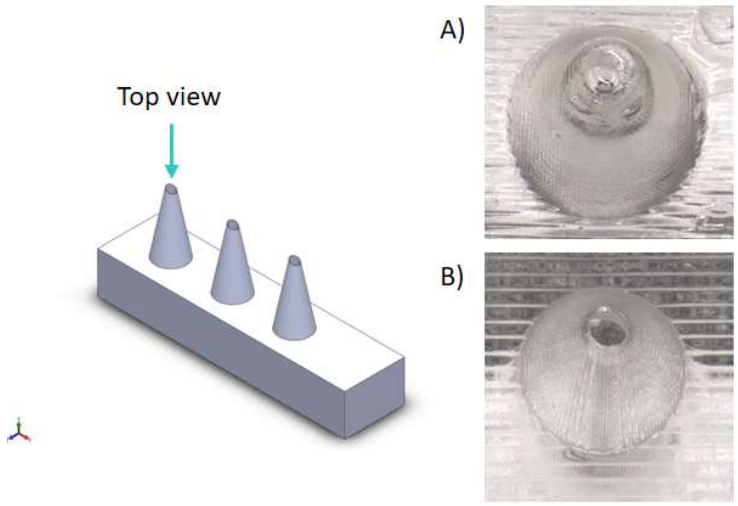

Figure 2. 15 Top view of A) clogged and B) hollow microneedle. Pictures done using the Keyence numerical microscope.

This phenomenon, called residual polymerization, can be minimized with the printing angle, the choice of the printing step or the resin precision. Nevertheless, these levers are not enough to obtain a straight 3mm long channel. To bypass this limitation, a new MNs design with a hybrid channel was created and successfully tested.

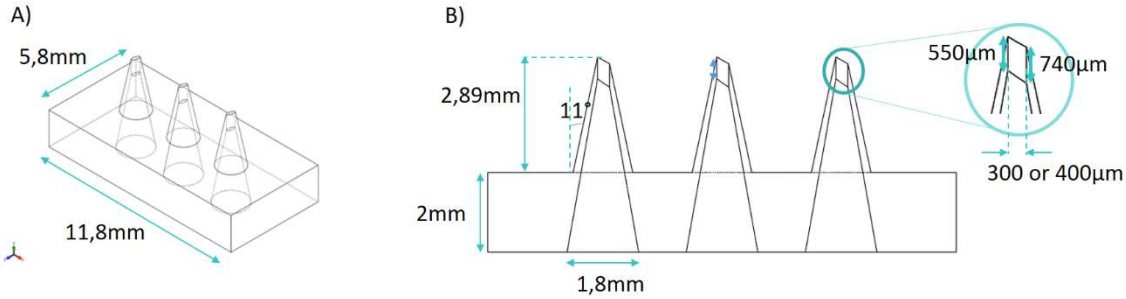

Figure 2. 16 Design of a three conic microneedles array. A) Overview of the MNs patch B) Sectional view of the array. The microneedles are designed with an 11° angle from the vertical axis. The channel is divided in two segments: a first conical part and a straight channel at the tip of 740µm long.

The MN has a conic body with a bevelled tip (45°). The channel, as presented on Figure 2. 16 is made of two segments. The first segment has a conic shape with a 1,8mm diameter at the base of the patch and 1,1mm at the base of the MNs. This first segment represents 75% of the channel length. Its large diameter allows the non-polymerized resin to flow out of the channel for the majority of the printing. The second segment of the channel starts at 740µm of the tip of the MN and is made of a straight, 400µm diameter channel. A straight channel

of this length was the maximum that could be obtained through the conducted tests. In further developments of the SmartRepro, a wide diameter on a large part of the channel will limit the capillary effect to bring the fluid from the tip of the MN to the microfluidic circuit where a pump will take over. This diameter issue is a limitation of the 3D printing technique. Further development will involve different techniques as the injection modelling techniques described in 2.2.1 section for which a straight, hundreds of microns of diameter channel will not be a major issue.

Alongside the MNs whose purpose is to sample interstitial fluids, another MNs design to anchor the patch on the cow ear was created. This microneedle, without channel should be as easy to implant as the other ones, help the patch to stay in place during its period of use and be as easy and painless as possible to remove. The result of this reflexion is presented in Figure 2. 17.

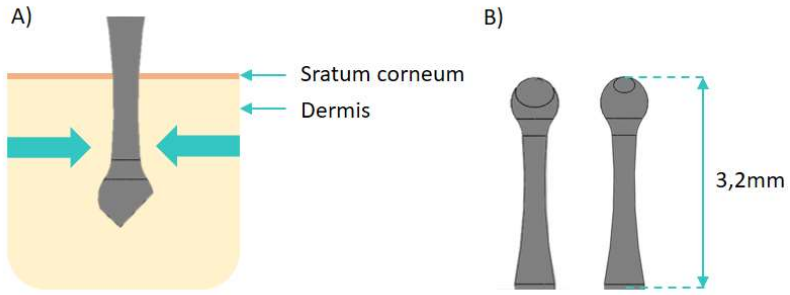

Figure 2. 17 Design of an « anchor » microneedle to help maintaining the microneedles patch on the cow ear during the four weeks of the oestral cycle.

The body of the microneedle is inspired by the famous Coca-Cola® bottle. The base and the top of the MN are flared while the centre of the MN has a fillet. This design will allow an easier and painless insertion under the skin. Once in place, the biological tissue should rearrange around the microneedle. Around the fillet, the tissues will reorganize themselves tighter than on the part of the microneedle located deeper in the tissues preventing them from unwanted withdraw. When the breeder will pull out the patch, the globally tapered design of the microneedle should keep the pain at an acceptable level for the cow.

This design was realized both to test the 3D printer performances but also with the idea to use this design in a more advance stage of the SmartRepro patch.

2.2.3 Fabrication – Printing protocols

For each 3D printer, a catalogue of compatible resin is given by the associated company. The choice of resin is induced by the resolution, the colour, the mechanical properties or the possible biocompatibility wanted for the final product.

For the Miicraft 3D printer, the SB – standard blend resin from Fun To Do (FTD) supplier was used. This resin is not from the Miicraft catalogue but is compatible with the Miicraft 125

series printer. The minimum microlayer height is 20µm which is interesting for microfluidic printing.

For the Formlabs Form 3 printer, two resins were also tested from their catalogue:

- BioMed Clear, a clear, rigid and biocompatible resin recommended by the company for long-term skin or mucosal membrane contact. The minimum microlayer height is 100 µm.
- Standard Black, a black resin. The minimum microlayer height is 25 µm.

The Formlabs resins have better accuracy than the resin compatible with the Miicraft printer but they were nonetheless selected as they have biocompatible products in their catalogue. The printers having respectively a 15µm and 25µm minimum microlayer height (related to printing accuracy), the selected resin should be exploited at the best of their potential.

Once the resin is chosen, it is poured into the printer tank. The designs made on SolidWorks® were load on the printer's software (MiiUtility for Miicraft and PreForm for the Formlabs printer). The loaded design is placed on a virtual reproduction of the printing platform.
From there, some parameters can be changed at the user's convenience. These parameters are introduced in Table 2. 6, together with their importance in obtaining hollow MNs.

Printing parameters	Importance
Base layer	**+**
Printing step	**++**
Curing time	**+++**
Supporting structure	**++**
Printing angle	**+++**

Table 2. 6 Impact of printing parameters playing a role in the presence printed microneedles (presence of the channel and quality of the overall look).

The base layer is a uniform layer of resin polymerised on the printing platform which thickness and polymerisation time are recommended by the manufacturer. The printed object will grow on this base (see Figure 2. 18), ensuring a better grip on the platform during the printing. Its role is to ensure that the MNs stay attached to the printing platform.

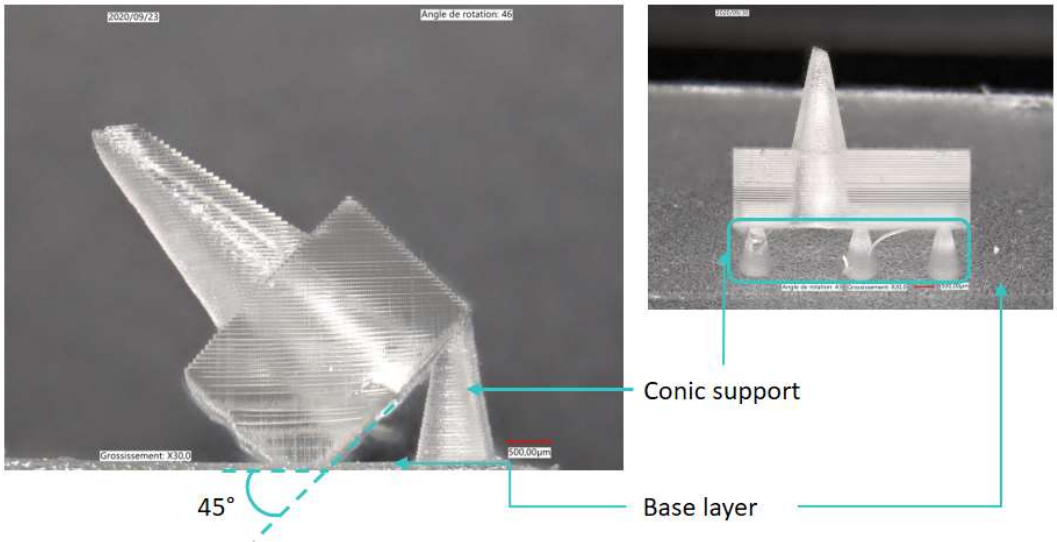

Figure 2. 18 Example of a microneedle (FTD resin) with its printing structure, side and front side. The microneedle has an angle of 45° toward the base layer (part hanging from the printing platform). According to the printed design, two to three conic supports are placed in between the base of the microneedle and the base layer. Pictures done using the Keyence numerical microscope.

Numerous combinations of printing step and curing time were tested. The two parameters have a clear impact on the presence of the channel and also the overall look of the MNs. The printing step is the thickness of each printed layer (or the height of the 3D pixel) which range from 15 µm to 100µm and the XY resolution is of 65µm. The curing time is the number of seconds during which the layer is insulated (ie polymerisation time). The parameters 15 µm and 4 seconds were finally applied.

Printing angles 0°, 20°, 30° and 45° were tested on the Miicraft printer as presented in Figure 2. 19.

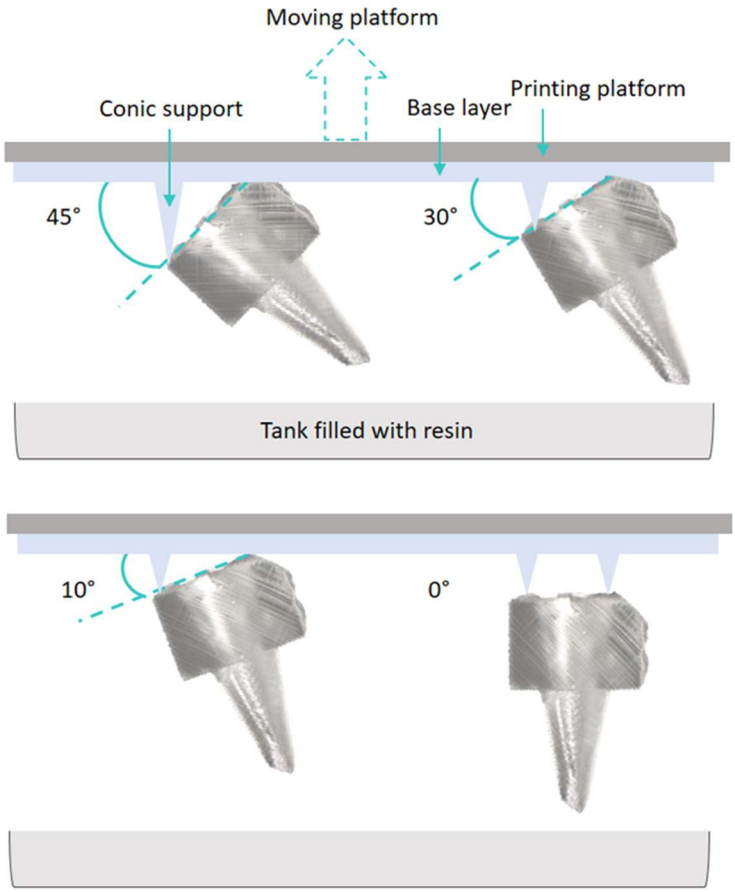

Figure 2. 19. Printing angles tested on the Miicraft 3D printer.

The 0° angle was abandoned right away as the MNs array fell off in the tank for most of the attempts. The conic supports (Figure 2. 18) could not support alone the weight of the MNs array near the end of the printing. No difference was seen between the three following angles concerning the external quality of the MNs. The difference between the three angles laid in the presence or not of the MN channel (see Figure 2. 15). The repeated attempts and comparison of the printed MNs led to the conclusion that the 45° tilt is more likely to help to have a channel. For the support structure, the goal is to create it as minimal as possible to be easily detached from the MNs patch after the printing but strong enough to support the structure during the printing, without breaking. The breaking of the support structure can lead the structure to fall from the printing platform and crash in the tank causing potential damage to the tank itself and making the whole batch unusable.

Printing speed and step, curing time of the resin for each step are also parameters that the user can change to his will.

For the two printers, the printing parameters are the following:

- Miicraft 125 series:
    - Curring time: 4sc
    - Gap adjustment: 0mm
    - Base layer: 2 (no unit)
    - Base curing: 25sc
    - Buffer layer: 4 (no unit)
    - Printing speed: slow

- Formlabs Form3:
    - Base density: 0.6 (no unit)
    - Printing layer: 25 µm (ie height of the 3D pixel)
    - Printing angle: 45°

A post printing treatment was needed for the two printers:
For the Miicraft printer, the printing platform is removed from the printer and the MNs patches are removed from the platform using a putty knife. The post printing recommendations from the supplier were tested (demineralized water and 180s ultrasonic bath) but were not enough for this project. The MNs patches are first immersed in isopropanol for 30s. The majority of the non-polymerized resin sticking to the MNs array is removed. The arrays are transferred into a fresh isopropanol solution and a new cleaning step using ultrasound for 10 minutes. It was found that this step provides cleaner MNs channels. The MNs arrays go under a final cleaning with isopropanol using a pipette and are dried using and air gun.
The Formlabs printer comes with its own post printing treatment devices. The process is similar to the one for the Miicraft printer but automated.

2.3 Microneedles characterization

One of the goals of this thesis was to validate a MNs design and a fabrication technique, respecting the constraints of the SmartRepro project. The 3D printing technique was selected, and numerous trials were realized on the 3D printers with always evolving printing parameters and post-printing treatments. The first step of characterization was focused on the visual aspect of the MN and was systematically realized after the post printing treatment. The observations were used to adjust the next printing process. For the final design, replicated with three different resins, the MNs were subject to a compression test to know if the resin could support the implantation into the ear of the cow.

2.3.1 Visual characterization

Visual characterization was realized using a Keyence VHX-7000 numerical microscope. This instrument delivers high resolution pictures (image sensor CMOS 4K) with the possibility to adjust the lighting, has a wide magnification spectrum (20x to 6000x) and integrate 2D and 3D measuring tools.

The following images display the first fabricated MNs designs (see Figure 2. 12) which played an important role in the preliminary stages of the 3D printing fabrication. These MNs were realized on the Miicraft 125 series printer only as the Formlabs one was not available yet at this time.

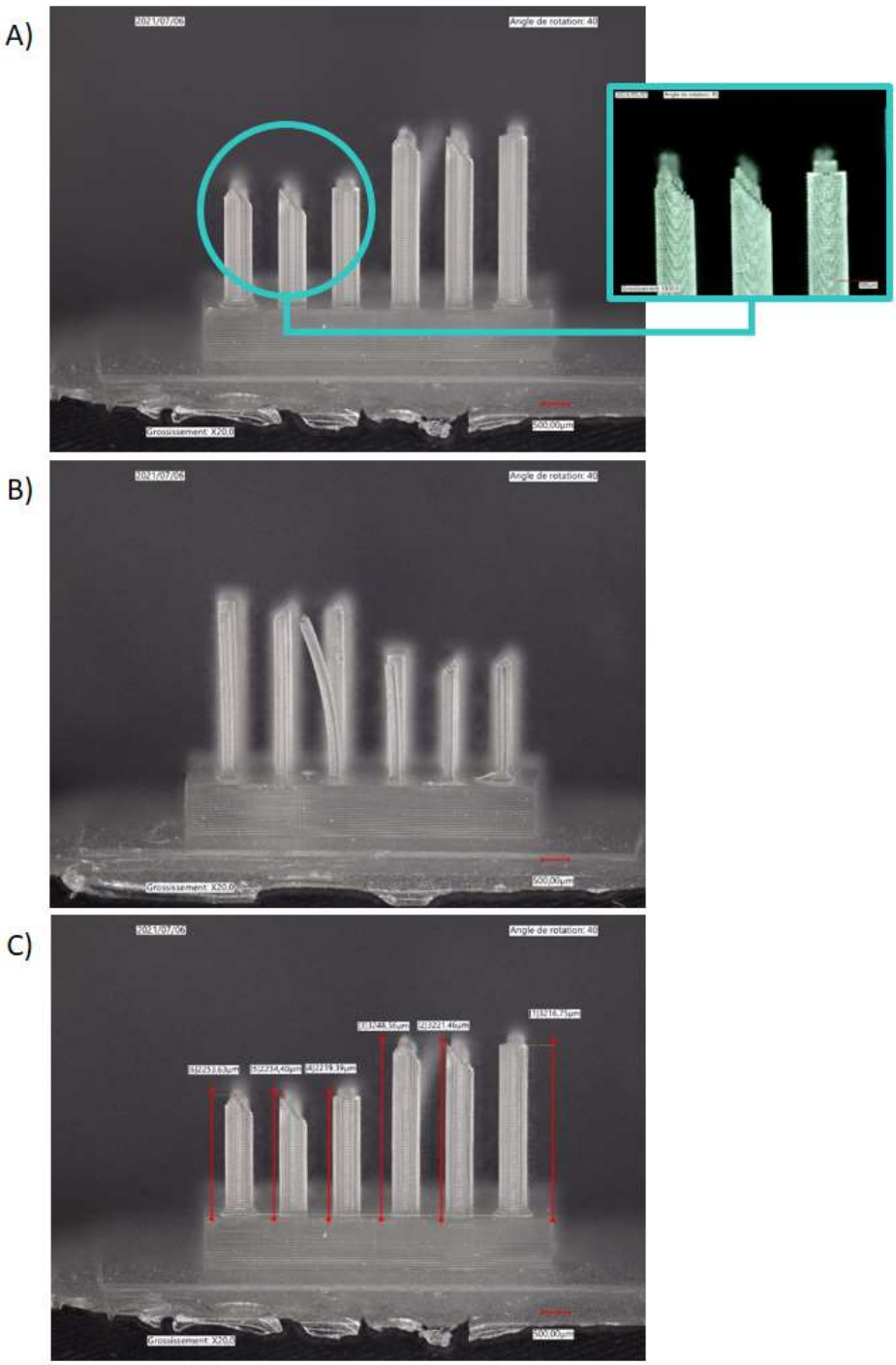

Figure 2. 20 Hollow microneedles printed using SB, standard blend resin from FTD, th e125 series Miicraft 3D printer and observed with the Keyence numerical microscope. A) Front view of the microneedles with their height and sectional view of the SolidWorks design with the two segments channel. Heights of the microneedles left to right: 2829 µm; 2806.94 µm; 2813 µm. B) Top view of the microneedles and the channels. C) Overview of the microneedles patch. D) Bottom view of the patch, inside a microneedle, diameter 1741 µm.

These MNs are printed according to the design presented in Figure 2. 12. Three external diameters were tested: 500 µm, 300vµm and 200vµm. If the 200vµm MNs do not seem to

have enough rigidity to stand by themselves (Figure 2. 20.B), the two other diameters stand on the base as expected. The external definition of the MNs is also satisfying: the three type of tips are well defined (Figure 2. 20.A) and a height difference between 0.5 and 2.4% between the design made on SolidWorks and the printed result. However, none of the MNs have the 2 to 3 mm long, 100 µm diameter channel which was part of the SolidWorks design.
If the external features can be printed with acute definition, series of tests have shown that obtaining a channel of few hundreds of microns of diameter and few millimeters in length is the real challenge for this MNs prototyping project.

The solution was found with the hybrid design for the channel as presented in Figure 2. 16. The two segments channel (conic and straight) printed with the parameters given in section 2.2.3 and a printing angle of 45° led to the fabrication of a hollow microneedle. Nonetheless, this result could be obtained only with the FTD resin and the Miicraft printer. The characteristics of the BioClear biocompatible resin and the standard Black resin associated with capacities of the Formlabs printer were not enough to obtain a hollow microneedle.

Figure 2. 21 presents the MNs obtained using the Figure 2. 16 design, the SB resin from FTD company and the Miicraft 125 series 3D printer.

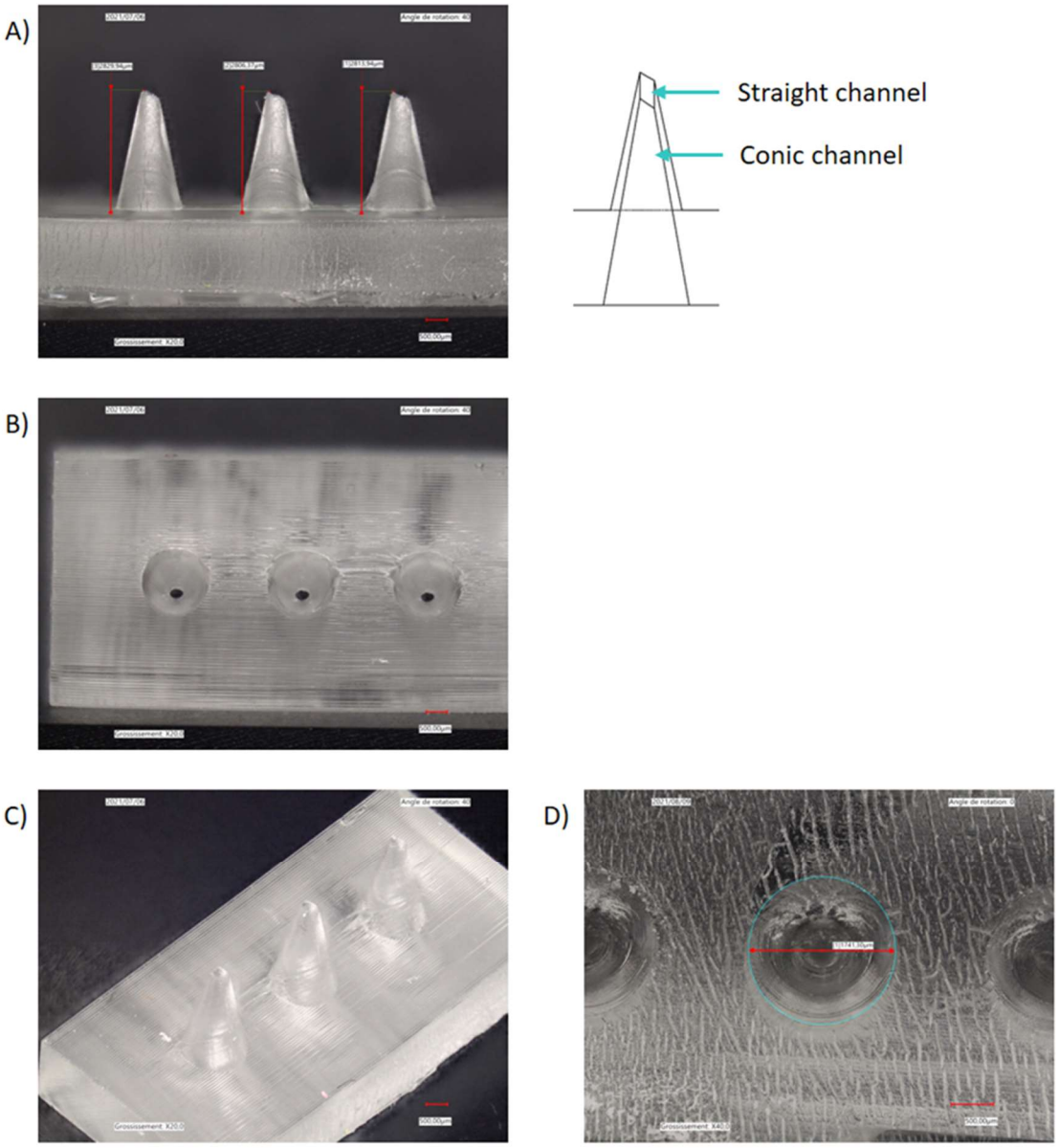

Figure 2. 21 Hollow microneedles printed using SB, standard blend resin from FTD, the 125 series Miicraft 3D printer and observed with the Keyence numerical microscope. A) Front view of the microneedles with their height and sectional view of the Solidworks design with the two segments channel. Heights of the microneedles left to right: 2829.94µm; 2806.37µm; 2813.94µm. B) Top view of the microneedles and the channels. C) Overview of the microneedles patch. D) Bottom view of the patch, inside a microneedle, diameter 1741.30µm.

2.3.2 Compression test

The final design realized in the three different resins has been subjected to a compression test. This test was performed to determine whether or not the design can handle the insertion in the cow ear without damage.

The compression tests were done using a TA.XT plus Texture Analyser. During the test, a force is gradually applied on the top of the microneedle from 1 mN to the set value. The force gauge shaft moves at 1 mm/s. When the force set point is reached, the force gauge shaft applies it during ten more seconds before releasing the pressure on the MNs patch. This time value was to mimic a manual insertion of the MN. The force is not continuously applied, and the gauge shaft has a vertical vibration motion to mimic what could undergo the MNs during the insertion in the ear of the cow when going different tissues.

For this compression test, two forces were applied to the MNs:

- 49N, the estimated force needed for MNs insertion under the human skin when doing it manually.
- 10N, the needed force to have 100% of the MNs inserted under human skin using a commercial applicator (stamp or motor driven micromodelling device) as tested by (Sabri et al., 2020).

The impact of the compression tests on the MNs structure is evaluated by measuring the height of the MNs before and after for the two compression tests (10 and 49N). The results are presented on Figure 2. 22 and Figure 2. 23.

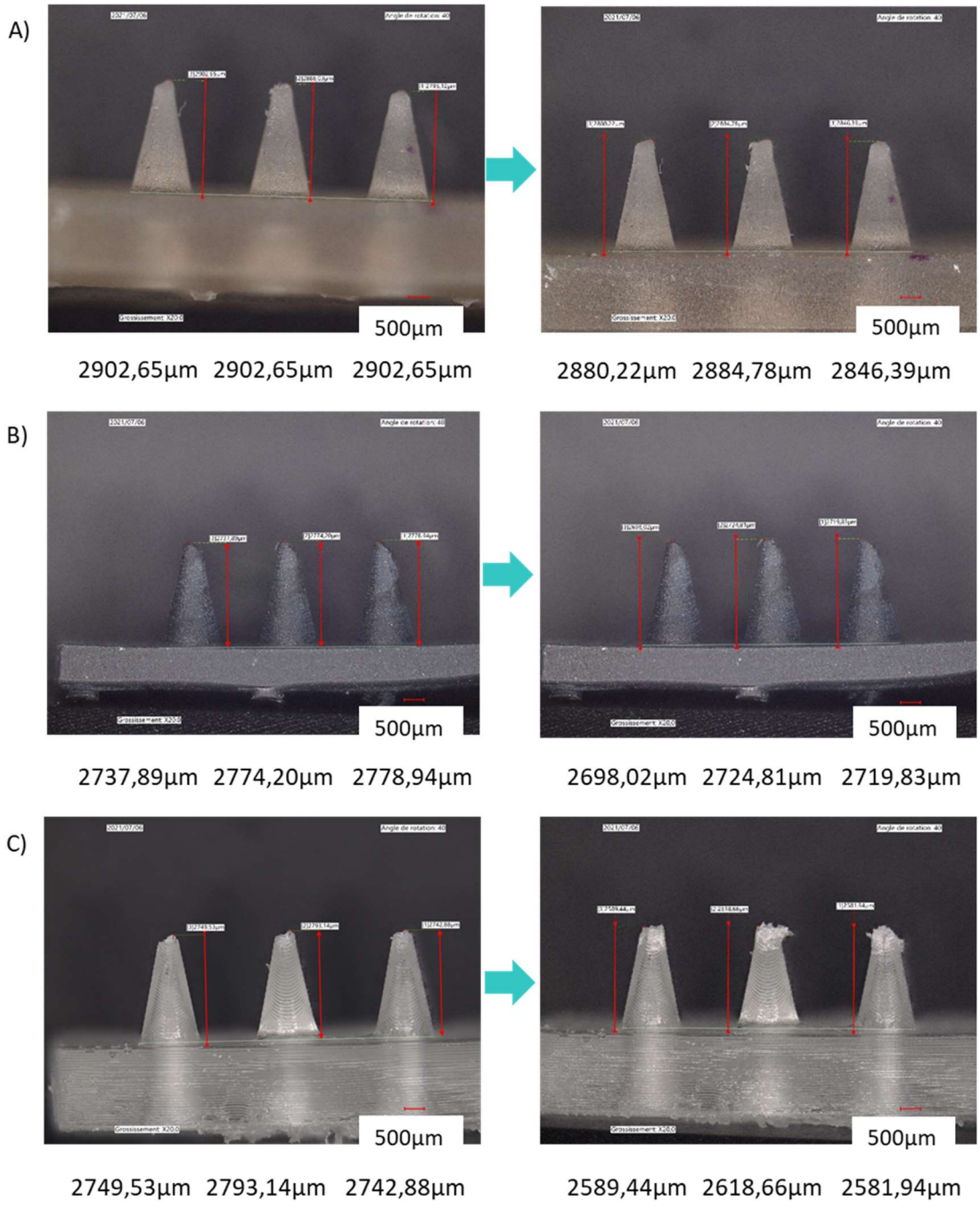

Figure 2. 22 Before / after the 10 N compression test and heights of the microneedles for the three type of resin: A) BioClear resin from Formlabs. B) Standard Black resin from Formlabs. C) FTD resin.

The 10 N compression test had very little impact on the Formlabs resins (Figure 2. 22 A) and B)) with no lateral deformation of the MN body. The height reduction was around 1% for the BioClear and around 2% for the Standard black Formlabs resins. The FTD resin (Figure 2. 22. C) was further damaged by the 10N compression test with no lateral deformation of the MNs but a clear destruction of the MN tip, weakening the rest of the MNs' body. The measurements after compression show a reduction of the height of 6%.

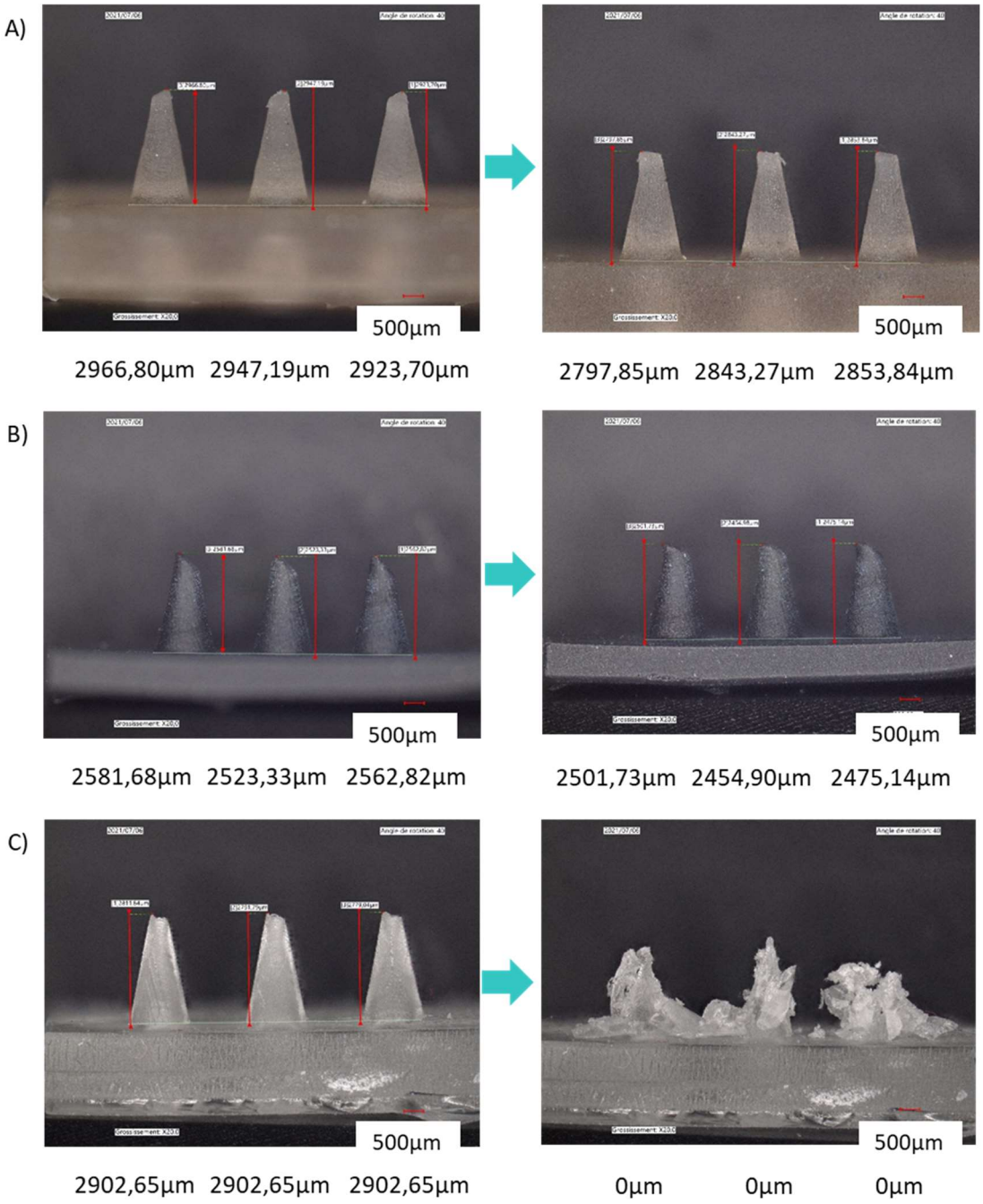

Figure 2. 23 Before / after the 49N compression test and heights of the microneedles for the three type of resin: A) BioClear resin from Formlabs. B) Standard Black resin from Formlabs. C) FTD resin.

The 49N compression results are shown in Figure 2. 23. For a force application five times higher than the previous test, the Formlabs resins did not suffer severe damage (Figure 2. 23. A and B). The tip of the MNs are flattened but the height loss is under 6% for the BioClear resin and under 4% for the Stand Black resin. In contrast, the 49 N test force destroyed 100% of the MNs made of the FTD resin.

Conclusion

A substantial part of this thesis was dedicated to the development of a first hollow MNs prototype.

The choice of the patch position on the cow is of critical importance to allow an easy application and removal of the patch for the breeder. It will also increase the chances for the device to remain in place despite the daily activities of the cow. Upstream of the thesis, a first round of ultrasound measures was realized on several parts of the cow to have an idea of the skin thickness on these localizations. The cow ear was preselected, and an important measurement campaign was realized on the ears of seven breeds (suckling and dairy). The best localization for the MNs implantation, based on the measurements presented in the article is the apex of the pinna, on the external side of the ear as presented in the article. This area offers the best compromise between a large implantation area and a similar thickness of tissues to pass through, considering all selected breeds.

The search for a MN fabrication process meeting our design requirements, which could be suitable to use in the first prototype versions of the patch (affordable, quick to make) led to the selection of the use of a 3D printer.
The design evolved along the different fabrication tests to end with a conic shape of 2.9 mm high for the external design. The creation of the channel was the main challenge of this part of this thesis. Pushing the 3D-printer to the maximum of its abilities and with some compromise on our side on the diameter of the channel, a first prototype of hollow MNs can be presented at the end of this thesis. The biocompatible aspect of the MN was not at the heart of this prototyping step but one biocompatible resin, the BioClear from Formlabs, was tested. If the composition of the resin did not allow the creation of the channel, good mechanical properties were highlighted when passed through the compression test. The next step of the development of the MNs could be oriented on its mechanical properties, now that it was proven that the design could be obtained using 3D printing.

Extensive capillarity testing was not conducted on the MNs. In the article (section 2.1.2) it was proven that fetal bovin serum can go through the MNs. However, the capillarity potential of the MN is not enough to conduct the fluid to the microfluidic network where a pump can take over. If the injection modelling technique could be a solution to bypass this issue, different paths can be explored before reaching this MNs stage of development. In this context, options like surface functionalisation should be investigated.

- Chapter 3 -

SGFETs sensors: from fabrication to understanding the sensor - target interaction

Introduction

The fluid sampled by the microneedles is subsequently analysed by a biosensor. Its role is to measure the level of the two reproductive hormones, progesterone and oestradiol, (see Chapter 1) in real time to predict the upcoming ovulation event.
In the sixties, the first biosensor was developed by Clark & Lyons, (1962) to detect glucose concentration using enzyme catalysis ($glucose + O_2\ glucose\ oxydase \Leftrightarrow gluconic\ acid + H_2O_2$) and a Clark oxygen electrode. Nearly fifty years later, a wide variety of biosensors has emerged with numerous detection techniques but they are all made of, at least, three components:

- A bioreceptor layer. The first layer, in contact with the studied environment, reacts specifically to the presence of the target.
- A transducer. This second layer translates the target detection event into a measurable signal.
- A signal processing system to potentially analyse and amplify the signal.

The performances of a biosensor are determined by different features depending on the application. In our case, two are of main importance for the first step of the sensor development:

- The selectivity of the sensor. The capacity to detect a specific target in a complex medium, as hormones in interstitial fluid in our case, while recognizing no other.
- The sensitivity of the sensor. Oestradiol and progesterone are present in low concentrations through the oestrus cycle of the cow mostly ranging under 10 pg/mL and 10 ng/mL respectively (Martin et al., 2013; J. B. Roelofs, 2005). The sensor's limit of detection determines the minimal amount of analyte (hormones here) that can be detected.

Apart of these two parameters, the response time of the sensor, its stability, reversibility, biocompatibility, size and also its cost are criterions that have an impact on the choice of sensor and detection strategy for a given application.

Through past decades, rise of microelectronic has enable the production of highly sensitive sensors at low cost with mass-production capacities. In this context, the discovery of highly conductive, lightweight, flexible, transparent, mechanically robust, Chemical vapour deposition (CVD) graphene has brought interest from the biosensors community. Its high specific area, due to its atomic layer thickness is particularly appealing for the detection of charged biological species. Using this technology, the Graphene-based Solution-Gated Field Effect Transistor (SGFET) is a very promising and sensitive sensor for the biodetection field (Phitsini Suvarnaphaet & Suejit Pechprasarn, 2017).

Such a sensor was developed in parallel to my thesis by Adrien Hugo, a PhD student from CEA Grenoble. A collaboration with him led to run electrochemical characterization tests with the SGFET, paving the way for the future hormones detection tests accordingly to the SmartRepro project needs.
Another partnership was created with Grapheal, a French start up based in Grenoble. This company also uses the Graphene-based SGFET technology but using different fabrication

protocols and characterization benches. In the context of the project, it appeared interesting to test the two sources of sensors and compare them in terms of manufacturing (quality, production time and cost) and performances.

In this chapter, the peculiarities of the two SGFETs sensors, from the fabrication process to the characterization bench, are presented.
With a series of tests, the goal was to understand the behaviour of the SGFETs and their detection structure in liquid environment. To do so, protocols were developed to detect molecules whose interaction mechanisms are well described in the literature. The type of detection structure chosen for the detection of hormones (SGFET sensor and additional detection structure) lays on the recognition and binding of target molecules, involving no enzymatic reactions and so no charges transfer, unlike the Clark and Lyons experiment mentioned above.
The results of the two types of SGFETS will be compared. From this comparison, we will determinate the best suited sensor to undergo the series of experiments on hormones detection.

3.1 Sensors presentation

The Graphene-based SGFET is a transistor with a graphene channel which is, when used in liquid conditions, directly exposed to the electrolyte. The intrinsic properties of graphene make this sensor highly sensitive and reactive to the charged species present at the electrolyte / Gr interface (Wang et al., 2016). The quality of the sensor and so its sensitivity is highly linked to the graphene quality from its growth to its transfer on the transistor substrate (Phitsini Suvarnaphaet & Suejit Pechprasarn, 2017).

Different techniques are available to obtain single layer of atomic graphene depending on its quality, size and cost. In this study, the graphene was grown by Chemical Vapor Deposition (CVD), a renowned technique that provides high quality graphene, reported for the first time by (Li et al., 2009).

During this thesis, two types of these SGFET sensors were fabricated and tested. If the fundamental function remains the same (SGFET sensors with CVD Gr as a channel), their technological fabrication process, substrate material and the way to manipulate the graphene differed.
This section presents their characteristics.

3.1.1 Si-SGFET

This version of the Graphene-based SGFET, called in this manuscript the Si-SGFET, is made at the Platefrome de Technologie Amont (PTA) clean room facilities at CEA Grenoble, following the protocol established by Adrien Hugo (2020). Figure 3. 1 presents the design of the transistor (A) and pictures of the final device (B) with variations in the transistor shapes.

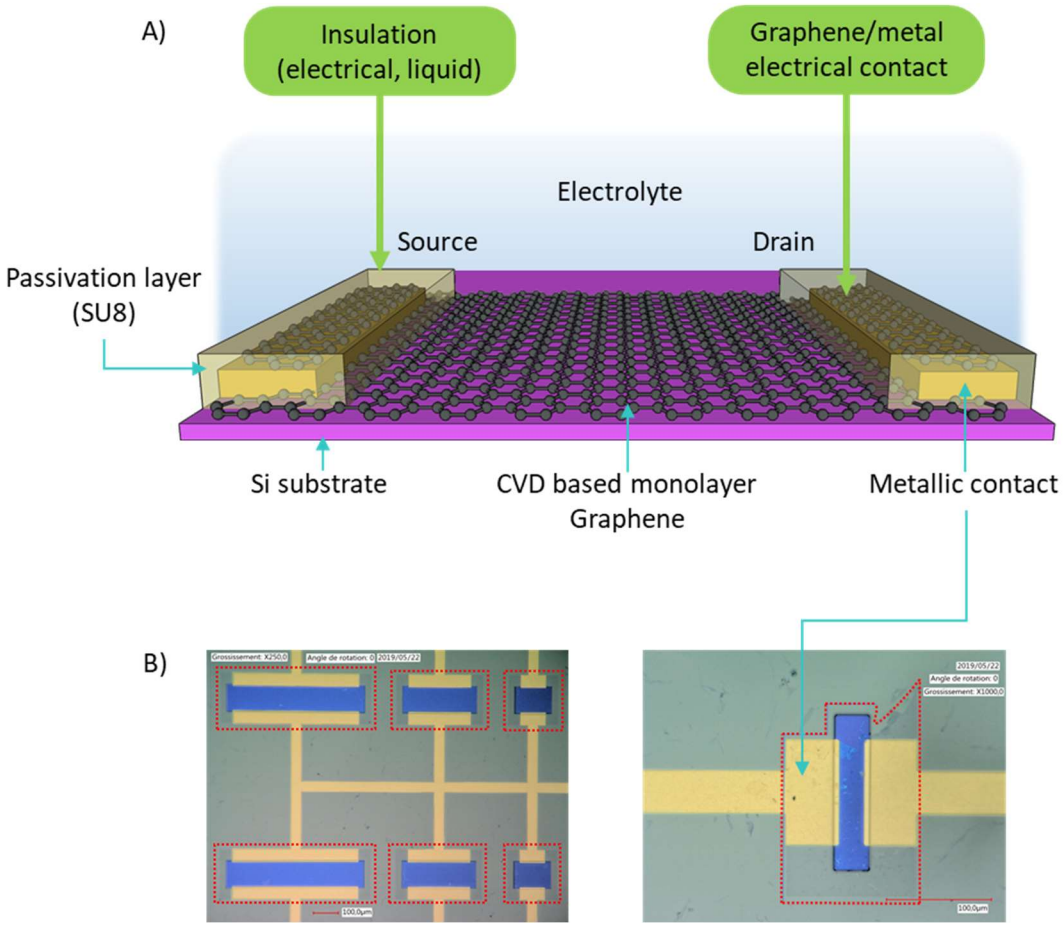

Figure 3. 1 Presentation of the Si-SGFET. A) Schematic view of the transistor composition, inspired by Adrien Hugo thesis manuscript. B) Examples of realized SGFET sensors. Graphene patches can be seen (red dotted lines) for each transistor as well as the rectangle window in the SU8 passivation layer, allowing part of the graphene patch to be in contact with the electrolyte (blue rectangles = opening in SU8, graphene in contact with electrolyte). Pictures realized using the Keyence VHX-7000 numerical microscope.

The Si-SGFET has two gold electrodes on silicon (Si) substrate. The graphene monolayer starts and ends on the top of the electrodes (source and drain) to ensure a good electrical contact and create the transistor channel. A passivation layer made of SU8 photoresist (about 2 µm thick) covers all the surface of the sensor except for the sensing areas (blue parts on Figure 3. 1.B) where the graphene lies.

It has been demonstrated by Yuan et al. (2013) that the Gr edges have a superior electrochemical reactivity compared to a pristine Gr basal plane (middle of the Gr sheet). The monolayer Gr sheet is polycrystalline and has several types of defects: carbon vacancies, dangling bonds, holes (Navalon et al., 2017). When the Si-SGFET is operating in liquid, a

difference of potential is applied between a reference electrode (Ag/AgCl electrode also called the gate here) and the Gr channel. The contact of the Gr edges or the basal plane defects (holes, grain boundaries) with the electrolyte will create active sites responsible for a catalytic activity (presence of oxygen groups, charge transfer interaction). These reactions, happening on the sensing area of the Gr will generate a current called leakage current ($I_{leakage}$) which may interfere with the signal of interest and drastically impact the sensor performance. If the basal plan defect can be partially controlled with the quality of the Gr and by handling with care, the passivation of the Gr edges (using SU8 resin here) significantly reduces the leakage current. This passivation layer also covers the metallic electrodes.

The quality of the fabrication of the Si-SGFET device is crucial to obtain good sensor quality and sensitivity, without Gr deterioration. A robust fabrication protocol was developed by Adrien Hugo to obtain high quality sensors. During the training to produce my own Si-SGFETs sensors, I helped Adrien Hugo to fine-tune the patterning of the Gr channel and the contact passivation step (see Figure 3. 2).

The key steps of the final fabrication protocol are presented Figure 3. 2.

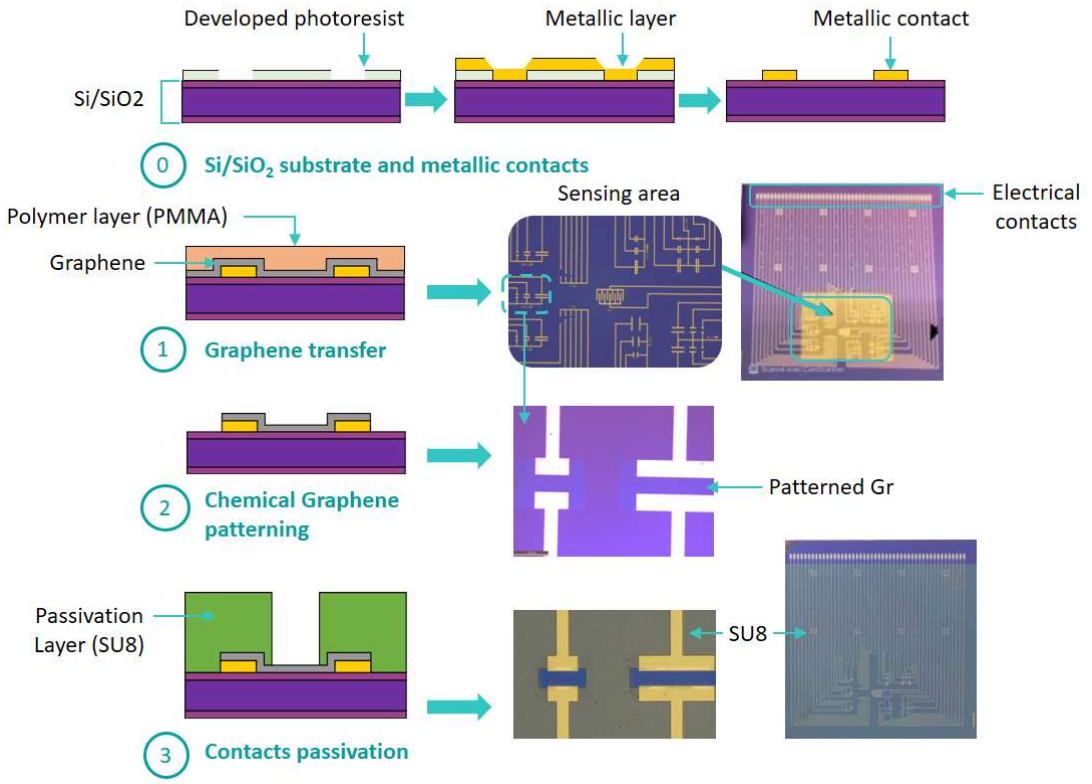

Figure 3. 2 Schematic presentation of the three main steps of fabrication of the Si-SGFET sensors.

On a Si/SiO_2 substrate, Au/Cr metal electrodes were microfabricated (Figure 3. 2, step 0). A sacrificial layer of photoresist was spin-coated on it. Using a mask, the photoresist is selectively insulated by UV light, creating the negative of electrodes patterns. A metallic composed of a Cr (Chromium) primer layer (15 nm) followed by an Au (Gold) layer (80 nm)

was sputtered on the Si/SiO_2. The photoresist and the metallic layer above are then removed and only the Au/Cr electrodes remain. This technique is broadly used in the microelectronic industry to create metal patterns (electrodes here) on a substrate (Si/SiO_2 here) using a sacrificial layer like a photoresist. The rest of the fabrication, described in (Hugo, 2020) can be summarized into three main steps, presented in Figure 3. 2 and developed below.

1. **Wet transfer of graphene on the Si substrate.**

The graphene is CVD grown on a copper layer by the Graphenea Company. A polymethyl methacrylate (PMMA) layer is added on the top of the Gr in the CEA clean rooms for Gr protection purpose and for ease of manipulation of the Gr during transfer on the Si chip. The transfer on the Si chip is also realized in a clean room environment following the process presented in Figure 3. 3.

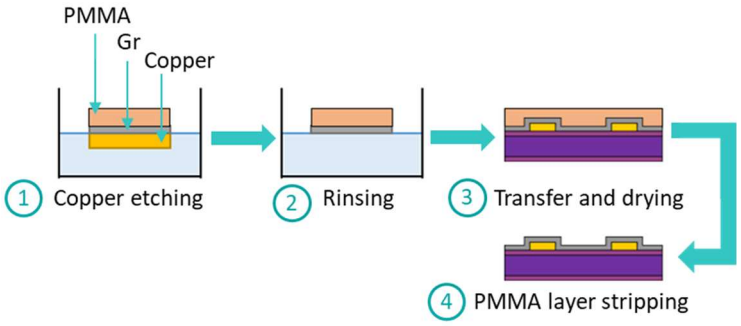

Figure 3. 3 Graphene transfer process. 1. Cu etching with ammonium persulfate solution. 2. Rinsing 5x in deionized water. 3. Transfer and drying overnight. 4. PMMA stripping using organic solvent.

2. **Transistor channel patterning.**

Using a copper (Cu) sacrificial layer to protect Gr from resin contamination and a lithography step, the graphene is patterned as rectangles on the top of each of the thirty-eight transistors on the chip.

During the collaboration with Adrien Hugo, I helped to improve this step. The protocol used at this time did not allow graphene patterning to be obtained as expected in a repeatable manner from one sensor to another. Graphene was often over-etched at the end of this step as shown on Figure 3. 4, left picture.

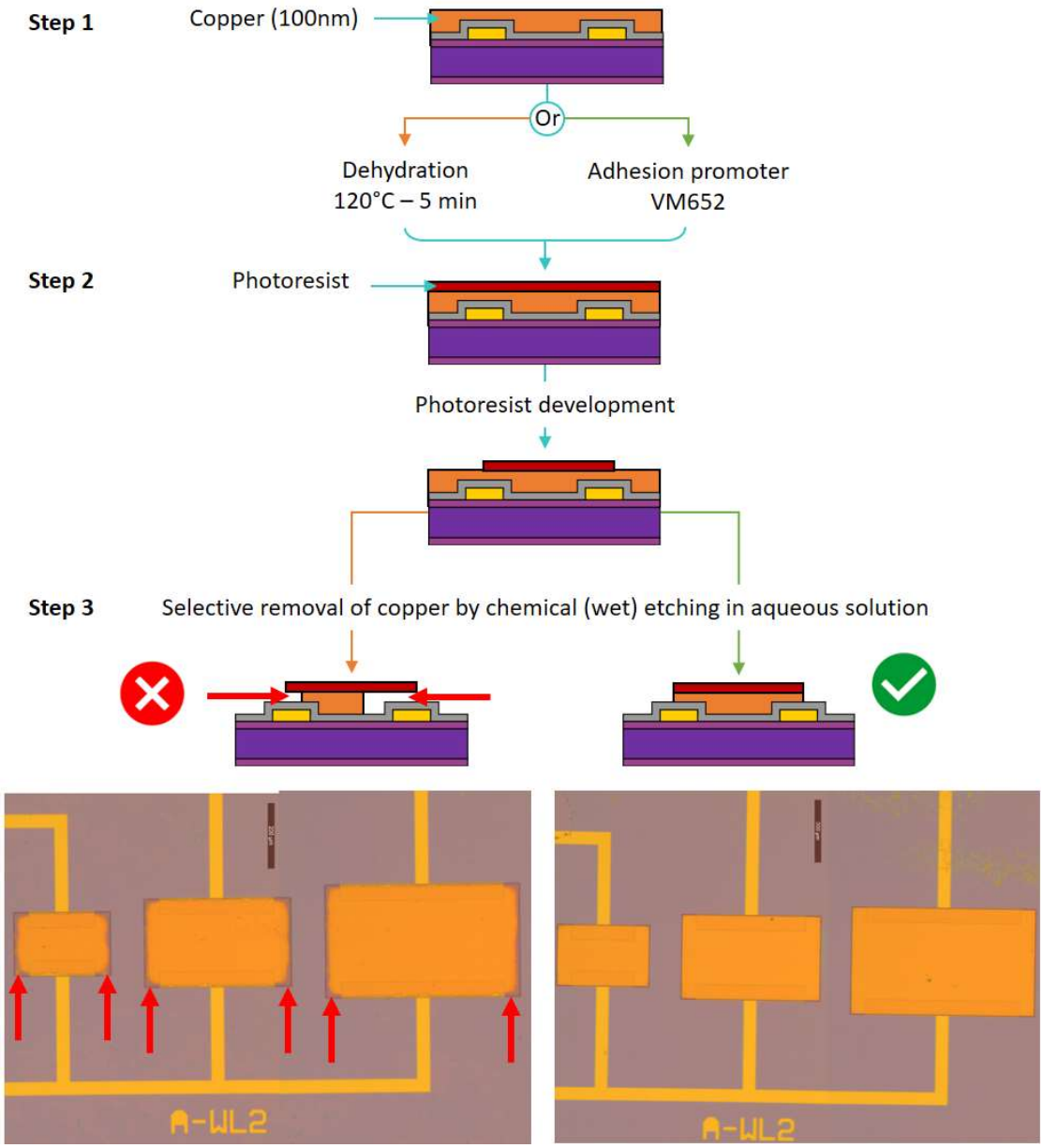

Figure 3. 4 Comparison of the wet resin development, before graphene patterning. On the left, a VM652 adhesion promoter is added on the copper before the addition of the photoresist. On the right, a soft bake (5 min, 120°C) is realized on the SGFETs before the addition of the photoresist. Over etching can be spotted on the edges of the patterned rectangles on the right picture when the same edges remain clean when the adherence promoter is used.

The patterning of the Gr consists of four steps:

- Deposit of a Cu layer on the top of Gr (step 1, Figure 3. 4).
- Deposit of a photoresist on the top of the Cu layer and patterning (step 2, Figure 3. 4). After the photoresist development, only the photoresist on top of the sensing areas remains.
- Patterning of the Cu layer by wet process (step 3, Figure 3. 4). The chip is immersed into a Cu etching solution (Ammonium persulfate (NH4)2S2O8 solution, 0.02 g/mL in deionized water). Within seconds, this solution attacks the Cu layer on the areas uncovered by the photoresist. As this etching technic is isotropic, the solutions may infiltrate underneath the photoresist protective layer, etching the Cu and leaving the

Gr unprotected on the sensing areas of the SGFET. This step requires precautions as the freshness of the etching solution components have an impact on the etching time. Visual observation is the only way to know when to remove the chip from the etching solution.

- Patterning of the Gr channels. Si-SGFETs are placed into a plasma that attacks the Gr in an anisotropic way. Only the Gr none protected by a Cu layer is etched. This method is slower than the wet etching, but it is automated and provides a better control of the material consumption.

The Cu is then eventually removed from the Gr surfaces and the result can be seen in Figure 3. 2, left picture.

The conservation of the Cu layer above the Gr channel is therefore of the utmost importance. Improving the adhesion of the resin layer to the Cu slows down the dissolution of the Cu underneath. A protocol was first tested to enhance this adhesion: the dehydration of the chip at 120°C during five minutes before the addition of the photoresist. The results (Figure 3. 4, left picture) show that the edge definition lacks cleanness and reproducibility from one chip to another. A new protocol was then tested with the use of an adherence promoter (reference: VM652) instead of the dehydration step (see Figure 3. 4, schematic). The results of this test are shown on Figure 3. 4, right picture. On this picture, the Cu underneath the photoresist remains un-etched. This technique therefore slowdowns Cu etching process enough so that the Gr channel is fully protected. This new protocol was kept in the fabrication protocol.

3. Passivation of the contacts.

The metallic electrodes are passivated using SU8 photoresist to prevent any electrochemical reaction to happen when the sensor is in operation in a liquid environment. This passivation step is also used to clearly define the graphene sensing area for each transistor as illustrated on Figure 3. 2. When the SU8 resist dries on the sensor, we can see a tendency to the creation of some cracks in the corner of the sensing areas. Tests were carried out in collaboration with Adrien Hugo to remove or reduce these cracks. Eventually, a soft bake (5min at 150°C on a hot plate) of the devices after the passivation layer drying allows to reduce or eliminate the SU8 cracks.

Each fabrication step is critical when processing graphene, since lattice defects or surface contamination can drastically affect its electrical properties. Having a clean graphene through the process is essential for a reproducible fabrication process and to obtain a suitable graphene-metal electrical contact.

From the transfer of the Gr on the Si/SiO_2 substrate to the end of the process flow, extra care was provided to protect the Gr single layer though the addition of protective layers and rinsing.

Microscopic, SEM (Scanning Electron Microscope), topographic and spectroscopic characterizations were realized all along the whole optimization of the fabrication process (Hugo, 2020). The results are highly promising and extremely good quality sensors were produced by using our process flow. In addition to the characterizations during the development of the fabrication process, microscopic observations were realized after each main step when producing the sensors (see Figure 3. 2) to ensure:

- The quality of the metallic tracks.

- The integrity of the Gr sheet and patterning quality. Manipulation of the monoatomic Gr sheet can create breaks or holes in the lattice. It is important to verify the condition of the lattice on the top of each SGFET.
- The integrity and quality of the SU8 passivation layer patterns.

To manufacture six chips as presented on Figure 3. 2, five days are necessary to one person. The different steps of the fabrication have to be realized in a sequential manner as there is no possibility to accomplish two steps in parallel. Furthermore, some steps like the Gr transfer (Figure 3. 3) are not suited for a future automation and this could be an obstacle in the perspective of a future industrialisation of the process.

3.1.2 Poly-SGFET

The second type of Graphene-based SGFET sensors is developed by Grapheal, a start-up located in Grenoble, France. If the type pf biosensor is the same (SGFET), the used materials and the manufacturing steps differ. The interest in starting a collaboration with Grapheal lies in two points for this thesis project:

- The manufacturing time of this second type of SGFET is significantly lower: the production of a week at the CEA could be made in a day at Grapheal. This is partly due to the fact that several fabrication steps can be realized in parallel which is a real time saver compared to the Si-SGFET fabrication.
- The characterization bench at Grapheal offers the possibility to test several SGFETs in parallel (up to sixteen) compared to one at a time using the CEA bench.

These three aspects allow the multiplication of the tests (reproducibility of the results, controls, concentration gradient…) over a short period of time. This was an interesting asset to exploit provided that they give similar results to the Si-SGFETs made in clean room.
Figure 3. 5 presents the structure of this second type of SGFET.

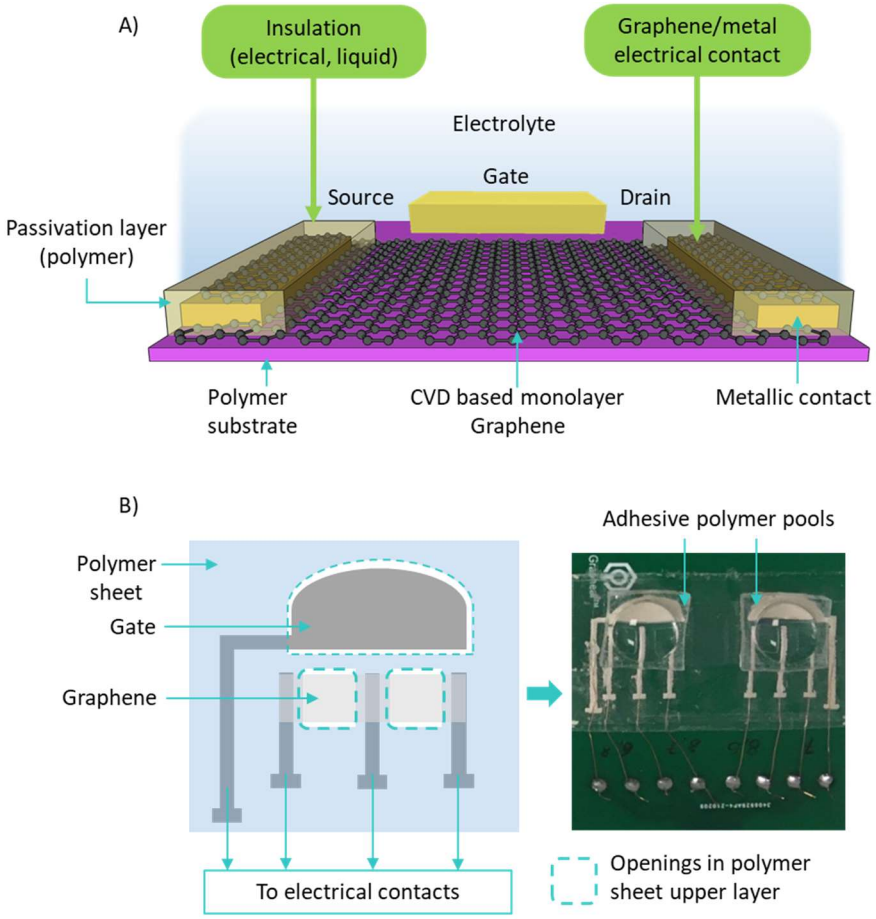

Figure 3. 5 Presentation of the Grapheal version of the SGFET. A) Schematic view of the transistor composition. B) Presentation of the SGFET Grapheal design and picture of a complete device (four sensing areas). One gate electrode is associated with two graphene sensing areas.

The sensor substrate is made of flexible polymer (Polyethylene terephthalate, PET) instead of Si. To differentiate this SGFET version from the Si-SGFET, it will be named Poly-SGFET with reference to the type of substrate used here.

The electrodes are screen-printed on it using a silver ink. The electrode design includes a common gate electrode as presented in Figure 3. 5. The Gr is CVD grown on a Cu sheet (in house or other sources) and transferred on a polymer layer to ease its manipulation. The Gr, pealed from its polymer layer using tweezers, is positioned in between the Source and Drain electrodes, as for the CEA sensor. The electrical contacts are kept safe from any contact with the electrolyte by adding another polymer layer (same as the substrate underneath the Gr), sealed to the first layer using heat. This last layer, which plays the same role as the SU8 resin for the SI-SGFET, is previously laser cut to allow the Gr to be in contact with the electrolyte.

Around ten devices as the one presented on Figure 3. 5.B (right) can be made in a day by one person.

3.2 Characterization benches: validation of the sensors' quality and electrochemical tests

Si-SGFETs and Poly-SGFETs were tested on their dedicated characterization benches. After the presentation of the characterization benches, the results for the Si-SGFET and Poly-SGFET will be presented and compared.

3.2.1 Si-SGFET

3.2.1.1 Characterization bench

The Si-SGFETs were characterized in dry and liquid conditions using an adapted characterization bench presented in Figure 3. 6.

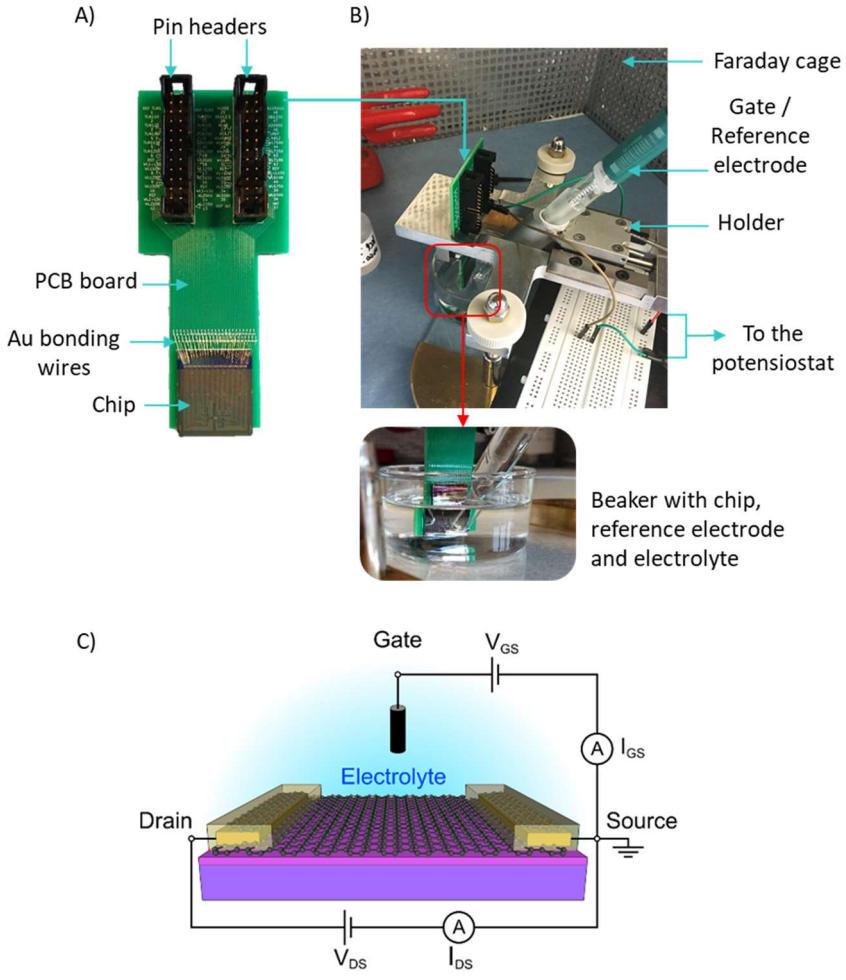

Figure 3. 6 SGFET experimental setup for CEA sensors with: A) Picture of the chip glued and wire-bonded to the PCB, B) Picture of the chip and reference electrode maintained in position by a home-made holder and soaking in a beaker, C) The electrical schematic of the setup.

First, the chip presented in Section 3.1.1 is bonded to a Printed Circuit Board (PCB) as presented in Figure 3. 6.A. The electrical contacts of the chip are wire-bonded using gold wires to the corresponding pads. Each contact can be individually addressed using the pin headers at the top of the PCB. Using a holder, the chip and an Ag/AgCl reference electrode are positioned in a beaker (Figure 3. 6.B). This holder allows the chip and the reference electrode to always have the same relative position (1 cm) in between them for all the tests. The electrodes are connected to a modular PGSTAT128N potentiostat from Metrohm. This potentiostat is equipped with a bi-potentiostat module to allow the control of both drain-source potential and gate current (Figure 3. 6.C). For all the measurements, the set up was placed into a Faraday cage to avoid background noise.

The measurements are realized with the NOVA 2.1.4 software from Methrom. Two type of measurements were performed on this software:

- A resistance test performed at 0 V gate voltage before the liquid characterization. This test gives an information on the Gr / metal contact interface.
- A field effect test performed in liquid conditions. This test is realized using a PBS 10^{-3}M (Phosphate Buffer Saline) solution with a Drain-Source polarization (V_{DS}) of 0.1 V. The Gate Source potential (V_{Gate}) evolved in a [-0.25V; 0.25V] scan window at a scan rate of 0.01 V/s. The scan window can possibly be extended to [-0.4 V; 0.4V] when needed. The drain source current (I_{DS}) as well as the Gate Source current (I_{GS} or also known as the leakage current, $I_{leakage}$) are recorded. The number of scans can be chosen to reach the stability of the sensor if needed.

An additional Python program was used to organize the files generated by the NOVA software for each test.

3.2.1.2 Extraction and exploitation of the data

Gr is a semimetal material, also classified as a zero gap semi-conductor. It is made of carbon atoms arranged in hexagonal structure, as shown in Figure 3. 7.A,B. Figure 3. 7.C showcases the unique energy band diagram of the Gr. Due to the presence of the π-orbitals, the energy spectrum has two energy bands: a valence band (at lower energies) and a conduction band (at higher energies). The conduction and valence bands intersect in some particular points as visible on Figure 3. 7.C. This point coincides with the Fermi level of the neutral system in the energy spectrum which is called the Dirac point. At this point, the Density of State (DOS) is zero but in the same time, there is no gap in the band structure, giving the Gr the name “zero gap semi-conductor”.

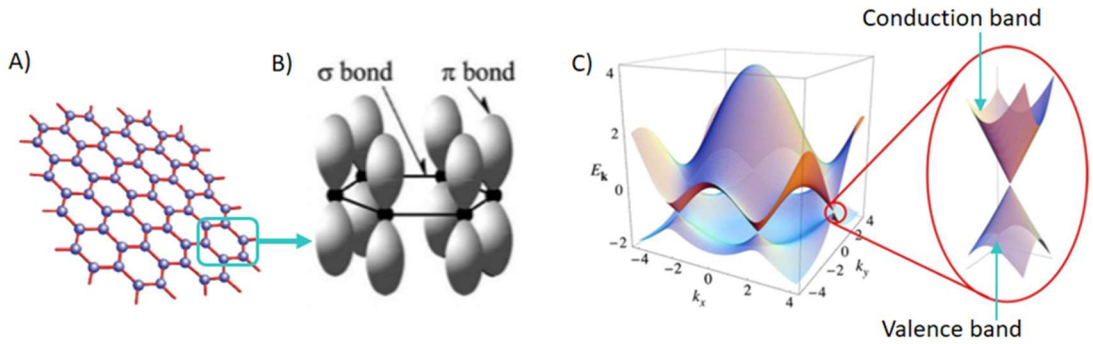

Figure 3. 7 A) Schematic of the graphene atomic monolayer, B) σ and π bonds and energy band diagram of the graphene. The figure is adapted from Basu et al. (2010) and Castro Neto et al. (2009)

The transition of the Gr channel electrons from the valence to the conduction band and the position of the Dirac point are visible during a field effect test, as described on Figure 3. 8, from (Hugo, 2020).

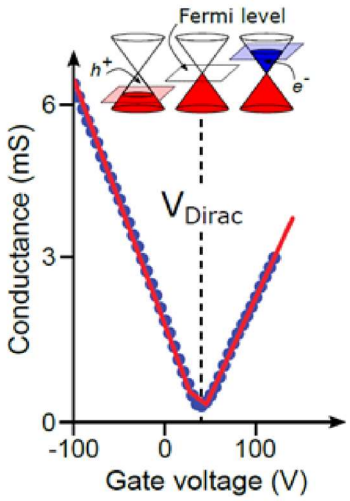

Figure 3. 8 Graphene channel characteristic transfer curve when subjected to different grid voltage. The conductance, proportional to the current is reported on the y-axis. Figure from Adrien thesis manuscript.

At the beginning of an experiment, only the bare Gr layer is present. A field effect test is run within the [-0,25V; 0,25V] V_{Gate} range and the black curve is schematized in Figure 3. 9.

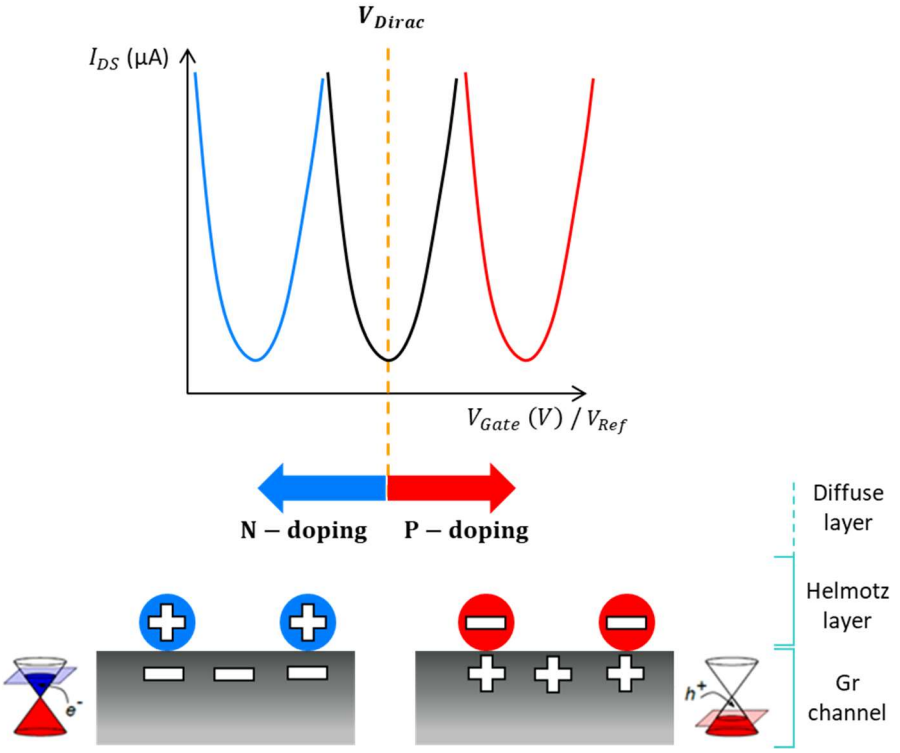

Figure 3. 9 Presentation of the transfer curve obtain when a field effect test is run and illustration of the effect of doping on the Dirac point of the curve

The Dirac point (V_{Dirac}), introduced previously is commonly used to localize the obtained transfer curve.

When biomolecules are introduced at the electrolyte / Gr interface (functionalization of the Gr or molecule detection), the organisation of the charges at the interface (Helmotz layer, Figure 3. 9) changes. These charges interact with the ones (electrons and holes) within the Gr layer. The thickness of this interface is controlled by the electrolyte composition (9.6 nm thick here in PBS 10^{-3}M). The new composition of the Helmotz layer shifts the neutrality point of the Gr/electrolyte interface (V_{Dirac}) to a new value. If the charges introduced at the interface are positive (blue case on Figure 3. 9), some electrons will accumulate in the conduction band of the Gr atomic layer, leading to an n-doping of the Gr. On the transfer curve, the result is a shift of the curve and so the Dirac point towards negative voltage values.

As introduced in the 3.1.1 section, the leakage current $I_{leakage}$ needs to be as minimal as possible to increase the SGFET performances. In the CEA characterization bench, $I_{leakage}$ is measured between the gate electrode and the transistor source, simultaneously with the drain-source current thanks to the bipotensiostat module. Typically, the leakage current for the CEA SGFETs is under 10 nA as illustrated on the following graph.

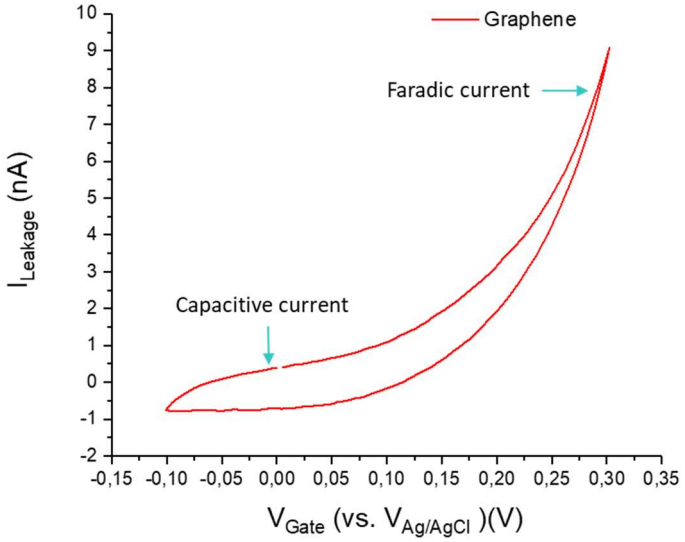

Figure 3. 10 $I_{leakage}$ curve for a Si-SGFET without any functionalization on the graphene channel. is measured in parallel of using the bipotensiostat module.

Within the appropriated voltage window, the leakage current remains reversible (capacitive current). When approaching the limit of this window, the leakage current increases quickly and may cause hysteresis. In aqueous conditions, applying potentials outside of this window can induce water electrolysis, producing O2 and H2 during the oxidation and reduction reactions (faradic current). The chemical modifications induced at the Gr / electrolyte interface and is irreversible and can damage the Gr structure. It is therefore essential to stay within a scanning window that avoids this phenomenon.
All the data were processed using the Origin, a scientific data processing and analysis software.

3.2.2 Poly-SGFET

During the collaboration with Grapheal, the characterization bench has been in constant evolution. Nevertheless, the characterization conditions and protocols of the two sources of sensors are close enough to enable the comparison of the results (see section 3.4).

3.2.2.1 Characterization bench

As for the CEA transistors, the Poly-SGFETs sensors are bonded on a PCB board. The contacts are made using traditional tin solder (Figure 3. 11.A right).

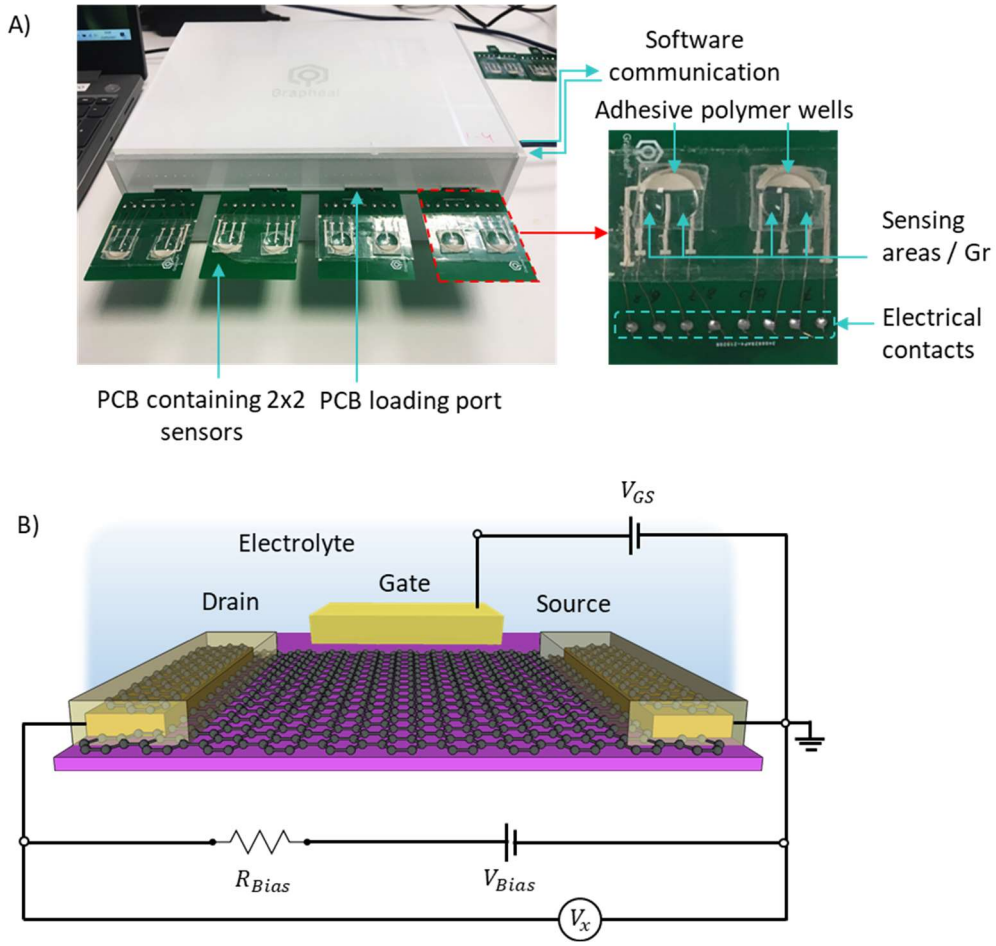

Figure 3. 11 SGFET experimental setup for Grapheal sensors with: A) Picture of PCBs loaded on the deck and close up on a PCB with 4 SGFETs, B) The electrical schematic of the setup.

Each PCB exhibits four Poly-SGFETs as presented in Figure 3. 11.A. Two Poly-SGFETs (sensing area in Figure 3. 11) share one Gate electrode and the same Drain electrode. These two Poly-SGFETs share also the same electrolyte, kept on the top of the electrodes by a polymer well. 200µL of solution can be poured in a well without leakage issues.

Four PCBs can be loaded in parallel on a deck developed by Grapheal (Figure 3. 11.A) so that a total of sixteen Poly-SGFETs can be tested at the same time. The deck is connected to several modules creating the voltage divider bridge presented in Figure 3. 11.B, to obtain the resistivity of the channel (R_{DS}).

$$V_x = \frac{V_{Bias} \times R_{DS}}{R_{Bias} + R_{DS}} \Rightarrow R_{DS} = \frac{R_{Bias} \times V_x}{V_{Bias} - V_x}$$

Among the components of the previous figure and formula, R_{Bias} had a value of 100 kΩ and V_{Bias} a value of -0,6V. During the test in liquid conditions V_{GS} swept in between 0,0V and 0,8V

and V_x was recorded. The Grapheal bench measures a resistivity whereas CEA bench measures a current. This will change the look of the transfer curve (upside down compared to Figure 3. 9) but the position of the Dirac point remains the same.

Before operating in a liquid environment, a capacitance measurement was performed on each SGFET, similar to the one done at the CEA, to quantify the quality of Gr / metal contact interface.

The measurements in liquid conditions were realized with the Grapheal software. Three types of measurements were performed:

- A resistance test, performed at 0 V gate voltage before the liquid characterization. This test gives an information on the Gr / metal contact interface.
- A field effect test. These tests were realized in a PBS 10^{-3}M solution. PB 10^{-3}M (PBS without the salt) could also be used to extend the Debye layer of a few nanometers. The Gate Source potential evolved in a maximal scan window of [0,0V; 0,8V] at a scan rate of 1 mV/s. The resistance R_{DS} in between the Drain and the Source was recorded.
- A live test, allowing to measure the R_{DS} through time. A gate voltage can be applied during the recording.

3.2.2.2 Extraction and exploitation of the data

The recorded data were exploited in the same way than for the Si-SGFET. The only difference is that the resistance R_{DS} is displayed on the plot instead of the I_{DS} current. The main point of interest in the plot is the position of the Dirac point and its shift from one functionalisation step to another. For this reason, this difference does not have any impact on the exploited data. $I_{leakage}$ was not recorded as the setup did not allow to measure a second parameter in parallel of R_{DS}. This way, the quality check of the Poly-SGFET is realized only at the beginning of a test, by measuring its resistance. If the doping of the Si-SGFETs was consistent from one batch to another one, the doping of the poly-SGFETs could vary from positive to negative doping. This did not affect the experiments conducted thereafter. All the data are processed using the Origin software as for the Si-SGFET data.

3.3 SGFETs functionalization and characterization of their behaviour

After the validation of the fabrication, the next step in the development of a sensor for biodetection is the characterization of its behaviour in liquid conditions, in presence of bioreceptors and targets.

Alava et al. (2013) demonstrated that single layer Gr is interesting for lab-on-chip analysis systems but they pointed out that some biomolecules may not keep their 3D integrity and functionality when in contact with Gr. For proteins, important deformations leading to the loss of their functions can be observed depending on the stability of their 3D folding structure. Various parameters can impact this stability like the nature of the sorbent or the number of

nonpolar amino acids and the energetics of the equilibrium between folded and denatured states.
To overcome this issue, linker molecules as PBASE (1-PyreneButyric Acid N-hydroxySuccinimide Ester) interface bioreceptors with the surface of Gr. The PBASE linker, presented on Figure 3. 12 (from Hugo, 2020) is widely used in the literature (Mukherjee et al., 2015; Park & Yan, 2013).

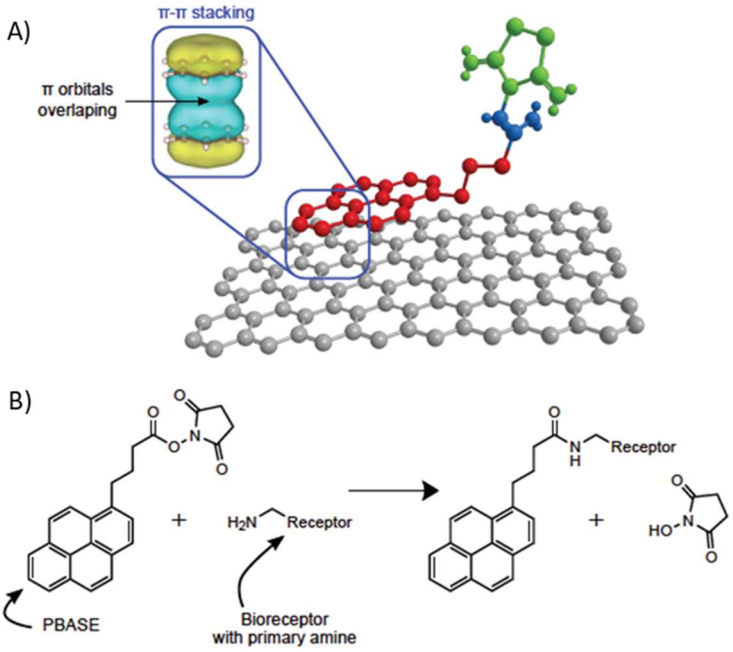

Figure 3. 12 A) PBASE interacting with graphene by π-π interactions. B) Chemical reactions of bioreceptors grafting to PBASE by nucleophilic attack of the primary amine on the NHS leaving group. From Adrien Hugo thesis manuscript.

It is made of an aromatic pyrene foot which interacts with the π electrons of the graphene layer through π-π interactions. A NHS ester group is attached to the pyrene feet (see Figure 3. 12.B). It is known to be a good leaving group having a nucleophilic reaction with the primary amines group contained in the proteins and in the side-chain of lysine amino acid residues.
This linker is an interesting option to link with proteins and keep them at proximity of the Gr while avoiding denaturation by stacking on the Gr.

Although PBASE is commonly used, it is not unambiguously and systematically proven that the biomolecules functionalized on the linker keeps its functionality (Alava et al., 2013). The PBASE has a certain rotation degree angle, showed in Figure 3. 13.A. This flexibility does not guaranty the orientation and the distance of the biomolecule relatively to the Gr. So even with this linker, there is still a non-negligible probability that it will stack on the Gr and be denaturised (Mann & Dichtel, 2013a).
Cooperative work between the CEA-LETI and Pr. William Dichtel from Northwestern university led to the design synthesis of a new and innovative linker, called the tripod (Mann et al., 2013; Mann & Dichtel, 2013b).

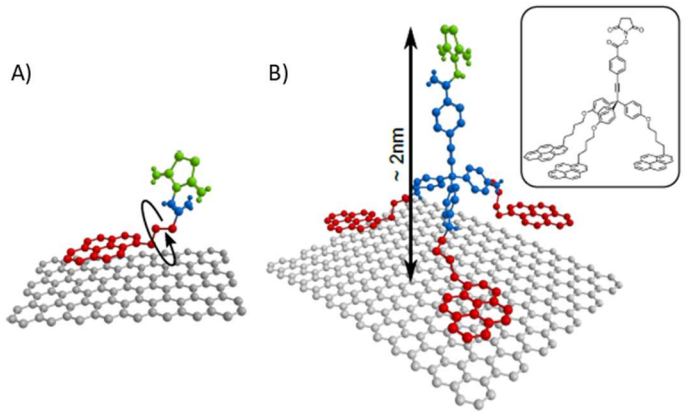

Figure 3. 13 A) Presence of a rotational degree of freedom along the carbon chain of the PBASE linker, B) Representation of the tripod linker stacked on graphene thanks to its three pyrene feet (red) projecting its functionality (green) away from the graphene surface. The atomic structure is shown in inset.

This molecule, presented in Figure 3. 13.B is composed by three pyrenes feet that are non-covalently adsorbed on the Gr, as for the PBASE linker. The three feet bring stability to the linker / functionalized protein structure (no linker flexibility) and avoid the protein denaturation. As for the PBASE, the tripod is equipped with a NHS functionality to bind to targeted biological molecules. The fact that there is no rotational degree of freedom in this linker and anchors the molecules at constant distance of the Gr.

Previous studies (Alava et al., 2013; Bharadwaj et al., 2016; Mann & Dichtel, 2013a, 2013b; C. Sun et al., 2015) have compared the two linkers and reported the following observations:

- The tripod – Gr interaction is more stable with a desorption rate in THF 1000 lower than the PBASE which is disappearing under 10 min. After 12 hours, the tripod was still present on the Gr at 86% of its initial coverage (Mann & Dichtel, 2013a). The tripod feature was also successfully tested in aqueous environment by Sun et al. (2015) to passivate graphitic regions of a graphene oxide substrate.
- The tripod has a slower charge transfer than the PBASE. The most likely hypothesis is that the tripod projects its active function further away from the Gr than the PBASE does. This hypothesis was confirmed by an additional work developed by Dichtel and his team (Mann & Dichtel, 2013b) on the tripod by testing several “foot motives”. They observed that the PBASE footprint larger was than the one of the pyrene moiety (1,7 mm^2 and 0.7 mm^2 respectively). The footprint of the tripod was 2.3 mm^2, a result very close from the expectation.
- The tripod can effectively maintain biomolecules away from Gr while protecting them from denaturation. Anti-E.Coli antibodies were immobilized onto PBASE, tripod and onto bare Gr (Mann & Dichtel, 2013a) . During the E.Coli cells recognition step, only the tripod showed a cell density noticeably different than the negative control tests. This result exhibits the fact that E.Coli cells demonstrate little or no affinity with the Anti-E.Coli antibodies adsorbed on bare Gr or on the PBASE linker, highlighting their loss of functionality. Other works (Alava et al., 2013; Bharadwaj et al., 2016) showcased similar results obtained with enzymes and proteins.

As displayed above, the tripod is a real asset in developing a SGFET sensor for biosensing applications and was functionalized on the Gr of our SGFET as the first layer of the biodetection structure.
Unlike for the Clark and Lyons experiment mentioned at the Chapter 3 introduction, the detection structure used in this thesis is based on the "capture" of target molecules. This strategy does not involve catalytic reactions where the product of an enzymatic reaction is detected by the transducer layer. Without electron transfer from this type of reaction, we had to investigate and understand the mechanisms of the Gr – tripod detection structure in aqueous environment. To do so, some proteins whose interaction mechanisms have been well described in the literature were used to functionalize the detection structure and to study the behaviour of our sensors.

The following article submitted for publication in ACS (Applied Materials & Interfaces) describes the realized tests and lead to the validation of an electrochemical model for both Si-SGFET and Poly-SGFET sensors.

Biological sensing using non-covalent functionalization of graphene-based solution gated field effect transistors

Article submitted on October, 2021 in ACS (Applied Materials & Interfaces)

Authors

Juliette Simon 1,2,3⸸, Adrien Hugo 1,2⸸, Thomas Alava 2 , Jason A. Mann 4, William R. Dichtel 4 , Fabienne Blanc 3, Vincent Bouchiat 5 and Pascal Mailley 1,2

1 University Grenoble Alpes, F-38000 Grenoble, France
2 CEA, LETI, Minatec Campus, F-38054 Grenoble, France
3 University Clermont Auvergne, VetAgro Sup, INRAE, UMR Herbivores, F-63122 Saint-Gènes-Champanelle, France
4 Department of Chemistry and Chemical Biology, Baker Laboratory, Cornell University, Ithaca, New York 14853-1301, United States
5 Grapheal, 25 Av. des Martyrs, 38042 Grenoble, France
⸸ First authors
Correspondence: Juliette.simon@cea.fr

Abstract:

Biosensors for medical or veterinary sciences have to be highly sensitive, easily adaptable for various type of detections, compact, minimally invasive, inexpensive and electable for mass-production. Through past decades, rise of microelectronic has enable the production of highly sensitive sensors at low cost with mass-production capacities.

In this context, the discovery of highly conductive, lightweight, flexible, transparent, mechanically robust, CVD graphene has brought interest from the biosensors community. Indeed, graphene high specific area due to its atomic thickness is particularly appealing for the detection of charged biological species. Previous work in our group demonstrated an innovative protocol for the fabrication of highly sensitive graphene-based Solution Gated Field Effect Transistor (SGFET). This study presents the results of the biological detection campaign realized to understand the behaviour of the charges at the sensor / electrolyte interface. Graphene was functionalized with a unique tripodal molecular compound and charged proteins. After each functionalization step, the evolution of the current in a [-0.25; 0.25V] voltage window was recorded. Unexpectedly the negatively charged proteins led to the n-doping of the Gr. Several tests on the selected proteins led to the validation of an electrochemical model of our detection structure based on our observations.

Keywords

SGFET; biosensors; CVD graphene; biological detection

Introduction

Biosensors have an increasing role in medical and veterinary science. To be competitive these biosensors have to be highly sensitive, easily adaptable for various types of detections, minimally invasive, compact unexpansive and be mass-produced. Through past decades, the rise of microelectronic has enabled the production of highly sensitive sensors at low cost with mass-production capacities. The first Field-Effect-Transistor (FET) based biosensors were introduced by Bergveld and coworkers (1970). These type of sensors called ISFET (Ion-Sensitive Field-Effect-Transistor) are made of a p-doped Si substrate with two n-doped areas (Source and Drain) separated by a Si/SiO2 channel. The potential applied between a reference electrode and the Si bulk substrate creates a channel between the Source and the Drain whereby the electrons flows when a difference of potential is applied between these two points. This type of device transduces a surface charge variation into a current modulation and is historically used for application such as pH sensing.

More recently, the discovery of highly conductive, lightweight, flexible, transparent, mechanically robust, Chemical Vapor Deposition (CVD) graphene has brought interest from the biosensors community (Bae et al., 2010; Li et al., 2009). Indeed graphene (Gr) high specific area due to its atomic thickness is particularly appealing for the detection of charged biological species as illustrated by Chen et al. (2012) and Mukherjee (2015).

Previous work in our group (Hugo, 2020) demonstrated a unique fabrication protocol of a Graphene-based Solution-Gated Field-Effect-Transistor (SGFET) technology operating in an

aqueous environment. The heightened electrical sensitivity of SGFET combined with the graphene characteristics is an encouraging path for a new generation of highly sensitive biosensors.

The graphene has a polarizable and hydrophobic surface, which can interact strongly with biomolecules. It is expected that the binding of a charged molecule induces a corresponding doping in the Gr single layer. Depending of the nature of the charge introduced at the Gr / electrolyte interface (positive or negative), the Gr channel will be doped accordingly (n-doping or p-doping respectively). The doping of the Gr channel can be observed with field effect tests before / after a recognition phenomenon as the transfer characteristic IDS/VG presented on Figure 1 will shift accordingly to the Gr doping.

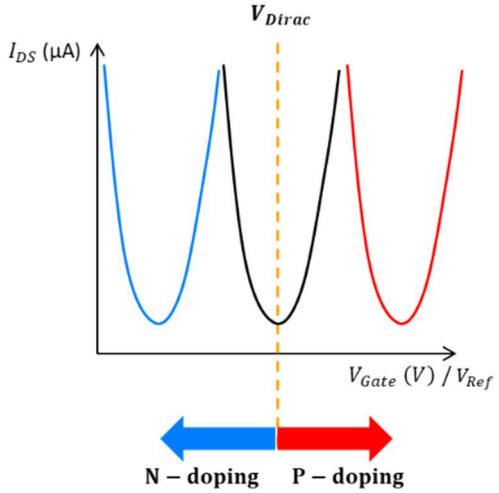

Figure 3. 14 Schematic of the transfer curve shift of a Graphene-based SGFET. Black curve represents the transfer curve before introduction of charged species at the graphene/electrolyte interface. The introduction of charged species induce an n or p-doping of the graphene channel, observable by a corresponding shift of the transfer curve.

The position of the transfer curve is usually indicated by the Dirac point, showed on Figure 3. 14, black curve. This point represents the Fermi level of the neutral system in the energy spectrum of the Gr.

However, it was shown that direct contact with graphene can deteriorate the function of some proteins like biomolecules (Katoch et al., 2012). To avoid this phenomena, a linker between the Gr and the molecule can be used to keep the molecule functionality away from the Gr surface. Alava and coworkers (Alava et al., 2013; Mann et al., 2011; Mann & Dichtel, 2013b) designed and tested an innovative tripodal linker (Figure 3. 15) that works around this challenge by anchoring proteins away from the Gr surface, preventing a loss of function and without disrupting graphene's desirable electronic structure. Compared to the commonly used in the literature P-BASE linker (1-pyrenebutanoic acid succinimidyl ester), the tripod has a series of advantages: no rotational angle (see Figure 3. 14), the functionality of the molecule is kept away from the Gr preventing the denaturation risk; a constant distance between the molecule and the Gr layer; a desorption rate 1000 times lower than P-BASE (Mann & Dichtel, 2013a).

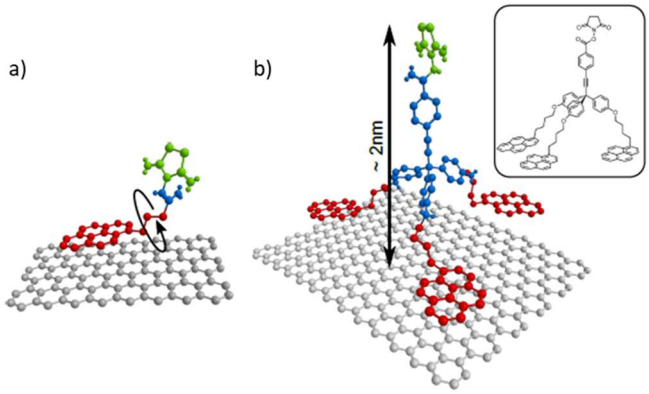

Figure 3. 15 . a) PBASE structure with NHS termination, non-covalently bonded to the Graphene lattice and with its rotational degree of freedom. b) Tripodal structure. Three pyrene feet are non-covalently bonded to the graphene layer. An NHS ester group is attached to the structure for further probe functionalization. Figure from (Hugo, 2020)

In the present article, Gr surface was non-covalently functionalized with the tripodal molecule as the first layer of the biodetection structure. The objective of this article is to detect a probe/target recognition phenomenon with this detection structure. Several model proteins whose interaction mechanisms are well described in the literature and without charge transfer during their recognition phenomena were selected and tested. The impact of the probe / target recognition was observed with the associated shift of the transfer curve. Avidin molecule and its derivative (neutravidin and streptavidin) were chosen along with biotin for a first probe / target complex. The functionalization steps are presented on Figure 3. 16.

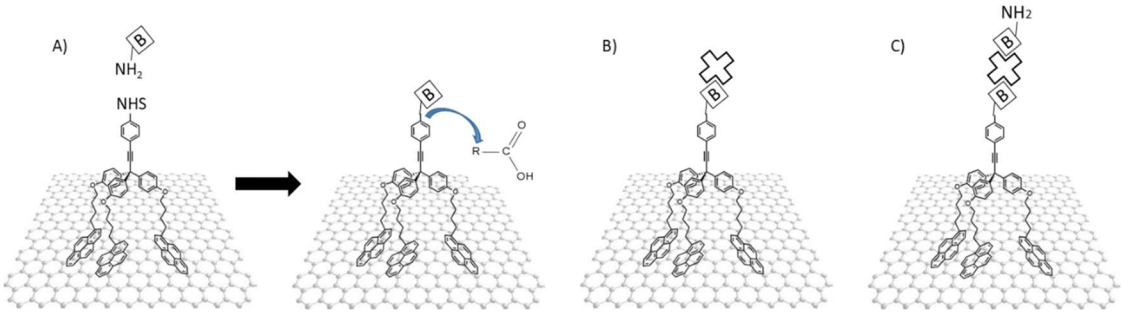

Figure 3. 16 Probe / target recognition steps using the graphene / tripod detection structure. a) Biotin derivated molecule (Biotitn-PEG-NH2) is functionalized on the tripod. B) One of the four binding sites of avidin or derivatives binds to biotin. c) A second biotin derivated molecule binds to a second recognition site of the avidin or derivative.

Avidin and its derivatives have a relatively low dissociation constant value: 10^{-14}M (streptavidin,(Duan et al., 2012)); 10^{-15}M (avidin: (Kamperman et al., 2019)); 10−11M (neutravidin, (Vermette et al., 2003)), ensuring a stable bond with biotin. These proteins have four binding sites. The detection of a second biotin can be done to have both small probe / large target and large probe / small target recognition phenomena in the same experiment. A second recognition system was tested with the Concanavalin A (Con A) and Methyl alpha D mannoside (Methyl α) molecules. In this configuration, a NH2 terminated Con A was functionalized on the tripod to further detect the Methyl α molecule. All these molecules being differently charged (see Table 1), the different shifts should induce different direction

shifts of the Dirac point. These data will help us to understand the inner mechanisms of the Gr / tripod detection structure during a probe / target recognition phenomena.

Material and methods

1. Chemicals and graphene

Avidin, Neutravidin, Streptavidin, Concanavalin A (NH2 terminated), Methyl alpha D mannoside, Biotin-PEG-NH2 were purchased from Fisher-Scientific. The tripodal molecule (NHS-Tripod) was provided by the William Dichtel's team from Northwestern University, Illinois. Tetrahydrofuran (THF, ≥99.9% purity) was purchased from Sigma-Aldrich. Single layer of graphene was purchased on copper foil from Graphenea company.

2. SGFET sensor

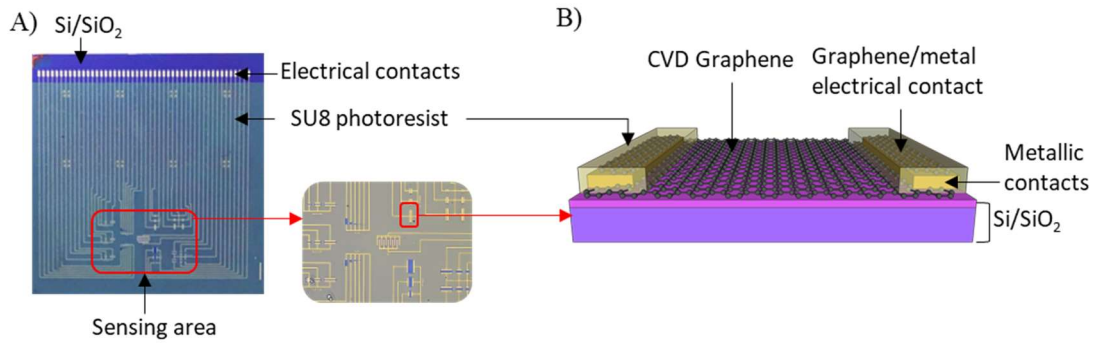

Figure 3. 17 . A) SGFETs device produced CEA clean rooms with close up on the sensing part B) Schematic of the architecture of a SGFET devices.

SGFET chips were produced in the PTA (Upstream Technological Platform) clean rooms (class 1000 or ISO6), located at the CEA Grenoble, France. The fabrication process and the graphene transfer method are described in (Hugo, 2020). The single layer of Gr is transferred on a Si/SiO2 substrate with pre-patterned electrodes. The Gr is patterned to fit in between the SGFET electrodes as presented in Figure 3. 17. Designed to perform to be operated in a liquid environment, electrical contacts of the chip are insulated to prevent any parasitic leakage current. SU8, a photosensitive resist, was used to passivate the metallic contacts while keeping the graphene areas exposed to the electrolyte.
A second source of SGFETs used for additional tests were provided by the Grapheal company (Grenoble, France).

3. Electrochemical setup

The SGFET chip was bonded to a Printed Circuit Board (PCB) (Figure 3. 18.B) via gold wires. Each electrode can be addressed individually using the pin headers at the top of the PCB. A homemade substrate holder was designed to hold the PCB and the reference electrode (Ag/AgCl). The electrodes were connected to modular PGSTAT128N potentiostat from Metrohm and the measurements were performed using the associated NOVA 2.1.4 software.

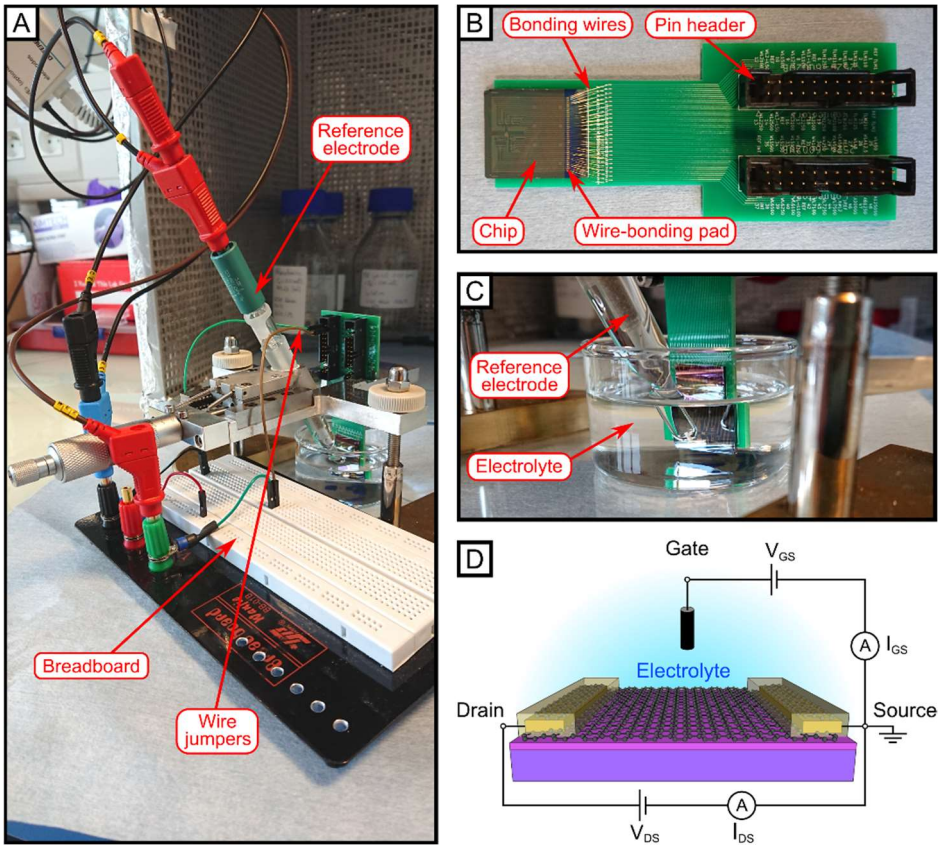

Figure 3. 18 (from (Hugo, 2020)(Hugo, 2020)) Electrochemical bench presentation. A) PCB with device glued on and wire-bounded. Each electrode on the chip is connected to a pin on the upper part of the PCB. B) Close up on the beaker containing the electrolyte, the reference electrode and the chip. C) Electrical schematic of the setup.

This potentiostat was equipped with a bi-potentiostat module that allows the control of both drain-source and gate-source potential (Figure 3. 18.D). IDS and IGS were recorded as shown on Figure 3. 18.D. The IDS measurement allows to follow the evolution of the SGFET doping while the IGS measurement gives information on the sensor quality. When the GFET is operating in liquid, a difference of potential is applied between a reference electrode (Ag/AgCl electrode also called the gate here) and the Gr channel. This can cause electrochemical reactions to happen between the reference electrode and the Gr channel. These reactions would be detectable by measuring the leakage current (IGS). For all the measurements, the set up was placed into a Faraday cage to prevent background noise.

4. Grafting and bio detection protocol

Electrochemical tests were conducted in between each functionalization step in a 10^{-3} M PBS (Phosphate Buffer Saline) solution at pH 7.6 within a [-0.25; 0.25V] potential window. These ionic strength was chosen to get a Debye length of approximately 9.6 nm. The NHS-Tripod linker is about 2 nm high, the avidin and derivated molecules have a diameter of approximately 5 nm, 8 nm for Con A (Mangold & Cloninger, 2006). Biotin-PEG-NH2 and Methyl α are small water-soluble organic molecule. The size of all these molecules allow the different recognition event to happen within the Debye layer.

The graphene surface was functionalized with the tripod linker by incubating the device in a 100 µM solution of NHS-Tripod. The sensor was then rinsed with pure THF (2 x 1 min) followed by deionized (DI) water (3 x 1min). The biotinylation of the tripod was realized with a 1 µg/L solution in 10^{-2}M PBS solution. After five minutes of functionalization, the sensor was rinsed with DI water (5 min). The targets recognition took place in 10^{-2}M PBS with a 50 µg/mL target concentration (30 min). Eventually, another biotin-NH2 molecule was added at the top of the avidin, streptavidin or neutravidin to test the ability of the sensor to detect two successive events.

For the second type of test, Con A (NH2 terminated) was functionalized on the top of tripod with a 50µg/mL solution in 10^{-2}M PBS solution. After 30 minutes, the sensor was rinsed with DI water (5 min). Recognition of the Methyl α protein took place in a 10^{-2}M PBS solution at 50µg/mL during 30 min.

Results and discussion

1. Assembly follow-up for targets detection

Avidin, Streptavidin and Neutravidin are biotin-binding proteins with four biotin-binding sites on each of them. Their isoelectric point makes them positively or negatively charged in this study experimental setting (see Table 3. 1). Con A is also a negatively charged protein which can bind to the non-charged Methyl α D protein. Figure 3. 19.A presents the transfer curves for the streptavidin test. From these data, the Dirac point was extracted as presented in Figure 3. 19.b for reasons of readability.

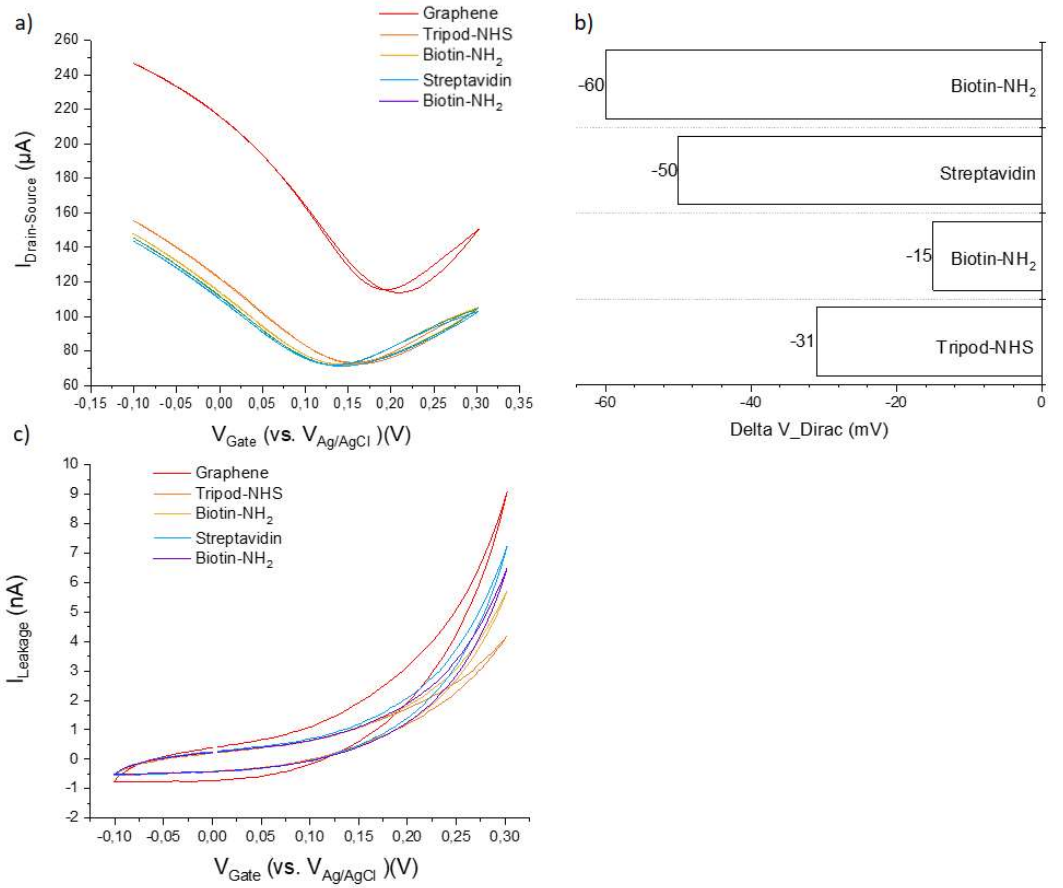

Figure 3. 19 Transfer curve (a), successive Dirac point (b) and leakage current (c) of the functionalized SGFET. Field effect tests were realized in PBS 10^{-3}M.

The first Dirac point shift is visible after the tripod functionalization on the Gr. The direction of the shift towards negative voltage values (ΔVDirac = -60 mV, Figure 3. 19.B) indicates an n-doping effect when a p-doping one is expected due to the presence of the NHS ester, an aromatic molecule which carries an electron donor group. The biotinylation, corresponding to the withdrawal of the NHS molecule (NHS / NH2 chemistry) induces a shift in the same direction (n-doping with ΔVDirac = -15 mV, Figure 3. 19.B). The negatively charged streptavidin protein causes a large left shift of the Dirac point (- 50 mV, Figure 3. 19.B). It was previously expected that a negatively charge protein would induce a p-doping of the Gr single layer but the reverse effect is observed on several steps of this test. As a last detection event another Biotin derivated molecule was functionalized and detected as a large n-doping can be observed on Figure 3. 19.B. It is interesting to point out that both small probe/ large target and large probe / small target detection were detected, even when the last recognition happened near the limit of detection of the SGFET (Debye layer).

Alongside the field tests realized at each functionalization or recognition step, the leakage current was measured. The corresponding curves are presented on Figure 3. 19.C The SGFET operates with a low leakage current under 10 nA. This current is drastically reduced after the Tripod functionalization, indicating that this step could help screening from the electrolyte the eventual graphene defects, which could be a source of leakage current.

Functionalization step	Molecule	Isolectric Point	Net charge in PBS 10^{-3}M - pH 7,6	Expected shift	Observed shift
Tripod	Tripodal linker				
Probe	Biotin-NH_2	--			
	Con A	5	negative		
Target 1	Streptavidin	5,6	negative		
	Neutravidin	6,3	negative		
	Avidin	10.5	positive		
	Methyl alpha	neutral	No charge		
Target 2	Biotin-NH_2				

Table 3. 1 Summary table of the different molecules used, their isoelectric point and their net charge in 10^{-3}M PBS medium. The expected doping following the functionalization of these molecules on the SGFET as well as the observed doping are presented on the right of the table (right shift: positive doping, left shift, negative doping).

For the Neutravidin and Avidin tests, shifts are equivalent to the streptavidin for the tripod and biotin functionalization steps as shown on Figure 3. 20.A. The Dirac point shift for the neutravidin recognition indicates an n-doping of the Gr, as for the streptavidin recognition. The Avidin which is positively charged in our experimental conditions and also shifts toward negative voltage values (-20 mV, Figure 3. 20.B). For the Con A functionalization on the tripod (Figure 3. 20.B) a negative shift of the Dirac point is observed (-10 mV). The Steptavidin, Neutravidin and Con A are negatively charged proteins and induces a shift toward negative values. If these results are not what were expected, they are nevertheless consistent. The Methyl α protein, detected by the Con A protein is not charged and generate a negligible 2mV shift as presented on Figure 3. 20.B (Dirac point detection ±5mV).

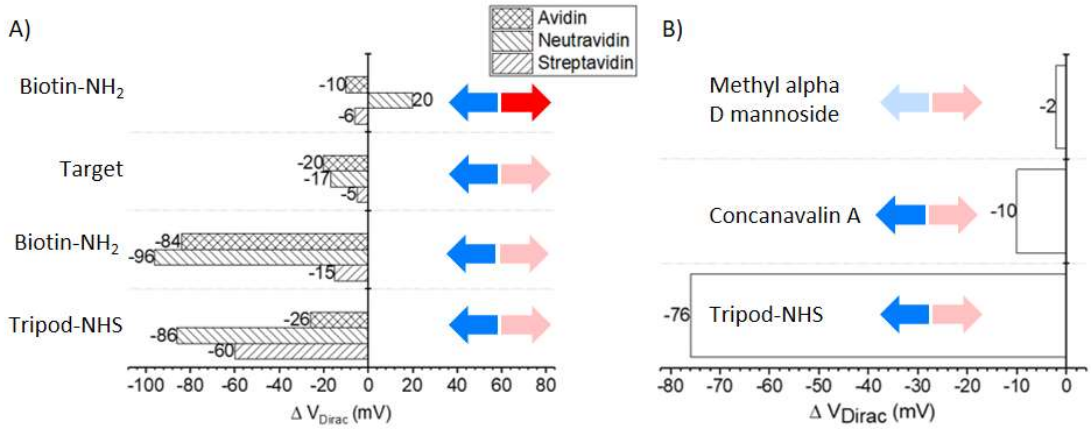

Figure 3. 20 Successive Dirac point for avidin, neutravidin and streptavidin tests (A) as well as for Con A test (A).

From the results of the negative and neutral molecules recognition, an electrochemical model can be proposed.
The immobilization of the negatively charge protein on the tripod, at 2 nm from the Gr can affect the ionic distribution of the Helmotz layer in between them. It is possible that, as presented in Figure 3. 21.B , the targeted protein is screened from the Gr layer by the excess of cations present in the EDL. The charges within the Gr react then to this ionic procession instead of reacting directly to the charge of the protein as visible on Figure 3. 21.A.

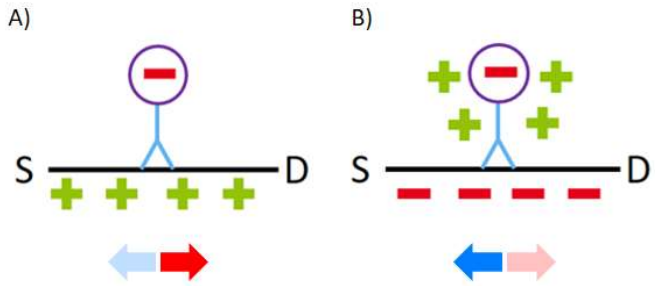

Figure 3. 21 Schematic interpretation of A) the expected and B) the actual electrochemical model for the SGFET sensor functionalized by the tripod linker.

2. The avidin case

This model presented above provides a possible explanation to interpret the negative shifts observed with negative charged proteins but it cannot explain the Avidin case (negative shift with a positive charged protein). It is reported in the literature that Avidin and bare Gr can form a stable complexe, primarily via hydrophobic forces along with electrostatic, and Van der Waals forces and hydrogen bonding interactions. (Macwan et al., 2017) work investigated this adsorption phenomena, demonstrating an attractive interaction in between avidin and bare Gr. This particular behaviour, schematizes on Figure 3. 21 could explain the right shift observed previously on Figure 3. 21.A.

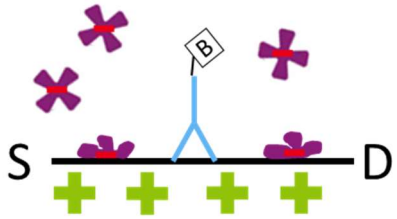

*Figure 3. SEQ Figure_3. * ARABIC 22 Schematic view of avidin's hypothetic behaviour during the SGFET functionalization.*

To validate this hypothesis, three trials were performed on the Graphene-based SGFETs from Grapheal. A replication of the test realized in Figure 3. 20 to ensure that the same behaviour occurs on the two types of sensors. An attempt at detecting Avidin without biotin derivated molecule functionnalized on the tripod linker. A second attempt at detecting Avidin with only the bare Gr layer.
For these three trials, the results shown on Figure 3. 23, present a shift of the Dirac point towards negative values for at the avidin step. The n-doping of the Gr layer for each of the three tests validates the avidin adsorption hypothesis. We can also see that the easier the

avidin has access to Gr (absence of biotin and then absence of biotin and tripod), the greater the shift.

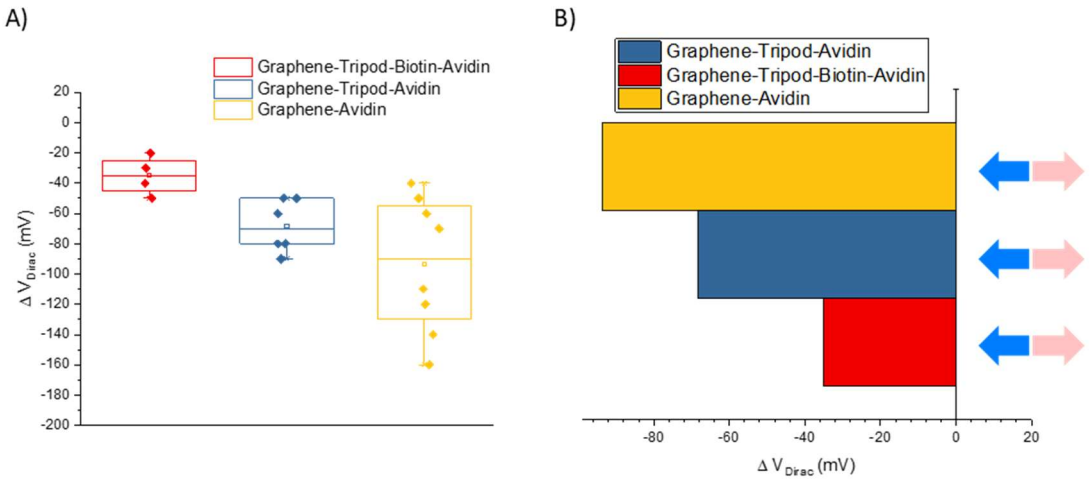

Figure 3. 23 A) Dirac point shift for the Biotin-Avidin recognition step (red), Tripod-Avidin recognition step (blue) and Graphene-Avidin recognition step. Each test was replicated four to eight times. B) Dirac point shift for the Biotin-Avidin recognition step (red), Tripod-Avidin recognition step (blue) and Graphene-Avidin recognition step. Each test was replicated between four and eight times. The mean value is presented here for each type of test.

Conclusion and opening

The primary objective of this study was to understand the behaviour of the developed SGFET sensor and tripodal linker when used for biosensing. The tripodal linker used to keep the proteins for being denaturised keeps a 2 nm space in between Gr surface and the targeted charged protein. This space impacted the electrochemical model of the SGFET sensor when is used in liquid environment. The charges in the single layer Gr channel react to the charged species present at the Gr / electrolyte interface. Due to the space in between the target proteins and the Gr, ions present in the electrolyte accumulate around the target, screening it from the Gr single layer. The Gr responds to this screen. In practice, when the detected charge is negative, cations accumulate around it and eventually the Gr channel is n-doped. This theory was tested with negatively or positively charged and neutral proteins. Only the Avidin, the only positively charged target, did not have the expected behaviour. The second objective of this study was to understand this specific behaviour. It was proved with additional tests that avidin has a great adsorption capacity on bare Gr unlike the other tested proteins. Even if some avidin do bind to the probe (Biotin-PEG-NH2), they will be screened by the ones adsorbed on the Gr. Our team is currently performing new studies in which new probes are tested to detect smaller molecules like hormones.

3.4 Comparison of CEA and Grapheal SGFETs

In the previous section, the results of the electrochemical characterization were discussed and the transfer function of the SGFETs was presented. During the thesis, two sources of SGFETs sensors were used: CEA (Si-SGFET) and Grapheal (poly-SGFET). The tests with avidin and streptavidin realised on the Si-SGFET sensors were also conducted on the Poly-SGFET sensors to compare them. Each test was realized on one Si-SGFET and one Poly-SGFET.

Figure 3. 24 and Figure 3. 25 present the successive ΔV_{Dirac} shifts through the whole experiment of avidin and streptavidin detection with the two types of SGFETs.

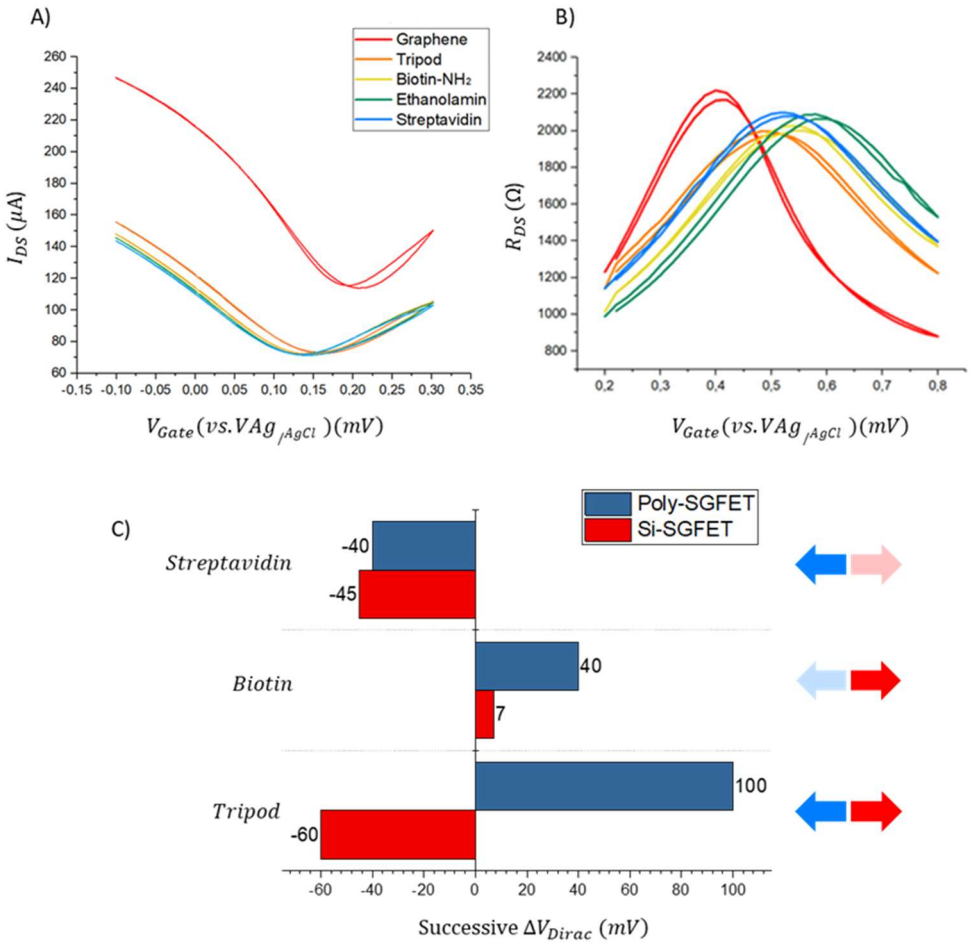

Figure 3. 24 Transfer curves for the Si-SGFET (A) and Poly-SGFET (B) and successive shifts (C) through the whole biosensing experiment of Streptavidin detection on the two sources of SGFET.

The first V_{Dirac} visible on Figure 3. 24.C (Gr + tripod) is on opposite direction for the two sensors. This is due to the original doping of the Gr, acquired during the sensor fabrication and manipulation before the test. Biotynilation induces a shift toward positive voltage values (p-doping of the Gr channel) in both cases. For the functionalization of streptavidin, a large

shift towards negative values (n-doping) and of similar amplitudes (-40 mV for Poly-SGFET and -45 mV for Si-SGFET) is visible on both sensors.

The avidin detection experiment was also duplicated on the Grapheal sensors and the results compared to the ones of the CEA SGFETs are shown in Figure 3. 25.

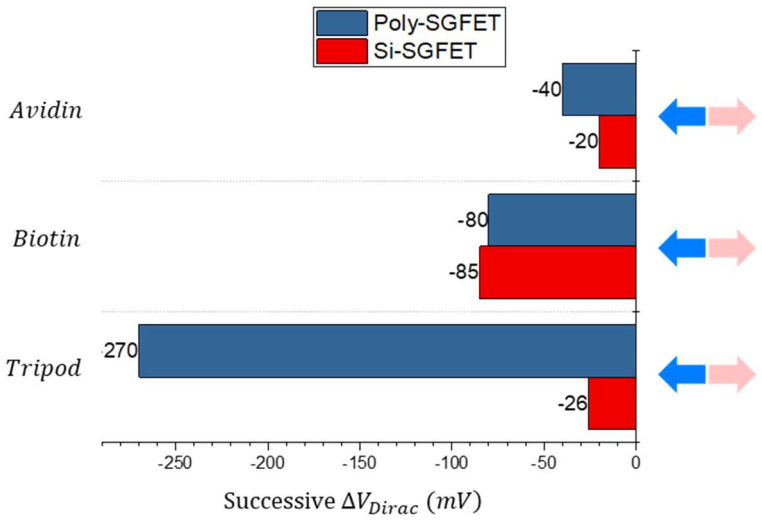

Figure 3. 25 Successive shifts (C) through the whole biosensing experiment of Avidin detection on the two sources of SGFETs

Both Si-SGFET and Poly-SGFET have an n-doped Gr at the beginning of the experiment. The fact that on both Figure 3. 24 and Figure 3. 25, the CEA sensors have a lesser doping than the Grapheal sensors comes from the fabrication methods and environment as the CEA SGFETs are produced in clean rooms. It was also found that depending of the manipulation or the source of the Gr monoatomic layer at Grapheal, the initial doping of the Gr could change. A resistivity measurement on the Gr sheet before the manufacturing of the sensor was realized to check on the doping.

The biotin induces a shift in the same direction (n-doping) but the Poly-SGFET presents a shift twice as important as for the Si-SGFET. As already discussed in part 3.3 this result is unexpected for a positive charged protein as an n-doping effect has already been observed and explained with negative charged molecules such as streptavidin. As suggested in the article of section 3.3, the hypothesis is that avidin is adsorbed on the Gr surface rather than on the Biotin-NH_2 molecule.

To recapitulate this Si-SGFET / Poly-SGFET sensors and characterization bench comparison:

The fabrication protocol of the Si-SGFET sensors ensures the production of high quality sensors with the verification of the quality all along the fabrication process. They can be produced by batches of five to six sensors (five days of fabrication).
The Poly-SGFET sensor fabrication protocol conditions are very different from the Si-SGFET ones. Apart from the Gr produced in a different facility, the Poly-SGFETs are fabricated in an electronic lab, without the precautionary measures to avoid contamination applied at the CEA. The production of a batch of five to six devices (PCBs) could easily be made within a day.

The characterization bench used for the Si-SGFETs can test one device at a time but has a bipotentiostat module allowing the user to perform two measurements in parallel (I_{DS} and $I_{leakage}$) with good accuracy (±5mV for the determination of the Dirac point).
The characterization bench for the Poly-SFGETs has less options to personalize the tests than for the CEA bench as Grapheal develops its own software. However, the Grapheal bench offers the significant advantage to allow testing up to sixteen Poly-SGFETs in parallel (or 4 PCBs as presented in Figure 3. 11). This feature is of high interest for the next steps of the biosensor development to move forward more quickly on the hormones detection tests. It was reported by the Grapheal team that the measurement of the Dirac point was within a ±10mV accuracy.

Conclusion

This chapter was dedicated to the development and characterization of a SGFET sensor for biosensing applications. It was given the opportunity to test two versions of a Graphene-based SGFET sensor.

The Si-SGFET version, developed in CEA is made in clean room facilities. The fabrication protocol is robust and produces high quality sensors, suitable for biosensing. The electrochemical setup offers potent, flexible and complete characterisation options in air and liquid environment. A SGFET electrochemical characterisation campaign was realized using this set up to test the Graphene-based SGFET sensors as well as the efficacy of the tripodal linker. Results shown that the Si-SGFET in conjunction with the tripod have good potential to be used as biosensors. The results also highlighted the impact of the tripod on the Si-SGFET behaviour leading to the proposition of an electrochemical model for the sensor.

If promising results were obtained with the Si-SGFETs, a second type of Graphene-based SGFETs sensors was also tested and compared to the Si-SGFET. The Grapheal French start-up has developed its own sensors, fabricated on classical electrical benches. The fabrication of these Poly-SGFETs is about five times quicker but the quality of the Gr/metallic contacts as well as the cleanness of the Gr atomic monolayer is not as guaranteed as for the Si-SGFET. Nevertheless, the obtained results shown comparable behaviour to the Si-SGFET one.

After the realization and characterisation of the microneedles presented in Chapter 2, the second main objective of this thesis was to develop a protocol for the detection of two hormones: progesterone and oestradiol. Due to the Covid-19 pandemic putting a hold on the experimental part of this thesis, time to design and realize a second detection campaign on Si-SGFET and associated characterization bench was not feasible. As the Poly-SGFETs shown promising results in the first campaign, I made the decision to conduct the hormones detection campaign exclusively on the Poly-SGFETs, allowing to duplicate and sequence tests much faster than with the Si-SGFETs. With this decision, the goal was to validate a detection

protocol before the end of the thesis. The next chapter will present the biosensing experiments realized to detect oestradiol and progesterone.

This first series of experiments and the results were presented at several conferences during the course of the thesis:

- Graphene 2020, largest European Conference & Exhibition in Graphene and 2D Materials for an oral contribution.
- Biosensors 2021, world largest conference on this theme for poster contribution.
- ESEAC 2022, International conference on Electroanalysis for an oral contribution. This conference was initially planned in 2020 but postponed to June 2022.

- Chapter 4 -

Hormones: from dosage to detection

Introduction

In Chapter 2, the location of the patch was chosen according to the following criteria:

- Ease of access and handling for the farmer
- Low risk of soiling and impact
- Optimal tissue thickness and composition for microneedle implantation.

In Chapter 3, we developed a sensor and tested it for biosensing applications. Chapter 4 is at the interface of the two previous chapters.

To definitively validate the location of the patch (apex of the pinna, external side), we need to ensure the presence of the two targeted hormones (progesterone and oestradiol) in the cow's ear interstitial fluid and determine their concentration throughout the oestrus cycle. This monitoring of hormone levels in the cow's ear has not been presented yet in the literature to our knowledge. However, this information is of primary importance to detect an ovulation event. To respond to this need of information, a fluids sampling campaign was carried out on ten cows at the INRAe centre (Clermont-Ferrand, France). The strategy, experimental set-up and the exploitation of the data collected are presented in the first part of this chapter.

Hormones are molecules difficult to detect essentially because of their small size. The choice of the probe to be functionalized on the tripod gave rise to an important investigation phase of the different methods available with the following specifications:

- A small size to ensure that the recognition will happen under the Debye length.
- A high selectivity to recognize only the targeted hormones and avoid a “false positive” event during the ovulation detection.
- The possibility for the sensor to release the targets every few hours. The hormones should not accumulate on the sensor over a period of days, as the measurement should be representative of an instant "t". In order to follow the evolution of the hormone levels, the sensor surface must be able to release the targets naturally or by using an external stimulus.

In the second part of this chapter, the hormones detection method will be investigated. From the one selected, functionalization and detection protocols will be developed.

4.1 Validation of the fluids sampling area

This part of this thesis is of great importance to validate the patch’s localisation on the cow and to determine the concentrations to be detected for each of the two hormones. An experiment was carried out by the SmartRepro team based at the UMRH (Unité Mixte de Recherche sur les Herbivores, INRAE Clermont-Ferrand) in order to measure progesterone and oestradiol concentrations in the ear derma of dairy cows. I took part to the sampling campaign and to data analyses. The INRAe Clermont-Ferrand team carried out the development of the hormone’s dosage.

4.1.1 Strategy

The sensor will have to detect the hormones in a mix of interstitial fluid and blood located in the ears of the cow. To this day, no data is available concerning the presence of reproductive hormones in the cow's ears (interstitial fluids or blood). The use of animal samples is therefore essential. It allows researchers to obtain reference data on the presence of progesterone (P4) and oestradiol (E2) in the fluids collected from the ear and to assess the range of variation of hormone concentrations in these fluids during the oestrus cycle.

As no available technology was found to collect interstitial fluids in sufficient amounts to measure hormone concentrations using standard analytical methods (ELISA and Radioimmunoassay (RIA)), we decided to collect capillary blood and assume that if hormones were found in ear capillaries, they may also be found in interstitial fluids.

This experimental strategy can be summarised in two mains actions:

- The monitoring of the dynamics of P4 and E2 concentrations in ear derma.
- The comparison of these results with hormone concentrations measured in systemic blood (caudal vein) and milk during the oestrus cycle.

4.1.1.1 Experimental design

Ten multiparous Prim'Holstein cows were selected according to their expected calving date (grouped calving on September 29, 2018 (± 2 days)). Forty-eight days after calving they underwent an oestrous synchronization treatment (PRID® Delta + PMSG protocol, (Med'Vet, 2021)) to synchronise their oestrus cycles. During the pre-experimental period (from calving to the end of the hormonal treatment, i.e. 48 days post-calving) cows were housed in an open free-stall barn. Two days before PMSG injection (D0) they were tied to allow milk and blood samples during the 33 days of the experimental period (from D-2 to D30) (Figure 4. 1). From calving to the end of the experimental period, cows were fed with an *ad libitum* complete diet composed by maize silage, grass silage, hay and concentrates (Table 4. 1). Amounts of each component of the diet was determined to meet cows' predicted net energy and metabolizable protein requirements (Inra, 2007).
The diet was distributed at 8:30 AM (2/3) and at 5:30 PM (1/3). Cows were fed individually and refusals were measured each day in order to know the intake of each animal. Refusals from the previous day were systematically removed before the morning meal was offered. 200 g of a mineral and vitamin supplement (Galaphos) were offered each day to each cow and salt and water were available *ad libitum*.

The experimental protocol is presented on Figure 4. 1. The 33-day experimental period (from D-2 to D30) was supposed to include the induced and the successive natural ovulation windows.

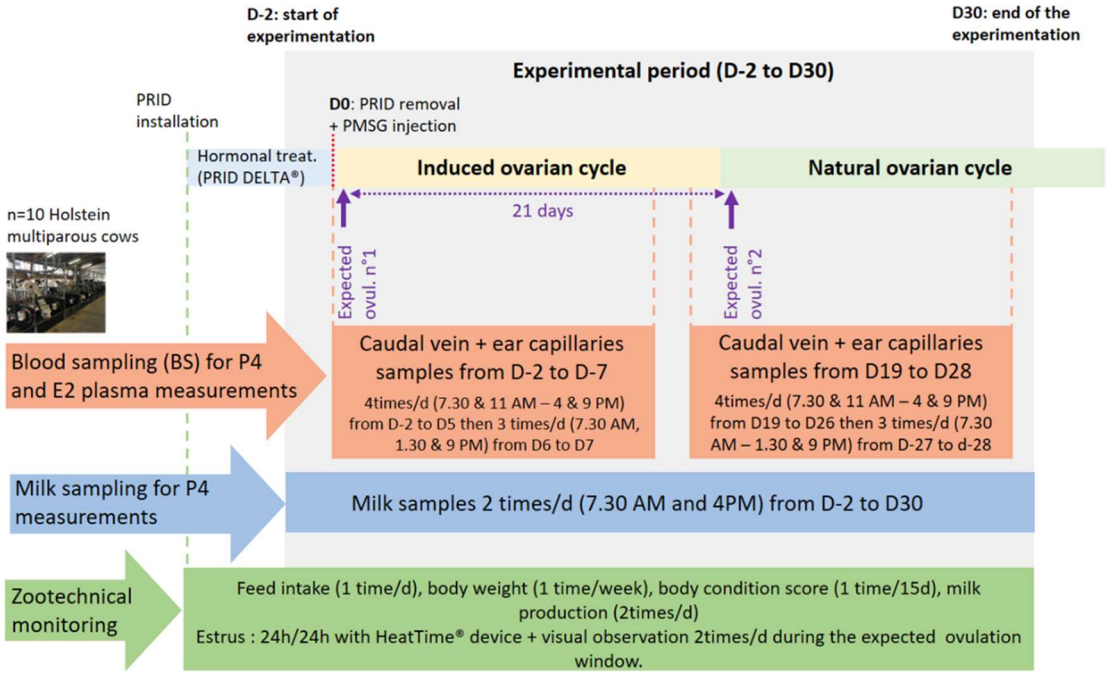

Figure 4. 1 Schematic representation of the experimental protocol developed to monitor progesterone (P4) and oestradiol (E2) concentrations in the epidermis of cow' ears around ovulation. Comparison with the kinetics observed in the caudal blood and milk.

	% MS
Maize silage	40.0
Grass silage	20.0
Hay	6.0
INRAe concentrates	28.5
Soybean meal	5.5

Table 4. 1 Composition of the basic ration for dairy cows. (MS = mass served)

4.1.1.2 Routine zootechnical measurements (Figure 4. 1):

This section presents the different parameters measured during the experiment. When the first four are routine measurements carried out for all types of experiments on cows, the fifth one has a direct link with the oestrus detection.

1. **Body weight:** Cows were weighed two times per day when leaving the milking parlour.
2. **Body condition:** Body condition score was assessed at the beginning of the trial before calving and then once every 15 days until the end of the experimental period. The notation system scales from 0 to 5 points the cow body outline (skeletal, bony, almost smooth, rounded, bulging due to fat).
3. **Feed intake:** Amounts of feed offered and refused were recorded individually every day. Dry matter (103°c for 24h), ash (550°c for 6h) and chemical composition (neutral and acid detergent fibre, starch, and fat content, crude protein) were analysed twice a week.

4. **Milk yield:** Milk yield was recorded daily at 8 am and 5 pm from calving to the end of the experimental period. Milk composition (fat and protein content, cells, lactose, urea) was assessed once a week during the experimental period.
5. **Oestrus detection:** all cows were equipped with the Heatime® heat monitoring system (cf Chapter 1) from day 10 postpartum to the end of the experimental period. Visual observation of oestrus expression was added around the expected ovulation days.

4.1.1.3 Measurement of progesterone and oestradiol levels around ovulation

Milk samples were collected every day from D-2 to D10 and from D12 to D30, at each milking (8 AM and 4:30 PM). Milk P4 profiles are thus quite complete along the experimental period except for a two-day period without measurements. Milk samples were stored at -20°c in 30 ml tubes without any preservative. Milk progesterone concentrations were assayed using a commercial ELISA kit (Ridgeway Research Ltd, UK). Dosage range, repeatability and reproducibility data of the assay are presented Table 4. 2.

Blood samples were collected four times a day at 7.30 AM, 11 AM, 4 PM and 9 PM from D-2 to D5 and from D19 to D26. They were reduced at 3 times a day (7.30 AM, 1.30 PM, 9 PM) from D6 to D8 and from D27 to D28. Plasma progesterone profiles are thus incomplete as we decided to limit blood sampling to the theoretical ovulation windows in order to prevent injuries on the caudal vein and ear capillaries. At each sampling time, blood samples were performed simultaneously from the caudal vein and from ear capillaries. Caudal blood was drawn into 9 ml evacuated tubes containing sodium heparin (Greiner) and ear capillary blood was collected into 200 µl minivette® POCT lithium heparin tubes (Sarstedt n°17.2112.200) after poking the skin with a lancet (penetration depth: 1.2 mm, blade width: 1.5 mm, Sarstedt n° 85.1019). Ear skin was disinfected with biseptine after each blood collection.

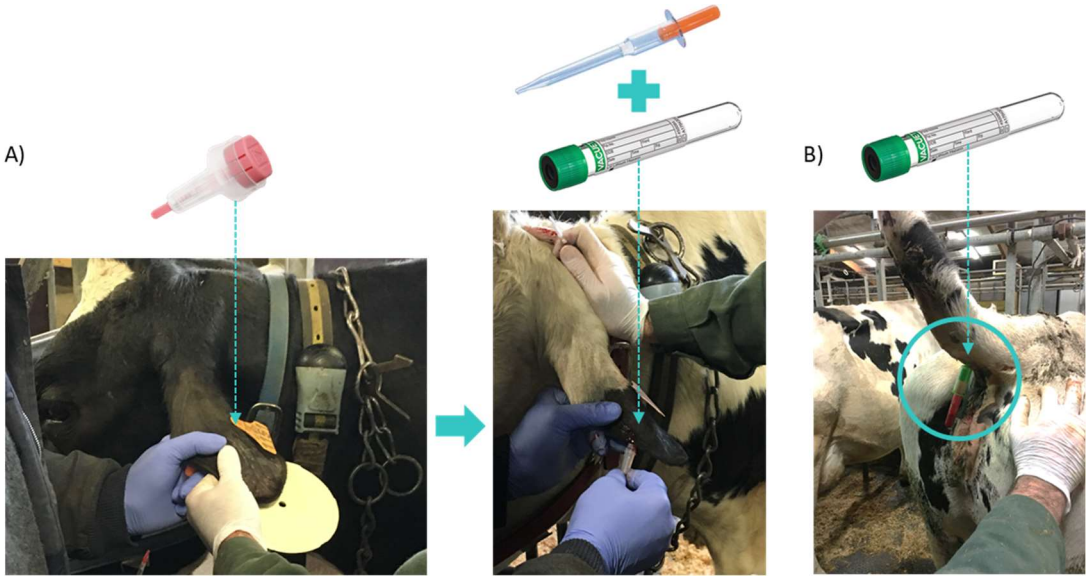

Figure 4. 2 Material and pictures of the blood sampling process from A) the ears capillaries (lancette to access the blood and minivette + tubes to collect it), B) the caudal vein (blood drawn in a tube).

Plasma was separated by centrifugation at 3000 g for 20 min at +4°C, was then distributed into 550 µL and 2000 µL tubes and stored at -20°c until analysed for P4 and E2 respectively. Plasma P4 concentrations were assayed using a commercial ELISA kit (Ridgeway Research Ltd, UK). Dosage range, repeatability and reproducibility data of the assay are presented Table 4. 2.

Type of assay	Dosage range	Validation range	CV Repeatability (ng/mL)			CV Reproducibility (ng/mL)		
			5	**10**	**40**	**5**	**10**	**40**
P4 in milk	0 to 50 ng/mL	4.75 to 50 ng/mL	6.73	4.30	2.53	4.04	12.13	4.66
			1.08	**10.8**	**15.338**	**1.08**	**10.8**	**15.338**
P4 in plasma	0 to 20 ng/mL	1.08 to 15.338 ng/mL	6.65	3.56	7.63	4.66	6.82	6.89

Table 4. 2 Milk and plasma progesterone dosing kits characteristics. CV = coefficient of variation

E2 concentrations were assayed using a commercial RIA kit (DSL4800 from Beckman Coulter). RIA is a highly selective bioanalytical method that measures the concentration of analytes (E2 here) in a solution using radiolabelled molecules in a stepwise formation of a complex with E2.

4.1.1.4 Data analysis

Milk P4 concentrations were plotted against days of experimentation to establish individual profiles over the oestrus cycle and to determine cows with normal vs abnormal cycles.

Milk P4 is usually assessed to analyse oestrous cycle in dairy cows whereas plasma P4 is the reference method used in suckling cows. Few studies have compared the two methods and comparisons were mainly performed through global correlations (Meisterling & Dailey, 1987; J. B. Roelofs et al., 2006). P4 measurements obtained from milk, caudal vein and ear capillaries were compared using the Bland-Altman method (Altman & Bland (1983)), which is considered the standard approach of agreement between two methods of measurement (Mansournia et al., 2021).

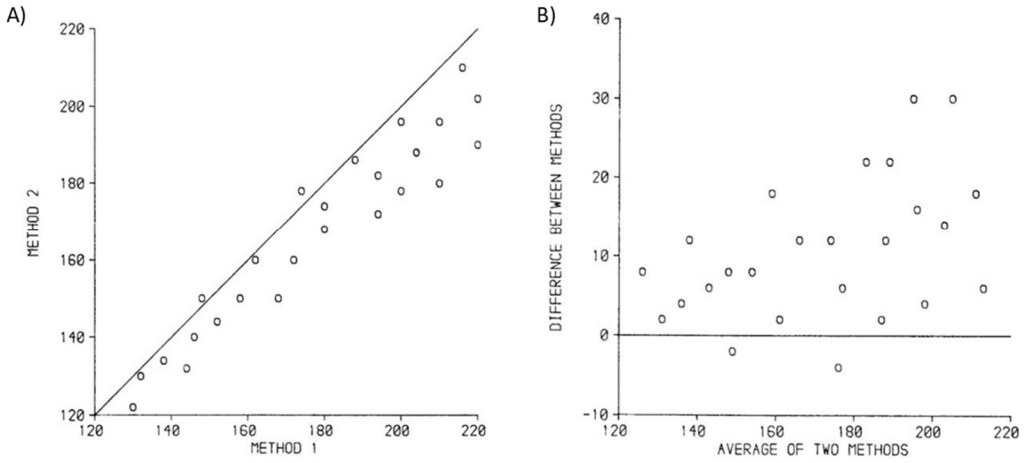

Figure 4. 3 Figure extracted from (Altman & Bland, 1983). A) Direct comparison of the two methods. B) Data presented in A) replotted to show the difference between the two methods against the mean of the two methods.

The Bland-Altman plot represents the difference between single measures of the two methods (A – B) against their mean ((A + B)/2) (Figure 4. 3.B). It was proposed as an alternative to the often-used correlation plot (Figure 4. 3.A) which has limits because "much of the plot will often be empty space. Also, the greater the range of measurements the better the agreement will appear to be." (Altman & Bland, 1983). In the Bland-Altman approach, the mean of the differences is the relative bias and their standard deviation is the estimate of error. The Bland-Altman plot also enables researchers to see if there is a correlation between the differences and the mean of measurements as shown in Figure 4. 3.B (higher differences for high values of the average measurement). The magnitude of disagreement (both error and bias), outliers and possible trends can thus be spotted easily.

Caudal plasma data were first compared to milk P4 concentrations, which was considered the reference, as data are available all along the experimental period. Then we compared progesterone concentrations from ear and caudal measurements to evaluate the agreement between the two sampling sites.

4.1.2 Results

For each cow, the P4 values from milk, caudal and ear plasma were plotted to have a first reading level. Additional statistical analysis using the Bland-Altman comparison method was used for a two-by-two comparison of the measurements from the three methods.

4.1.2.1 Progesterone concentrations

1. **Description of the progesterone profiles**

The variation levels of progesterone were tracked during the oestrus cycle following the hormonal treatment (see section 4.1.1.1). Ten complete profiles of milk progesterone concentration were available but only five account for a complete oestrus cycle (Figure 4. 4,

cows n°2632, n° 2014, n°5461, n°6582, n°6543). Ear plasma P4 measurements are quite incomplete for the first theoretical ovulation window as we encountered difficulties to collect enough amounts of blood from capillaries at the beginning of the experimental period.

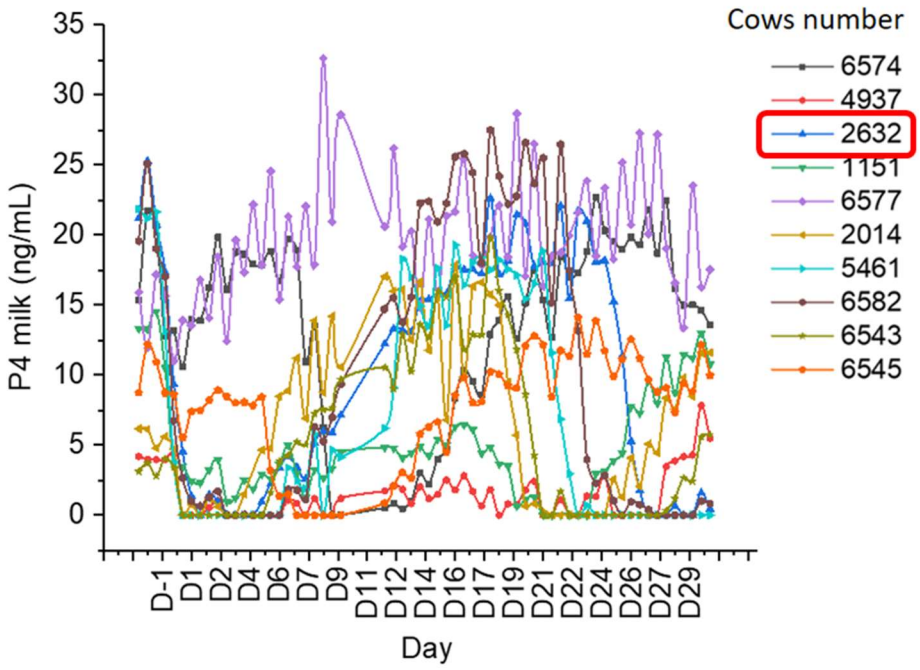

Figure 4. 4 The ten cows' progesterone concentration profiles throughout the all experiment for milk dosages. Cow n°2632 profile will be later analysed on this chapter.

As reported in Figure 4. 4, a large variability was found between milk progesterone profiles of individual animals. It is known that not all cows respond equally to hormone treatment in terms of temporality or intensity (Grimard et al., 2003). Among the ten cows, three presented abnormal oestrus cycles (acyclicity for cow n°4937, interruption of cyclicity for cow n° 1152 and prolonged luteal phase for cow n° 6577). The particularities of each profile can be better observed in Figure 4. 5.

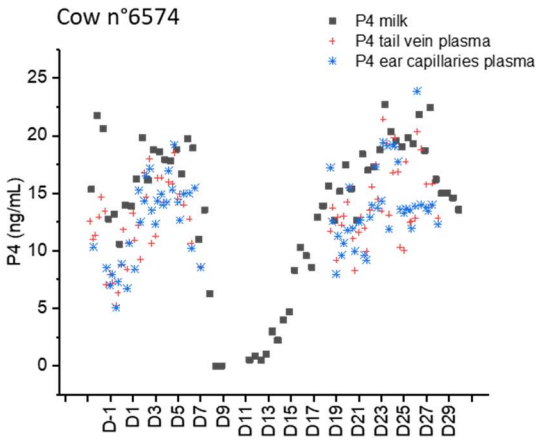
Cow n°6574
P4 milk
P4 tail vein plasma
P4 ear capillaries plasma
P4 (ng/mL)
0
5
10
15
20
25
D-1
D1
D3
D5
D7
D9
D11
D13
D15
D17
D19
D21
D23
D25
D27
D29

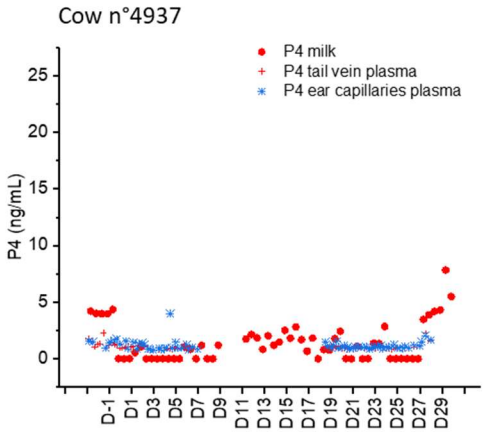
Cow n°4937
P4 milk
P4 tail vein plasma
P4 ear capillaries plasma
P4 (ng/mL)
0
5
10
15
20
25
D-1
D1
D3
D5
D7
D9
D11
D13
D15
D17
D19
D21
D23
D25
D27
D29

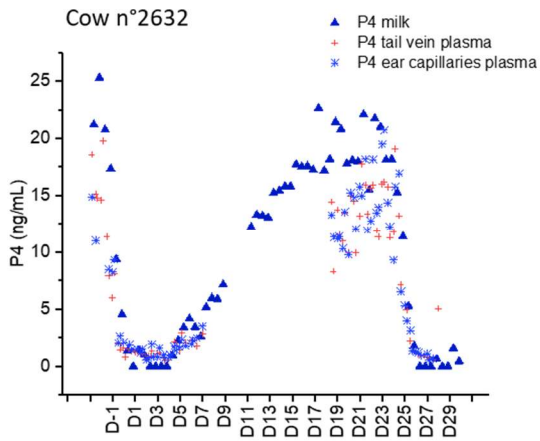
Cow n°2632
P4 milk
P4 tail vein plasma
P4 ear capillaries plasma
P4 (ng/mL)
0
5
10
15
20
25
D-1
D1
D3
D5
D7
D9
D11
D13
D15
D17
D19
D21
D23
D25
D27
D29

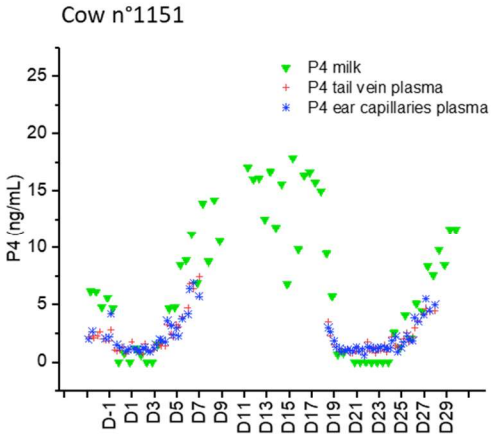
Cow n°1151
P4 milk
P4 tail vein plasma
P4 ear capillaries plasma
P4 (ng/mL)
0
5
10
15
20
25
D-1
D1
D3
D5
D7
D9
D11
D13
D15
D17
D19
D21
D23
D25
D27
D29

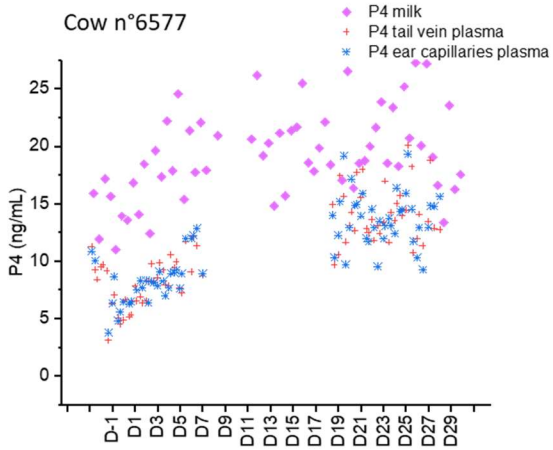
Cow n°6577
P4 milk
P4 tail vein plasma
P4 ear capillaries plasma
P4 (ng/mL)
0
5
10
15
20
25
D-1
D1
D3
D5
D7
D9
D11
D13
D15
D17
D19
D21
D23
D25
D27
D29

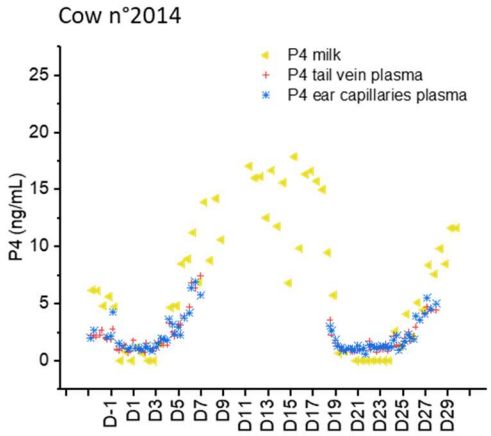
Cow n°2014
P4 milk
P4 tail vein plasma
P4 ear capillaries plasma
P4 (ng/mL)
0
5
10
15
20
25
D-1
D1
D3
D5
D7
D9
D11
D13
D15
D17
D19
D21
D23
D25
D27
D29

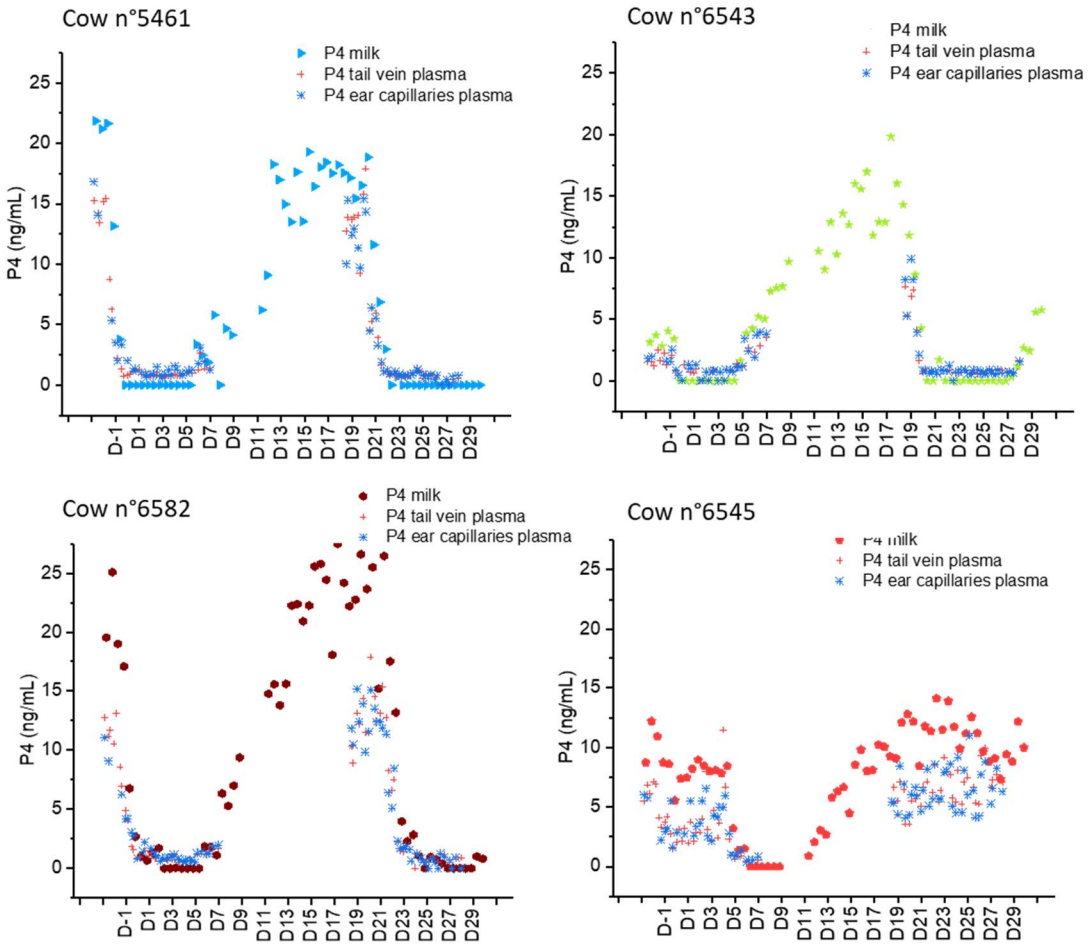

Figure 4. 5 All ten cows' profiles for progesterone levels in milk, caudal vein plasma and ear capillaries plasma. The progesterone levels in milk are the same colour in Figure 4. 4 and here.

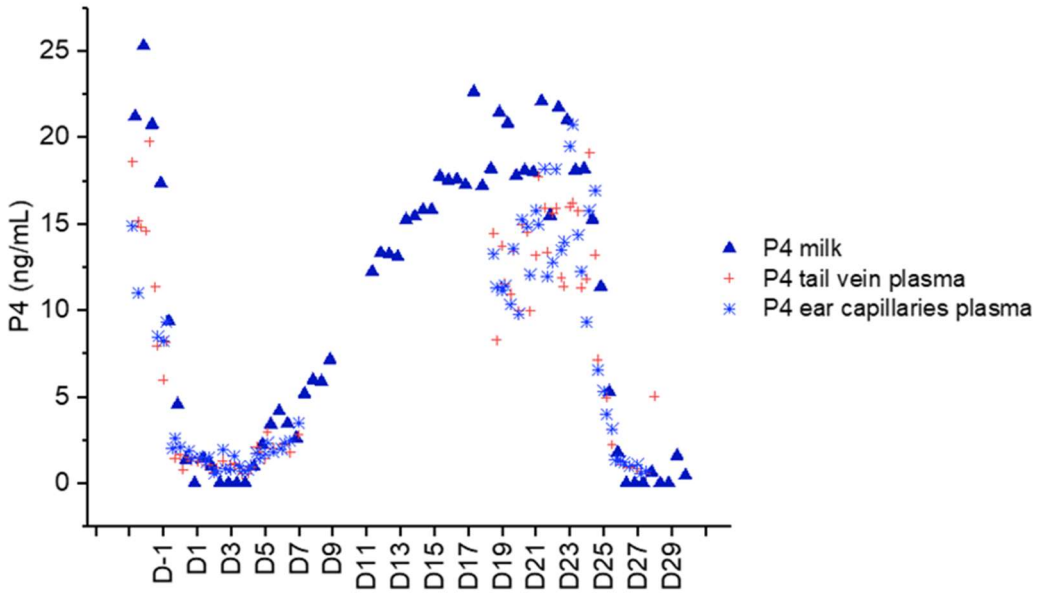

Figure 4. 6 Progesterone concentration profiles of cow n°2632 from three sampling places: the milk (blue triangle), the caudal vein plasma (red) and the ear capillaries plasma (blue snowflake).

Figure 4. 6 shows a normal ovarian profile with two ovulation periods (low P4 concentrations) delimiting an 18 days luteal phase (P4>5ng/ml) (cf Chapter 1). The decrease in plasma progesterone data (tail and ear) is synchronised with the decrease in milk P4 concentrations.

2. **Comparisons of progesterone concentrations from milk, caudal and ear plasma**

Milk P4 concentrations are on average higher than plasma caudal concentrations (8.7±7.9 ng/ml *vs* 5.1±5.3 ng/ml, p<0.001). Such a difference between milk and plasma P4 levels has already been reported in dairy cows (Dobson,H et al., 1975; Meisterling & Dailey, 1987; Rabiee et al., 2002). No difference was observed between mean of caudal and ear concentrations for plasma P4 (5.1±5.3 ng/ml *vs* 5.0±5.2 ng/ml, p=0.52) during the entire cycle.

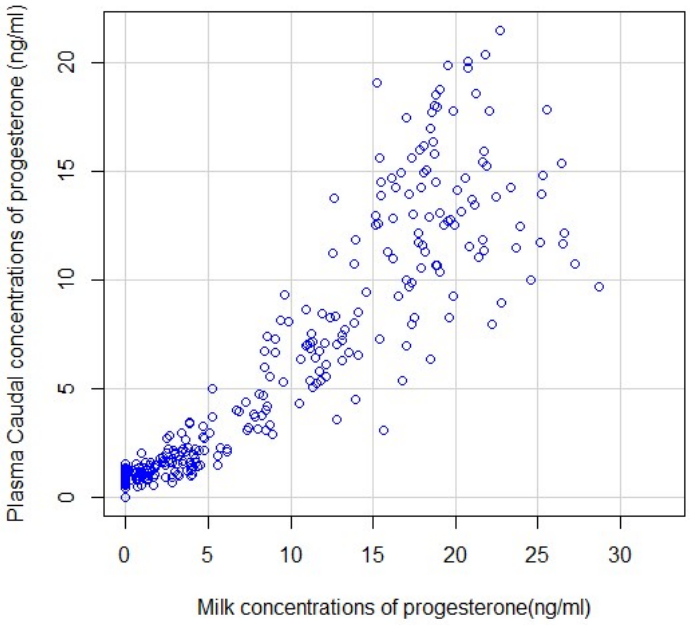

Figure 4. 7 Comparison of milk and caudal plasma progesterone values. Data from the ten cows are included.

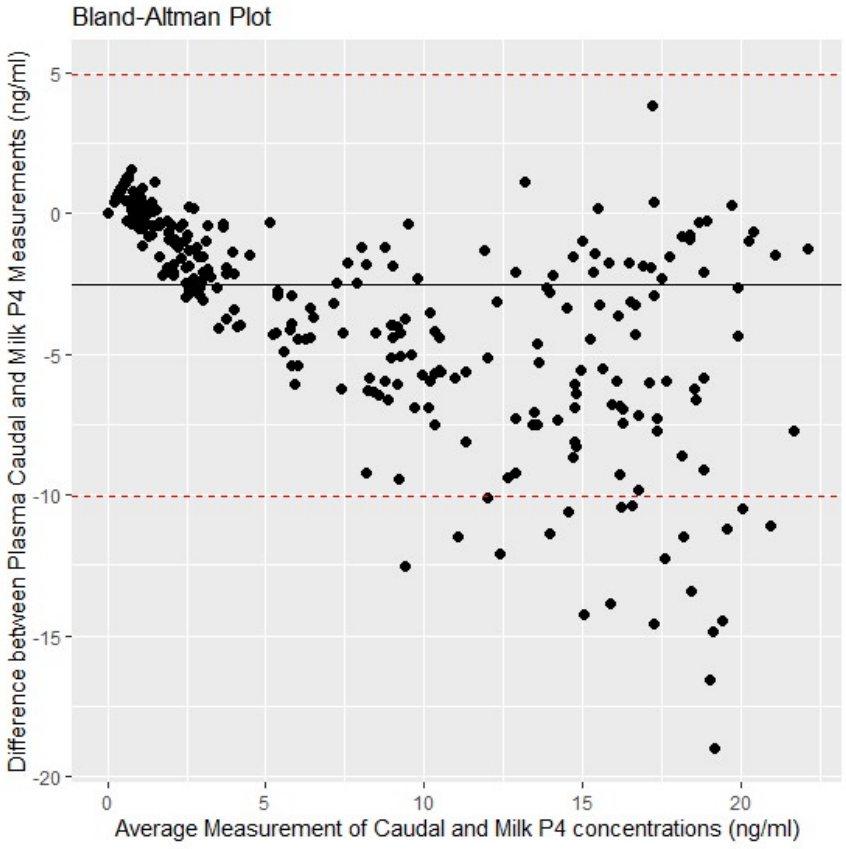

Figure 4. 8 Bland-Altman plot for milk and caudal plasma progesterone values. Data from the ten cows are included.

Figure 4. 7 shows that concentrations of progesterone in milk and in caudal plasma are correlated (r_spearman = 0.93, p<0.001)

The mean of differences between plasma caudal and milk progesterone concentrations is negative (-2.55±3.82 ng/ml, p<0.001) meaning that there is a bias between the two methods. The Bland-Altman plot (Figure 4. 8) clearly shows an association between the difference and the mean of single measurements of caudal and milk progesterone concentrations. The agreement of the two measurements is high for low P4 values (<5ng/ml) but decreases when entering the luteal phase (P4>5 ng/ml). For P4 values higher than 5 ng/ml, differences between caudal plasma and milk measurements increase with the mean of P4 concentration, with some differences being higher than 10 ng/ml. These results mean that thresholds used to define the characteristics of P4 profile have to be defined separately for plasma and milk measurements as already done by Roelofs et al (2006). Comparison between milk and caudal plasma P4 concentrations is more relevant to assess changes in P4 along the oestrus cycle than to determine true values of P4 levels.

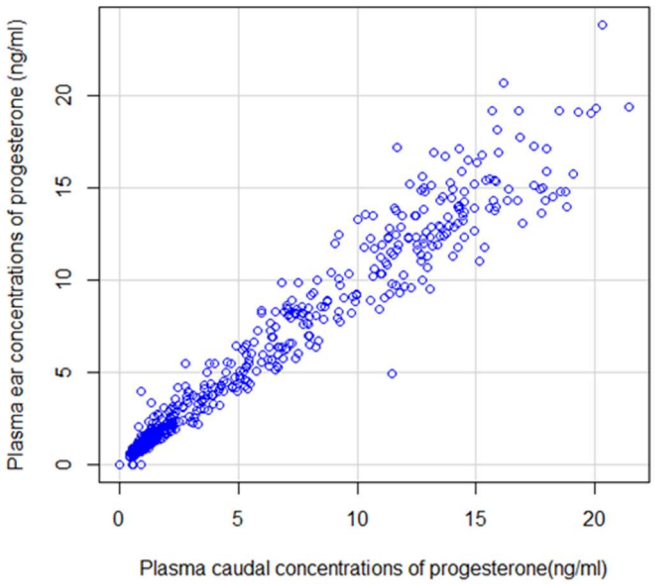

Figure 4. 9 Comparison of caudal plasma and ear capillaries plasma progesterone values. Data from the ten cows are included.

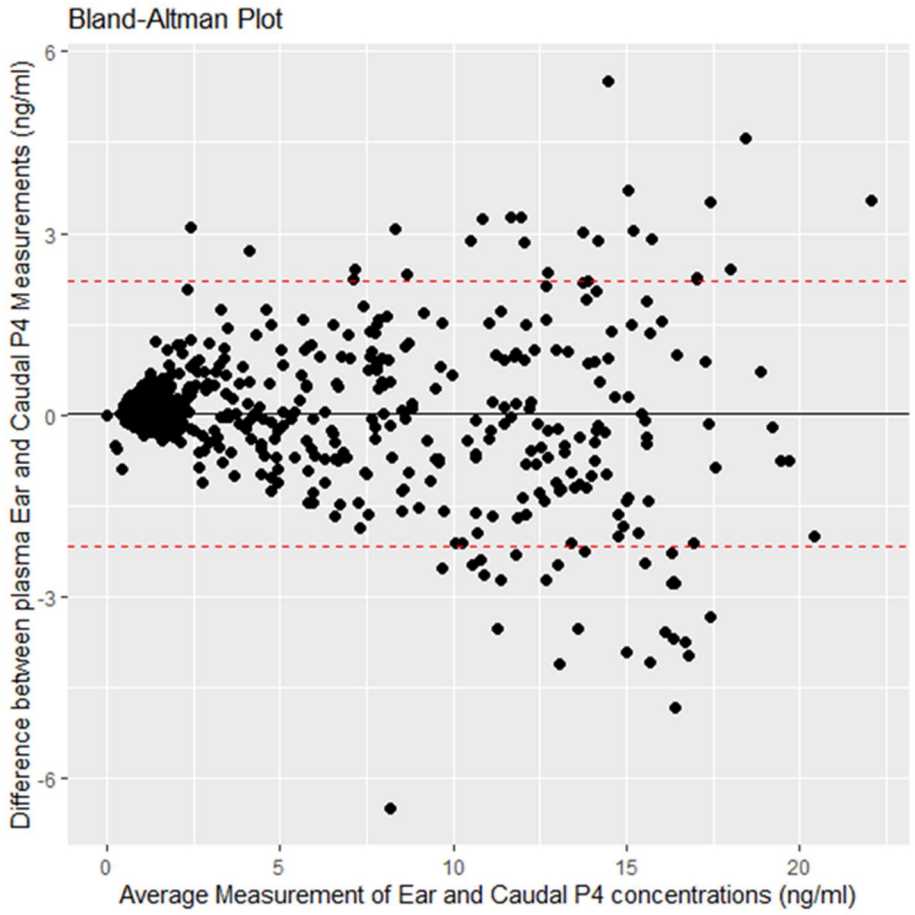

Figure 4. 10 Bland-Altman plot for caudal plasma and ear capillaries plasma progesterone values. Data from the ten cows are included.

Figure 4. 9 compares the P4 plasma concentrations from the caudal vein and the ear capillaries. The correlation between the two sites is high and significant (r_spearman = 0.97, p<0.001). P4 values appear to be close to the regression line, meaning that the concentration of caudal and ear plasma progesterone agree all along the oestrus cycle, with a better agreement as the ovulation is approaching (data closer to the regression line when P4 is lower than 5 ng/ml).

The mean of the differences between caudal and ear progesterone concentrations is close to zero (0.027±1.11 ng/ml, p=0.53) meaning that there is no bias between the two methods. The Bland-Altman plot (Figure 4. 10) shows that there is no association between the differences and the mean value of P4 concentration, meaning that P4 values from the two sites are in good agreement. The variability in P4 differences increases for P4 > 10 ng/ml but the differences mainly stay under ±5 ng/mL.

This analysis allows us to conclude that the evolution of the P4 level in the ear capillary is comparable in timing with the levels observed in the caudal vein. We can therefore validate that it would be possible to measure progesterone dynamics along the oestrus cycle with a patch implanted on the external side of the apex of the pinna.

4.1.2.2 Oestradiol concentrations

E2 concentrations were significantly lower than for the P4 by a factor of 1000. After several trials to dose E2 using different ELISA kits, the decision was made by the INRAe team to use RIA method. The trials to develop an adapted protocol to dose the E2 using RIA are still ongoing during the redaction of the manuscript. For this reason, statistical analysis cannot be realized for now.

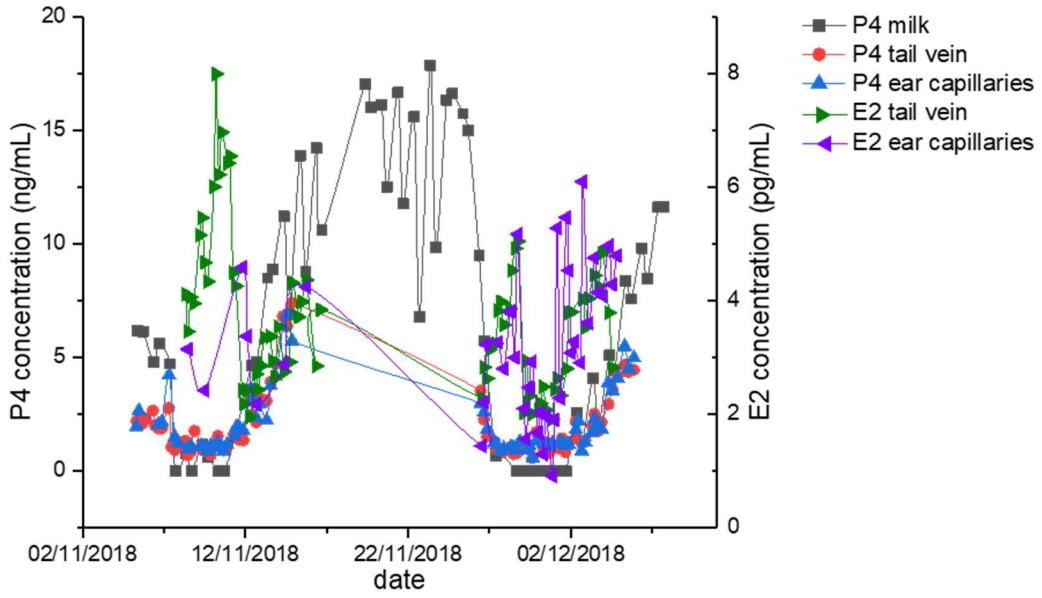

Figure 4. 11 Plot of P4 and E2 variations all through the experiment (induced and natural cycle) for cow n°2014.

Figure 4. 11 presents the different profiles obtained for P4 and E2 hormones during the experiment. For the first oestrus cycle (induced), the E2 coming from the tail vein plasma presents a peak at 8 pg/mL, which coincides with the low plateau of P4. For the second cycle, the peak is not as neat as the precedent one and the concentration does not exceed 5 pg/mL.

The concentration variations of E2 coming from the ear capillaries are more difficult to analyse for both cycles for this cow. During the first cycle, maximal concentrations are recorded around 5 pg/mL but do not present a peak. During the second oestrus, E2 concentrations remain noisy but seem to follow the same behaviour than for the E2 plasma from the tail vein, with equivalent concentrations. Data from the nine other cows are needed to conclude on the E2 level comparison between the tail vein and the ear capillaries.

To conclude on this part, the levels of P4 measured in the milk and in the plasma (tail vein and ear capillaries) showed that the variation of hormone level happens simultaneously along the oestrus cycle. Plasma from the caudal vein and the ear capillaries displays similar levels of hormone during the cycle as well (Figure 4. 10) indicating that the ear is a suitable emplacement to follow the evolution of P4 level to detect an oestrus event.

For the E2, preliminary results indicate that the hormone is present in the ear in similar concentrations than in the tail vein plasmas. E2 variations in the two plasmas seems to

happen concurrently. The levels of E2 appear to be 1000 times lower than for the P4 at their maximal concentration, which should be taken into account in the development of the sensor.

4.2 Going tiny: toward the detection of oestradiol and progesterone

In Chapter 3, the Si-SGFET and Poly-SGFET sensors were tested for biodetection and the Poly-SGFET was selected at the end of the trial to be used for hormone detection. For reasons presented in Chapter 1, aptamers are promising probes to detect small molecules like hormones. The following section presents the selection and functionalisation of the probe on the SGFET-Tripod detection structure.

4.2.1 Choice of the aptamers for progesterone and oestradiol detection

Aptamers are short single-stranded nucleic acid ligands that are capable of binding almost any targets. Their dissociation constant (K_D) is in the micromolar to nanomolar range and is reported to have exceptional specificities (Zhuo et al., 2017). Aptamers are artificially made using the SELEX method, developed in the nineties (Ellington & Szostak, 1990; Tuerk & Gold, 1990b). In the literature a broad spectrum of aptamers have already been synthetized to bind specifically numbers of molecules like proteins, cells or organic compounds (Bayat et al., 2018).

In this context, several teams around the world have already synthetized various aptamers for oestradiol and progesterone detection. To select the aptamer sequences for functionalisation of the Poly-SGFET sensor, we search for sequences used by several research laboratories. The use of an aptamer that has been successfully tested by several teams provides more guarantees on the robustness of recognition.

4.2.1.1 Oestradiol

Aptamers for oestradiol detection are subject to numerous articles (128 on Scopus database in September 2021) as the hormone is a common indicator for various clinical conditions such as precocious puberty, infertility and tumours in the ovaries (R. Wang et al., 2016). Among the developed aptamers, Alsager and co-workers (2015) as well as other research teams (J. Liu et al., 2015; Zhu et al., 2015) have generated an aptamer with highly sensitive detection of E2.
The E2 aptamer presented in these articles is a 22 bases oligonucleotide created out of a 75 bases oligonucleotide synthetized by (Alsager et al., 2014). Based on Alsager article (2015), the truncated version of the aptamer has several advantages:

- The dissociation constant of the aptamer (K_D) decreases when the number of bases is lowering. This was achieved by simply removing flanking nucleotides on either sides of the inner core of the aptamer. The 75, 35 and 22 bases versions were tested and the associated K_D were 25nM, 14nM and 11 nM.

- A shorter aptamer will eventually prevent other molecules to bind as the sequence offers less oligonucleotides combinations.

For this project, having a truncated version of the aptamer also increases the chances that the active part of the aptamer is in the sensor's detection zone, under the Debye length.

In addition to these results, Hilder and co-worker (2017) has run computational modelling over several version of a wide range of E2 aptamers in the literature. This study gives more information about the properties of the aptamer binding affinity, important binding positions, minimal binding sequence or mutations to enhance binding. Sequences presented on Figure 4. 12 were tested in this article.

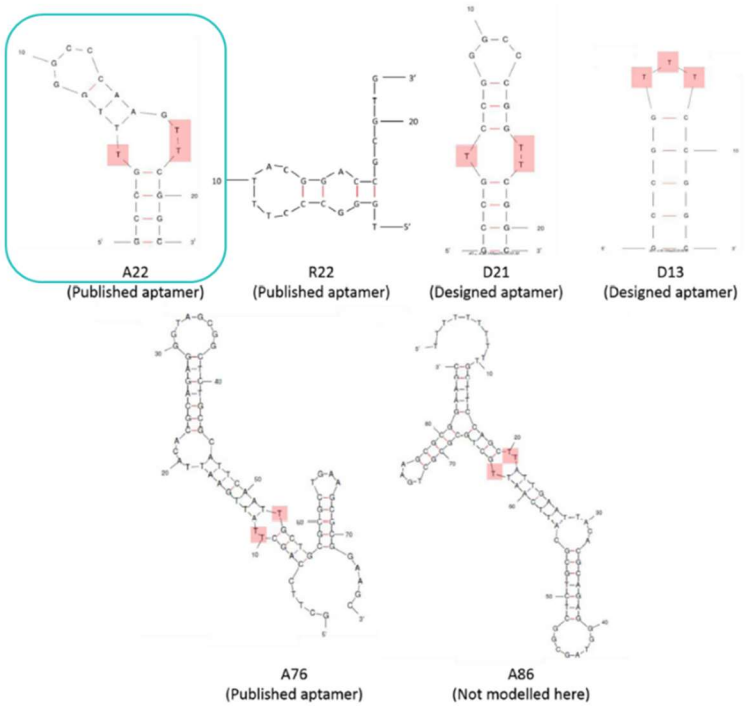

Figure 4. 12 Extracted from (Hilder & Hodgkiss, 2017). Representative 2D structure of E2-specific aptamers from the literature, tested via computational modelling. The thymine (T) bases implicated in the T-loop binding region are highlighted in red. ***The A22 aptamer is the one selected for E2 detection in this thesis.***

The computational modelling confirmed ae stronger target binding of the 22 bases aptamer compared to the 76 bases aptamer (A22 and A76 respectively on Figure 4. 12). K_D is also slightly lower than in the Alsager article with 10.95 nM instead of 11 nM.
Based on the use of this aptamer in the literature and the additional data provided by the Hilder and co-workers article, the 22 bases aptamer was chosen for E2 detection.

4.2.1.2 Progesterone

Compared to the oestradiol binding aptamers, significantly less articles were found on the development of progesterone aptamers. Alhadrami and co-workers (2017), based on previous work (Jimenez et al., 2015), shortened a 60 bases long aptamer for P4 detection:
5'-GCATCACACACCGATACTCACCCGCCTGATTAACATTAGCCCACCGCCCACCCCCGCTGC-3'
to a 25 bases version: 5'-GATTAACATTAGCCCACCGCCCACC-3'.

The dissociation constant appeared to decrease by a factor of 16 when shortening the original sequence to obtain a 2.1 nM value.
The aptamer was also tested with E2 hormone in this article to validate its discrimination against this hormone. The results obtained by fluorescence measurements are presented on Figure 4. 13. Non-significant cross reactivity was observed with, among others, the E2 compound.

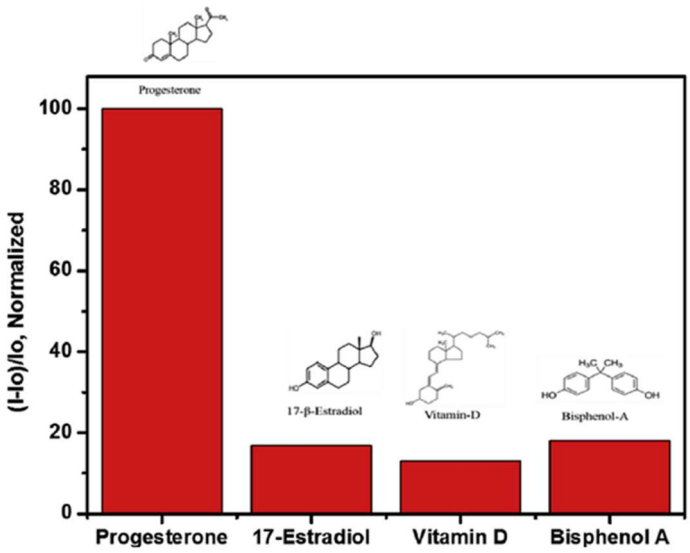

Figure 4. 13 Extracted from (Alhadrami et al., 2017). Cross reactivity of the progesterone aptamer against 17-β-oestradiol, vitamin-D, Bisphenol A, obtained by fluorescence measurements.

Based the results of this paper, the 25 bases, P4 aptamer developed and tested aptamer from the Alhadrami article (2017) was selected for P4 detection.

4.2.2 Adaptation and validation of the detection structure stability

Once the aptamers for E2 and P4 selected, a functionalization strategy was set up to anchor it on the top of the Gr / Tripod detection structure described in Chapter 3.

4.2.2.1 Recognition of the complementary DNA strand strategy

The stability of the detection structure including the graphene, tripod and aptamer is crucial to ensure the further detection of hormones. Prior to the hormones detection assays, functionalization protocols were tested and refine until validation of the stability of the detection structure.

To validate the stability of the structure, a two steps strategy was developed. First, the aptamer is functionalized on the tripod and a field effect test is realized (Figure 4. 14.A). By comparison with the previous field effect test (tripod functionalization on Gr), a first estimation of the success of the grafting is done. To validate the stability in time of the structure, the aptamer complementary DNA strand is introduced (Figure 4. 14.B). A last field

effect test is then realized. If a new shift of the Dirac point is observed, this means that the complementary DNA strand has been successfully grafted on the aptamer.

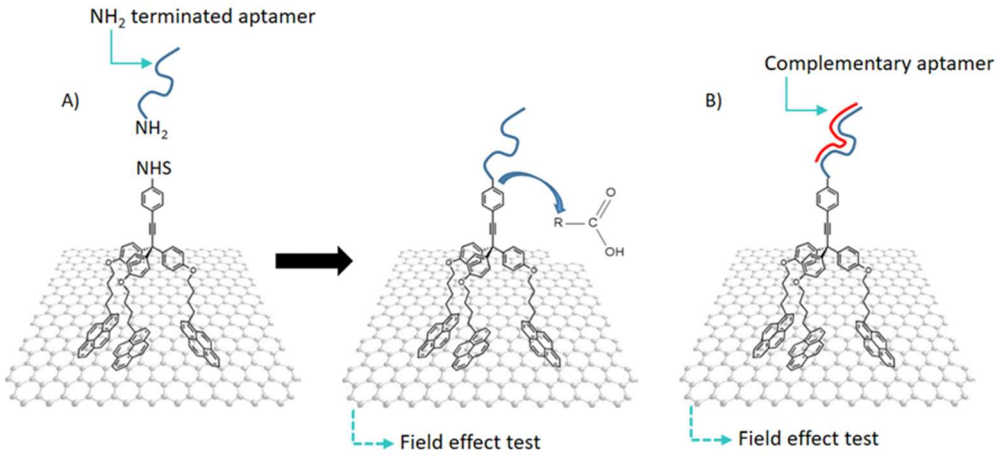

Figure 4. 14 Scheme of the aptamer functionalization validation strategy. A) The aptamer, NH_2 terminated is functionalized on the tripod-NHS and a field effect test is realized. B) The complementary aptamer binds to the aptamer. The associated shift observed on the field effect test validates the stability of the detection structure.

4.2.2.2 Material and methods

E2 and P4 aptamers as their complementary sequences were ordered from Eurogentec with the following addition to the initial sequence:

- Addition of five thymines bases (T) at the 5' end to add a degree of freedom to the aptamer once functionalized on the tripod.
- Addition of an amine (NH_2) at the 5' end for functionalization on the tripod (NHS terminated).

In total, four sequences were ordered:

P4 aptamer sequence (modified): 5' NH_2 – TTT-TTG-ATT-AAC-ATT-AGC-CCA-CCG-CCC-ACC 3'
P4 complementary aptamer sequence: 5' GGT-GGG-CGG-TGG-GCT-AAT-GTT-AAT-C 3'
E2 aptamer sequence (modified) 5' NH_2 – TTT-TTG-CCG-TTT-GGG-CCC-AAG-TTC-GGC 3'
E2 complementary sequence: 5' GCC-GAA-CTT-GGG-CCC-AAA-CGG-C 3'

Resuspension of the aptamers was realized in a PBS solution (10^{-3}M) according to the supplier recommendations and concentration of the obtained solution was verified using a Nanodrop (spectrophotometer device). Stock solutions were kept at -20°C in between utilisations as recommended by the supplier.

Functionalisation of the aptamer takes place after the non-covalent functionalisation of the tripod linker on the Gr and the associated field effect test (cf Chapter 3). The aptamer functionalization and binding stability experiment includes ten steps:

1. Aptamer solution preparation at 10µM in $NaHCO_3$ buffer (pH= 8,3) from Thermo Fisher. The concentration was chosen to obtain a saturation situation of the aptamer (Reynaud et al., 2021). The basic pH was found to help the NHS-NH_2 reaction to occur.
2. The well containing the electrolyte on the top of the sensing part of the sensor (Gr area) was rinse three times with $NaHCO_3$ buffer.
3. 100µL of the prepared aptamer solution was poured in the well for a one-hour long functionalisation. This step was followed using real time analysis on the Grapheal software.
4. The well was rinsed three times using a rinsing buffer (see recipe in Appendice B).
5. 200µL of PBS 10^{-3}M was poured into the well and a field effect test was carried out.
6. 200µL of rinsing buffer was poured into well and let there for five minutes to ensure that nothing aside the Gr-tripod-aptamer detection structure was present on the detection structure.
7. A 1µM complementary aptamer solution was prepared in a hybridation buffer (see recipe Appendice C).
8. 100µL was poured in the well and the chip was incubated at 57°C (for all types of aptamers) during 15 min according to the aptamer supplier advices.
9. The well was rinsed three times using DI water.
10. 200µL of PBS 10^{-3}M was poured into the well and a field effect test was carried out.

As for the previous trials presented in Chapter 3, we looked at the shift of the Dirac point (V_{Dirac}) after each functionalisation step. The results are presented on Figure 4. 15.

4.2.2.3 Results

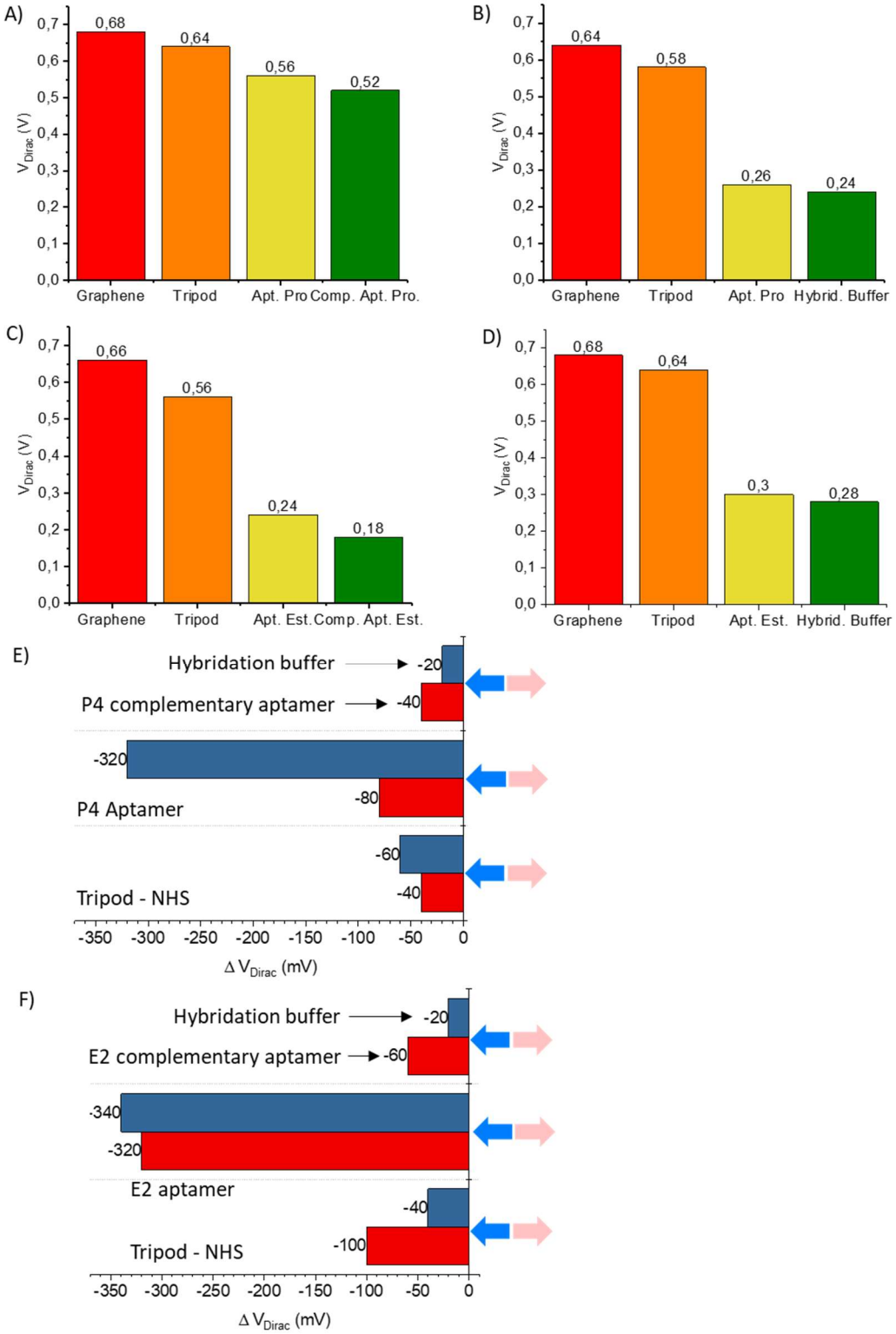

Figure 4. 15 Successive Dirac points of the functionalized SGFETs for A) & B) the functionalisation of the P4 and E2 complementary aptamer as the final step and C) & D) only the presence of the hybridation buffer (without the respective complementary aptamer). E) & F) are the comparison of the Δ V_{Dirac} in between each step for the two different tests (with complementary aptamer in blue or with only the hybridation buffer in red).

The test presented on Figure 4. 15.A was repeated six times with the same Dirac point shift (-40 mV) for the P4 complementary aptamer recognition. In the case of the E2 complementary aptamer recognition, the test was carried out eleven times with a consistent shift of -60 mV for this step. This repeatability of these results indicates the successful and stable grafting of the aptamer on the tripod. DNA has a global negative charge due to its backbone structure made of phosphate. Based on the model proposed in Chapter 3 (Figure 3. 21), the Dirac point is supposed to shift toward negative tension values when molecule binding is negatively charged. The results on Figure 4. 15.E and .F supports this model.

A hybridation buffer was used to help the two DNA strands recognition in each test. The buffer, whom the recipe is presented in the Appendice C could also have an impact on the Dirac point shift. It contains among other components some salmon DNA (10 mg/mL) which role is to block the sensing surface of the SGFET (non occupied by the tripod). This prevents any other molecules present in the electrolyte from being deposited on the Gr and could induce unknown Dirac point shift.
A second type of test was realized to know the impact of the hybridation buffer and salmon DNA on the -40 and -60 mV sifts observed for the P4 and E2 complementary DNA strand respectively. Results are presented Figure 4. 15.C & .D. From the protocol given previously, step 7 to 10 where modified as only the hybridation buffer was used.
The following field effect tests showed a Dirac point shift of -20 mV for all tests, which were conducted four times with the P4 aptamer and four times with the E2 aptamer. A comparison of the shifts of the Dirac points is visible on Figure 4. 15.E & .F. Eventually, the recognition of the complementary aptamers is a success as the the Dirac point shift due to their binding to the aptamers is of -20 ±10 mV for P4 and -40±10 mV for E2 if we take into account the margin of error linked to the measurement.

We can conclude that the developed protocol allows a stable grafting of the two aptamers on the tripodal linker.

4.3 Hormones detection

The validation of the detection structure stability led to the hormones detection trials, using the Graphene based SGFETs from Grapheal.

4.3.1 Experiment strategy

The hormones detection assays realized during the thesis includes three main steps:

1. **Validation of the detection protocol.** As presented on Figure 4. 16.A, once the aptamer is grafted on the tripodal linker, the associated hormone solution is poured in the sensor's well. The concentration of the solution is 14 ng/mL for the P4 hormone and 8 pg/mL for the E2 hormone. These concentrations correspond to the highest levels of hormones measured in the caudal vein plasma in section 4.1.1.4. After a ten minutes incubation time, as recommended in Alsager (2015), a field effect test is run and the Dirac point is compared to the one obtained after the aptamer grafting step.

A shift superior to ±10 mV (margin of error for the Poly SGFET, cf Chapter 3) will be attributed to the hormone recognition by the detection structure.
In parallel, as in the section 4.2.2, a test with only the binding buffer, without the hormone is realized to evaluate the impact of the binding buffer on the Dirac point shift.

2. **Validation of the selectivity of the two aptamers.** This test is designed to ensure the discrimination of the P4 aptamer toward E2 hormone and the discrimination of the E2 aptamer toward P4 hormone. As for the previous test, the comparison of the Dirac points before and after the introduction of the hormones are compared. It is expected that the obtained shift is 0V, minus the impact of the binding buffer on the Dirac point shift which will also be measured.
3. **Concentration range assays.** Once the hormones detection protocol validated, a range of P4 and E2 concentrations will be tested in an attempt to test the sensitivity of the Poly SGFET (14, 7 and 0 ng/mL for P4 and 20 ng/mL, 8, 2 and 0pg/mL for E2).

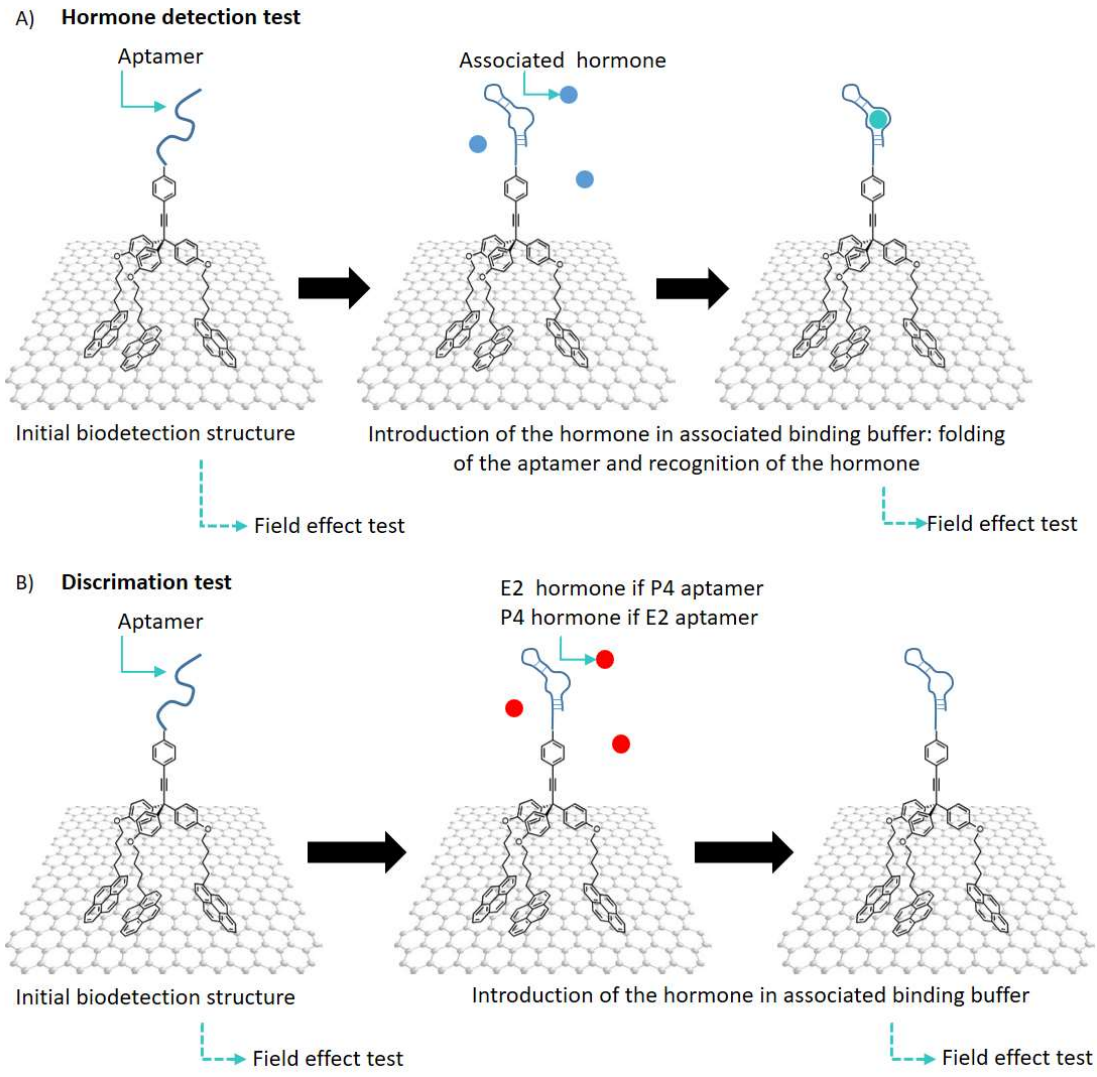

Figure 4. 16 Schematic of the hormone detection experiment strategy. In both cases, the aptamer, is functionalized on the tripod and a field effect test is realized. A) The introduction of the associated hormone in binding buffer should led to the hormone recognition. A field effect test will validate or not the recognition by comparison of the two Dirac points. B) The introduction of the wrong hormone should lead to no Dirac point shift in the second case.

4.3.2 Material and methods

Hormones

E2 and P4 hormones were purchased from Sigma Aldrich and stock solution were prepared following advised protocol from the supplier:

- P4 stock solution was prepared in DMSO (Dimethyl sulfoxide) at 1 mg/mL concentration and kept at -20°C in between uses.
- E2 stock solution was prepared in pure ethanol at 1mg/mL concentration and kept at -20°C in between uses.

Buffers

Both Alsager (2015) and Alhadrami (2017) developed all-in-one biding and rinsing buffer for to use with the aptamer sequences used in this PhD. These buffers were recreated and used in our tests.

- P4 binding and rinsing buffer: 50mM Tris-HCL, keeping the buffer solution at pH 7.5; 150nM NaCl and 5mM $MgCl_2$.
- E2 binding and rinsing buffer: 2mM Tris-HCl and pH 7,5; 10nM NaCl; 0.5 mM KCl; 0,2 mM $MgCl_2$; 0,1mM $CaCl_2$; 5% ethanol, added in the buffer / hormone mix to help the hormone dissolution.

The buffers were kept at 5°C until further use.

Detection protocol

1. Aliquots of different hormones concentrations, based on the results obtained from the dosages on the cow were realized.

For P4, a 14 ng/mL and 7 ng/mL were prepared. The first concentration correspond roughly to the high plateau before the oestrus (see Figure 4. 6). The second one is on the way to the concentration fall to 0 ng/mL, just a few hours before the oestrus.

For E2, a larger range of concentration was used. E2 levels are 1000 lower than P4 levels with a maximum peak at 8 pg/mL. As it was not sure to be able to detect such small concentration at the stage of the sensor and characterisation platform development, we started the detection protocol with an E2 concentration of 14 ng/mL. We then move to concentrations that are more realistic in our application with an 8 pg/mL and 2 pg/mL solutions (see Figure 4. 11).

2. Once the aptamer grafted on the tripod, 100µL of the buffer solution was poured in the sensor well for 5 minutes.
3. 100µL of the hormones solutions were then poured in the sensor well and led to incubate 10 minutes at room temperature. This step was followed using real time analysis on the Grapheal software.
4. The well was rinsed three times using a DI water.
5. 200µL of PBS 10^{-3}M was poured into the well and a field effect test was carried out.

4.3.3 Results

In this section, the focus will be on the hormones detection by the Poly SGFET. The steps prior to the aptamer grafting on the tripod will not be addressed as they were already discussed in the previous chapter.

4.3.3.1 Results for progesterone assay

The results of the detection assays with the P4 aptamer can be separated in two parts as presented on Figure 4. 17:

- The tests to detect the P4.

- The tests to determine if the chosen P4 aptamer discriminate the E2.

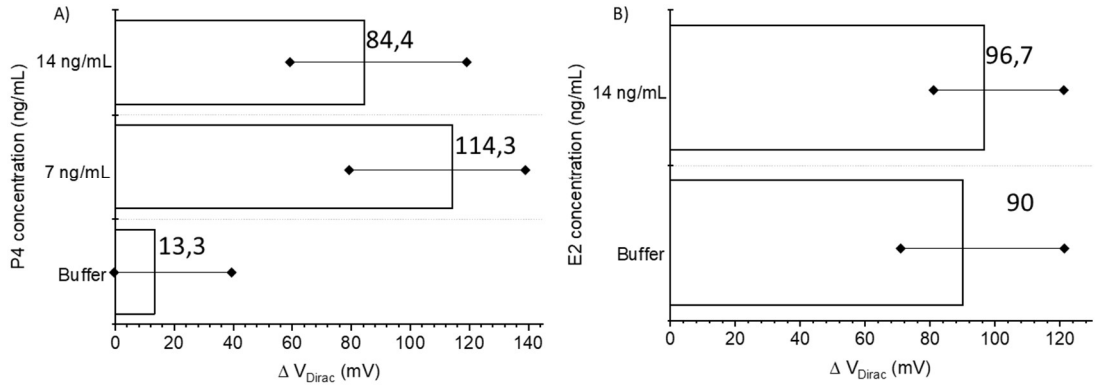

Figure 4. 17 V_{Dirac} shifts of the detection by the progesterone aptamer of A) three concentrations of progesterone and B) two concentrations of oestradiol. For each concentration, the minimal, mean and maximal shifts value are indicated.

On Figure 4. 17.A, three concentrations are tested.
For the 14 ng/mL concentration, seven sensors were tested with Dirac point shifts ranging from 60 to 120 mV and a mean value of 84.4 mV. For the 7 ng/mL concentration, seven sensors were tested. The Dirac shift varying from 80 to 140 mV with a mean value of 114.3 mV. Finally, the test with only the binding buffer allow us to observe its impact on the two previous shifts as realized on nine Poly SGFETs. The Dirac point ranges between 0 and 40 mV with a mean value of 13.3 mV.

From these first results, it is clear that the P4 hormone detection was a success with a large shift of the Dirac point for the 14 and 7 ng/mL concentration, the impact of the biding buffer and the possible measurement error of ± 10 mV taking into consideration. However, it was expected to observe a smaller Dirac point shift for the 7 ng/mL than for the 14 ng/mL concentration. This tendency, visible after testing each concentration seven times has not yet found an explanation.

Results for the P4 aptamer / E2 hormone discrimination test are presented on Figure 4. 17.B. An E2 detection test was performed using a 14 ng/mL solution on five sensors. The resulting shifts were included in a [80; 100 mV] range and with a mean value of 96.7 mV. Another test was realized to evaluate the impact of the E2 binding buffer on the previous shift. This test was performed on three sensors and a shift ranging from 70 to 120 mV was recorded with a mean value of 90 mV. By also taking into account the ± 10 mV margin of error, we can consider than the 14 ng/mL and 0 ng/mL shift are equivalent. The discrimination of the P4 aptamer toward the E2 hormone is therefore validated.

If the overall results allow us to say that hormone detection has indeed taken place, the difference in results for the same test is much greater than the +10mV of measurement error expected. This observation is valid for all the tests performed with the Poly SGFET and can partially be attributed to the fact the reproducibility of the Poly-SGFET sensors is not yet enough. This point should be investigated and improved in the next stages of the sensor's development.

4.3.3.2 Results for oestradiol assay

The results of the detection assays with the E2 aptamer are as for the previous section presented in two parts:

- The tests to detect different concentrations of E2.
- The tests to evaluate the E2 aptamer response to the presence of P4 hormone.

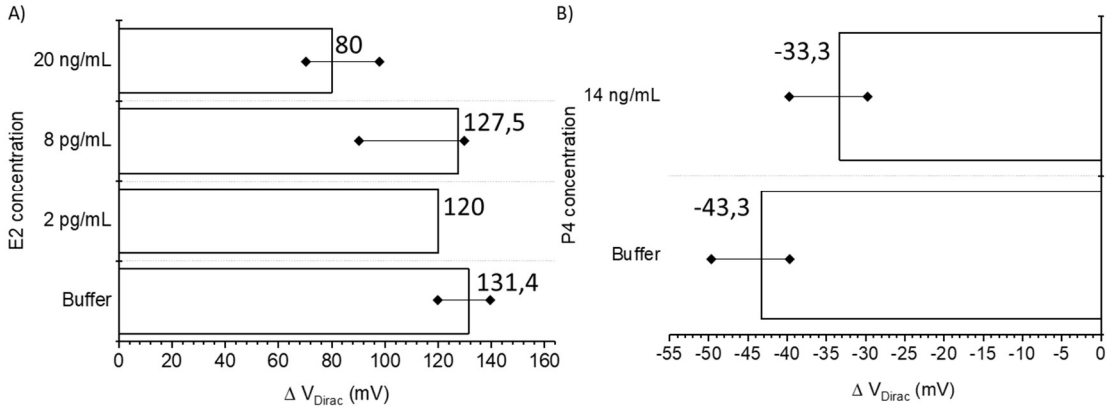

Figure 4. 18 V_{Dirac} shifts of the detection by the oestradiol aptamer of A) four concentration of oestradiol and B) two concentrations of progesterone.

During the oestrus cycle, the E2 hormone has a peak of concentration during the oestrus event, a few hours before the ovulation. This peak was around 8 pg/mL in the caudal vein plasma (see section 4.1.2.2). A first series of E2 detection test was realized and the results are presented in Figure 4. 18.A. For a concentration of 8 pg/mL, corresponding to the E2 peak value, four sensors were tested with a Dirac point shift ranging from 90 to 150 mV and a mean value of 127 mV.

A second test, with a concentration of 2 pg/mL was realized on two sensors. Both showed a shift of 120 mV which is very close from the result obtained with the 8 pg/mL concentration. The influence of the binding buffer on the previously recorded shifts was investigated on seven sensors. The resulting Dirac point shifts are ranging from 120 to 140mV with a mean value of 131.4 mV. This result is overlapping with the 8 and 2 pg/mL concentrations. If we subtract the impact of the buffer on the two previous results, a zero-value shift is obtained meaning that no detection took place. To know if the issues was the sensitivity of the sensor or the detection protocol, a test with a concentration 10 000 times higher, in the same range that the maximal P4 concentration, was realized. A 20 ng/mL E2 solution was used on five sensors. The results showed a shift in the 70 – 90 mV range, with a mean value of 80 mV. This value, far from the 8 pg/mL and 2 pg/mL shifts give a -51 mV shift once the impact of the E2 buffer deduced.

This last result highlights the lack of sensitivity of the Poly SGFET sensor when detecting pg/mL concentrations. If the fall of the P4 concentration is already a good indicator of the upcoming oestrus, the dosing of E2 brings a more accurate estimate of the ovulation moment and confirms the event. This is why this technical lock should be addressed in the next step of the SmartRepro project.

On Figure 4. 18.B the results of the tests to verify the E2 aptamer selectivity against the P4 hormone are presented. A concentration of 14 ng/mL of P4 solution was first put to the test

on six sensors. The resulting point of Dirac evolves between -30 and -40 mV with a mean value of -33.3 mV. As for the precedent tests, the impact of the P4 binding buffer was evaluated. The test, carried out on three sensors presented Dirac points ranging from -40 to -50 mV. The two tests give similar results when taking into account the ±10 mV error margin. Alhadrami and co-workers (Alhadrami et al., 2017) also showed in their results that the P4 aptamer has a small but real response to the presence of P4 (see Figure 4. 13). More tests should be conducted to see if this 10 mV difference between the two results mean can be reduced to conclusively show a clear discrimination of the E2 aptamer toward P4 hormone.

Conclusion

The last part of this thesis was dedicated to the development of the patch core: the detection of the two targeted hormones (oestradiol and progesterone).
This objective required two main elements:

- To know the order of magnitude of the hormones concentrations as well as their dynamics throughout the oestrus cycle to recognize the oestrus event.
- To have an efficient probe for each hormone.

In the absence of data in the literature on the dynamics of progesterone and oestradiol levels in the cow's ear, an animal experiment had to be set up by INRAe. During this experiment, the hormones levels of ten cows were followed during two oestrus cycles. Three type of samples were collected: milk, caudal vein plasma and ear capillaries plasma. From the collected data, several conclusions can be used in this project.
If a large variablity can be found on the recorded profiles of P4, trends can be identified by comparing the results from the three sampling sites.
The variation in P4 concentrations seems to be synchronised at all three sites. However, although the concentrations seem to be equivalent in both plasma (ear and tail) over the whole cycle, they are generally lower than in milk (8.7±7.9 ng/ml vs 5.1±5.3 ng/ml). The measurement of P4 in tail vein plasma is a reference method. The fact that the ear capillaries plasma gives results close to those the caudal vein in concentration and dynamic, especially near the oestrus event, allow us to validate the patch localisation on the external side of the apex of the pinna for the P4 hormone.
For the E2 hormone, several dosage trials reveal very low levels of E2 in the ear and caudal vein plasma. The first results, obtained at the end of this thesis for one cow and two sampling locations (caudal vein and ear capillaries), showcased concentrations in the pg/mL range with a peak around 8pg/mL when approaching the ovulation. With the current data, it seems that as for the P4, the caudal vein and ear capillaries concentration have similar profiles in concentration and dynamic. However, additional data will be needed to make a decision about the external side of the apex of the pinna is validated for E2 real time monitoring or not.

To detect the hormones, two aptamers were selected from the literature. A protocol to functionalize them on the Poly-SGFET / tripodal linker complex was developed. Once the stability of the detection structure was validated for the two aptamers, series of trials were set up to detect hormones. A satisfactory discrimination of the P4 aptamer against E2 hormone and of the E2 aptamer against the P4 hormone was obtained. A successful hormone detection was realized for both oestradiol and progesterone for concentrations in the ng/mL range. However, trials to detect pg/mL oestradiol concentration were unsuccessful. In order to detect the low E2 concentration few improvement to the actual set up could be made. A first trial could consist in enhancing the hormone binding signal. In a second time, the measurement software associated with the Poly-SGFET could be improved to reduce the measurement margin error which is currently of ±10 mV. This would allow the Dirac shifts to be detected with more accuracy and would have an impact on the repeatability of the tests.

For the further development of the sensor, several steps are still to be validated. When using the sensor on the cow, the hormone measurement will have to be continuous. To be able to accurately reflect the hormone level at a given time, the sensor will have to be regularly cleaned of the hormones previously accumulated on the sensor. This cleaning can be done naturally (dissociation of the aptamer/hormone pair after a certain period of time) or by heating the sensor for example. Preliminary tests were done by leaving the hormone / aptamer complex for 4 hours in DI water. No shift of the Dirac point, which could be associated with dissociation of the complex, was observed after this time. Finally, tests including circulating fluids and a more complex environment such as plasma should be carried out to get closer from the application.

Conclusion & perspectives

This thesis work focused on the development of the first technological building blocks of the SmartRepro ovulation detection patch. The work was organised around three axes dealing with different scientific fields: finding the location of the patch on the cow, developing hollow MNs to reach and transport the interstitial fluid/blood mixture containing the hormones, developing a biosensor to dose the hormones (E2 and P4) in real time.

The emplacement of the patch on the cow was the first axis addressed, as it would have an impact on how to reach the fluid. A set of specifications was drawn up to guide the research. The chosen location must be easily accessible to the farmer, allowing for simple installation and removal of the patch, without the assistance of a veterinarian. The chosen area should also be protected from the cow's daily activities, allowing the patch to remain in place for approximately 30 days (duration of the oestrus cycle). According to these primary requirements, the cow's ear was pre-selected. No literature on the anatomy of the cow's ear tissue was found and a measurement campaign was carried out on ears of 7 breeds of cows (dairy and suckling). For each cow, 3 samples were taken from different areas and histological sections were taken and analysed. From the acquired data, it was found that the optimal location is the apex of the pinna, external side of the ear. This area offers the best compromise between a large implantation area and a similar thickness of tissues to penetrate, considering all selected breeds. This site has a large implantation depth window (DeepDe[3] : 1403 ±589 µm) and a rather uniform SupDe sublayer for all breeds (SupDe[4]: 1323±404µm) which could lead to the design of a single patch for all suckling and dairy breeds.

The MNs developed during the thesis were designed to reach the middle of the DeepDe layer. Several studies have shown that only 50-60% of the MNs penetrate below the epidermis and the final length of the MNs was about 3mm. If many hollow MNs are present in the literature, they generally have a height of a few hundreds of micrometres. The realisation of a channel of 3mm high and few hundreds of micrometres in diameter was a real challenge and many technologies have been considered to create these MNs. For this phase of prototyping, the main objective was to prove that hollow MNs could be made. Thanks to 3D printing, I was able to design the first prototypes of hollow MNs with channel diameter from 300µm to 400µm.
3D printing is perfect for this stage of the project's development because it allows to test a large number of designs at a reduced cost and with short manufacturing time (1 hour of printing to obtain 6 MNs arrays). The resin used to make the MNS is not biocompatible. However, a test was carried out with a biocompatible resin (Formlabs Company). Like many biocompatible resins on the market, its definition was lower than the resin used during this

[3] Deep Derma
[4] Superficial Derma

thesis and the channel clogged during printing. However, the biocompatible resin showed good resistance during compression tests at 10 and 49 N which is interesting for the insertion stage of the MNs. The research or creation of a biocompatible ink that would allow a channel to be obtained and that could withstand the stresses undergone during the insertion of the patch and throughout its use would be a very interesting route to explore. New designs could also be tested to help anchor the device in the cow ear while taking into account the pain factor for the animal from the application to the removal of the patch. Increasing the capillarity of the channel using surface chemistry should also be an important point to develop to ease the transfer of the fluid from the sampling area to the biosensor. For a more advanced stage in the development of MNs, other techniques such as injection moulding should also be explored to reduce the diameter of the channel and increase the capillarity performance of the MN.
The work on cow ear tissue and the creation of the hollow microneedles were reported in an article, currently under review for the journal Biosystem Engineering.

The third axis of work of this thesis concerned the development of a biosensor to monitor in real time the evolution of E2 and P4 hormones in the cow's ear (blood and interstitial fluid). The choice of the technology was made by considering its sensitivity, its selectivity, its potential to be miniaturised for future integration into an embedded system and its price with a view to future industrialisation. SGFET biosensors were selected for this project. CVD Gr, classified as a semi-metal has many interesting properties for biosensor application: highly conductive, lightweight, flexible, transparent and mechanically robust. Its high specific area due to its atomic thickness is particularly appealing for the detection of charged biological species. In parallel to my thesis, a CEA PhD student, Adrien Hugo demonstrated a unique, robust and reproducible fabrication protocol of a Graphene-based Solution-Gated Field-Effect-Transistor (SGFET) technology operating in an aqueous environment. After training for the fabrication of robust and reproducible Si-SGFET sensors, we were able to collaborate on the refinement of certain fabrication steps as well as on the first electrochemical characterizations of the sensor in a liquid environment.

The detection structure is composed of three layer: the Gr monolayer, the tripod and a probe. To avoid denaturation of the target proteins by contact with the Gr, a unique tripodal linker was first non-covalently functionalized on the Gr for all tests through well-known π-stacking interaction between the pyrene groups and the Gr. This linker keeps the bioreceptors and targets at a fixed distance from the Gr in order to avoid possible denaturation by contact with the Gr.

In a first step, molecules whose interactions are well known in the literature (Biotin, avidin, streptavidin, neutravidin, Con A and Methyl alpha D) were detected. The evolution of the Gr doping for each molecule detected (negatively or positively charged) allowed me to understand the behaviour of charges at the Gr/electrolyte interface. In parallel with the characterisation of Si-SGFETs, a collaboration with the start-up Grapheal (Grenoble, France) allowed me to test another version of SGFETs. The Poly-SGFETs made at Grapheal have a less robust and less reproducible fabrication process than the Si-SGFETs but a duplication of the

experiments conducted on the Si-SGFETs gave comparable results. The sensors developed by Grapheal as well as their electrochemical characterisation bench have significant advantages: five times faster fabrication of the sensors and the possibility of testing up to 16 sensors in parallel instead of one for Si-SGFETs. This collaboration at the end of the thesis enabled me to meet the objectives we had set at the beginning of the thesis for this axis. The detection of P4 and E2 hormones was thus made possible, despite the delays caused by Covid-19 and other technical problems throughout this thesis.

For the detection of target hormones, aptamers, short strands of oligonucleotides, were chosen as probes. Aptamers can bind their target with high specificity and affinity. They can be reversibly denatured, enabling the biorecognition layer regeneration for real-time monitoring purpose. This feature is of high interest for real time measurement through the entire oestrus cycle. They are also considerably smaller than antibodies (≈2 nm), and have the ability to bring the target closer to the surface by conformational changes induced by the binding event, which is appealing for working in complex solutions such as blood. Each aptamer was chosen on the basis of its sensitivity and selectivity towards the target hormone but also on its ability to discriminate the other hormone. Protocols for grafting the aptamers onto the tripod and detecting the hormones in a simple medium were set up. The results validate the detection of both hormones by their respective aptamers for ng/mL concentrations. In both case, the aptamers demonstrated a good discrimination of P4 in the case of the E2 aptamer and E2 in the case of the P4 aptamer.

The work on the electrochemical characterization of the Si-SGFET was reported in an article, currently under review for the ACS journal. This work and the hormone detection results were also selected by the following conferences:

- Graphene 2020, largest European Conference & Exhibition in Graphene and 2D Materials for an oral contribution.
- Biosensors 2021, world largest conference on this theme for poster contribution.
- ESEAC 2022, International conference on Electroanalysis for an oral contribution. This conference was initially planned in 2020 but postponed to June 2022.

During this thesis, an experiment to determine the hormone levels in the interstitial fluid/blood mix of the ear capillaries was conducted at INRAe. The level and dynamics of hormones during two oestrus cycles in the ear were compared with two reference methods: caudal plasma and milk. Although the results show a certain synchronisation of the evolution of the levels between the three sources, the hormone levels differ. Thus, while P4 is present at ng/mL levels in the ear, E2 concentration are a thousand time lower. Concentrations in the ng/mL range could be detected but this was not the case for pg/mL levels. Several paths could be explored to increase the biosensor sensitivity towards E2. First, continue the development of the Poly-SGFETs with a more reproducible quality and a reduction of the uncertainty window in the measurement (currently ± 10mV). A more specific E2 aptamer could also be created using the SELEX method, with a lower K_D. Amplifying the detection signal could also be a solution with the grafting of a polyanion (molecule or chemical complex having negative charges at several sites) at the end of the aptamer sequence. The conformational change of the aptamer when binding with the target (hormone) would bring the polyanion closer to the Gr surface which would react accordingly. During this thesis, the electrochemical tests were

performed using DC current and only the analyte within the Debye length could be detected. In PBS 10^{-3} M medium, the Debye length was around 9 nm but this value considerably decreases when working in a complex medium such as blood. In future studies tests using frequency modulation using EIS technique (Electrochemical Impedance Spectroscopy) using small amplitude AC current could be used to overcome this limitation.

In addition to the different development paths presented in this section for the next phase of the SmartRepro project, microfluidic integration of the MNs and the biosensor as well as pumping solutions will also have to be developed in a future stage of the project. In the longer term, it would be also interesting to develop new aptamers to detect the presence of other hormones related to the oestrus cycle of the cow. For example, LH has a higher concentration than E2 at peak. This solution could be a real asset for the patch and stands out from existing solutions. Indeed, this solution is not currently envisaged for predicting ovulation in cows for several reasons (J. B. Roelofs, 2005):

- LH peak cannot be detected by blood tests because the samples would have to be taken very frequently and this operation would be too invasive for the cow.
- LH cannot be measured in the milk.

A last long term perspective for the SmartRepro project would be the validation that the MNs can sample interstitial fluids for the thirty days use of the patch.

This thesis work paved the way for further promising development of the SmartRepro ovulation detection tool. The main contribution of this work consists in finding the patch emplacement on the cow, the development of hollow MNs array as well as the development of a biosensor for E2 and P4 detection.

Appendices

Appendice A

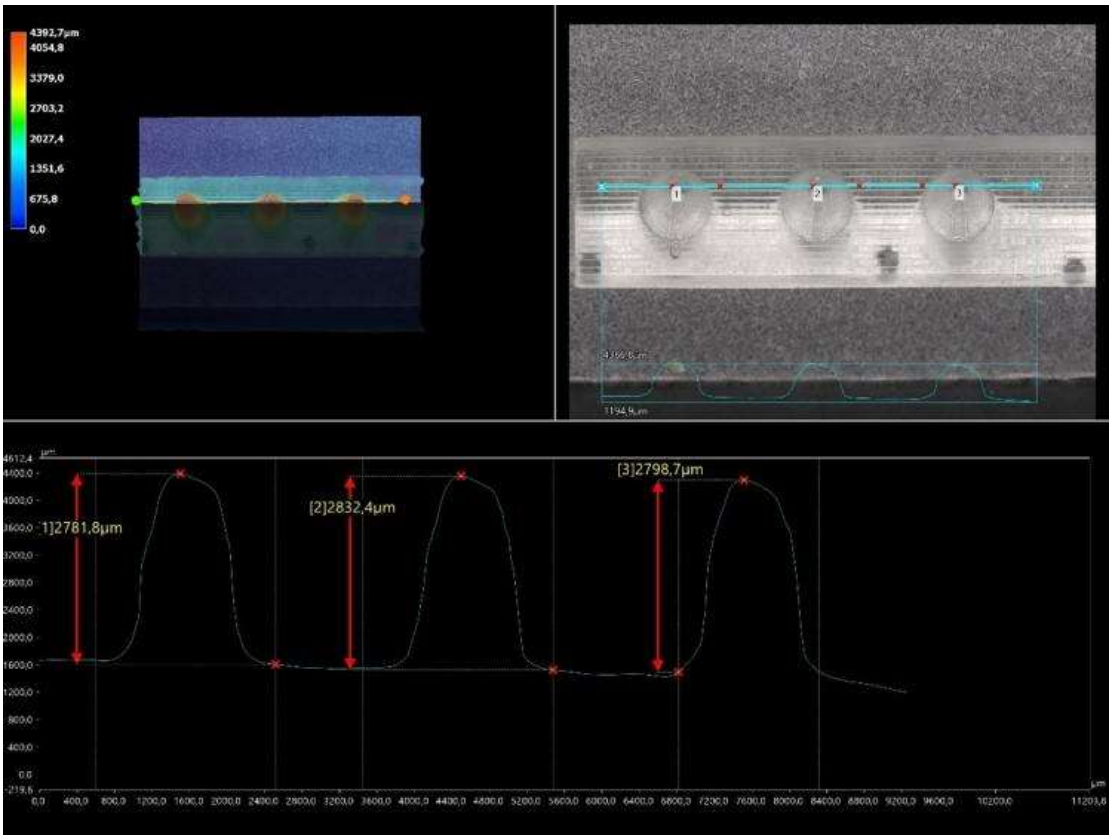

Microneedle cross-section measurements using a VHX 7000-970F numerical microscope and associated software. The three microneedle heights are measured from base to tip.

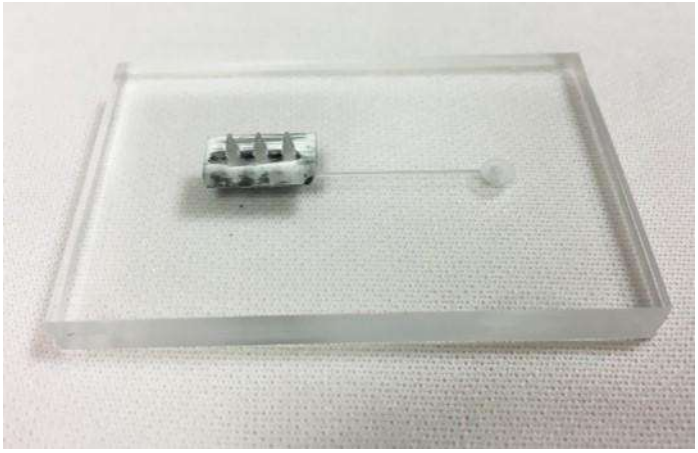

Connection of the microneedle array to a microfluidic channel for fluidic tests.

Appendice B – Rinsing buffer recipe

Recipe from CREAB (Chimie pour la Reconnaissance et l'Étude d'Assemblages Biologiques) CEA laboratory.

Products	Supplier	References	Quantity for 1L
PBS tablets	Sigma Aldrich	P4417	5 (PBS 10x)
NaCl	Sigma Aldrich	S3014	23.375 g
Tween 20	Sigma Aldrich	274348	1.5 mL
H_20 (pure water)	/	/	Fill up to 1L

1. Dertermine the volume to prepare
2. Weigh the NaCl
3. Dissolve NaCl and PBS tablets with pure water into volumetric flask
4. Add the needed volume of Tween 20
5. Complete to the gauge line and homogenize.
6. Filter the solution with a 0,22µm filter

The solution can be kept 6 months at -20°C and 15 days at +4°C.

Appendice C – Hybridation buffer recipe

Recipe from CREAB (Chimie pour la Reconnaissance et l'Étude d'Assemblages Biologiques) CEA laboratory.

Products	Supplier	References	Quantity for 1L
PBS tablets	Sigma Aldrich	P4417	1 (PBS 10x)
NaCl	Sigma Aldrich	S3014	4.675 g
Tween 20	Sigma Aldrich	274348	4 mL
Denhart 50x	Sigma Aldrich	D2532	0.2 mL
Salmon DNA (10 mg/mL)	Sigma Aldrich	D9156	0.3 mL
H_20 (pure water)	/	/	Fill up to 1L

1. Dertermine the volume to prepare
2. Weigh the NaCl
3. Dissolve NaCl and PBS tablets with pure water into volumetric flask
4. Add the needed volume of Denhart and Salmon DNA
5. Add the needed volume of Tween 20
6. Complete to the gauge line and homogenize.
7. Filter the solution with a 0,22µm filter

The solution can be kept 6 months at -20°C and 15 days at +4°C.

Bibliography

Afzal, A., Mujahid, A., Schirhagl, R., Bajwa, S., Latif, U., & Feroz, S. (2017).Gravimetric Viral Diagnostics: QCM Based Biosensors for Early Detection of Viruses. *Chemosensors*, *5*(1), 7. https://doi.org/10.3390/chemosensors5010007

Agreste. (2020). *GRAPH'AGRI 2020—Produits agroalimentaires—Bovins*.

Ahlman, T., Berglund, B., Rydhmer, L., & Strandberg, E. (2011). Culling reasons in organic and conventional dairy herds and genotype by environment interaction for longevity. *Journal of Dairy Science*, *94*(3), 1568–1575. https://doi.org/10.3168/jds.2010-3483

Alava, T., Mann, J. A., Théodore, C., Benitez, J. J., Dichtel, W. R., Parpia, J. M., & Craighead, H. G. (2013).Control of the Graphene–Protein Interface Is Required To Preserve Adsorbed Protein Function. *Analytical Chemistry*, *85*(5), 2754–2759. https://doi.org/10.1021/ac303268z

Alawneh, J., Williamson, N., & Bailey, D. (2006). Comparison of a camera-software system and typical farm management for detecting oestrus in dairy cattle at pasture. *New Zealand Veterinary Journal*, *54*(2), 73–77. https://doi.org/10.1080/00480169.2006.36615

Alhadrami, H., Chinnappan, R., Eissa, S., Rahamn, A. A., & Zourob, M. (2017). High affinity truncated DNA aptamers for the development of fluorescence based progesterone biosensors. *ANALYTICAL BIOCHEMISTRY*, *525*, 78–84. https://doi.org/10.1016/j.ab.2017.02.014

Allain, Thomas, & Chanvallon. (2012). *Détection automatisée des chaleurs en élevage bovin laitier: Quel outil choisir?* Institut de l'élevage.

Allice. (2021). *Insémination—Reproduction*. Https://Www.Allice.Fr/.

Allrich, R. D. (1993). Estrous Behavior and Detection in Cattle. *Veterinary Clinics of North America: Food Animal Practice*, *9*(2), 249–262. https://doi.org/10.1016/S0749-0720(15)30644-7

Alsager, O. A., Kumar, S., Willmott, G. R., McNatty, K. P., & Hodgkiss, J. M. (2014). Small molecule detection in solution via the size contraction response of aptamer functionalized nanoparticles. *Biosensors and Bioelectronics*, *57*, 262–268. https://doi.org/10.1016/j.bios.2014.02.004

Alsager, O. A., Kumar, S., Zhu, B., Travas-Sejdic, J., McNatty, K. P., & Hodgkiss, J. M. (2015). Ultrasensitive Colorimetric Detection of 17β-Estradiol: The Effect of Shortening DNA Aptamer Sequences. *Analytical Chemistry*, *87*(8), 4201–4209. https://doi.org/10.1021/acs.analchem.5b00335

Altman, D. G., & Bland, J. M. (1983). Measurement in Medicine: The Analysis of Method Comparison Studies. *The Statistician*, *32*(3), 307. https://doi.org/10.2307/2987937

At-Taras, E. E., & Spahr, S. L. (2001). Detection and Characterization of Estrus in Dairy Cattle with an Electronic Heatmount Detector and an Electronic Activity Tag. *Journal of Dairy Science*, *84*(4), 792–798. https://doi.org/10.3168/jds.S0022-0302(01)74535-3

Bae, S., Kim, H., Lee, Y., Xu, X., Park, J.-S., Zheng, Y., Balakrishnan, J., Lei, T., Ri Kim, H., Song, Y. I., Kim, Y.-J., Kim, K. S., Özyilmaz, B., Ahn, J.-H., Hong, B. H., & Iijima, S. (2010). Roll-to-roll production of 30-inch graphene films for transparent electrodes. *Nature Nanotechnology*, *5*(8), 574–578. https://doi.org/10.1038/nnano.2010.132

Bahadır, E. B., & Sezgintürk, M. K. (2016). A review on impedimetric biosensors. *Artificial Cells, Nanomedicine, and Biotechnology*, *44*(1), 248–262. https://doi.org/10.3109/21691401.2014.942456

Baines, I. C., & Colas, P. (2006). Peptide aptamers as guides for small-molecule drug discovery. *Drug Discovery Today*, *11*(7–8), 334–341. https://doi.org/10.1016/j.drudis.2006.02.007

Bard, A. J., & Faulkner, L. R. (2001). *Electrochemical methods: Fundamentals and applications* (2nd ed). Wiley.

Bascom, S. S., & Young, A. J. (1998). A Summary of the Reasons Why Farmers Cull Cows. *Journal of Dairy Science*, *81*(8), 2299–2305. https://doi.org/10.3168/jds.S0022-0302(98)75810-2

Basu, J., Basu, J. K., & Bhattacharyya, T. K. (2010). The evolution of graphene-based electronic devices. *International Journal of Smart and Nano Materials*, *1*(3), 201–223. https://doi.org/10.1080/19475411.2010.510856

Bayat, P., Nosrati, R., Alibolandi, M., Rafatpanah, H., Abnous, K., Khedri, M., & Ramezani, M. (2018). SELEX methods on the road to protein targeting with nucleic acid aptamers. *Biochimie*, *154*, 132–155. https://doi.org/10.1016/j.biochi.2018.09.001

Bazin, I., Tria, S. A., Hayat, A., & Marty, J.-L. (2017). New biorecognition molecules in biosensors for the detection of toxins. *Biosensors and Bioelectronics*, *87*, 285–298. https://doi.org/10.1016/j.bios.2016.06.083

Beaudeau, F., Ducrocq, V., Fourichon, C., & Seegers, H. (1995). Effect of Disease on Length of Productive Life of French Holstein Dairy Cows Assessed by Survival Analysis. *Journal of Dairy Science*, *78*(1), 103–117. https://doi.org/10.3168/jds.S0022-0302(95)76621-8

Becton Dickinson. (2002). *Microneedle for delivering a substance into the dermis* (Becton Dickinson and Company Patent No. 2413769).

Bedere, N. (2017). *Aptitude des vaches laitières à se reproduire en systèmes pâturants contrastés: Quelle vache pour quel système?* 207.

Bergveld, P. (1970). Development of an Ion-Sensitive Solid-State Device for Neurophysiological Measurements. *IEEE Transactions on Biomedical Engineering*, *BME-17*(1), 70–71. https://doi.org/10.1109/TBME.1970.4502688

Bhalla, N., Jolly, P., Formisano, N., & Estrela, P. (2016). Introduction to biosensors. *Essays in Biochemistry*, *60*(1), 1–8. https://doi.org/10.1042/EBC20150001

Bharadwaj, B. K., Nath, D., Pratap, R., & Raghavan, S. (2016). Making consistent contacts to graphene: Effect of architecture and growth induced defects. *Nanotechnology*, *27*(20), 205705. https://doi.org/10.1088/0957-4484/27/20/205705

Blanc, Paccard P., Gatien J., De La Torre A., Ponsart C., Egal D., Krauss D., Delval E., & Agabriel J. (2010). Caractérisation de l'oestrus chez la vache allaitante: Quantification des manifestations comportementales et facteurs de variation. *Renc. Rech. Ruminants*, *17*, 121–124.

Blavy, P., Derks, M., Martin, O., Höglund, J. K., & Friggens, N. C. (2016). Overview of progesterone profiles in dairy cows. *Theriogenology*, *86*(4), 1061–1071. https://doi.org/10.1016/j.theriogenology.2016.03.037

Blavy, P., Friggens, N. C., Nielsen, K. R., Christensen, J. M., & Derks, M. (2018). Estimating probability of insemination success using milk progesterone measurements. *Journal of Dairy Science*, *101*(2), 1648–1660. https://doi.org/10.3168/jds.2016-12453

Boyd. (1984). *Aids to oestrus detection—A review*. 60–67.

Boyer, C. N., Griffith, A. P., DeLong, K. L., Boyer, C. N., Griffith, A. P., & DeLong, K. L. (2020). *Reproductive Failure and Long-Term Profitability of Spring- and Fall-Calving Beef Cows*. https://doi.org/10.22004/AG.ECON.298435

Brielmann. (2014). *La solution Anemon pour des vaches connectéesUn système performant pour la détection électronique des chaleurs bovines*. *7*.

Brzáková, M., Svitáková, A., Čítek, J., Veselá, Z., & Vostrý, L. (2019). Genetic parameters of longevity for improving profitability of beef cattle1. *Journal of Animal Science*, *97*(1), 19–28. https://doi.org/10.1093/jas/sky390

Cao-An Vu, & Wen-Yih Chen. (2020). *Predicting Future Prospects of Aptamers in Field-Effect Transistor Biosensors*.

Castro Neto, A. H., Guinea, F., Peres, N. M. R., Novoselov, K. S., & Geim, A. K. (2009). The electronic properties of graphene. *Reviews of Modern Physics*, *81*(1), 109–162. https://doi.org/10.1103/RevModPhys.81.109

Champeau. (2020). *Dissolving microneedles for an optimal transdermal delivery of an active principle used in photodynamic therapy: Development and proof of concept*. École doctorale Biologie-Santé de Lille.

Chanvallon, Grimard, Chastant, & Bidan. (2015). Expression et détection des chaleurs dans les troupeaux bovins allaitants. *Institut de l'élevage*, 27.

Chastant-Maillard, & Saint-Dizier. (2016). *Elevage de précision*. France Agricole.

Chen, S., Zhang, Z.-B., Ma, L., Ahlberg, P., Gao, X., Qiu, Z., Wu, D., Ren, W., Cheng, H.-M., & Zhang, S.-L. (2012). A graphene field-effect capacitor sensor in electrolyte. *Applied Physics Letters*, *101*(15), 154106. https://doi.org/10.1063/1.4759147

Chua, B., Desai, S. P., Tierney, M. J., Tamada, J. A., & Jina, A. N. (2013a). Effect of microneedles shape on skin penetration and minimally invasive continuous glucose monitoring in vivo. *Sensors and Actuators A: Physical*, *203*, 373–381. https://doi.org/10.1016/j.sna.2013.09.026

Chua, B., Desai, S. P., Tierney, M. J., Tamada, J. A., & Jina, A. N. (2013b). Effect of microneedles shape on skin penetration and minimally invasive continuous glucose monitoring in vivo. *Sensors and Actuators A: Physical*, *203*, 373–381. https://doi.org/10.1016/j.sna.2013.09.026

Chung, H., Li, J., Kim, Y., Van Os, J. M. C., Brounts, S. H., & Choi, C. Y. (2020). Using implantable biosensors and wearable scanners to monitor dairy cattle's core body temperature in real-time. *Computers and Electronics in Agriculture*, *174*, 105453. https://doi.org/10.1016/j.compag.2020.105453

Clark, L. C., & Lyons, C. (1962). ELECTRODE SYSTEMS FOR CONTINUOUS MONITORING IN CARDIOVASCULAR SURGERY. *Annals of the New York Academy of Sciences*, *102*(1), 29–45. https://doi.org/10.1111/j.1749-6632.1962.tb13623.x

Claus, R., Karg, H., Zwiauer, D., von Butler, I., Pirchner, F., & Rattenberger, E. (1983). Analysis of Factors Influencing Reproductive Performance of the Dairy Cow by Progesterone Assay in Milk-Fat. *British Veterinary Journal*, *139*(1), 29–37. https://doi.org/10.1016/S0007-1935(17)30586-9

Cutullic. (2010). *Concurrence entre lactation et reproduction chez la vache laitière*.

Cutullic, E., Delaby, L., Causeur, D., & Disenhaus, C. (2006). *Facteurs de variation de la détection des chaleurs chez la vache laitière conduite en vêlages groupés*. 4.

Cutullic, E., Delaby, L., Causeur, D., Michel, G., & Disenhaus, C. (2009). Hierarchy of factors affecting behavioural signs used for oestrus detection of Holstein and Normande dairy cows in a seasonal calving system. *Animal Reproduction Science*, *113*(1–4), 22–37. https://doi.org/10.1016/j.anireprosci.2008.07.001

Dalton, J. C., Nadir, S., Bame, J. H., Noftsinger, M., Nebel, R. L., & Saacke, R. G. (2001). Effect of Time of Insemination on Number of Accessory Sperm, Fertilization Rate, and Embryo Quality in Nonlactating Dairy Cattle. *Journal of Dairy Science*, *84*(11), 2413–2418. https://doi.org/10.3168/jds.S0022-0302(01)74690- 5

Damborský, P., Švitel, J., & Katrlík, J. (2016). Optical biosensors. *Essays In Biochemistry*, *60*(1), 91–100. https://doi.org/10.1042/EBC20150010

Davis, S. P., Prausnitz, M. R., & Allen, M. G. (2003). Fabrication and characterization of laser micromachined hollow microneedles. *TRANSDUCERS '03. 12th International Conference on Solid-State Sensors, Actuators and Microsystems. Digest of Technical Papers (Cat. No.03TH8664), 2, 1435–1438.* *https://doi.org/10.1109/SENSOR.2003.1217045*

Dieleman, S. J., Bevers, M. M., Van Tol, H. T. M., & Willemse, A. H. (1986). Peripheral plasma concentrations of oestradiol, progesterone, cortisol, LH and prolactin during the oestrous cycle in the cow, with emphasis on the peri-oestrous period. *Animal Reproduction Science*, *10*(4), 275–292. https://doi.org/10.1016/0378-4320(86)90003-5

Dijkhuizen, A. A., Stelwagen, J., & Renkema, J. A. (1985). Economic aspects of reproductive failure in dairy cattle. I. Financial loss at farm level. *Preventive Veterinary Medicine*, *3*(3), 251–263. https://doi.org/10.1016/0167-5877(85)90020-0

Disenhaus, Cutullic, Blanc, Gatien, Agabriel, Hetreau T, Michel G, Paccard P., Badinand F, Egal D., & Ponsart C. (2008). Caractéristiques comparées de la cyclicité après vêlage de différentes races bovines. *Renc. Rech. Ruminants*.

Dobson,H, Midmer, SE, & Fitzpatrick, RJ. (1975). *Relationship between progesterone concentrations in milk and plasma during bovien estrous cycle*. *96*(10), 222–223. https://doi.org/10.1136/vr.96.10.222

Donnelly, R. F., Morrow, D. I. J., McCarron, P. A., David Woolfson, A., Morrissey, A., Juzenas, P., Juzeniene, A., Iani, V., McCarthy, H. O., & Moan, J. (2009). Microneedle Arrays Permit Enhanced Intradermal Delivery of a Preformed Photosensitizer. *Photochemistry and Photobiology*, *85*(1), 195–204. https://doi.org/10.1111/j.1751-1097.2008.00417.x

Donnelly, R. F., Singh, T. R. R., Garland, M. J., Migalska, K., Majithiya, R., McCrudden, C. M., Kole, P. L., Mahmood, T. M. T., McCarthy, H. O., & Woolfson, A. D. (2012). Hydrogel-Forming Microneedle Arrays for Enhanced Transdermal Drug Delivery.

Advanced Functional Materials, *22*(23), 4879–4890. https://doi.org/10.1002/adfm.201200864

Dowling, D. (1955). The thickness of cattle skin. *Australian Journal of Agricultural Research*, *6*(5), 776. https://doi.org/10.1071/AR9550776

Duan, X., Li, Y., Rajan, N. K., Routenberg, D. A., Modis, Y., & Reed, M. A. (2012). Quantification of the affinities and kinetics of protein interactions using silicon nanowire biosensors. *Nature Nanotechnology*, *7*(6), 401–407. https://doi.org/10.1038/nnano.2012.82

Elias, P. M. (2012). Structure and Function of the Stratum Corneum Extracellular Matrix. *Journal of Investigative Dermatology*, *132*(9), 2131–2133. https://doi.org/10.1038/jid.2012.246

Ellington, A. D., & Szostak, J. W. (1990). In vitro selection of RNA molecules that bind specific ligands. *Nature*, *346*(6287), 818–822. https://doi.org/10.1038/346818a0

Felix, F. S., & Angnes, L. (2018). Electrochemical immunosensors – A powerful tool for analytical applications. *Biosensors and Bioelectronics*, *102*, 470–478. https://doi.org/10.1016/j.bios.2017.11.029

Firk, R., Stamer, E., Junge, W., & Krieter, J. (2002). Automation of oestrus detection in dairy cows: A review. *Livestock Production Science*, 14.

Fisher, A. D., Morton, R., Dempsey, J. M. A., Henshall, J. M., & Hill, J. R. (2008). Evaluation of a new approach for the estimation of the time of the LH surge in dairy cows using vaginal temperature and electrodeless conductivity measurements. *Theriogenology*, *70*(7), 1065–1074. https://doi.org/10.1016/j.theriogenology.2008.06.023

Fowler, J. M., Wong, D. K. Y., Halsall, H. B., & Heineman, W. R. (2008). Recent developments in electrochemical immunoassays and immunosensors. In *Electrochemical Sensors, Biosensors and their Biomedical Applications* (pp. 115–143). Elsevier. https://doi.org/10.1016/B978-012373738-0.50007-6

Friggens, N. C., & Chagunda, M. G. G. (2005). Prediction of the reproductive status of cattle on the basis of milk progesterone measures: Model description. *Theriogenology*, *64*(1), 155–190. https://doi.org/10.1016/j.theriogenology.2004.11.014

Fritz, J., Cooper, E. B., Gaudet, S., Sorger, P. K., & Manalis, S. R. (2002). Electronic detection of DNA by its intrinsic molecular charge. *Proceedings of the National Academy of Sciences*, *99*(22), 14142–14146. https://doi.org/10.1073/pnas.232276699

Gardeniers, H. J. G. E., Luttge, R., Berenschot, E. J. W., de Boer, M. J., Yeshurun, S. Y., Hefetz, M., van-t Oever, R., & van den Berg, A. (2003). Silicon micromachined hollow microneedles for transdermal liquid transport. *Journal of Microelectromechanical Systems*, *12*(6), 855–862. https://doi.org/10.1109/JMEMS.2003.820293

Gerstel, M. S., & Place, V. A. (1971). *(54) DRUG DELIVERY DEVICE*. 13.

Gill, H. S., & Prausnitz, M. R. (2007a). Coated microneedles for transdermal delivery. *Journal of Controlled Release*, *117*(2), 227–237. https://doi.org/10.1016/j.jconrel.2006.10.017

Gill, H. S., & Prausnitz, M. R. (2007b). Coating Formulations for Microneedles. *Pharmaceutical Research*, *24*(7), 1369–1380. https://doi.org/10.1007/s11095-007-9286-4

Gold L. (1995). *Oligonucleotides as research, diagnostic, and therapeutic agents*.

Gold, V. (Ed.). (2019). *The IUPAC Compendium of Chemical Terminology: The Gold Book* (4th ed.). International Union of Pure and Applied Chemistry (IUPAC). https://doi.org/10.1351/goldbook

Grimard, B., Humblot, P., Ponter, A. A., Chastant, S., Constant, F., & Mialot, J. P. (2003). Efficacité des traitements de synchronisation des chaleurs chez les bovins. *INRAE Productions Animales*, *16*(3), 211–227. https://doi.org/10.20870/productions-animales.2003.16.3.3661

Gumbrecht, W., Schelter, W., Montag, B., Rasinski, M., & Pfeiffer, U. (1990). Online blood electrolyte monitoring with a ChemFET microcell system. *Sensors and Actuators B: Chemical*, *1*(1), 477–480. https://doi.org/10.1016/0925-4005(90)80253-V

Hadley, G. L., Wolf, C. A., & Harsh, S. B. (2006). Dairy Cattle Culling Patterns, Explanations, and Implications. *Journal of Dairy Science*, *89*(6), 2286–2296. https://doi.org/10.3168/jds.S0022-0302(06)72300-1

Hélène M.E.P.P Boÿreau. (2019). *Les freins au développement de l'IA en élevage allaitant*. Faculté de médecine de Créteil.

Henry, S., Mcallister, D. V., Allen, M. G., & Prausnitz, M. R. (1998). *Microfabricated microneedles: A novel approach to transdermal drug delivery*. *87*(8), 4.

Hilder, T. A., & Hodgkiss, J. M. (2017). The Bound Structures of 17 beta-Estradiol-Binding Aptamers. *CHEMPHYSCHEM*, *18*(14), 1881–1887. https://doi.org/10.1002/cphc.201700363

Homola, J. (2003). Present and future of surface plasmon resonance biosensors. *Analytical and Bioanalytical Chemistry*, *377*(3), 528–539. https://doi.org/10.1007/s00216-003-2101-0

Hostiou, N., Fagon, J., Chauvat, S., Turlot, A., Kling-Eveillard, F., Boivin, X., & Allain, C. (2017). *Impact of precision livestock farming on work and human-animal interactions on dairy farms. A review*. 9.

Huangxian Ju, Guosong Lai, & Feng Yan. (2017). *Immunosensing for Detection of Protein Biomarkers* (Elsevier).

Hugo, A. (2020). *Graphene-based liquid-gated transistors for biosensing*. Université Grenoble Alpes.

Hutton, A. R. J., Quinn, H. L., McCague, P. J., Jarrahian, C., Rein-Weston, A., Coffey, P. S., Gerth-Guyette, E., Zehrung, D., Larrañeta, E., & Donnelly, R. F. (2018). Transdermal delivery of vitamin K using dissolving microneedles for the prevention of vitamin K deficiency bleeding. *International Journal of Pharmaceutics*, *541*(1–2), 56–63. https://doi.org/10.1016/j.ijpharm.2018.02.031

Inra. (2007). *Tables d'alimentation des bovins, ovins, caprins Besoins des animaux - Valeurs des aliments: Tables Inra 2010*. Editions Quae.

Iqbal, M., Gleeson, M. A., Spaugh, B., Tybor, F., Gunn, W. G., Hochberg, M., Baehr-Jones, T., Bailey, R. C., & Gunn, L. C. (2010). Label-Free Biosensor Arrays Based on Silicon Ring Resonators and High-Speed Optical Scanning Instrumentation. *IEEE Journal of Selected Topics in Quantum Electronics*, *16*(3), 654–661. https://doi.org/10.1109/JSTQE.2009.2032510

Jimenez, G. C., Eissa, S., Ng, A., Alhadrami, H., Zourob, M., & Siaj, M. (2015). Aptamer-Based Label-Free Impedimetric Biosensor for Detection of Progesterone. *ANALYTICAL CHEMISTRY*, *87*(2), 1075–1082. https://doi.org/10.1021/ac503639s

Kamperman, T., Koerselman, M., Kelder, C., Hendriks, J., Crispim, J. F., de Peuter, X., Dijkstra, P. J., Karperien, M., & Leijten, J. (2019). Spatiotemporal material functionalization via competitive supramolecular complexation of avidin and biotin analogs. *Nature Communications*, *10*(1), 4347. https://doi.org/10.1038/s41467-019-12390-4

Katoch, J., Kim, S. N., Kuang, Z., Farmer, B. L., Naik, R. R., Tatulian, S. A., & Ishigami, M. (2012). Structure of a Peptide Adsorbed on Graphene and Graphite. *Nano Letters*, *12*(5), 2342–2346. https://doi.org/10.1021/nl300286k

Ke, H., Liu, M., Zhuang, L., Li, Z., Fan, L., & Zhao, G. (2014). A Fetomolar Level 17β-estradiol Electrochemical Aptasensor Constructed On Hierachical Dendritic Gold

Modified Boron-Doped Diamond Electrode. *Electrochimica Acta*, *137*, 146–153. https://doi.org/10.1016/j.electacta.2014.06.014

Kerbrat, & Disenhaus. (2004). Proposition for an Updated Behavioural Characterization of the Oestrus Period in Dairy Cows. *Applied Animal Behaviour Science*.

Kiddy, C. A. (1977). Variation in Physical Activity as an Indication of Estrus in Dairy Cows. *Journal of Dairy Science*, *60*(2), 235–243. https://doi.org/10.3168/jds.S0022-0302(77)83859-9

Kim, Y. S., Jung, H. S., Matsuura, T., Lee, H. Y., Kawai, T., & Gu, M. B. (2007). Electrochemical detection of 17β-estradiol using DNA aptamer immobilized gold electrode chip. *Biosensors and Bioelectronics*, *22*(11), 2525–2531. https://doi.org/10.1016/j.bios.2006.10.004

Kim, Y.-C., Park, J.-H., & Prausnitz, M. R. (2012). Microneedles for drug and vaccine delivery. *Advanced Drug Delivery Reviews*, *64*(14), 1547–1568. https://doi.org/10.1016/j.addr.2012.04.005

Knight, C. H. (2020a). Review: Sensor techniques in ruminants: more than fitness trackers. *Animal*, *14*, s187–s195. https://doi.org/10.1017/S1751731119003276

Knight, C. H. (2020b). Review: Sensor techniques in ruminants: more than fitness trackers. *Animal*, *14*, s187–s195. https://doi.org/10.1017/S1751731119003276

Kochhar, J. S., Quek, T. C., Soon, W. J., Choi, J., Zou, S., & Kang, L. (2013). Effect of Microneedle Geometry and Supporting Substrate on Microneedle Array Penetration into Skin. *Journal of Pharmaceutical Sciences*, *102*(11), 4100–4108. https://doi.org/10.1002/jps.23724

Kohler, S., Brielmann, C., & Hug, K. (2010). *Détection automatique des chaleurs chez les bovins*. 4.

Kuramitz, H., Matsuda, M., Thomas, J. H., Sugawara, K., & Tanaka, S. (2003). Electrochemical immunoassay at a 17β-estradiol self-assembled monolayer electrode using a redox marker. *The Analyst*, *128*(2), 182–186. https://doi.org/10.1039/b209590b

Larrañeta, E., Lutton, R. E. M., Woolfson, A. D., & Donnelly, R. F. (2016a). Microneedle arrays as transdermal and intradermal drug delivery systems: Materials science, manufacture and commercial development. *Materials Science and Engineering: R: Reports, 104, 1–32. https://doi.org/10.1016/j.mser.2016.03.001*

Larrañeta, E., Lutton, R. E. M., Woolfson, A. D., & Donnelly, R. F. (2016b). Microneedle arrays as transdermal and intradermal drug delivery systems: Materials

science, manufacture and commercial development. Materials Science and Engineering: R: Reports, 104, 1–32. https://doi.org/10.1016/j.mser.2016.03.001

Lee, K., Lee, C. Y., & Jung, H. (2011). Dissolving microneedles for transdermal drug administration prepared by stepwise controlled drawing of maltose. Biomaterials, 32(11), 3134–3140. https://doi.org/10.1016/j.biomaterials.2011.01.014

Li, X., Cai, W., An, J., Kim, S., Nah, J., Yang, D., Piner, R., Velamakanni, A., Jung, I., Tutuc, E., Banerjee, S. K., Colombo, L., & Ruoff, R. S. (2009). Large-Area Synthesis of High-Quality and Uniform Graphene Films on Copper Foils. Science, 324(5932), 1312–1314. https://doi.org/10.1126/science.1171245

Liu, J., Bai, W., Niu, S., Zhu, C., Yang, S., & Chen, A. (2015). Highly sensitive colorimetric detection of 17β-estradiol using split DNA aptamers immobilized on unmodified gold nanoparticles. Scientific Reports, 4(1), 7571. https://doi.org/10.1038/srep07571

Liu, X., Wang, X., Zhang, J., Feng, H., Liu, X., & Wong, D. K. Y. (2012). Detection of estradiol at an electrochemical immunosensor with a Cu UPD|DTBP–Protein G scaffold. Biosensors and Bioelectronics, 35(1), 56–62. https://doi.org/10.1016/j.bios.2012.02.002

Lopez, H., Bunch, T. D., & Shipka, M. P. (2002). Estrogen concentrations in milk at estrus and ovulation in dairy cows. *Animal Reproduction Science*, *72*(1–2), 37–46. https://doi.org/10.1016/S0378-4320(02)00074-X

Lopez, H., Satter, L. D., & Wiltbank, M. C. (2004). Relationship between level of milk production and estrous behavior of lactating dairy cows. *Animal Reproduction Science*, *81*(3–4), 209–223. https://doi.org/10.1016/j.anireprosci.2003.10.009

Lucy, M. C. (2001). Reproductive Loss in High-Producing Dairy Cattle: Where Will It End? *Journal of Dairy Science*, *84*(6), 1277–1293. https://doi.org/10.3168/jds.S0022-0302(01)70158-0

Luo, X., & Davis, J. J. (2013). Electrical biosensors and the label free detection of protein disease biomarkers. *Chemical Society Reviews*, *42*(13), 5944–5962. https://doi.org/10.1039/C3CS60077G

Macwan, I., Khan, M. D. H., Aphale, A., Singh, S., Liu, J., Hingorani, M., & Patra, P. (2017). Interactions between avidin and graphene for development of a biosensing platform. *Biosensors and Bioelectronics*, *89*, 326–333. https://doi.org/10.1016/j.bios.2016.07.024

Mangold, S. L., & Cloninger, M. J. (2006). Binding of monomeric and dimeric Concanavalin A to mannose-functionalized dendrimers. *Organic & Biomolecular Chemistry*, *4*(12), 2458. https://doi.org/10.1039/b600066e

Mann, J. A., Alava, T., Craighead, H. G., & Dichtel, W. R. (2013). Preservation of Antibody Selectivity on Graphene by Conjugation to a Tripod Monolayer. *Angewandte Chemie International Edition*, *52*(11), 3177–3180. https://doi.org/10.1002/anie.201209149

Mann, J. A., & Dichtel, W. R. (2013a). Noncovalent Functionalization of Graphene by Molecular and Polymeric Adsorbates. *The Journal of Physical Chemistry Letters*, *4*(16), 2649–2657. https://doi.org/10.1021/jz4010448

Mann, J. A., & Dichtel, W. R. (2013b). Improving the Binding Characteristics of Tripodal Compounds on Single Layer Graphene. *ACS Nano*, *7*(8), 7193–7199. https://doi.org/10.1021/nn402599x

Mann, J. A., Rodríguez-López, J., Abruña, H. D., & Dichtel, W. R. (2011). Multivalent Binding Motifs for the Noncovalent Functionalization of Graphene. *Journal of the American Chemical Society*, *133*(44), 17614–17617. https://doi.org/10.1021/ja208239v

Mansournia, M. A., Waters, R., Nazemipour, M., Bland, M., & Altman, D. G. (2021). Bland-Altman methods for comparing methods of measurement and response to criticisms. *Global Epidemiology*, *3*, 100045. https://doi.org/10.1016/j.gloepi.2020.100045

Martin, O., Friggens, N. C., Dupont, J., Salvetti, P., Freret, S., Rame, C., Elis, S., Gatien, J., Disenhaus, C., & Blanc, F. (2013). Data-derived reference profiles with corepresentation of progesterone, estradiol, LH, and FSH dynamics during the bovine estrous cycle. *Theriogenology*, *79*(2), 331-343.e4. https://doi.org/10.1016/j.theriogenology.2012.09.025

McAllister, D. V., Wang, P. M., Davis, S. P., Park, J.-H., Canatella, P. J., Allen, M. G., & Prausnitz, M. R. (2003). Microfabricated needles for transdermal delivery of macromolecules and nanoparticles: Fabrication methods and transport studies. *Proceedings of the National Academy of Sciences*, *100*(24), 13755–13760. https://doi.org/10.1073/pnas.2331316100

Med'Vet. (2021). *PRID® Delta Système*. Med'Vet. https://www.med-vet.fr/medicament-prid-delta-1-55-g-systeme-de-diffusion-vaginal-p506

Mehrotra, P. (2016). Biosensors and their applications – A review. *Journal of Oral Biology and Craniofacial Research*, *6*(2), 153–159. https://doi.org/10.1016/j.jobcr.2015.12.002

Meisterling, E. M., & Dailey, R. A. (1987). *Use of Concentrations of Progesterone and Estradiol-17 in Milk in Monitoring Postpartum Ovarian Function in Dairy Cows1*. *70*(10), 8.

Mollarasouli, Kurbanoglu, & Ozkan. (2019). The Role of Electrochemical Immunosensors in Clinical Analysis. *Biosensors*, *9*(3), 86. https://doi.org/10.3390/bios9030086

Moore, S. G., Aublet, V., & Butler, S. T. (2021). Monitoring estrous activity in pasture-based dairy cows. *Theriogenology*, *160*, 90–94. https://doi.org/10.1016/j.theriogenology.2020.11.002

Morales-Narváez, E., Baptista-Pires, L., Zamora-Gálvez, A., & Merkoçi, A. (2016). Graphene-Based Biosensors: Going Simple. *Advanced Materials*, n/a-n/a. https://doi.org/10.1002/adma.201604905

Mottram, T. (2016). Animal board invited review: Precision livestock farming for dairy cows with a focus on oestrus detection. *Animal*, *10*(10), 1575–1584. https://doi.org/10.1017/S1751731115002517

Mukherjee, S., Meshik, X., Choi, M., Farid, S., Datta, D., Lan, Y., Poduri, S., Sarkar, K., Baterdene, U., Huang, C.-E., Wang, Y. Y., Burke, P., Dutta, M., & Stroscio, M. A. (2015). A Graphene and Aptamer Based Liquid Gated FET-Like Electrochemical Biosensor to Detect Adenosine Triphosphate. IEEE Transactions on NanoBioscience, 14(8), 967–972. https://doi.org/10.1109/TNB.2015.2501364

Navalon, S., Dhakshinamoorthy, A., Alvaro, M., Antonietti, M., & García, H. (2017). Active sites on graphene-based materials as metal-free catalysts. Chemical Society Reviews, 46(15), 4501–4529. https://doi.org/10.1039/C7CS00156H

O'Connor, M. L. (2009). Estrus Detection. In Current Therapy in Large Animal Theriogenology (2nd ed., p. 9).

Oh, J., Park, H., Do, K., Han, M., Hyun, D., Kim, C., Kim, C., Lee, S., Hwang, S., & Shin, S. (2008). Influence of the delivery systems using a microneedle array on the permeation of a hydrophilic molecule, calcein. European Journal of Pharmaceutics and Biopharmaceutics, 69(3), 1040–1045. https://doi.org/10.1016/j.ejpb.2008.02.009

Olatunji, O., Das, D. B., Garland, M. J., Belaid, L., & Donnelly, R. F. (2013). Influence of Array Interspacing on the Force Required for Successful Microneedle Skin Penetration: Theoretical and Practical Approaches. Journal of Pharmaceutical Sciences, 102(4), 1209–1221. https://doi.org/10.1002/jps.23439

Olowu, R. A., Arotiba, O., Mailu, S. N., Waryo, T. T., Baker, P., & Iwuoha, E. (2010). Electrochemical Aptasensor for Endocrine Disrupting 17β-Estradiol Based on a Poly(3,4-ethylenedioxylthiopene)-Gold Nanocomposite Platform. Sensors, 10(11), 9872–9890. https://doi.org/10.3390/s101109872

Ovsianikov, A., Chichkov, B., Mente, P., Monteiro-Riviere, N. A., Doraiswamy, A., & Narayan, R. J. (2007). Two Photon Polymerization of Polymer?Ceramic Hybrid Materials for Transdermal Drug Delivery. International Journal of Applied Ceramic Technology, 4(1), 22–29. https://doi.org/10.1111/j.1744-7402.2007.02115.x

Palmer, M. A., Olmos, G., Boyle, L. A., & Mee, J. F. (2010). Estrus detection and estrus characteristics in housed and pastured Holstein–Friesian cows. Theriogenology, 74(2), 255–264. https://doi.org/10.1016/j.theriogenology.2010.02.009

Park, J., & Yan, M. (2013). Covalent Functionalization of Graphene with Reactive Intermediates. Accounts of Chemical Research, 46(1), 181–189. https://doi.org/10.1021/ar300172h

Pereira, R. L., Nascimento, I. C., Santos, A. P., Ogusuku, I. E. Y., Lameu, C., Mayer, G., & Ulrich, H. (2018). Aptamers: Novelty tools for cancer biology. Oncotarget, 9(42), 26934–26953. https://doi.org/10.18632/oncotarget.25260

Pesquero, N. C., Carvalho, F. C., Faria, R. C., Roque-Barreira, M.-C., & Bueno, P. R. (2017). ArtinM Binding Effinities and Kinetic Interaction with Leukemia Cells: A Quartz Crystal Microbalance Bioelectroanalysis on the Cytotoxic Effect. Electroanalysis, 29(6), 1554–1558. https://doi.org/10.1002/elan.201700093

Petrone, N., Dean, C. R., Meric, I., van der Zande, A. M., Huang, P. Y., Wang, L., Muller, D., Shepard, K. L., & Hone, J. (2012). Chemical Vapor Deposition-Derived Graphene with Electrical Performance of Exfoliated Graphene. Nano Letters, 12(6), 2751–2756. https://doi.org/10.1021/nl204481s

Phitsini Suvarnaphaet, & Suejit Pechprasarn. (2017). Graphene-Based Materials for Biosensors: A Review. Sensors, 17(10), 2161. https://doi.org/10.3390/s17102161

Pimentel, E. C. G., & König, S. (2012). Genomic selection for the improvement of meat quality in beef. *Journal of Animal Science*, *90*(10), 3418–3426. https://doi.org/10.2527/jas.2011-5005

Piro, B., Shi, S., Reisberg, S., Noël, V., & Anquetin, G. (2016). Comparison of Electrochemical Immunosensors and Aptasensors for Detection of Small Organic Molecules in Environment, Food Safety, Clinical and Public Security. *Biosensors*, *6*(1), 7. https://doi.org/10.3390/bios6010007

Ponsart, Frappat, Gatien, Chanvallon, Fabienne Blanc, Disenhaus, Seegers, Ribaud, Salvetti, & Paccard. (2010). *La détection par les éleveurs des chaleurs des vaches: Des pratiques et des logiques de décision très diverses*.

Prausnitz, M. R. (2004). Microneedles for transdermal drug delivery. *Advanced Drug Delivery Reviews*, *56*(5), 581–587. https://doi.org/10.1016/j.addr.2003.10.023

R Development Core Team. (2008). *R: A language and environment for statistical computing*. R Foundation for Statistical Computing.

Rabiee, A. R., Macmillan, K. L., & Schwarzenberger, F. (2002). Plasma, milk and faecal progesterone concentrations during the oestrous cycle of lactating dairy cows with different milk yields. *Animal Reproduction Science*, *74*(3–4), 121–131. https://doi.org/10.1016/S0378-4320(02)00169-0

Ranasinghe, R. M. S. B. K., Nakao, T., Yamada, K., & Koike, K. (2010). Silent ovulation, based on walking activity and milk progesterone concentrations, in Holstein cows housed in a free-stall barn. *Theriogenology*, *73*(7), 942–949. https://doi.org/10.1016/j.theriogenology.2009.11.021

Reynaud, L., Bouchet-Spinelli, A., Janot, J.-M., Buhot, A., Balme, S., & Raillon, C. (2021). Discrimination of α-Thrombin and γ-Thrombin Using Aptamer-Functionalized Nanopore Sensing. *Analytical Chemistry*, *93*(22), 7889–7897. https://doi.org/10.1021/acs.analchem.1c00461

Rodgers, J. C., Bird, S. L., Larson, J. E., Dilorenzo, N., Dahlen, C. R., DiCostanzo, A., & Lamb, G. C. (2012). An economic evaluation of estrous synchronization and timed artificial insemination in suckled beef cows1. *Journal of Animal Science*, *90*(11), 4055–4062. https://doi.org/10.2527/jas.2011-4836

Roelofs, J. B. (2005). *When to inseminate the cow? Insemination, ovulation and fertilization in diary cattle.* [Wageningen Universiteit]. ISBN 90-8504-285-2

Roelofs, López-Gatius, F., Hunter, R. H. F., van Eerdenburg, F. J. C. M., & Hanzen, Ch. (2010). When is a cow in estrus? Clinical and practical aspects. *Theriogenology*, *74*(3), 327–344. https://doi.org/10.1016/j.theriogenology.2010.02.016

Roelofs, Soede, N. M., Voskamp-Harkema, W., & Kemp, B. (2008). The effect of fenceline bull exposure on expression of oestrus in dairy cows. *Animal Reproduction Science*, *108*(1–2), 226–235. https://doi.org/10.1016/j.anireprosci.2007.08.002

Roelofs, Van Eerdenburg, F. J. C. M., Hazeleger, W., Soede, N. M., & Kemp, B. (2006). Relationship between progesterone concentrations in milk and blood and time of ovulation in dairy cattle. *Animal Reproduction Science*, *91*(3–4), 337–343. https://doi.org/10.1016/j.anireprosci.2005.04.015

Roelofs, van Eerdenburg, F. J. C. M., Soede, N. M., & Kemp, B. (2005). Various behavioral signs of estrous and their relationship with time of ovulation in dairy cattle. *Theriogenology*, *63*(5), 1366–1377. https://doi.org/10.1016/j.theriogenology.2004.07.009

Romanyuk, A. V., Zvezdin, V. N., Samant, P., Grenader, M. I., Zemlyanova, M., & Prausnitz, M. R. (2014). Collection of Analytes from Microneedle Patches. *Analytical Chemistry*, *86*(21), 10520–10523. https://doi.org/10.1021/ac503823p

Roxhed, N., Griss, P., & Stemme, G. (2008). Membrane-sealed hollow microneedles and related administration schemes for transdermal drug delivery. *Biomedical Microdevices*, *10*(2), 271–279. https://doi.org/10.1007/s10544-007-9133-8

Roxhed, N., Samel, B., Nordquist, L., Griss, P., & Stemme, G. (2008). Painless Drug Delivery Through Microneedle-Based Transdermal Patches Featuring Active Infusion. *IEEE Transactions on Biomedical Engineering*, *55*(3), 1063–1071. https://doi.org/10.1109/TBME.2007.906492

Rutten, C. J., Steeneveld, W., Inchaisri, C., & Hogeveen, H. (2014). An ex ante analysis on the use of activity meters for automated estrus detection: To invest or not to invest? *Journal of Dairy Science*, *97*(11), 6869–6887. https://doi.org/10.3168/jds.2014-7948

Rutten, C. J., Steeneveld, W., Oude Lansink, A. G. J. M., & Hogeveen, H. (2018). Delaying investments in sensor technology: The rationality of dairy farmers' investment decisions illustrated within the framework of real options theory. *Journal of Dairy Science*, *101*(8), 7650–7660. https://doi.org/10.3168/jds.2017-13358

Sá Filho, M. F., Penteado, L., Reis, E. L., Reis, Tomás. A. N. P. S., Galvão, K. N., & Baruselli, P. S. (2013). Timed artificial insemination early in the breeding season improves the reproductive performance of suckled beef cows. *Theriogenology*, *79*(4), 625–632. https://doi.org/10.1016/j.theriogenology.2012.11.016

Sabri, A. H., Cater, Z., Ogilvie, J., Scurr, D. J., Marlow, M., & Segal, J. (2020). Characterisation of mechanical insertion of commercial microneedles. *Journal of Drug Delivery Science and Technology*, *58*, 101766. https://doi.org/10.1016/j.jddst.2020.101766

Saint-Dizier, M., & Chastant-Maillard, S. (2012a). Towards an Automated Detection of Oestrus in Dairy Cattle: Automated Oestrus Detection in Dairy Cattle. *Reproduction in Domestic Animals*, *47*(6), 1056–1061. https://doi.org/10.1111/j.1439-0531.2011.01971.x

Saint-Dizier, M., & Chastant-Maillard, S. (2012b). Towards an Automated Detection of Oestrus in Dairy Cattle: Automated Oestrus Detection in Dairy Cattle. *Reproduction in Domestic Animals*, *47*(6), 1056–1061. https://doi.org/10.1111/j.1439-0531.2011.01971.x

Saint-Dizier, M., & Chastant-Maillard, S. (2015). Methods and on-farm devices to predict calving time in cattle. *The Veterinary Journal*, *205*(3), 349–356. https://doi.org/10.1016/j.tvjl.2015.05.006

Saumande, J., & Humblot, P. (2005). The variability in the interval between estrus and ovulation in cattle and its determinants. *Animal Reproduction Science*, *85*(3–4), 171–182. https://doi.org/10.1016/j.anireprosci.2003.09.009

Schöning, M. J., & Poghossian, A. (2006). Bio FEDs (Field-Effect Devices): State-of-the-Art and New Directions. *Electroanalysis*, *18*(19–20), 1893–1900. https://doi.org/10.1002/elan.200603609

Seegers, H. (2006). *Economics of the reproductive performance of dairy herds*. 12.

Shafiee, H., Lidstone, E. A., Jahangir, M., Inci, F., Hanhauser, E., Henrich, T. J., Kuritzkes, D. R., Cunningham, B. T., & Demirci, U. (2014). Nanostructured Optical Photonic Crystal Biosensor for HIV Viral Load Measurement. *Scientific Reports*, *4*, 4116. https://doi.org/10.1038/srep04116

Silper, B. F., Robles, I., Madureira, A. M. L., Burnett, T. A., Reis, M. M., de Passillé, A. M., Rushen, J., & Cerri, R. L. A. (2015). Automated and visual measurements of estrous behavior and their sources of variation in Holstein heifers. I: Walking activity and behavior frequency. *Theriogenology*, *84*(2), 312–320. https://doi.org/10.1016/j.theriogenology.2014.12.029

Souteyrand, E., Cloarec, J. P., Martin, J. R., Wilson, C., Lawrence, I., Mikkelsen, S., & Lawrence, M. F. (1997). Direct Detection of the Hybridization of Synthetic Homo-Oligomer DNA Sequences by Field Effect. *The Journal of Physical Chemistry B*, *101*(15), 2980–2985. https://doi.org/10.1021/jp963056h

Steinbach, S., Jalili-Firoozinezhad, S., Srinivasan, S., Melo, M. B., Middleton, S., Konold, T., Coad, M., Hammond, P. T., Irvine, D. J., Vordermeier, M., & Kapur, V. (2021). Temporal dynamics of intradermal cytokine response to tuberculin in Mycobacterium bovis BCG-vaccinated cattle using sampling microneedles. *Scientific Reports*, *11*(1), 7074. https://doi.org/10.1038/s41598-021-86398-6

Stensaas, S. S., & Stensaas, L. J. (1978). Histopathological evaluation of materials implanted in the cerebral cortex. *Acta Neuropathologica*, *41*(2), 145–155. https://doi.org/10.1007/BF00689766

Sun, C., Walker, K. L., Wakefield, D. L., & Dichtel, W. R. (2015). Retaining the Activity of Enzymes and Fluorophores Attached to Graphene Oxide. *Chemistry of Materials*, *27*(12), 4499–4504. https://doi.org/10.1021/acs.chemmater.5b01954

Sun, D., Guo, T., Ran, Y., Huang, Y., & Guan, B.-O. (2014). In-situ DNA hybridization detection with a reflective microfiber grating biosensor. *Biosensors and Bioelectronics*, *61*, 541–546. https://doi.org/10.1016/j.bios.2014.05.065

Svobodová, M., Skouridou, V., Botero, M. L., Jauset-Rubio, M., Schubert, T., Bashammakh, A. S., El-Shahawi, M. S., Alyoubi, A. O., & O'Sullivan, C. K. (2017). The

characterization and validation of 17β-estradiol binding aptamers. *The Journal of Steroid Biochemistry and Molecular Biology*, *167*, 14–22. https://doi.org/10.1016/j.jsbmb.2016.09.018

Tuerk, C., & Gold, L. (1990a). Systematic evolution of ligands by exponential enrichment: RNA ligands to bacteriophage T4 DNA polymerase. *Science*, *249*(4968), 505–510. https://doi.org/10.1126/science.2200121

Tuerk, C., & Gold, L. (1990b). Systematic evolution of ligands by exponential enrichment: RNA ligands to bacteriophage T4 DNA polymerase. *Science*, *249*(4968), 505–510. https://doi.org/10.1126/science.2200121

Vailes, L. D., & Britt, J. H. (1990). Influence of footing surface on mounting and other sexual behaviors of estrual Holstein cows. *Journal of Animal Science*, *68*(8), 2333. https://doi.org/10.2527/1990.6882333x

Van Eerdenburg, F. J. C. M., Karthaus, D., Taverne, M. A. M., Mercis, I., & Szenci, O. (2002). The Relationship between Estrous Behavioral Score and Time of Ovulation in Dairy Cattle. *Journal of Dairy Science*, *85*(5), 1150–1156. https://doi.org/10.3168/jds.S0022-0302(02)74177-5

Van Eerdenburg, F. J. C. M., Loeffler, H. S. H., & van Vliet, J. H. (1996). Detection of oestrus in dairy cows: A new approach to an old problem. *Veterinary Quarterly*, *18*(2), 52–54. https://doi.org/10.1080/01652176.1996.9694615

Van Vliet, & Van Eerdenburg. (1996). Sexual activities and oestrus detection in lactating Holstein cows. *Applied Animal Behaviour Science*.

Velasco-Garcia, M. N., & Mottram, T. (2001). Biosensors in the livestock industry: An automated ovulation prediction system for dairy cows. *Trends in Biotechnology*, *19*(11), 433. https://doi.org/10.1016/S0167-7799(01)01841-8

Verbaan, F. J., Bal, S. M., van den Berg, D. J., Dijksman, J. A., van Hecke, M., Verpoorten, H., van den Berg, A., Luttge, R., & Bouwstra, J. A. (2008). Improved piercing of microneedle arrays in dermatomed human skin by an impact insertion method. *Journal of Controlled Release*, *128*(1), 80–88. https://doi.org/10.1016/j.jconrel.2008.02.009

Vermette, P., Gengenbach, T., Divisekera, U., Kambouris, P. A., Griesser, H. J., & Meagher, L. (2003). Immobilization and surface characterization of NeutrAvidin biotin-binding protein on different hydrogel interlayers. *Journal of Colloid and Interface Science*, *259*(1), 13–26. https://doi.org/10.1016/S0021-9797(02)00185-6

Vestergaard, M., Kerman, K., & Tamiya, E. (2007). An Overview of Label-free Electrochemical Protein Sensors. *Sensors*, *7*(12), 3442–3458. https://doi.org/10.3390/s7123442

Voskerician, G., Shive, M. S., Shawgo, R. S., Recum, H. von, Anderson, J. M., Cima, M. J., & Langer, R. (2003). Biocompatibility and biofouling of MEMS drug delivery devices. *Biomaterials*, *24*(11), 1959–1967. https://doi.org/10.1016/S0142-9612(02)00565-3

Walsh, S. W., Williams, E. J., & Evans, A. C. O. (2011a). A review of the causes of poor fertility in high milk producing dairy cows. *Animal Reproduction Science*, *123*(3–4), 127–138. https://doi.org/10.1016/j.anireprosci.2010.12.001

Walsh, S. W., Williams, E. J., & Evans, A. C. O. (2011b). A review of the causes of poor fertility in high milk producing dairy cows. *Animal Reproduction Science*, *123*(3–4), 127–138. https://doi.org/10.1016/j.anireprosci.2010.12.001

Wang, C., Cui, X., Li, Y., Li, H., Huang, L., Bi, J., Luo, J., Ma, L. Q., Zhou, W., Cao, Y., Wang, B., & Miao, F. (2016). A label-free and portable graphene FET aptasensor for children blood lead detection. *Scientific Reports*, *6*(1), 21711. https://doi.org/10.1038/srep21711

Wang, P. M., Cornwell, M., Hill, J., & Prausnitz, M. R. (2006). Precise Microinjection into Skin Using Hollow Microneedles. *Journal of Investigative Dermatology*, *126*(5), 1080–1087. https://doi.org/10.1038/sj.jid.5700150

Wang, R., Chon, H., Lee, S., Cheng, Z., Hong, S. H., Yoon, Y. H., & Choo, J. (2016). Highly Sensitive Detection of Hormone Estradiol E2 Using Surface-Enhanced Raman Scattering Based Immunoassays for the Clinical Diagnosis of Precocious Puberty. *ACS Applied Materials & Interfaces*, *8*(17), 10665–10672. https://doi.org/10.1021/acsami.5b10996

Wilke, N., Mulcahy, A., Ye, S.-R., & Morrissey, A. (2005). Process optimization and characterization of silicon microneedles fabricated by wet etch technology. *Microelectronics Journal*, *36*(7), 650–656. https://doi.org/10.1016/j.mejo.2005.04.044

Wu, Y. X., & Kwon, Y. J. (2016). Aptamers: The “evolution” of SELEX. *Methods*, *106*, 21–28. https://doi.org/10.1016/j.ymeth.2016.04.020

Xu, Z. Z., McKnight, D. J., Vishwanath, R., Pitt, C. J., & Burton, L. J. (1998). Estrus Detection Using Radiotelemetry or Visual Observation and Tail Painting for Dairy Cows on Pasture. *Journal of Dairy Science*, *81*(11), 2890–2896. https://doi.org/10.3168/jds.S0022-0302(98)75849-7

Yang, Z., Ma, F., & Xu, K. (2017). Grain boundaries guided vibration wave propagation in polycrystalline graphene. *RSC Advances*, *7*(40), 24667–24673. https://doi.org/10.1039/C7RA03744A

Yih, J.-N., Chu, Y.-M., Mao, Y.-C., Wang, W.-H., Chien, F.-C., Lin, C.-Y., Lee, K.-L., Wei, P.-K., & Chen, S.-J. (2006). Optical waveguide biosensors constructed with subwavelength gratings. *Applied Optics*, *45*(9), 1938–1942. https://doi.org/10.1364/AO.45.001938

Yuan, W., Zhou, Y., Li, Y., Li, C., Peng, H., Zhang, J., Liu, Z., Dai, L., & Shi, G. (2013). The edge- and basal-plane-specific electrochemistry of a single-layer graphene sheet. *Scientific Reports*, *3*, 2248. https://doi.org/10.1038/srep02248

Zhou, X., Liu, L., Hu, M., Wang, L., & Hu, J. (2002). Detection of hepatitis B virus by piezoelectric biosensor. *Journal of Pharmaceutical and Biomedical Analysis*, *27*(1–2), 341–345. https://doi.org/10.1016/s0731-7085(01)00538-6

Zhu, B., Alsager, O. A., Kumar, S., Hodgkiss, J. M., & Travas-Sejdic, J. (2015). Label-free electrochemical aptasensor for femtomolar detection of 17 beta-estradiol. *BIOSENSORS & BIOELECTRONICS*, *70*, 398–403. https://doi.org/10.1016/j.bios.2015.03.050

Zhuo, Z., Yu, Y., Wang, M., Li, J., Zhang, Z., Liu, J., Wu, X., Lu, A., Zhang, G., & Zhang, B. (2017). Recent Advances in SELEX Technology and Aptamer Applications in Biomedicine. *International Journal of Molecular Sciences*, *18*(10), 2142. https://doi.org/10.3390/ijms18102142

Zurovsky, Y., Mitchell, G., & Hattingh, J. (1995). Composition and viscosity of interstitial fluid of rabbits. *Experimental Physiology*, *80*(2), 203–207. https://doi.org/10.1113/expphysiol.1995.sp003840

Abstract

In cattle herds using animal insemination (80% of dairy and 13% of suckling cows), reproductive management involves a decisive step that consists of detecting the ovulation time. This step conditions the success of the reproduction and, consequently, the economic results of the farm. Traditionally, ovulation detection is done by observing the sexual behaviour (oestrus or heat) that cows express in the 25 to 30 hours preceding ovulation. However, oestrus detection faces two major problems: 1/ the increase in herd size, which makes this activity particularly time-consuming, and 2/ a reduction in oestrus expression (in duration and intensity) observed in animals with high milk production potential. Defects in oestrus expression challenge the tools used to help detect ovulations based on the recording of sexual behaviour and lead to the development of tools based on the monitoring of physiological signals (hormonal dynamics) that announce ovulation. This thesis, supported by INRAE, VetAgro Sup and CEA, aims to create a first prototype for monitoring the reproductive hormones in the form of a portable patch capable of measuring hormone concentrations during the ovarian cycle from interstitial fluid samples. This device will be able to predict the occurrence of ovulation associated with a peak in oestradiol, after the fall in progesterone and will warn the breeder. In this context, this thesis work aimed to develop the first technological building blocks of the patch. The first step was the design and creation of hollow microneedles (MNs). Their role is to collect the interstitial fluids (between the cells of the dermis) in which the hormones are present. Parallel research for the location of the patch on the cow helped to define the length required for the MNs to reach the targeted tissues. Secondly, the development of a microfluidic network to deliver the fluids from the MNs to a measurement chamber. The third and final part developed during this thesis was the biosensor for hormone detection. Using graphene-based SGFET (solution-gated-field-effect-transistors) technology, various biological detection tests were realized using model molecules to understand the biosensor's response in liquid environment. Finally, hormones detection tests were performed using aptamers (small single-stranded DNA) as probes. To be competitive on the market, the patch will have to be easy to use for the farmer without veterinary assistance, to be affordable, made of biocompatible materials and comfortable enough not to be a source of discomfort for the cow. The communication between the patch and the farmer is not part of the objectives of this thesis and will be developed later on the SmartRepro project.

Résumé

Dans les troupeaux bovins pratiquant l'insémination animale (80% des vaches laitières et 13% des vaches allaitantes), la gestion de la reproduction passe par une étape déterminante: la détection des ovulations. Cette étape conditionne la réussite de la reproduction et, de ce fait, les résultats économiques de l'exploitation. Traditionnellement, la détection des ovulations se fait par l'observation des comportements sexuels (œstrus ou chaleurs) que les vaches expriment dans les 25 à 30 heures qui précèdent l'ovulation. La détection des œstrus se heurte toutefois à deux problèmes majeurs : 1/ l'agrandissement de la taille des troupeaux qui rend cette activité particulièrement chronophage et 2/ une réduction de l'expression de l'œstrus (en durée et en intensité) observée chez les animaux à fort potentiel laitier. Les défauts d'expression des œstrus remettent en question les outils d'aide à la détection des ovulations basés sur l'enregistrement des comportements sexuels et orientent les réflexions vers le développement d'outils s'appuyant sur le suivi de signaux physiologiques (dynamiques hormonales) annonciateurs de l'ovulation. Le projet de cette thèse, porté par l'INRAE, VetAgro Sup et le CEA, est de créer un premier prototype de monitoring des hormones de la reproduction sous forme d'un patch portable capable de mesurer les concentrations en hormones au cours du cycle ovarien à partir de prélèvements de fluides interstitiels. Ce dispositif sera en mesure de prédire l'occurrence d'une ovulation associée à un pic d'œstradiol détecté après la chute de progestérone et d'en avertir l'éleveur. Dans ce contexte, ces travaux de thèse ont visé à développer les premières briques technologiques du patch. La première étape fut la conception et la création de microaiguilles (MAs) creuses. Leur rôle est de collecter les fluides interstitiels (entre les cellules du derme) dans lesquels les hormones sont présentes. Une recherche en parallèle de l'emplacement du patch a permis de définir la longueur requise pour les MAs afin d'atteindre les tissus cibles situés dans le derme. Deuxièmement, le développement d'une carte microfluidique pour amener les fluides des MAs jusqu'à la chambre de mesure. La troisième et dernière partie développée au cours de cette thèse est le biocapteur pour la détection des hormones. En utilisant la technologie SGFET (solution-gated-field-effect-transistors) à grille de graphène, différents tests de détection biologiques ont été réalisés avec des molécules modèles pour comprendre la réponse de ce type de capteur émergent avant de passer à la détection des hormones en utilisant des aptamères (petit ADN simple brin) comme sondes. Pour être compétitif sur le marché, le patch devra être facile d'utilisation pour l'éleveur sans aide vétérinaire, peu coûteux, suffisamment confortable pour ne pas être source d'inconfort pour la vache et être développé avec des matériaux biocompatibles pour ne pas induire de réactions inflammatoires. La communication entre le patch et l'éleveur ne fait pas partie des objectifs de thèse et sera développée ultérieurement.